Rules of Molecular Self-Organization: Emergence, Control and Predictability

SIGILL: UNIVERSITAT: LUDOVIC: MAXIM:

Carsten L. Rohr

München 2011

Rules of Molecular Self-Organization: Emergence, Control and Predictability

Dissertation

am Lehrstuhl für Experimetalphysik

Prof. J. O. Rädler

Fakultät für Physik

Ludwig-Maximilians-Universität München

Carsten L. Rohr

Juni 2011

Betreuer: Dr. B. Hermann

Erstgutachter: Prof. Dr. Joachim O. Rädler

Zweitgutachter: PD Dr. Markus Lackinger

Datum der Prüfung: 15.6.2011

Contents

ZUSAMMENFASSUNG **III**

ABSTRACT **V**

1 INTRODUCTION **1**

1.1 MISSING RULES AND PREDICTABILITY 1
1.2 AIMS OF THE THESIS 3
1.3 STRUCTURE OF THE THESIS 4

2 SELF-ORGANIZATION **5**

2.1 CONCEPT 5
2.2 MOLECULAR SELF-ORGANIZATION 6

3 SCANNING TUNNELING MICROSCOPY **9**

3.1 SCANNING TUNNELING MICROSCOPY 9
3.2 TUNNEL THEORY 13
3.3 TUNNELING THROUGH MOLECULAR ADLAYERS 17
3.4 SUBSTRATES 19
3.5 SOLUTION CASTING 20
3.6 IMAGE PROCESSING 22

4 MOLECULAR SYSTEMS **25**

4.1 SUPRAMOLECULAR CHEMISTRY 25
4.2 FRÉCHET-DENDRONS 26

5 COMPLEX ENERGY LANDSCAPES **29**

5.1 ENERGY LANDSCAPES 29
5.2 METASTABLE STATES 30
5.3 PHASE TRANSFORMATIONS 31
5.4 EMERGENCE 31

6 COMPUTATIONAL TOOLS 33
6.1 FORCE FIELDS IN MOLECULAR MECHANICS SIMULATIONS 34
6.2 DENSITY FUNCTIONAL THEORY SIMULATIONS 35
6.3 INTERACTION-SITE MODEL IN MONTE-CARLO SIMULATIONS 38
7 CONCEPTS OF SELF-ORGANIZED MOLECULES 41
7.1 2D SYMMETRY GROUPS 41
7.2 CHIRALITY 45
7.3 HIERARCHICAL ORGANIZATION 46
8 SUMMARIES OF PUBLICATIONS 49
9 PUBLICATIONS 55
9.1 SIZE MATTERS IN OSTWALD´S RULE OF STAGES: MULTIPHASE TRANSFORMATIONS CAUSED BY STRUCTURAL COMPLEXITY 55
9.2 MOLECULAR JIGSAW: PATTERN DIVERSITY ENCODED BY ELEMENTARY GEOMETRICAL FEATURES 59
9.3 MOLECULAR SELF-ORGANIZATION: PREDICTING THE PATTERN DIVERSITY AND LOWEST ENERGY STATE OF COMPETING ORDERING MOTIFS 67
9.4 PREDICTING THE INFLUENCE OF A *P2*-SYMMETRIC SUBSTRATE ON MOLECULAR SELF-ORGANIZATION WITH AN INTERACTION-SITE MODEL 75
9.5 SIMULATING PATTERNS FOR MOLECULAR SELF-ORGANIZATION ON SURFACES USING INTERACTION-SITE MODELS 91
9.6 MULTI-HIERARCHICAL ASSEMBLY VIA MOLECULAR FLEXIBILITY 101
9.7 SURFACE CONTROL OF CHIRALITY, ORIENTATION AND HIERARCHICAL ASSEMBLY OF SELF-ORGANIZED MONOLAYERS 109
9.8 A VERSATILE FRÉCHET-DENDRON COMPOUND UNIFIES HOST-GUEST AND TEMPLATED HETEROGENEOUS SELF-ASSEMBLY 115
10 PERSPECTIVES 125
10.1 FROM PREDICTION AND COMPLEXITY IN SELF-ORGANIZATION 125
10.2 TOWARDS DESIGN AND FUNCTIONALITY 127
REFERENCES 129
APPENDIX 141
A BOOK CHAPTER: DIE SUCHE NACH DEM TIEFSTEN TAL: SELBSTORGANISATION VON MOLEKÜLEN IN GESCHLOSSENEN SYSTEMEN 141
B ORGANIC SUPERCONDUCTORS REVISITED 165
ACKNOWLEDGMENTS 173

Zusammenfassung

Diese Arbeit stellt die Frage nach der Vorhersagbarkeit von komplexen selbstorganisierten Molekülmustern und versucht mit Hilfe von kognitiven Ansätzen und Simulationsmethoden Antworten zu geben. Dazu wurden die Anordnungen von Fréchet-Dendronen, dem phasenreichsten zweidimensionalen System, mittels Rastertunnelmikroskopie abgebildet. Bisher führen die fehlenden Regeln oder Simulationen für molekulare Selbstorganisation zu einem Molekül-Design nach dem Versuch-und-Irrtum-Prinzip. Mittels klarer Algorithmen können mögliche Ausgänge vor dem Experiment vorherzusagt werden, was ein gezieltes Experimentdesign ermöglicht. Diese Arbeit gliedert sich in drei Teilbereiche:

1. *Verstehen und Kontrolle der Eigenschaften und Phasenvielfalt von Fréchet-Dendronen*
    - Die Untersuchung einer Reihe von ähnlichen Molekülen mit steigender Komplexität ergibt, dass bei der Umwandlung vom metastabilen Ausgangsmuster zur thermodynamischen Endanordnung mit größerer Komplexität schrittweise mehr Zwischenmuster angenommen werden. Diese Komplexitätsabhängigkeit der von Ostwald vor 100 Jahren aufgestellten Stufenregel wird als Emergenzphänomen erklärt, das durch eine zunehmend zerfurchtere Energielandschaft entsteht.
    - Fréchet-Dendronen erzeugen mit Gastmolekülen sowohl Wirt-Gast-Anordnungen als auch polymorphe Muster in Abhängigkeit von der elektronischen Struktur des Gastmoleküls. Dies ist das erste Mal, dass ein Molekül diese beiden Klassen der heterogenen Musterbildung vereint. Erklärt wird dieser Effekt durch den dualen Wechselwirkungscharakter des Moleküls.
2. *Entwicklung eines Monte-Carlo-Modells zur Mustervorhersage*
    - Ein stark abstrahiertes Wechselwirkungsmodell von Fréchet-Dendronen wird auf der Basis von Molekularmechanik-Simulationen entwickelt. Dieses Modell prognostiziert in Monte-Carlo-Simulationen nicht nur Phasenvielfalt,

sondern auch deren lokale und globale Anordnungen in Übereinstimmung mit dem Experiment.
- Eine Weiterentwicklung des Wechselwirkungsmodells mit unterschiedlichen Konformationen reproduziert das komplexeste Muster exakt, zusätzlich zu den bereits gefundenen Phasen. Eine Energieanalyse des Modells zeigt, dass die niedrigste Energie für dasjenige Muster gefunden wird, das dem thermodynamischen Endzustand im Experiment entspricht.
- Mit Hilfe des Modells werden die erwarteten Anordnungen auf einem modifizierten $p2$-symmetrischen Substrat vorhergesagt, die in der Folge auch experimentell bestätigt werden. Damit werden erstmalig die selbstorganisierten Muster für neue experimentelle Bedingungen prognostiziert.

3. *Auffinden von allgemeinen Beziehungen zwischen molekularem Baustein und resultierendem Muster*
   - Das hierarchische Entstehen der Muster, gekoppelt mit einem Rekombinationsprozess der Bausteine auf jeder Hierarchieebene, führt zu der gefundenen Phasenvielfalt. Dies ist das erste Beispiel für multihierarchische Anordnung in 2-D selbstorganisierten Systemen.
   - Grundlegende Eigenschaften der Molekülbausteine wie Asymmetrie, multiple Wechselwirkungen und Flexibilität bedingen Mustereigenschaften wie Rotationssymmetrie, hierarchischen Anordnungen und multiple Phasen.
   - Mit Hilfe einer veränderten Oberfläche werden durch diese Prinzipien gezielt die Chiralität, Orientierung und Anordnungshierarchie eines Musters verändert.

Für eine ausführlichere Zusammenfassung der im Rahmen dieser Arbeit entstandenen Veröffentlichungen wird auf Kapitel 9 verwiesen.

Abstract

This thesis describes approaches with computational as well as cognitive methods to pattern prediction, deriving rules for 2D molecular self-organization from a large set of scanning tunneling microscopy images on a set of Fréchet Dendron molecules.

Up to date understanding and directing self-organization of supramolecular monolayers based on innovative modeling approaches presents a major prerequisite for reliable applications towards surface functionalization, sensors, catalysis, as well as molecular electronic devices. There is an urge for an understanding of self-organization rather than following a trial and error method. Although all the forces contributing to molecular self-organization are known, no systematic approach, rule based or simulation based, can predict the properties of the observed patterns in advance.

Fréchet Dendrons exhibit the highest phase variety for molecular self-organization on surfaces and are investigated by scanning tunneling microscopy and multiple modeling techniques. This pattern diversity is here found to stem from the first instant of multi-hierarchical assembly found for 2D molecular self-organization caused by the molecules´ high conformational freedom. A comparison between molecules of increasing complexity shows that the pattern diversity is the result of emergent transient states due to an increasingly rugged energy landscape.

In this thesis an interaction-site model is developed that successfully condenses the essential molecular properties of the Fréchet Dendrons, as determined by multiscale modeling. In a Monte Carlo approach this model successfully predicts the various local and global ordering motifs of Fréchet Dendron self-organization. This confirms that only geometry as well as a few salient weak interaction sites encode these structural motifs.

The different forms of organization created by Fréchet Dendrons were modeled and relevant features in the orderings were identified. General building

block properties could be determined that lead to specific features of higher level structures, for example symmetry, hierarchical assembly and orientations. From this insight general rules governing molecular self-organization could be determined. This implies that basic properties of the building blocks necessitate the properties of the resulting pattern.

Lastly these insights were employed by creating a surface modified with *n*-alkanes to change the surface´s characteristics. The possible assembly patterns on this surface were predicted using the interaction site model and successive experiments found a change in pattern symmetry, orientation and hierarchical assembly.

With these insights and modelling tools changes in designing a new molecular building block can take place. More time spent in front of the whiteboard, will lead to a more conscious and more controlled form of self-organization.

1 Introduction

1.1 Missing rules and predictability

The process of self-organization is the way by which nature creates complexity from the inanimate world of galaxies, sand dunes and molecules to the living realm of membranes, swarm dynamics and consciousness[1]. Molecular self-organization provides one of the two approaches to create structures at the nanoscale.

> "*…self-assembly is one of the few practical strategies for making ensembles of nanostructures. It will therefore be an essential part of nanotechnology*."
>
> G.Whitesites[2]

On surface the organization of supramolecular monolayers constitutes a major challenge important for surface functionalization[3], sensors,[4] catalysis,[5] and molecular electronic devices[6]. In recent years research has uncovered an enormous variety of patterns which are combined in the two dimensional structural database 2DSD[7]. Increasingly different patterns are created by one and the same molecule[8-14], leading to coexistence and dynamical behavior like phase transformations[15].

> "*Once the mechanisms controlling the self-ordering phenomena are fully understood, the self-assembly and growth processes can be steered to create a wide range of surface nanostructures from metallic, semiconducting and molecular materials.*"
>
> K. Kern and co-workers,[3].

This statement by Kern describes the possibilities of molecular self-organization and raises the main prerequisite, *understanding*, for this development. The main difficulty lies in making reliable predictions[16] and controlling[17] the complex molecular ordering on the nanometer scale. As de Feyter put it bluntly in 2008:

> "*When faced with the question how a given molecule is going to adsorb on a well-known surface, the answer is often vague and most often the "I-don't-know" approach is the most honest one.*"
>
> S. de Feyter and co-workers[18]

This raises the question of how to deal with this uncertainty and complexity. One chemical approach is to reduce complexity by creating very specific key-lock interactions at the applied molecules to avoid uncertainty in the outcome[19-21]. This tecton[16] approach deals with complexity by simplifying it. Other approaches to understand pattern formation in molecular self-organization rely on the shape of the molecule[22] for an explanation.

Modeling approaches to understand specific self-organized systems like density-functional-theory[23, 24] or molecular mechanics or dynamics[25-27] usually provide an explanation *after* the experiment has been performed, since random starting configurations exceed the computational power available. Coarse graining with interaction site model[28, 29] or other simplified models implemented for Monte Carlo methods[25-27] could present a possible alternative. Nevertheless predictive methods are still missing.

> "*... the increasing complexity of the assembly units used makes it generally more difficult to control the supramolecular organization and predict the assembling mechanisms. This creates a case for developing novel analysis methods and ever more advanced modeling techniques*"
>
> de Vita and co-workers[30]

The development of predictive computer simulations would no doubt change the approach for synthesizing molecules for self-organization. But even more appealing would be the derivation of simple rules governing the self-organization process. This would replace the current trial and error approach for synthesizing the right molecule that organizes in a specific manner.

> "*Engineering is not easy. It requires a set of rules which allows predicting the outcome of the self-assembly process with a high degree of reliability.*"
>
> S. de Feyter and co-workers[18]

> *"Through progressive discovery, understanding, and implementation of the rules that govern the evolution from inanimate to animate matter and beyond, we will ultimately acquire the ability to create new forms of complex matter."*
>
> J. M. Lehn, [4]

These rules would not only have to cover properties like symmetry, chirality[31-33] and hierarchy[34] within self-organized patterns but might also go into the more complex realm of heterogeneous assembly[35-40].
This opens three questions for this thesis:

1. How can the new complexity in self-organization be explained?
2. Is it possible to predict molecular pattern in advance using simulations?
3. What are the rules governing molecular self-organization?

1.2 Aims of the Thesis

1. *Understand the mechanisms behind the phase variety and complex phase transformations observed in Fréchet Dendrons.*

Fréchet Dendrons show the highest phase variety for molecular self-organization on surfaces. The patterns coexist and phase transform on the surface within minutes to hours. The influences of the molecular flexibility as well as the properties of the molecular building blocks are regarded as possible reasons. The temporal and energetic relationship between the phases of specific molecules is investigated. A comparison between molecules of increasing complexity explores the question of emergence within self-organized systems.

2. *Develop in cooperation a simulation model capable of predicting the pattern variety of the Fréchet Dendron system.*

So far it has been impossible to predict the pattern for a self-organized monolayer prior to the experiment. In this thesis an interaction site model is developed in cooperation with theorists. This simulation approach drastically reduces the molecular complexity to increase the number of simulated molecules as well as the simulation time scale. These two conditions are prerequisites for the possible prediction of patterns from an unordered state. The model is tested on the phase rich Fréchet Dendron system.

3. *Abstract rules of self-organization from the complex behavior of Fréchet Dendrons which are also applicable to other molecules.*

Rules governing more complex forms of self-organization, like hierarchical assembly, are absent and a trial and error approach prevails when a specific pattern outcome is desired. Here the different forms of patterns created by Fréchet Dendrons are modeled and common features in the orderings are identified. The derived rules are checked against the literature of self-organized systems and possible experimental realizations are tested.

1.3 Structure of the Thesis

After a consideration of the current research and the identification of key questions, the aims of this thesis are worked out in chapter one. The thesis is then divided into two large parts, one introducing concepts and techniques important to the topic, while the second half comprises the results of the research.

The chapters in the first half are grouped by topic. In the beginning chapter two introduces self-organization in general and then more specifically for molecular monolayers. With this general concept covered, the experimental site encompassing the scanning tunneling microscope (STM) and its background theory and image acquisition are introduced in chapter three. The molecular aspect is introduced in chapter four defining supramolecular chemistry and the employed system of Fréchet Dendrons. The connection between energy landscapes, phase transformations and emergence in self-organization is made in chapter five. The basis for three different simulation approaches molecular mechanics, density functional theory and interaction site modeling are explained next in chapter six. In the last chapter seven, three properties of self-organization, namely symmetry, chirality and hierarchy will be discussed.

In the beginning of the results the publications are briefly summarized. The first starts with emergent phases for increasing molecular complexity. The next four publications introduce and then highlight different aspects of an interaction site model which successfully reproduces an experimental pattern variety and predicts results prior to the experiment. The following two publications introduce rules for molecular self-organization and utilize a modified surface assembly. The last publication combines two previously separate fields of heterogeneous self-organization. In the end these findings are put into context and possible future prospects are discussed.

The appendix features a popular science book chapter on emergence and a publication about organic superconductors, not part of this thesis.

2 Self-Organization

2.1 Concept

Pattern formation and destruction are the two basic processes driving change in our universe. Self-organization refers to a class of pattern formation in a wide range of systems[2], from inanimate objects to self-determined agents the individual parts are connected by the process of pattern formation that leads to the creation of structure and order within. This process is internal and happens by interactions inherent to the system, requiring no external influences to drive the pattern formation. Self-organization is often defined by what it is not. In self-organized systems there is no global plan directing the individual parts, no external blueprint or template, no order imposed by any sort of outstanding leader or guide, though there might by a self-organized hierarchical order, see chapter 7.3.

A very useful definition for self-organization is given by Scott Camazine[1]: "*Self-organization is a process in which **pattern** at the **global level** of a system emerges solely from numerous **interactions** among the **lower-level components** of the system. Moreover, the **rules** specifying interactions among the system's components are executed using only **local information**, without reference to the global pattern. In short, the pattern is an **emergent property** of the system, rather than a property imposed on the system by an external ordering influence.*" This definition requires the appearance of a pattern within a system. The pattern can be spatial or temporal in nature or a combination of both. It needs to be present at the global level of the system. A self-organized system requires multiple parts and a means of interaction between the parts of the system, which can be direct or indirect interaction. The pattern is not structured by an outside influence but by the interactions between the components. Nevertheless an outside influence (temperature change, predator etc.) can trigger a pattern or pattern change. The interactions follow rules, which are strictly local in nature, global templates or plans in this definition. Lastly the pattern can by characterized as an emergent property, see chapter 5.4.

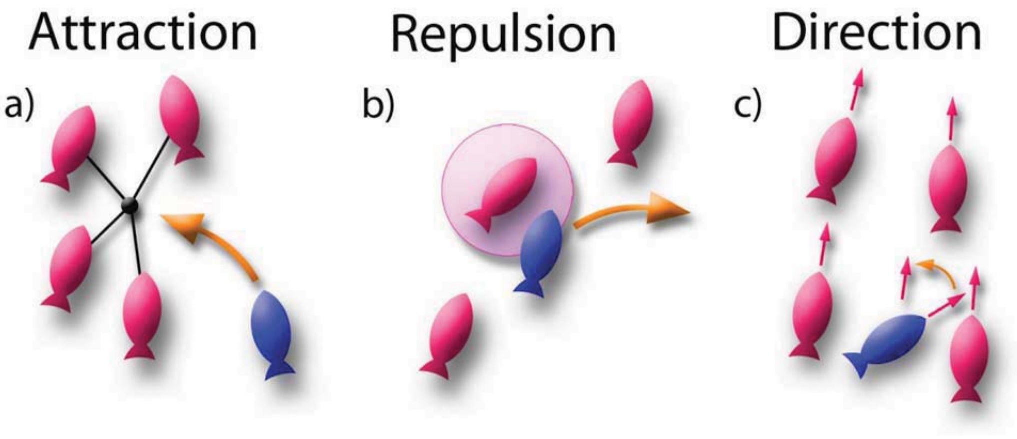

Figure 1. Fish schools and individual directives: The self-organization behavior of fish schools is driven by three rules that individuals adhere to in their local environment. a) Stay in the center of the group. b) Leave space for maneuvering. c) Match the movement direction of your local neighbors.

This definition will here be illustrated by schools of fish. The individual fish form a spatial arrangement of a closed swarm with regular distances to their nearest neighbors and a general swarm direction. The interaction of the different individuals within a school is governed by three rules. These rules strictly apply to the local environment of the individual, see figure 1. 1. Stay in the center of the group (Avoid unoccupied space around you). 2. Leave (local) space for maneuvering. 3. Match the movement direction of your local neighbors.[1] No internal global plan or external template creates this behavior.

In the following, this definition of self-organization will now be applied to the ordering phenomena of molecular systems.

2.2 Molecular Self-Organization

Self-organization at the molecular level is one of two approaches to create structures at the nanometer scale. The route employed by molecular self-organization, also known as bottom-up approach, creates complex structures out of relatively simple ones. In contrast, the top-down approach imposes predefined structure by a global template or plan.

---

[1] This third rule is found in flocks of birds or schools of fish, but is missing in swarms of insects. Therefore insect swarm behavior looks distinctly different and more chaotic.

When checking the previously employed definition for self-organization for applicability on the molecular scale, similarities but also restrictions appear. Individual molecules can form patterns in the absence of external stimuli. For this process to occur, local interactions need to govern the ordering. The basic local nonspecific interactions at the molecular scale are attraction, repulsion and orientation. The most basic attractive force is the van der Waals force. The Pauli Exclusion Principle prevents the overlap of molecules, while electrostatic and in particular dipolar forces, orient molecules with respect to each other, see figure 2.

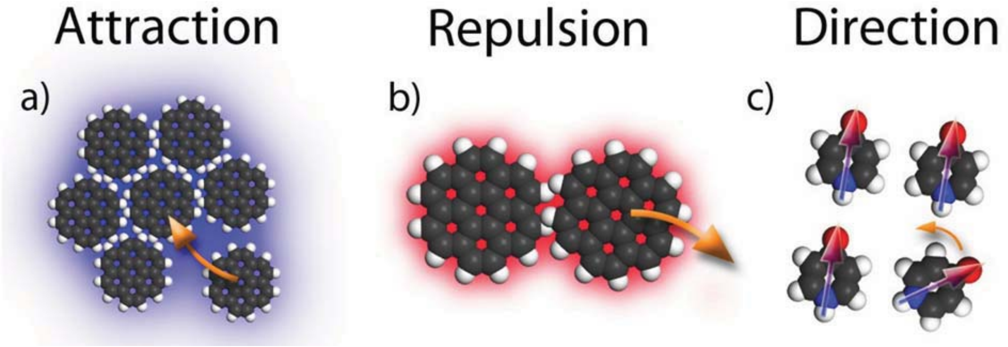

Figure 2. Molecular self-organization: Three basic non covalent interactions on the molecular scale that lead to molecular self-organization. a) Van der Waals forces attract molecules to another. b) The Pauli repulsion prevents molecules from overlapping. c) Electrostatic forces orient molecules with respect to their local environment.

The necessity for non-covalent bonds is given by the local character of the interactions, which requires the possibility of reconfiguration to adapt to local changes not possible with covalently bonded molecular meshes. In the case of surface bound self-organization, the possibility of a templating influence of the substrate can impede the ordering process and predetermine possible orderings. For the influence of the surface properties on the organization process see chapter 7.1.

A distinctly different form of self-organization can be found, when specific key-lock interactions are employed. Here the interactions carry a specific information component, which allows for a greater directed engineering ability[4]. The additional information component usually leads to distinctly different assembly components with highly individualistic interactions depending on the specificity of the interacting parts. Biochemical and biological molecules employ this kind of self-organization between heterogeneous parts.

A primary example of information carrying building blocks is the specificity of DNA assembly[41, 42]. Only sequences of bases fitting their counter strand bind together to form an essentially one-dimensional strand see figure 3a. Nevertheless the assembly into two and three dimensional structures is also possible. In the holiday junction for example, where four only partially fitting DNA strands organize into a cross like shape, see figure 3b. With the use of sticky DNA endings this network can be repeated in two dimensions, see figure 3c.

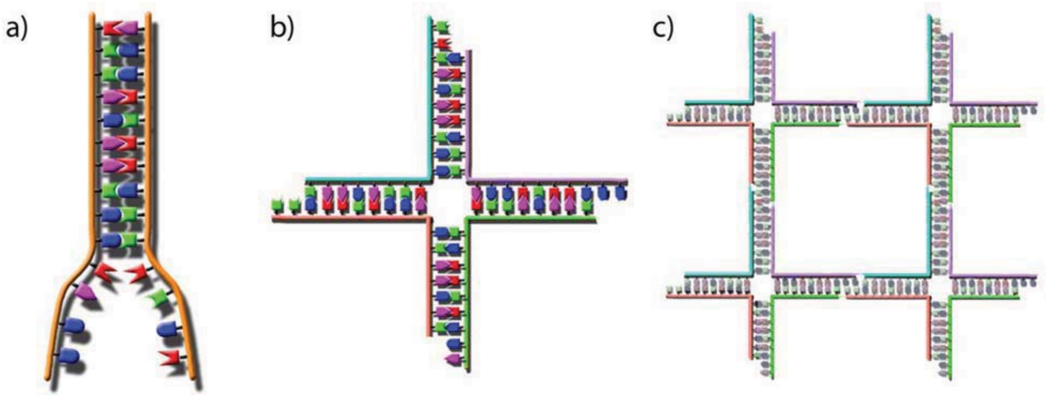

Figure 3. Information and DNA self-assembly: In DNA assembly information is encoded in the base sequence of individual self-assembly building blocks. a) Preprogrammed DNA strands only assemble with their fitting counterpart. b) A Holiday junction as simple example of two-dimensional DNA organization. c) Structure repetition using sticky ends within the DNA structure.

Great strides have been made with information encoded DNA self-assembly in the recent years[43] and similarities and overlap between the two areas of molecular self-organization become apparent. This work focuses on the non-specific form of self-organization, its emergent patterns and the prediction thereof. The detection of the self-organization and the emerging patterns inherent to the studied systems require a tool with sub-molecular resolution, as scanning tunneling microscopy can provide.

3 Scanning Tunneling Microscopy

3.1 Scanning Tunneling Microscopy

In 1981 scanning tunneling microscopy (STM) was invented by G. Binning und H. Rohrer[44]. With this device it became possible to image surfaces with atomic resolution. STM was not only employed for the atomic characterization of innumerable substrates and their electronic standing waves[45, 46], but also atomic and molecular adlayers[47], the observation and induction of chemical reactions[48], surface chirality[5], conformational switching[49-51], spin polarization[52] as well as atomic positioning[53].

Scanning tunneling microscopy relies on the quantum mechanical tunneling effect. The tip and the substrate have an applied bias voltage U_{Bias} and form an open circuit. Under classical conditions this barrier could not be overcome by the electrons. When considering quantum mechanics, their waves do not end abruptly at the barrier, but decay exponentially. If the barrier is thin enough, the probability function extends into the region beyond the barrier and electrons are able to tunnel through the barrier. The tunneling current is inversely exponential with respect to the tip – surface distance, see chapter 3.2. This implies on the one hand that the interaction is extremely short ranged[2], on the other hand it allows the precise height detection of the surface, if for example the tip is held constant. The tunneling current is generally in the order of 10^{-9} to 10^{-12} A.

Piezo-actuators allow tip – substrate positioning with sub-angstrom precision. Their working principle relies on an electric property of anisotropic crystals and certain ceramic materials. The dimensions of the piezo-electric material will change, depending on the direction and strength of the applied voltage within the range of nanometers. A three dimensional movement is achieved by arranging three such piezos perpendicular to each other. In most modern STM setups so-called single tube-piezos[54] are employed, see figure 4.

---

[2] The tunneling current is reduced to 1% of its original value if the tip surface distance is increased by 1 angstrom.

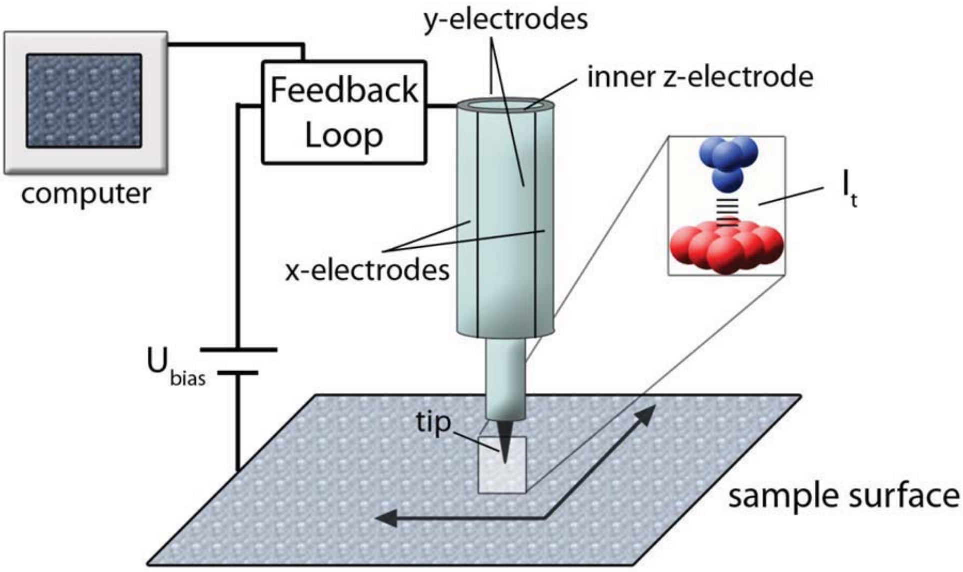

Figure 4. The scanning tunneling microscope: A bias voltage U_{Bias} applied between the atomically sharp tip and the surface allows electrons to tunnel the small distance, creating a pico ampere current I_{T}. A feedback loop adjusts the position of the tip via piezo elements to keep the tunneling current constant, while the piezo change is recorded to produce the surface image.

The tunneling current I_{T} is used as the set point signal, which a feedback loop tries to keep constant. In this constant current mode two datasets are recorded during a scanning process. One uses the movement of the z-piezo while scanning the surface, providing the main information about the substrate. The second dataset records the actual values of the measured tunneling current as an error signal. Due to the inertia of the feedback control, this set point value still contains some information about the substrate.

The feedback loop aims to keep the tunneling current I_{T} at a chosen set point by correcting the z-position of the tip. In most cases a proportional-integral-derivative (PID) control circuit is employed adjusting the z-piezo height to keep the preset current set point as constant as possible. The three components of the feedback proportional, integral and derivative can be adjusted by changing the values for the three parameters K_P, K_I and K_D individually, see figure 5.

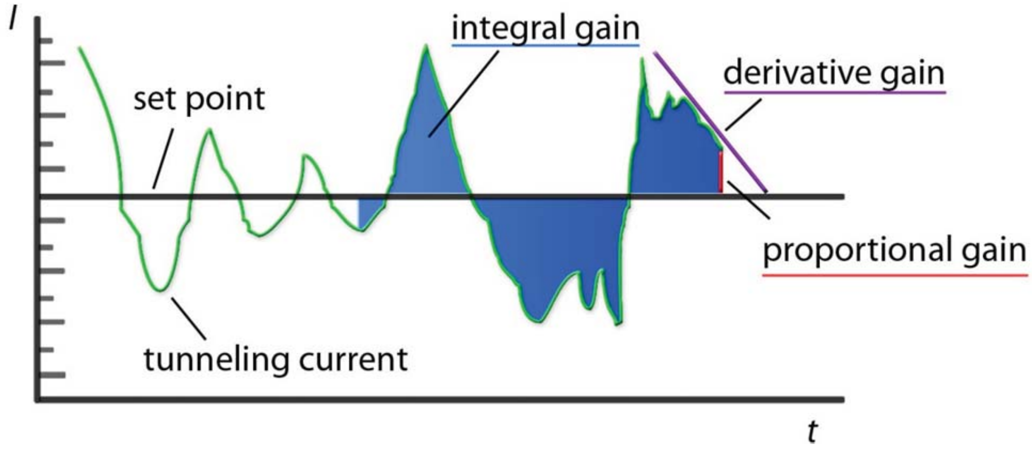

Figure 5. The feedback loop (PID): The tunneling current should be kept to a specific set point. The proportional gain *P* reacts proportional to the difference between set point and tunneling current. The integral gain *I* integrates the past deviances from the set point, while the derivative gain *D* uses the slope of the current curve with respect to the set point.

The proportional gain multiplies the factor K_P to the difference of set point and the measured tunneling current, the error signal *e(t)*. The resulting bias *u(t)* is applied to the z-component of the piezo-tube to counter the direction of the error signal.

$$u(t) = K_P \cdot e(t)$$

The integral gain integrates over past values of the error signal multiplied by the factor K_I resulting in a bias voltage, which is then applied to the z-piezo. The integral gain reduces oscillations of an overshooting feedback.

$$u(t) = K_I \int_0^t e(\tau) d\tau$$

The derivative gain is used less often to minimize the overshoot of the feedback response. Here, the factor K_D is multiplied to the derivate of the error signal.

$$u(t) = K_D \frac{d}{dt} e(t)$$

Turning off the feedback loop will switch the microscope to constant height mode. In this mode the full information of the surface corrugation is found in the tunneling current. Its use is only advisable on flat non tilted surfaces.

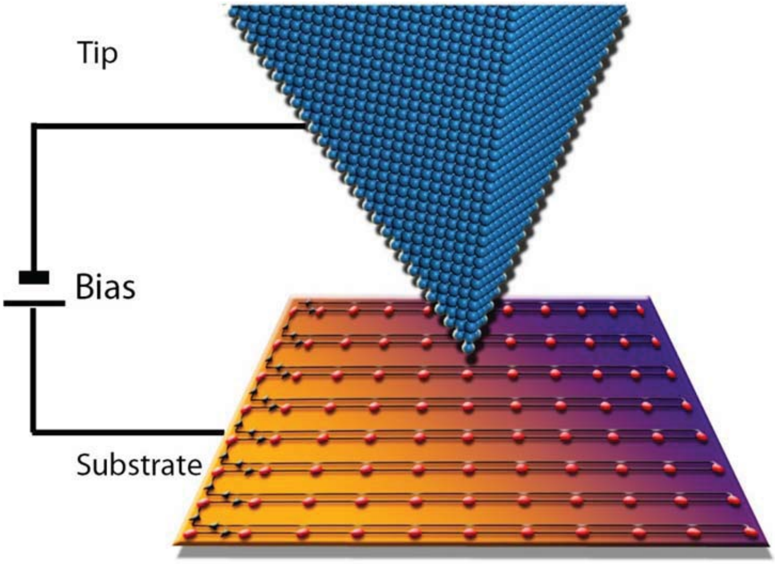

Figure 6. Scanning movement: The tip uses a raster movement to sample the surface of the substrate. This motion results in a fast scan direction along the x-axis and a slow scan along the y-axis.

A typical scanning movement for a forward scan is illustrated in figure 6. At intervals of equal distance measurement values are taken. The movement that results along the x-axis is called the fast scan direction, whereas the movement along the y-axis is the slow scan direction.

The STM tip records a mixture of the surface elevation, the electronic local density of states (LDOS) near the Fermi level[55]. If molecular adlayers are imaged, it is expected that electrons can tunnel from the highest occupied molecular orbitals (HOMOs) into lowest unoccupied molecular orbital (LUMO) of the tip, or vice versa depending on the sign of the applied voltage. The orbitals contributing to this process depend on the strength of the applied bias and integrate all orbitals from the Fermi energy up to the applied bias, see chapter 3.3.

The extended geometry of the tip is always convoluted with the measured surface structures resulting in broader STM features within a measurement as the tip passes above a corrugated surface. This needs to be kept in mind for the simulation of STM measurements, see chapter 6.2.

Moving the tip to a different location on the substrate also may result in some distortion during the first few lines of the measurement. This effect is referred to as piezo creep. The piezo-electric material needs some time to adjust its dimensions to abrupt changes in the applied voltage. The strong inhomogeneous electric field between tip and substrate can be used to manipulate the substrate structure[56].

The measurements in this thesis were made with a Nanoscope III employed with low current converter. The images were taken at ambient conditions.

3.2 Tunnel Theory

Two different effects are important to provide a reliable theory of the tunneling: Firstly the emergence of a local van-der-Waals force, secondly the exchange interaction itself. The close proximity of tip and substrate leads to a distortion of the undisturbed electron wave functions of both tip and substrate. This distortion gives rise to the van-der Waals force. This modification of the undisturbed wave functions will be treated by a stationary-state perturbation calculation. The process of quantum transmission in the tunneling process itself can be treated by time-dependent perturbation theory after the approach of Bardeen and Oppenheimer[57]. There are more sophisticated modeling approaches available[58] [59], which explain more of the intricate effects[60] seen in STM measurements over the years.

Tersoff and Hamann used a simplified tip geometry to demonstrate the ability of the STM to measure a surface of constant density of states near the Fermi level[61]. However for an adequate explanation of the atomic resolution of the STM, the description of the tip geometry has to be expanded to include so-called dangling bond states as has been shown by C. J. Chen[62]. The following chapters now give a step-by-step derivation for the tunneling current following the method of the Modified Bardeen Approach.

To describe the van-der-Waals force with perturbation calculations, a separation surface is drawn between tip and substrate, see figure 7a. The potentials describing the two subsystems U_S and U_T, for the substrate (S) and tip (T) respectively, are defined to satisfy two conditions.

$$U_S + U_T = U \text{ and } U_S \cdot U_T = 0$$

The product of the two potentials of the two subsystems equals zero in the entire space. Only in the interaction region, in close proximity to the apex of the tip, the potential barrier is substantially lowered. Outside of this region however, the potential equals the reference point of energy, the vacuum level U.

The free and disturbed potentials of the substrate, U_{S0} and U_S are shown in figure 7b. If the perturbation potential $V_S = U_{S0} - U_S$ is known, time-independent perturbation theory can be applied to derive the perturbed wave functions ψ_μ. In principle though, the wave functions are solutions of the Schrödinger equation

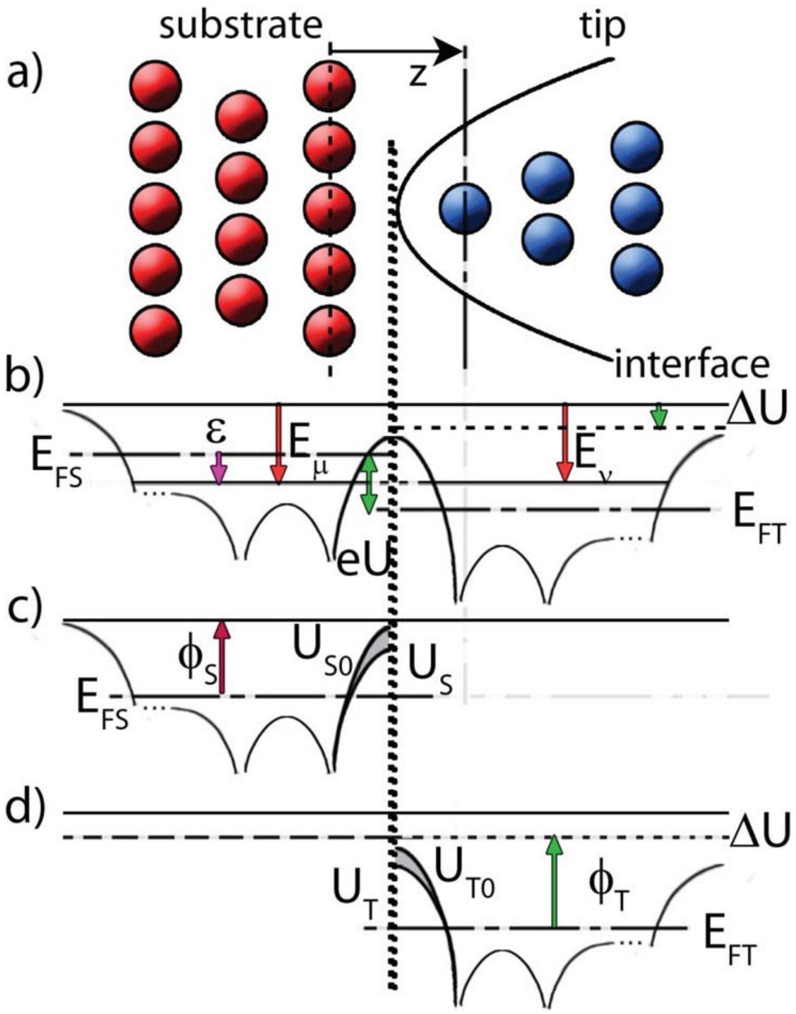
substrate
tip
a)
z
interface
b)
ε
E_μ
E_ν
ΔU
E_{FS}
E_{FT}
eU
c)
ϕ_S
U_{S0}
U_S
E_{FS}
d)
ΔU
U_T
U_{T0}
ϕ_T
E_{FT}

Figure 7. Perturbation theory at the tip-sample gap: a) Atoms at the tip and the sample interface. b) An energy scheme of the tip-substrate system is shown. (b) The potential surface of the complete system. E_{FS} and E_{FT} refer to the Fermi level, E_μ and E_ν to the energy levels of substrate and tip, respectively. U denotes the potential of the complete system. c-d) disturbed and undisturbed potential of substrate and tip respectively.

$$(T + U_S)\psi_\mu = E_\mu \psi_\mu$$

The same is true for the tip.

$$(T + U_T)\chi_\nu = E_\nu \chi_\nu$$

Knowing the modified wave functions ψ_μ and χ_ν, the two subsystems can once again be combined and the time-dependent evolution of the complete system be examined.

The time-dependent Schrödinger equation gives the wave function of the complete system. Using time-dependent perturbation theory the transition probability can subsequently be determined from the expansion coefficients. In first-order perturbation theory this transition probability is also known as Fermi's Golden Rule.

At the beginning of the calculation each subsystem is in its disturbed but stationary state, as described above. At the time $t > 0$ the perturbation potential of the tip U_T is switched on and the system as a whole starts to evolve following the time-dependent Schrödinger equation

$$i\hbar\frac{\partial\Psi}{\partial \mathrm{t}} = (T + U_S + U_T)\Psi$$

Expanding the time-dependent wave function Ψ into χ_ν:

$$\Psi = \sum_\nu a_\nu(t)\chi_\nu e^{-\frac{iE_\nu t}{\hbar}}$$

At $t = 0$, the state of the system still should be ψ_μ, thus the expansion coefficients will have to be

$$a_\nu(t) = \langle\chi_\nu|\psi_\mu\rangle e^{-\frac{i(E_\mu - E_\nu)t}{\hbar}} + c_\nu(t)$$

using $c_\nu(0) = 0$. Substituting a_υ leads to the following form of the wave function Ψ of the combined system:

$$\Psi = \psi_\mu e^{-\frac{iE_\mu t}{\hbar}} + \sum_\nu c_\nu(t)\chi_\nu e^{-\frac{iE_\nu t}{\hbar}}$$

The first term describes how Ψ would evolve if U_T would not have been switched on, the second term describes the perturbation induced by U_T.

Using this wave function and expanding by $< \chi_\nu|$ gives the condition for the $c_\nu(t)$:

$$i\hbar\dot{c}_\nu(t) = \langle\chi_\nu|U_T|\psi_\mu\rangle e^{-\frac{i(E_\mu - E_\nu)t}{\hbar}} + \sum_\lambda \langle\chi_\nu|U_S|\chi_\lambda\rangle c_\lambda(t) e^{-\frac{i(E_\lambda - E_\nu)t}{\hbar}}$$

The transition probability from a state ψ_μ of the substrate to a state χ_ν of the tip, $P_{\mu\nu}$, can now be derived from the expansion coefficients $c_\nu(t)$:

$$P_{\psi_\mu \rightarrow \chi_\nu} = P_{\mu\nu} = \left|\int_0^t \dot{c}_\nu(t)dt\right|^2$$

The transition rate $\omega_{\mu\nu}$ in first order perturbation theory is given by P/τ and its calculation leads to Fermi's Golden Rule

$$\omega_{\mu\nu}^{(1)} = \frac{2\pi}{\hbar}\left|M_{\mu\nu}\right|^2\frac{dN}{dE}$$

with the tunneling matrix element

$$M_{\mu\nu} = \left\langle \chi_\nu \middle| U_T \middle| \psi_\mu \right\rangle = \int_{V_{Tip}} \chi_\nu^* U_T \psi_\mu dV_{Tip}$$

To calculate the tunneling current I all the states within the tip and the substrate and their occupation probabilities have to be used, as well as the interplay of these states described by the matrix element $M_{\mu\nu}$.

For an arbitrary energy level ε (see figure 7) the contribution of the states of substrate (S) and tip (T) to the tunneling current corresponds to the density of states (DOS) ρ, resulting in the following factors $\rho_S(E_{FS} - eU + \varepsilon)$ and $\rho_T(E_{FT} + \varepsilon)$ where E_{FS} and E_{FT} denote the Fermi level E_F of the substrate and tip, respectively. To find an expression for the occupation probabilities, the tunneling current is divided into two parts: (i) transition from an occupied state of the surface to an unoccupied state of the tip and (ii) transition from an occupied state of the tip to an unoccupied state of the surface, as shown in figure 8.

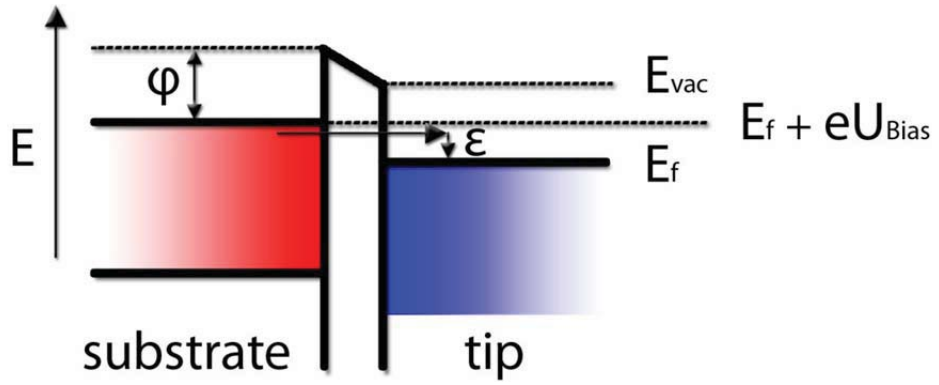

Figure 8. The tunneling current: The Fermi level difference of tip and sample plus the applied bias voltage results in the possible tunneling current. The energy of a state is measured in reference to the Fermi level E_F of substrate (S) and tip (T). At an arbitrary energy ε, electrons can tunnel from an occupied state of the substrate into an unoccupied state of the tip. Φ is the work function of the surface.

Using the Fermi-Energy as the reference level, the occupation probabilities F for case (i) are then given by:

$$F_{\rightarrow} = f_S(\varepsilon - eU)[1 - f_T(\varepsilon)]$$

using the Fermi-Dirac distribution

$$f(E) = \frac{1}{1 + e^{\frac{E - E_F}{kT}}}$$

For the transition in the reverse direction the occupation probabilities are:

$$F_{\leftarrow} = f_T(\varepsilon)[1 - f_S(\varepsilon - eU)]$$

Therefore, combining both occupation probabilities:

$$F_{\rightarrow} - F_{\leftarrow} = f_S(\varepsilon - eU) - f_T(\varepsilon)$$

This results in the expression for the total tunneling current:

$$I = \frac{4\pi e}{\hbar}\int_{-\infty}^{\infty}[f_S(E_{FS} - eU + \varepsilon) - f_T(E_{FS} + \varepsilon)] \cdot \rho_S(E_{FS} - eU + \varepsilon)\rho_T(E_{FS} + \varepsilon)|M|^2 d\varepsilon$$

The matrix element M depends exponentially on the tip-substrate distance. This fact is responsible for the atomic resolution of the STM. Since only the outermost atom at the apex of the tip contributes significantly to the tunneling current, the adjacent atoms´ contribution is negligible.

The tunneling current with a simplified tip geometry (s-wave function) was shown by Tersoff and Hamann in 1983 and reproduces a typical STM image of a gold substrate mapping a surface of constant density of states[61]. The s-wave approximation is a common method used for simulations images of scanning tunneling microscopy, see chapter 6.2. To explain the atomic resolution of an STM image one requires more states of the tip surface to be taken into account. Using localized p_z and d_{z^2}-dangling bonds C. J. Chen derived an expression for the tunneling current explaining the atomic resolution of an STM[62].

3.3 Tunneling through molecular adlayers

Using the derived formula for the tunneling current with some assumptions can clarify the tunneling through a molecular adlayer. Initially assuming a non-scanning tip at a certain point above the substrate and using Tersoff and Hamanns approximation[61] of the tunneling matrix elements by

$$|M|^2 \propto e^{-2\kappa d} \qquad \kappa = \sqrt{\frac{2m\phi}{\hbar}}$$

where d is the distance between tip and sample, m is the electron mass and ϕ the work function of tip and sample. When additionally approximating the density of states of tip and substrate by homogenously filled bands up to the Fermi-level, they both contribute only a factor to the current. If now a molecule is introduced into the tunneling gap that has a small interaction with the surface and the tip, its energy level will now open up a new tunneling channel for the tunneling current. For this channel the current becomes

$$I \propto e^{-2\kappa d}\sum_{\varepsilon_i}\frac{\gamma_S\gamma_T}{\gamma_S + \gamma_T}[f_S(E_{FS} - eU + \varepsilon_i) - f_T(E_{FS} + \varepsilon_i)]$$

with γ denoting the coupling constants between the tip and the molecular energy level and the substrate and the molecular energy level. For a molecule introduced into the tunneling gap the effective tunneling distance d is reduced, enhancing contribution of this channel and possibly dominating the current.

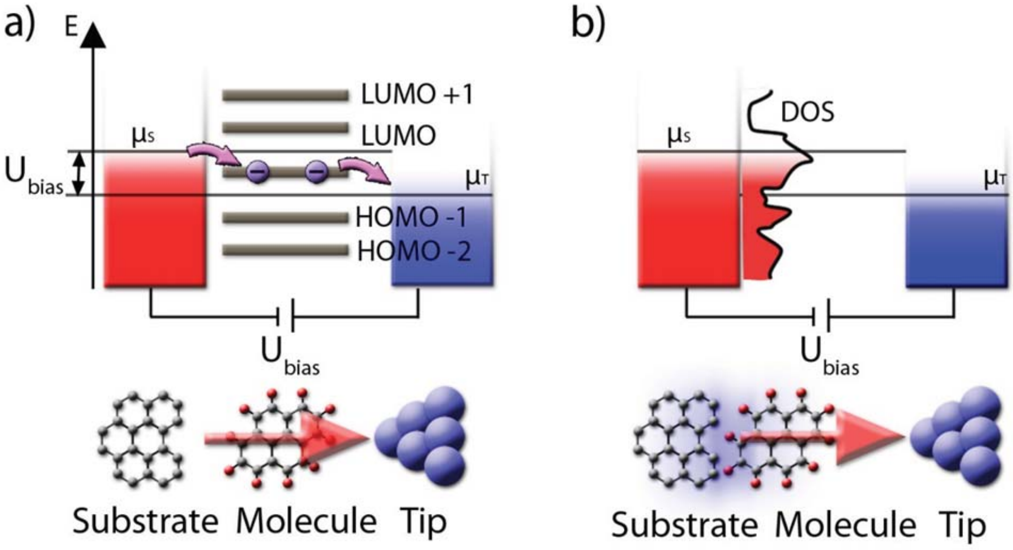

Figure 9. Tunneling through molecules: a) Tunneling from the substrate through one orbital (e.g. HOMO) of a, from the surface decoupled molecule into the tip with applied bias voltage. b) Strong molecule-substrate interactions lead to a smeared out density of states for the tunneling.

In the simplest case only one energy level of the molecule, either its highest occupied molecular orbital (HOMO) or its lowest unoccupied molecular orbital (LUMO), depending on the bias is used for the tunneling, see figure 9a. The orbital needs to lie between the energy of the tip and the substrate, when a bias is applied to be used for tunneling. If multiple molecular orbitals fall into this region all of them contribute to the current. In the case of a strong coupling between molecule and substrate, often the case for metal substrates, the energy levels form a more distributed combined density of states instead of distinct molecular orbitals, see figure 9b. Such a decoupling can be experimentally achieved by employing a thin insulating NaCl layer [63] compared to the use of the pure metal surface[64].

For a simulation of STM images the tunneling current through the electronic structure of the adsorbate-substrate can be calculated. The various techniques use Hückel approximations and first-principle self-consistent methods, mainly density functional theory (DFT)[65].

3.4 Substrates

STM measurements put several demands on a possible substrate for self-organization. The substrates need to show atomically flat terraces of the size of some hundred molecules for molecular self-organization. The substrate has to be inert for ambient experiments as well as conducting under these conditions. Due to the limited range of the piezo-actuators a reasonably flat substrate is advisable to avoid unnecessary crashing of the tip. These conditions are found in the properties of highly-oriented-pyrolytic-graphite (HOPG).

Graphite is one of the allotropes of carbon, a multilayer crystal with the layer sequence ABA. Within a layer the carbon atoms are connected into planar sp^2-hybridized hexagonal rings with a unit cell size of 0,246 nm. Successive layers are weakly linked by π-interactions between the delocalized electrons within a sheet and have a distance of 0,3 nm, see figure 10a. Consequently, an adsorbate of aromatic molecules can be stabilized by π-stacking interactions with the substrate.

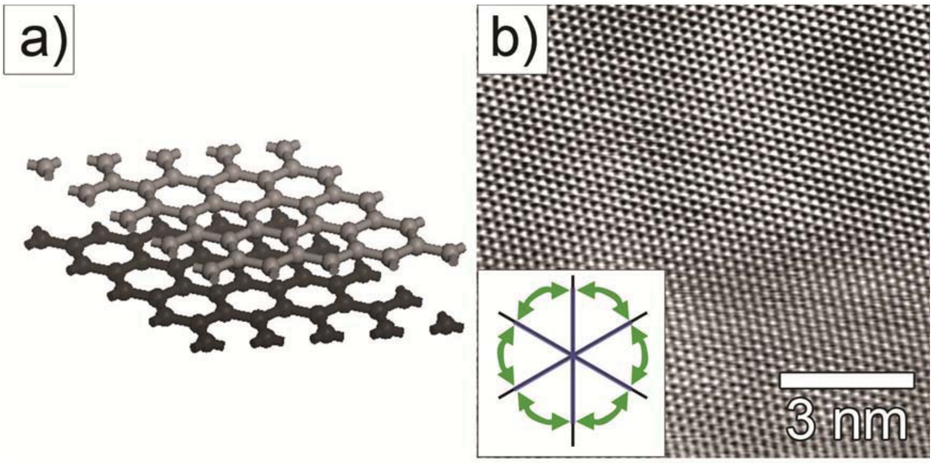

Figure 10: The graphite substrate: a) HOPG shows a hexagonal structure of sheets arranged in a layered structure. b) STM measurement of the HOPG surface with individual atoms (10 nm x 10 nm). The surface shows six-fold rotational symmetry as well as mirror symmetry.

Due to the consecutive stacking in an ABA pattern, every other carbon atom has a nearest neighbor in the layer below, while every other does not. This fact is reflected in a typical STM image of graphite, instead of showing every atom only every other atom is visible because of increased conductivity[66]. The surface exhibits a six-fold rotational symmetry and additional mirror symmetry, see also chapter 7.1. In STM measurements step edges of individual graphite layers are visible. This stacking behavior of the different layers can lead to different kinds of defects, the most common of which is the Moiré pattern[67]. This purely electronic hexagonal superstructure is caused by non-aligned layers of graphite.

The preparation of clean and atomically flat HOPG surfaces for consecutive experiments can easily be done by drawing off the top layers with adhesive tape and thus readying the substrate for molecular self-organization.

3.5 Solution Casting

To apply molecules onto the substrate a variety of approaches can be taken depending on the experimental conditions and limitations imposed by the molecules. Thermal evaporation and organic molecular beam epitaxy [68] sublimate molecules onto the surface. Langmuir-Blodgett deposition uses a film of molecules at a liquid-air interface or at a liquid-liquid interface which is transferred onto the substrate[69]. Electrospray deposition sprays molecules through a hole into the vacuum chamber with the help of an ionized transport gas[70]. The pulse injection method uses a fast opening valve for the injection of the molecule containing solvent directly into vacuum onto the sample[71].

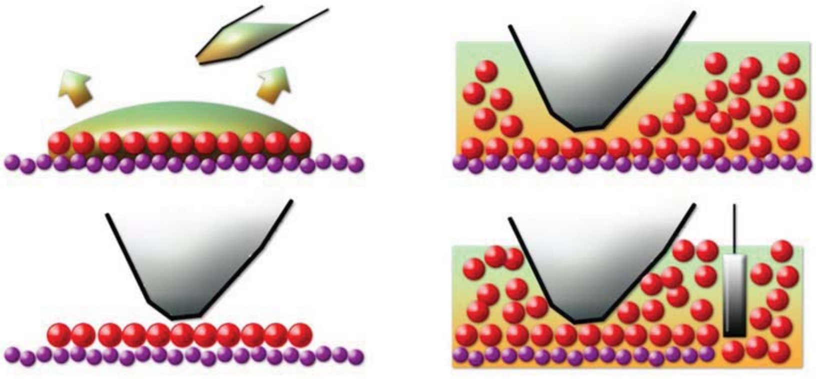

Figure 11. Application of molecules: left) Solution casting applies the solvent molecules onto the substrate and lets the solvent evaporate. Right) Measurements can also be taken with the tip immersed in a non-evaporating solvent or use a counter electrode for electrochemical measurements.

When the STM is operated in ambient conditions sample deposition via solution casting or at the liquid-solid interface is used most commonly. The liquid-solid interface is investigated by operating the tip submerged in the solvent[72]. Typically the solvent is non-conductive and has a low vapor pressure to keep the solvent from evaporating, see figure 11 right. When the STM operates in air, in general a thin water film is always present on the surface. STM at the liquid-solid interface avoids this film by replacing it with the controlled solvent environment.

In solution casting a droplet of the solution containing the molecules is placed on the substrate. While the solvent evaporates, the molecules remain on the surface, see figure 11 left. Typically, millimolar solutions with only small quantities of substance are used. The solvent should not adsorb onto the substrate and evaporate long enough to allow molecular organization. Solution casting on a heated substrate accelerating the evaporation is referred to as sizzling [73].

When a droplet with solved molecules is evaporating the more common case is that the size of the droplet stays constant, while its thickness diminishes[74]. This evaporation process can be measured in the changing parameter of the contact angle θ. To look at the material transport and deposition during the solution casting process a model droplet with the following specifications is used, see figure 12.

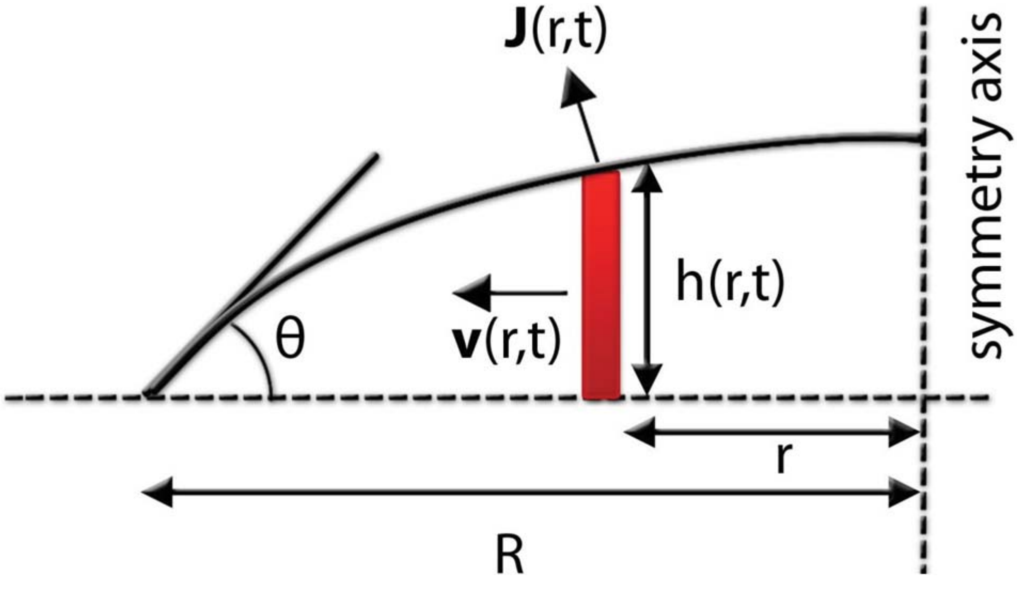

Figure 12. Scheme of a droplet: The evaporative flux ***J**(r,t)* reduces the height *h(r,t)* at every point *r*. At constant radius *R* this results in a radially outward pointing net velocity of the transported material ***v**(r,t)*. The contact angle θ is reduced during the evaporation.

For the droplet to keep its Radius R constant during the evaporative flux ***J(r,t)*** solvent needs to be transported to the perimeter with a velocity ***v(r,t)***. The flux ***J(r,t)*** is given by

$$\boldsymbol{J}(r,t) = -D\boldsymbol{\nabla}\varphi$$

with D being the diffusion constant and φ the concentration at the surface. At the boundary of the droplet the normal derivative diverges for the evaporative flux as r approaches the contact line. This divergence is of the form

$$|J(r,t)| \propto (R-r)^{-\frac{\pi-2\theta}{2\pi-2\theta}} \qquad \lim_{\theta\to 0}\frac{\pi-2\theta}{2\pi-2\theta} = 1/2$$

for the contact angle θ. To replace the diverging flux near the perimeter a diverging velocity *v(r)* transporting material is required.

$$v_{r\to R} \propto |J(r,t)| \propto (R-r)^{-\frac{\pi-2\theta}{2\pi-2\theta}}$$

Due to this transport velocity within the droplet all the mass *M(r,0)* within a wedge shaped part of the droplet will be transported to the perimeter within the time t.

$$t = \int_{r_t}^{R}\frac{1}{v}dr \propto (R-r_t)^{1+\frac{\pi-2\theta}{2\pi-2\theta}}$$

In leading order, the outward current *h(r,t)**v(r,t)*** must stay constant with time in order to replenish the constant evaporation flux ***J***. Thus ***v*** must diverge as the evaporation time ends. This diverging velocity leads to a diverging displacement of any point $r>0$. Thus all initial points $r>0$ are carried to the perimeter before the drying time t_f. This means that all the material within a droplet is transported to the perimeter, leaving a ring of dried materials and possibly a monolayer within the middle.

3.6 Image processing

To access the information contained within the measurements different forms of processing aid in the highlighting of individual features of the image and reduce nose or distortions.

In the flattening process a polynomial of zero to second order is subtracted from each line of the measurement. This technique compensates for the tilt of the substrate with respect to the scan section.

Drift is caused by thermal expansion or the warming up of the electronics during STM measurements[75]. This thermal expansion results in the relative motion of tip and substrate addition an additional component of motion to the regular raster movement of the tip, which is not accounted for in the images.

Because of the drift, features within the image may appear elongated or shortened, depending on direction of the drift motion in respect to the scanning movement. Common remedies are the cooling of the system, or in the case of room temperature experiments, an adequate waiting period until thermal equilibrium is reached within the system.

With respect to time critical processes involving for example phase transformations, which happen within minutes of the sample casting an alternative to waiting might be desirable. For these cases a simple algorithm for correcting the drift distortion was developed. It employs two images of opposite scan direction (up- and down-scan) with two recognizable features in each image that have constant distance. The original length of this distance is not needed; therefore two arbitrary features that appear in both images will suffice. The method assumes a constant drift velocity and direction, and a constant feature distance over the scanning time of the two images.

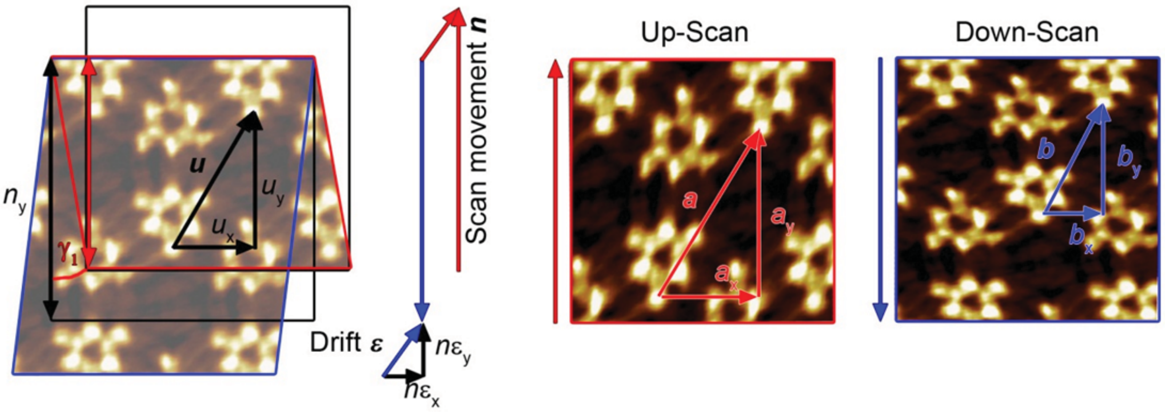

Figure 13: Drift correction: A drift motion ε present during scanning is added to the regular scan movement n, resulting in distorted images. The up and down scan are changed in height and skew to the left and right respectively. The vector between to features u present in both up a and down scan b can be used to extract the drift vector and correct both images accordingly.

In this problem the two scanning dimensions can be looked at separately. The drift in y-direction ε_y creates an elongation or compression of the image, while the drift in x-direction ε_x results in skewing the image. In y-direction the length of the normal scan movement n_y for example is shortened by the drift movement ε_y, see figure 13. This results in an elongation of all features in y-direction within the image. That means that the same original y-distance u_y of two features within the two images appears as

$$a_y = u_y\left(1 + \frac{\varepsilon_y}{n_y}\right) \qquad b_y = u_y\left(1 - \frac{\varepsilon_y}{n_y}\right)$$

To correct for the distortion in y-direction the parameter ε_y can be found by

$$\varepsilon_y = \frac{|a_y - b_y|}{a_y + b_y} n_y$$

to drift correct both images. For the correction of the x-portion of the drift ε_x the fraction of the drift for the two features ε_x is calculated via

$$\varepsilon_x = \frac{|a_x - b_x|}{a_x + b_x} n_x$$

To arrive at the two skew angles γ_1 and γ_2 for the x-correction

$$\gamma_1 = +\tan^{-1}\left(\frac{\varepsilon_x}{n_y - \varepsilon_y}\right) \ \gamma_2 = -\tan^{-1}\left(\frac{\varepsilon_x}{n_y + \varepsilon_y}\right)$$

Other forms of drift correction[76] utilize for example knowledge about the dimensions of certain structures on the surfaces from other sources.

Correlation averaging[77] is used to enhance the signal to noise ratio within an image. This algorithm requires identical structures, which are repeated within an image to calculate an average of this structure with reduced noise. A section of the image containing at least one of the repeated structures is cross correlated with the complete image. The local maxima of the correlation map are calculated and maxima above a certain threshold are selected. The image sections corresponding to the maxima are then selected. The images´ height is then summated pixel by pixel and the sum divided by the number of images. This technique helps to reduce random noise from the measurement, whereas periodically appearing structures are kept at constant height, enhancing self-organized periodic structures.

4 Molecular Systems

4.1 Supramolecular Chemistry

The term supramolecular chemistry was introduced in 1978 by J.-M. Lehn[78, 79]: "*Just as there is a field of molecular chemistry based on the covalent bond, there is a field of supramolecular chemistry, the chemistry of molecular assemblies and of the intermolecular bond.*" In another definition, J.-M. Lehn states in his Nobel Lecture [80]:"*Supramolecular chemistry may be defined as chemistry beyond the molecule, bearing on the organized entities of higher complexity that result from the association of two or more chemical species held together by intermolecular forces, not by covalent bonds.*"

These intermolecular forces can be hydrogen and van der Waals forces, seen in key-lock recognition or host-guest assembly, metal coordination bonds or even reversible covalent bonds, such as disulfide bridges.

Three different meanings of "supramolecular" are currently in use:

(a) intermolecular interactions;

(b) applied coordination chemistry;

(c) a strategy of controlled organization of multiple separate components.

I. Dance recommends the use of the adjective intermolecular weak interactions between molecules, employing the term coordination chemistry for metal coordination complexes. The term supramolecular he reserves for "*the philosophies and strategies of grand assembly*"[81], where molecular self-organization enters the field.

Weak chemical bonds, i.e. non-covalent bonds, are namely the hydrogen bond, the van-der-Waals and the π-π-interaction. As the strongest of the non-covalent bonds, the hydrogen bond is a direct consequence of the asymmetric electron density in the "classical" X–H…Y (X, Y = O, N) hydrogen bond, with energies of 20–40 kJ mol^{-1}[82]. Due to the high electronegativity of the acceptor, the hydrogen atom gains a positive partial charge. In turn, this hydrogen atom can interact with the electronegative oxygen atom of a second molecule, thus establishing a directed intermolecular interaction force. The concept of hydrogen bonds is extrapolated by many researchers to include weaker electrostatic interactions and termed "weak" or "unconventional" hydrogen bonds.

Van der Waals forces comprise two types of interactions, dispersion forces and Debye forces. Dispersion forces, also known as London forces, result from a temporary fluctuation of the electron density that creates a dipole moment, which in turn induces a complementary dipole moment an adjacent non-polar molecule (induced dipole – induced dipole interaction). Debye forces on the other hand act upon molecules possessing a permanent dipole moment. This induces a permanent dipole moment in the non-polar molecule (dipole – induced dipole interaction). The interaction energies for van-der-Waals forces vary between 0.5 and 5 kJ mol^{-1} and thus are smaller than the interaction energy of hydrogen bonds.

The π-π interaction operates between the orbitals of delocalized π electrons of two aromats. Hunter et al. give a description for π-π interactions: "*The key feature of the model is that it considers the σ -framework and the π - electrons separately and demonstrates that net favorable π–π interactions are actually the result of π–σ attractions that overcome π–π repulsions*" [83]. Therefore a π–σ attraction rather than a π–π electronic interaction leads to the favorable interaction. The electrostatic contribution strongly determines the geometry of π-stacking and van der Waals interactions are responsible for the magnitude of the observed effect. Both T-shaped and face-to-face, geometries can be explained in that way.

Weak intermolecular interactions are ideally suited for self-organization since it is possible to embed information in them that guide the self-organization process [78, 84, 85].

4.2 Fréchet-Dendrons

Dendrimers are highly branched polymers, which polymerize from AB$_x$-type polymers. The word is derived from the greek δενδρον, which means tree, and μερος, which means part. Dendrimers are highly branched, but structurally perfect molecules. They are prepared via iterative synthesis[86]. Dendrimers are synthesized in a stepwise manner by repeating synthetic steps. Each repeat adds an additional layer of branches, called generation to the molecules. This can be seen by following one of the branches. Each branching point raises the counter by one generation. Second-generation dendrimers are called dendron. Two major synthetic routes exist: the divergent route where synthesis proceeds outwards from the center and the convergent approach synthesizing from the outside-in. Fréchet-type dendrimers were the first dendrimers constructed by the convergent approach[87, 88]. This approach to dendrimers has been ideal to construct dendrimers, when lower generations are needed. A large number of studies have employed Fréchet-type dendrimers[89, 90].

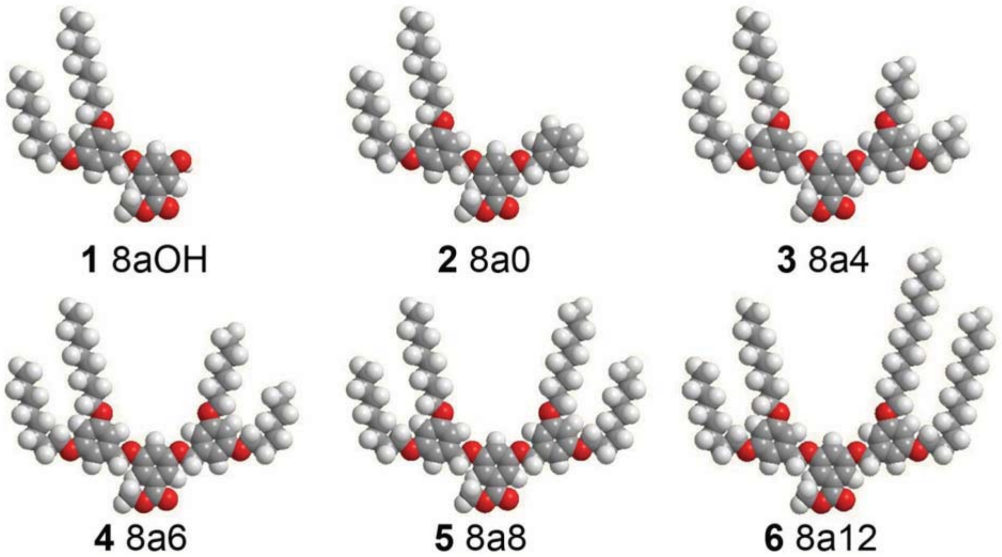
1 8aOH
2 8a0
3 8a4
4 8a6
5 8a8
6 8a12

Figure 14. Fréchet dendrons: 1-6 The six different employed Fréchet dendrons in order of increasing complexity. The numbers denominate the length of the alkoxy chain on each side.

The synthesis of the Fréchet-dendrons used for this thesis was conducted in the group of Professor E. Constable at the University of Basel, Switzerland, where also other dendrons have been employed for self-organization[91], [49], [92], [86, 93]. The asymmetric second-generation Fréchet dendron consist of three phenyl rings, two of which are functionalized by two pairs of alkoxy chains, a octyloxy pair of fixed length and a second pair, whose length varies within the employed molecules and increases their complexity[94], see figure 14. These arms are responsible for van der Waals and weak unconventional hydrogen bonds resulting in the high tendency of these molecules to self-assemble in layers (not just on the surface, but also in three dimensional crystals[95]). Alkyl-alkyl interactions are considered as important supramolecular synthon for self-assembled monolayers[96]. Additionally the Fréchet dendrons show liquid-crystalline properties.

Each phenyl-ring is adjacent to two ether units making them electron-rich. This results in a lower ionization potential of the phenyl rings, leading to stronger interaction between the adlayers electronic levels and the surface Fermi level. The enhanced tunneling probability pronounces the phenylrings in STM measurements. Therefore the molecular core acts as a STM-marker. The dendritic structure of the molecule provides conformational freedom to rotate about the internal C–C and C–O bonds, making this molecule highly flexible. This is in contrast to many other compounds used STM studies which are mainly rigid and flat (e. g. porphyrins and phthalocyanines[97-100]). The molecular flexibility is a strong contributing factor in facilitating the phase variety seen for these molecules, see chapter 9.6.

5 Complex Energy Landscapes

5.1 Energy Landscapes

The potential energy of a molecule is in most cases strongly dependent on its conformation. This is most vividly shown in the process of protein folding[101, 102], but can also be employed for less complex molecules[103]. Here the different degrees of conformational freedom span a hyper surface in conformational space with different energies associated with each of the relevant coordinates[104]. This energy landscape can fall into one of two broad categories. It either features one or multiple energetic minima. At the energetic minimum, a small displacement in any variable increases the potential energy. The energy surfaces of complex systems usually have many different of local minima; the lowest one is the global minimum, see figure 15.

In energy landscapes a displacement relates to a change in order parameter. Seemingly basic systems can feature a complex set of local minima with the lowest being the global minimum[105]. Where equilibrium behavior is concerned, only the relative energies of the minima count. For dynamic behavior of the system on the other hand the properties of the connections between the minima are of importance. The pathways between the minima fundamentally influence the relaxation of the system. These local minima are likely energetic traps for the system dynamics, representing points of frustration, where competing interactions balance out, leading to the creation of metastable states.

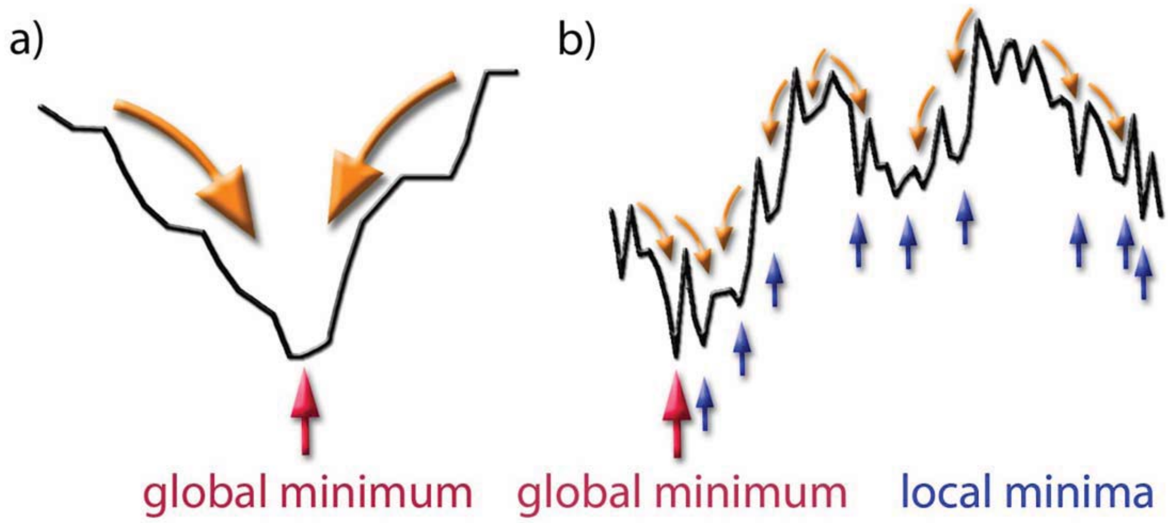

Figure 15. Energy landscapes: a) The global energetic minimum in a potential landscape with only one minimum is reached over time independent of the starting point within the landscape. b) Complex systems exhibit usually rugged energy landscapes with multiple local minima in addition to the global minimum, causing the system to freeze in the metastable state of a local minimum.

5.2 Metastable States

A self-organization state or a phase is a structure or region, which is uniform in its properties, such as symmetry, molecular composition or unit cell size. To talk about metastable states, a distinction between stability and equilibrium has to be made. A state is in equilibrium within the energy landscape, if its derivative along all coordinates is zero. That point can still be unstable, e.g. balancing a pencil on its tip. For a stable equilibrium it is required that the second derivate of the energy landscape is larger than zero.

Such a state is metastable if it is stable only with respect to small fluctuations. Larger fluctuations will cause the system to change its state. Finally the thermodynamically stable state will be reached, nevertheless how long this process of relaxation within the energy landscape takes is a problem of kinetics. An additional restriction follows from the appearance of a metastable state. The relaxation lifetime of the metastable state must be within the observation timescale. Such a relaxation towards the global minimum requires the overcoming a barrier within the energy landscape. The height of this barrier is the ultimate factor controlling the kinetic rate. The occurrence of metastable states is linked with small fluctuation amplitudes, limiting relaxations to small barrier heights within the energy landscape, rather than relaxing into the global equilibrium[106].

5.3 Phase Transformations

In phase transitions at least one of the order parameters has to change. This change in general is accompanied by either a change in the first derivative of thermodynamic free energy or the second derivative. This classification by Ehrenfest states that a first-order transition is continuous in thermodynamic free energy, while the first derivative of is discontinuous. At the transition point, the thermodynamic functions, except for the Gibbs energy, show discontinuous behavior in a P-T ensemble. First-order transition can be seen as discontinuous transitions, while second order transitions can be characterized as continuous transitions.

In general, the degree of order changes in a phase transformation from one phase to another. This approach of using an order parameter derives from mean field theory. With increasing temperature the observed phase usually possesses a lower level of ordering, while the order parameter at high temperatures is essentially zero and the state is unordered.

5.4 Emergence

Self-organized systems often show emergent properties. Emerging properties are for Goldstein [107] "*the arising of novel and coherent structures, patterns and properties during the process of self-organization in complex systems.*" Here the properties of the self-organized system could not be anticipated by the simple summation of the properties of the individual components. These properties are system-wide and usually present a phase transition with the change of one of the systems parameter, e. g. the number of building blocks. They arise from the nonlinear interactions of the system's components.

One simple and illustrative example is the emergence of translational repeat units due to competing interactions between spheres. In this example the two interactions are a provided by a the short range attraction between the spheres on the one hand and a corrugated surface of slightly larger corrugation size then the diameter of the spheres and on the other, see figure 16 a,b. Each individual interaction can be minimized. If on the other hand more and more spheres are added to the surface a minimization process starts first favoring the attraction between the spheres. If the two interactions are of similar magnitude at some point a behavior bifurcation occurs resulting in a large gap between adjacent spheres. The emergent pattern now globally shows a new larger translational symmetry not present in any of the components, see figure 16c.

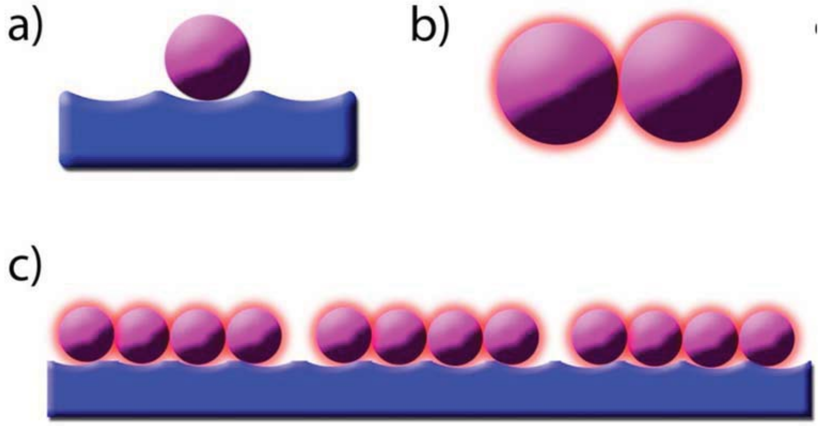

Figure 16. Competing Interactions and Emergence: a) The sphere tries to lie as low as possible within the corrugated surface. b) Two spheres have a short range attractive interaction. c) At a certain number of constituents a behavior transition occurs resulting in an emergent pattern of global ordering. This ordering is not found within the individual interactions, but results from the interaction between the two interactions and only becomes prominent a large enough number of building blocks.

With the increasing number of components in this example the energy landscape became more rugged for each subsequently added sphere until a phase transition occurred forcing the system into a state, where both interactions could be partially satisfied. Here the emergent behavior stems not from the interactions itself, but from the interactions of the two interactions, which only becomes significant in a system with a large enough number of constituents.

Another possibility causing emergence is the increasing complexity respective degrees of freedom of the constituents, not their number. Here also the energy landscape becomes more rugged, resulting in additional local minima and the appearance of additional phases, see chapter 9.1.

In the process of creating functional monolayers ever more complex building blocks are employed for self-organization. Therefore emergent behavior, desired or undesired is to be expected along the way. Is it possible to extrapolate from previous knowledge to predict the behavior of systems prone to emergent behavior or is this impossible by the very definition of emergence?

6 Computational Tools

With the advent of computer in the last 50 years simulations have become an invaluable tool for material scientists. Molecular simulations can be based on quantum mechanics (e.g. density functional theory), classical mechanics (e. g. molecular mechanics and dynamics) or generic interaction site models. Each approach has its costs and benefits in terms accuracy, computational costs and explanatory/predictive power.

Quantum mechanics is the basis for the theoretical description of chemistry. Ab initio (first principles) quantum mechanics calculations employ the most basic natural constants such as the velocity of light, masses and charges of nuclear particles. Differential equations are used to directly calculate molecular properties and geometries.

The Schrödinger equation $\mathcal{H}\Psi = E\Psi$ is the basis from which all chemical properties are derived. E is the energy of the system, Ψ the wave-function defining the coordinates of the atoms and H is the Hamiltonian operator comprising both the potential and kinetic energy.

One approximation, the Born-Oppenheimer approximation[108], differentiates the atoms into electrons and nuclei, which are much heavier and slower than electrons. Therefore the electrons are seen as moving in a potential around a fixed nucleus. This assumption leads to an effective electronic energy E which depends on relative nuclear coordinates of the nuclei R.

$$\text{electrons: } \mathcal{H}\Psi(\mathrm{r};\mathrm{R}) = E(R)\Psi(\mathrm{r};\mathrm{R})$$
$$\text{nuclei:} \mathcal{H}\Phi(\mathrm{R}) = E(R)\Phi(\mathrm{R})$$

For the description of the structure and change with time of the molecular model the movement of the nuclei in the potential $E(\mathrm{R})$ suffices. Calculating *E(R)* is still very costly so that empirical force fields can be employed to approximate *E(R)*. Neglecting quantum mechanical effects of the nuclei due to their relatively large mass derives at the Newtonian equation of motion:

$$-\boldsymbol{\nabla}_R V = m\frac{d^2\boldsymbol{R}}{dt^2}$$

Molecular dynamic simulations (MD) solve the time dependent equation, while molecular mechanics (MM) explores the static properties of the molecular model.

In the Linear Combination of Atomic Orbitals (LCAO) approximation the wave-function Ψ is the product of orbitals containing one electron. These basis functions and their orbital coefficients define the energy of the system. Hartree-Fock method to derive those coefficients referred to as the self-consistent-field (SCF) theory[109].

6.1 Force fields in Molecular Mechanics Simulations

The empirical potential energy force fields *E(R)* employed in MM simulations are parameterized into different contributions.

$$E_{pot} = E_{bond} + E_{angle} + E_{torsion} + E_{vdW} + E_{el} + E_{cross}$$

The different contributions to energy of the molecule(s) are the energy of the bonds that are stretched or compressed, molecular angles that are displaced from their resting position and dihedral angles that are twisted to name the valence terms. Additionally contributing are the van der Waals forces and electrostatic contributions. The last term reflects cross term energies that appear within between the valence terms.

Using Taylor expansion till the second order for the valence terms and a Lenard-Jones and Coulomb potential for the van der Waals and electrostatic contribution respectively the individual contributions appear as

$$E = \sum_{bond} k_b(b_0 - b)^2 + \sum_{angle} k_\vartheta(\vartheta_0 - \vartheta)^2 + \sum_{torsion} k_\varphi(1 + \cos(n\varphi))^2$$
$$+ \sum_{vdW} \frac{A}{r_{ij}^{12}} + \frac{B}{r_{ij}^{6}} + \sum_{el} \frac{Q_i Q_j}{r_{ij}}$$

The “Universal Force Field”[110-112] employed in this thesis is describes geometries and conformational energies in organic molecules, inorganic main group elements, as well as metal complexes. It was used within the context of the Forcite Plus module of Materials Studio 4.4. MM methods are generally not to be employed with free electron gas systems like metals, which cannot be accurately described.

The energy of the molecular system can be minimized by changing the coordinates of the different atoms within the system. Different minimization algorithms can be employed for that[113]. The simplest approach is the steepest gradient approach, which works well for a structure far from its equilibrium. The conjugated gradient approach is more useful for a system close to the optimal geometry[114], while there are other methods combining different approaches, like SMART.

Molecular mechanics energy minimizations are limited in the respect, that within the energy landscape only the nearest local minima is reached, which is in general not the global minimum. Therefore the end conformation of minimization depends critically on the starting conformation requiring an already quote developed understanding of the molecular conformation within a pattern. Molecular dynamics simulations with integrated annealing steps allow for the probing of different minima but do not necessarily home in on the global minimum.

6.2 Density Functional Theory Simulations

The simulation of images obtainable by scanning probe microscopy needs to describe the tunneling current measured by STM. Using the Tersoff-Haman approximation[61] that the tunneling conductivity at a given point is proportional to the electronic local density of states (LDOS) at the Fermi level at the center of an s-wave tip, a method is needed to calculate the LDOS and the corresponding energy. Since classical methods e. g. MM only rely on nuclei positions and describe the electronic part by an empirical force field they cannot be employed. For small systems solving the Schrodinger equation is a plausible way of proceeding usually employing Born-Oppenheimer[108] and Hartree-Fock[109] approximations and subsequently solving for the *non-local* exchange potential with high scaling numbers for the calculations with increasing number of electrons[115].

An approach avoiding to solve the Schrodinger equation is the density functional theory (DFT). DFT describes many electron systems in its quantum mechanical ground state. Here the Born-Oppenheimer approximation is also employed, but in contrast to MM the focus lies on the electronic part of the Hamiltonian H_e, while the nuclei provide an external potential V_{ext} for the repulsing electrons V_{ee}.

$$H_e = T_e + V_{ee} + V_{ext} = -\frac{1}{2}\sum_{i=1}^{N_e} \nabla_i^2 + \sum_{i>j} \frac{1}{|\boldsymbol{r}_i - \boldsymbol{r}_j|} - \sum_{i=1}^{N_e} V_{ext}(\boldsymbol{r}_i, \boldsymbol{R})$$

Kohn and Hohenberg´s[116] theorem states that two systems with the same number of electrons N_e have the same sum $T_e + V_{ee}$ and are only distinguished by the external potential V_{ext}. It further says that the external potential V_{ext} is determined by the electronic ground state density n_0. If the electronic ground state density n_0 is given then the ground state wave function can be determined $\Psi_0 = \Psi[n_0]$. From that it follows, that all expectation values are also a functional of n_0, in particular the ground state energy E_0:

$$E_0 = E[n_0] = \langle \Psi[n_0] | T_e + V_{ee} + V_{ext} | \Psi[n_0] \rangle$$

The second theorem of Hohenberg and Kohn states that it is sufficient to minimize the expectation value for the energy

$$\begin{aligned} E[n] &= \langle \Psi | T_e + V_{ee} | \Psi \rangle + \int n(\boldsymbol{r})\, V_{ext}(\boldsymbol{r}, \boldsymbol{R}) d\boldsymbol{r} \\ &= T_e[n] + V_{ee}[n] + \int n(\boldsymbol{r})\, V_{ext}(\boldsymbol{r}, \boldsymbol{R}) d\boldsymbol{r} \\ &= F[n] + \int n(\boldsymbol{r})\, V_{ext}(\boldsymbol{r}, \boldsymbol{R}) d\boldsymbol{r} \end{aligned}$$

to derive at the electron density at the ground state. $F[n]$ is the same functional for all systems containing N_e electrons and is known as the Hohenberg-Kohn functional. The two theorems combined result in basic formula of density functional theory:

$$\delta \left[E[n] - \mu \left(\int n(\boldsymbol{r}) d\boldsymbol{r} - N_e \right) \right] = 0$$

If the kinetic T_e and electron-electron functional V_{ee} could be found, direct minimization of the energy would be possible. Kohn and Sham[117] approximated the two functionals by using a system of N_e non-interacting electrons representing the new orbitals ϕ_i for the modified system.

$$E_{KS}[n] = \langle \Psi_{KS}[n] | T_{KS} + V_{KS} | \Psi_{KS}[n] \rangle$$

With the solutions ϕ_i for the Schrodinger equation

$$\left[-\frac{\hbar^2}{2m} \nabla^2 + V_{KS}(\boldsymbol{r}) \right] \phi_i = \varepsilon_i \phi_i(\boldsymbol{r})$$

With a practical choice of the modified potential V_{KS} as

$$V_{KS} = V_{ee} + V_{ext} + (T_e - T_{KS})$$

the orbitals ϕ_i are equally solutions for the original problem. A large proportion of the electron-electron interaction will be a classical Coulomb interaction – or Hartree energy, while the rest of the error made due to non-interacting kinetic energy and using classical electron-electron interaction are combined in the *exchange correlation functional* V_{XC}:

$$V_{KS} = V_{ext} + \int \frac{n(\boldsymbol{r}')}{|\boldsymbol{r} - \boldsymbol{r}'|} d\boldsymbol{r}' + V_{XC}$$

To approximate the unknown exchange correlation functional V_{XC} different approaches are feasible. In the simplest approach, the local density approximation (LDA) the functional is only dependent on the local electron density at the place of its calculation:

$$V_{XC}[n] = \int \varepsilon_{XC}(n) n(\boldsymbol{r}) d^3\boldsymbol{r}$$

If additionally to the electron density $n(\mathbf{r})$, the gradient of the density $\nabla n(\mathbf{r})$ for both spins is included the approach is termed generalized gradient approach (GGA):

$$V_{XC}[n_\uparrow, n_\downarrow] = \int \varepsilon_{XC}(n_\uparrow, n_\downarrow, \nabla n_\uparrow, \nabla n_\downarrow) n(\boldsymbol{r}) d^3\boldsymbol{r}$$

The GGA provides a more accurate description of the local electronic density of states than the LDA, but even more accurate descriptions are possible.

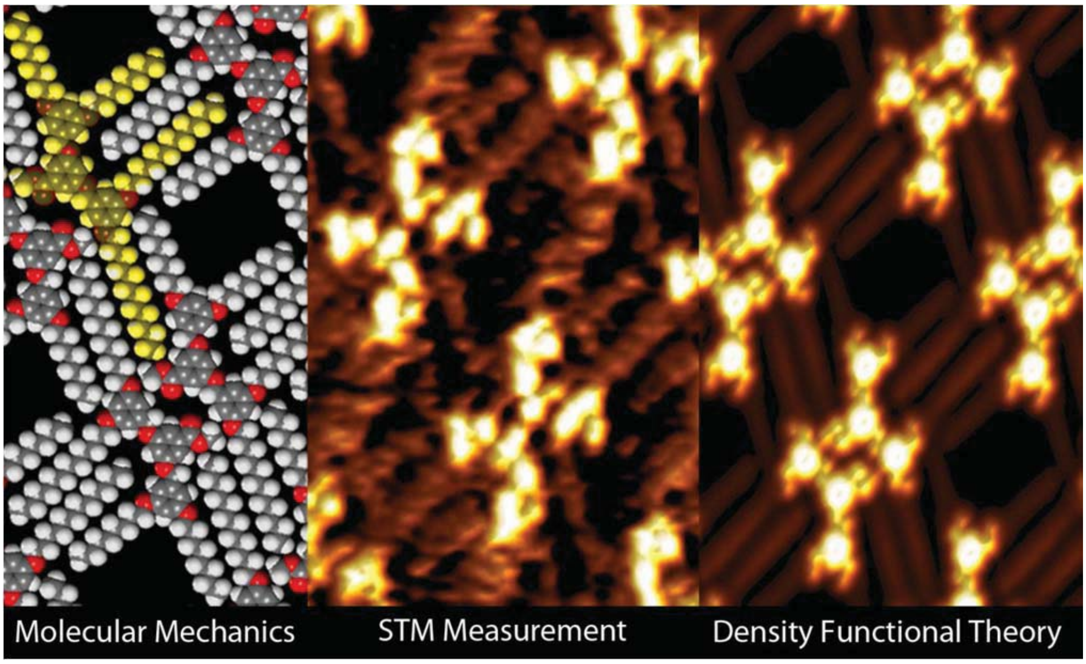

Figure 17. Simulation and measurements: For the simulation of the STM image (middle) a stating conformation for molecular mechanics model was derived and energy minimized using a Universal force field (left) [110-112]. The atomic positions were subsequently employed as input into the GGA DFT calculations (PW´91) [118] to derive at the contours of the integrated local density of states (ILDOS) (right) to compare to the measurement.

The integrated local density of states (ILDOS), which correlates with the expected STM image, was derived at in this thesis by employing the CASTEP module of Materials Studio 4.4. The GGA exchange correlation functional (PW´91) was used.

Since only a delta function tip would reproduce the exact ILDOS of the surface by not an extended tip, this effect was simulated. To account for the extension of a real tip the density contours of the ILDOS of the free molecules were convoluted by a Gaussian function with a blurring size of a 0.13 nm × 0.13 nm Gauss function, mimicking the roughly 0.26 nm diameter of the tunneling d_z orbital.

6.3 Interaction-Site Model in Monte-Carlo Simulations

The methods discussed so far could in principle be used to map the energy landscape of molecular self-organization for small enough systems via simulated annealing. In that technique, barriers dividing local energetic minima can be overcome, leading to a more global mapping of the landscape. In practice simulating the whole quantum mechanical system or even doing classical force-field simulations for tens to hundreds of atoms per molecule computational to expensive.

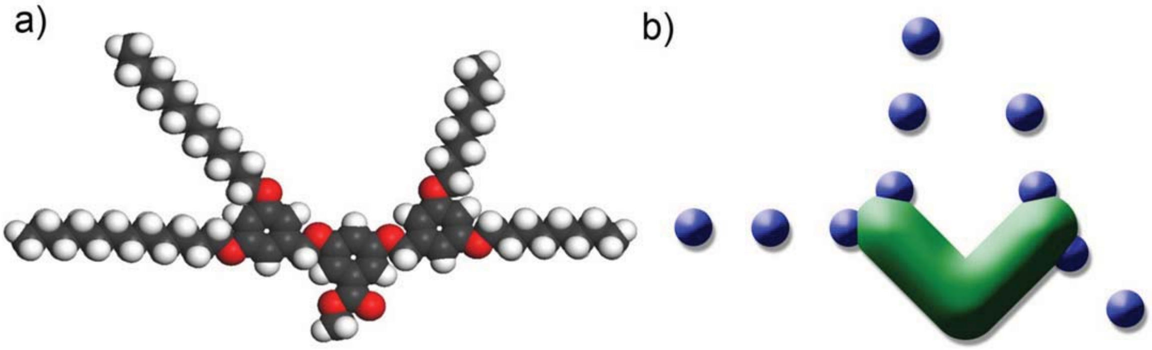

Figure 18. Interaction site model: Left) Molecular mechanics model of the Fréchet Dendron 8a12 with 150 atoms and many internal degrees of freedom. Right) The Interaction site model of the same molecule with ten effective interaction site and not internal degrees of freedom drastically reduces the computational costs for simulating many of those models.

In an interaction site model the number of interaction centers and degrees of freedom of the molecule can be reduced to a few effective interactions, as well as reducing the degrees of freedom possible for that model. As example for an interaction site model the Fréchet Dendron 8a12 in figure 18 can be seen. The already approximated molecular mechanics model incorporating 150 interacting atoms and many internal degrees of conformational freedom, see figure 18 left, compares to the rigid interactions-site model with 10 interaction site and only one rotational degree of freedom for the whole molecule, see figure 18 right.

For the simulated annealing systems with N interaction site molecules ranging from some hundreds to a few thousands molecules are prepared[119]. To calculate expectation values of any observable A in such a complex system a Monte-Carlo approach to the partition function of the system is useful[120]. The self-organized system is a canonical. For the partition function

$$Z = \int d\boldsymbol{r}^N e^{-\frac{E(\boldsymbol{r}^N)}{k_B T}}$$

of the canonical ensemble, the probability density $N(\boldsymbol{r}^N)$ for the system in a particular configuration $\boldsymbol{r}^N$ becomes

$$N(\boldsymbol{r}^N) = \frac{e^{-\frac{E(\boldsymbol{r}^N)}{k_B T}}}{Z}$$

With the number of points n_i per unit volume in the configuration space around $\boldsymbol{r}^N$ and the total number of points L in configuration space it is possible to compute averages of observables

$$\langle A \rangle \approx \frac{1}{L} \sum_i n_i A(\boldsymbol{r}_i^N)$$

For the generation of points in configuration space with probabilities proportional to the Boltzmann factor first random configurations are generated. The new configuration which lies near the old one is then produced with a corresponding Boltzmann factor. The possible acceptance of this new configuration is governed by the Metropolis algorithm[121, 122] which accepts the new configuration under

$$acc(old \to new) = \begin{cases} \dfrac{N(new)}{N(old)} \; if \; N(new) < N(old) \\ \quad 1 \; if \; N(new) \geq N(old) \end{cases}$$

In one MC step on average every molecule is updated once. Trial configurations attempt to rotate a randomly selected molecule, which is the only degree of freedom in this model. The new configuration is accepted following the Metropolis scheme. The temperature is gradually lowered until the system reaches a stable configuration. This way it is possible to *predict* ordering motifs of a self-organizing molecule *a priori* from random starting configurations, sampling the different points of the energy landscape, with an interaction site model.

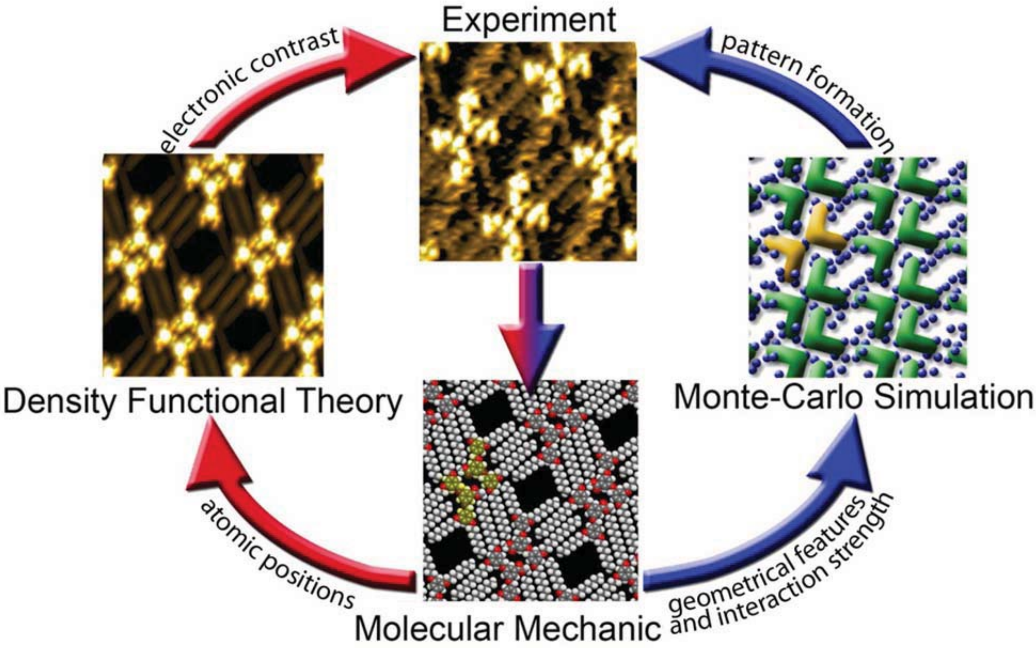
Experiment
electronic contrast
pattern formation
Density Functional Theory
Monte-Carlo Simulation
atomic positions
geometrical features and interaction strength
Molecular Mechanic

Figure 19. Simulation methods: The methods in the red circle provide a testable approach to arrive at an atomistic model of the pattern, while the blue circle predicts pattern by mapping the energy landscape of a self-organized system.

The three different simulation methods work together in this thesis in understanding and predicting the observed patterns in molecular self-organization. From the experiment the starting configuration for the energy minimization of the molecular mechanics model is derived. The MM model provides the atomic positions for the DFT simulation resulting in a simulated STM image, which can be compared to the real measurement, see figure 19 left circle. This way the MM model can be tested. The MM model contributes the conformational geometry and the interaction strength for the interaction site model on the Monte-Carlo simulation. The MC model derives possible patterns by sampling the energy landscape and predicts self-organization results, see figure 19 right circle.

7 Concepts of Self-Organized Molecules

7.1 2D Symmetry Groups

To characterize the patterns formed in two dimensional molecular self-organization symmetry operations are used to describe the pattern. Symmetry operations in n-dimensional space are operations $f\colon \mathbb{R}^n \to \mathbb{R}^n$ that if applied to an object $M \subset \mathbb{R}^n$, preserve a specific property of this object.

$$f(M) = M, f|_M = id_M$$

An object is symmetric if more than the identity operation is applicable to it. Possible symmetry operations in two dimensions are rotations and mirror operations, which are called point groups since they map at least one point onto itself. Additional to that there are translational symmetries and glide mirror symmetries.

The unit cell of a pattern contains all the two dimensional symmetry operations of the pattern. In three-dimensions there exist 230 symmetry groups, while two-dimensional systems can be grouped into 17 plane symmetry groups. Five basic types of translational symmetries exist: parallelogrammatic (oblique), rectangular, rhombic, square and hexagonal. If mirror, rotational and glide mirror symmetries are incorporated, the categories results in the aforementioned 17 plane symmetry groups. Figure 20 shows each group with its respective symmetries. In experimental observations these symmetry groups are represented in different proportions. In general higher symmetric patterns exhibiting mirror symmetries are rarest[7]. The plane group describes the symmetries of the unit cell of a pattern. These symmetries are reflected in the properties of the patterns belonging to the same plane group. Knowing the symmetry of the employed molecules and the symmetry of the used substrate certain inferences can be drawn.

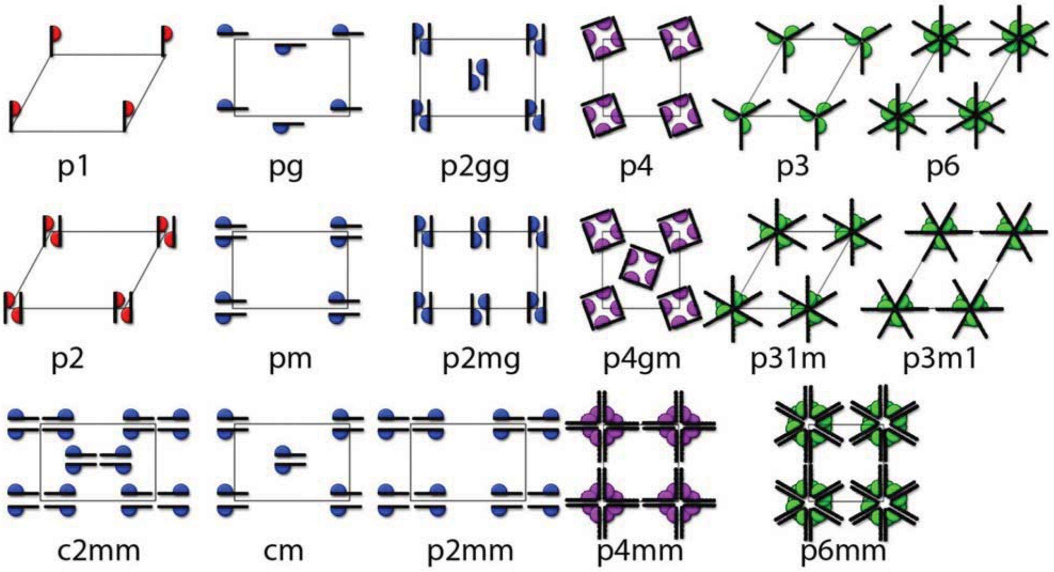

Figure 20. 2D Symmetry groups: 17 different plane symmetry groups can be found in two dimensions. They are by definition translational symmetric and they can feature rotational, mirror or glide mirror symmetries.

Number of molecular orientations: The number of energetically most favorable equivalent molecular orientations depend on the symmetries of the molecules and the symmetries of the substrate. Rotational molecular symmetries can reduce the number of observed orientations N_{Orient}, which is given by the cardinal number (number of elements) of the substrate rotational symmetry group ($C_{\mathrm{i\text{-}Surf}}$) divided by the cardinal number of the largest subgroup ($C'_{\mathrm{k\text{-}Mol}}$) of the molecular rotational symmetry group ($C_{\mathrm{j\text{-}Mol}}$), which is also a subgroup of $C_{\mathrm{i\text{-}Surf}}$[123].

$$N_{Orient} = \frac{|C_{i-Surf}|}{|C'_{k-Mol}|}$$

with

$$C'_{k-Mol} \subseteq C_{i-Surf} \wedge C'_{k-Mol} \subseteq C_{j-Mol} \wedge \forall C'_{l-Mol} \subseteq C_{i-Surf}\colon |C'_{l-Mol}| \leq |C'_{l-Mol}|$$

As an example in figure 21a) a molecule (4-[trans-2-(pyrid-4-yl-vinyl)]benzoic acid) [124]without rotational symmetry or mirror symmetry is shown on a surface with fourfold rotational symmetry and mirror symmetry. Assuming a single energetically most favorable position on the surface, the molecule can adsorb in four different orientations with discrete relative angles of 90°. If the molecule is either a) not mirror symmetric (in 2D) or b) mirror symmetric but the direction of its mirror axis does not fit any mirror axes of the substrate, then the number of energetically most favorable positions doubles. The position of the molecule can be described by mirroring the existing position along one of the substrate mirror axes.

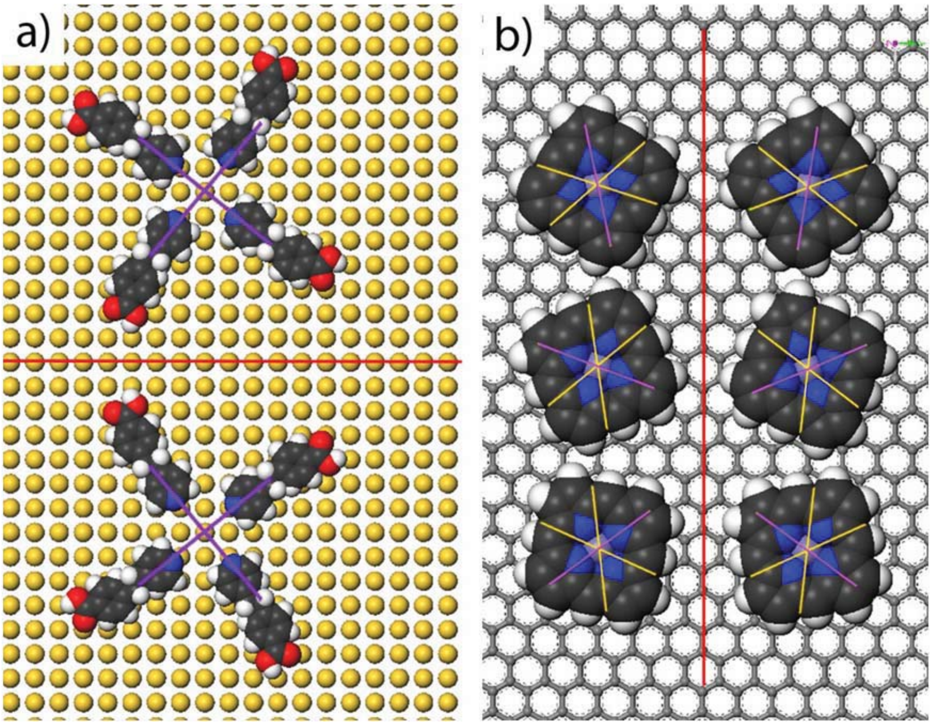

Figure 21. Domain orientations on a surface: Number of energetically equal orientations on the surface. a) Adsorption of a molecule without rotational or mirror symmetry on a fourfold rotational and mirror symmetric surface resulting in eight distinguishable molecular orientations on the surface, four of which are mirror symmetric to one another. b) Adsorption of a fourfold rotational and mirror symmetric iron-porphyrin on a six-fold rotational and mirror symmetric substrate resulting in six distinguishable orientations, three of which are mirror-symmetric to each other.

In mathematical terms the cardinal number of the rotational symmetry group of the molecule ($C_{1\text{-Mol}} = \{\Gamma_{0°=360°}\}$) on a fourfold rotational substrate ($C_{4\text{-Surf}} = \{\Gamma_{0°=360°}, \Gamma_{90°}, \Gamma_{180°}, \Gamma_{270°}\}$) is $N_{Orient} = \frac{|C_{4-Surf}|}{|C'_{1-Mol}|} = \frac{4}{1} = 4$. This number doubles because of the substrate mirror symmetry as described above. This means in this particular case no three- or six-fold rotational assemblies are possible, but four- and twofold assemblies can be expected with the possibility of glide mirror and mirror symmetries.

In figure 21 b) a fourfold rotational symmetric iron porphyrin with mirror symmetry is shown on a six-fold rotational and mirror symmetric HOPG substrate. For the observed orientations of a molecular square ($C_{4\text{-Mol}}$ = {$\Gamma_{0°=360°}$, $\Gamma_{90°}$, $\Gamma_{180°}$, $\Gamma_{270°}$}) on the surface of HOPG ($C_{6\text{-Surf}}$ = {$\Gamma_{0°=360°}$, $\Gamma_{60°}$, $\Gamma_{120°}$, $\Gamma_{180°}$, $\Gamma_{240°}$, $\Gamma_{300°}$}) the cardinal number of the subgroup $C'_{2\text{-Mol}}$ = {$\Gamma_{0°=360°}$, $\Gamma_{180°}$} is relevant. This results in $N_{Orient} = \frac{|C_{6-Surf}|}{|C'_{2-Mol}|} = \frac{6}{2} = 3$, which is the cardinal number of C_3 = {$\Gamma_{0°=360°}$, $\Gamma_{120°}$, $\Gamma_{240°}$} equal to the observed orientations. If a substrate, e.g. HOPG with rotationally allowed orientations $|C_3|$, exhibits mirror symmetries at 3 mirror axes, this results to $|D_6|$ (twice as many) energetically most favored molecular orientations, unless the mirror axis of the adsorbed molecules falls onto one of the mirror axes of the substrate. The latter is only rarely the case and molecules most often show local organizational chirality[125], see also chapter 7.2 The most complex pattern a porphyrin of this type could form on graphite is a threefold rotational pattern with possible mirror symmetries. No fourfold or six-fold pattern would be possible due to the symmetry of the molecule. Hence, the orientations of the molecules on the substrate are strongly influenced by the interplay of substrate and molecule symmetries, see chapter 9.5.

Number of pattern orientations: In general the number of possible molecular orientations can be divided by the cardinal number of the rotational group of the self-organized pattern to give the number of possible distinguishable domain orientations on the surface. If the pattern is chiral and the surface mirror symmetric, this number has to be multiplied by a factor of two, see also chapter 9.7.

Example: A chiral twofold rotational symmetric pattern shows on a six-fold rotational and mirror symmetric HOPG surface $N_{Orient} = \frac{|C_{6-Surf}|}{|C'_{2-Pattern}|} = \frac{6}{2} = 3$ domain orientations on the surface. This number doubles to six, due to the fact that the surface is mirror symmetric and the pattern chiral (allowing both chiralities on the surface), see chapter 7.2.

Symmetry modification of the surface: With the strong influence of the surfaces´ symmetry operations on the possible patterns, their symmetry, orientations and chirality the question arises how the surface symmetry can be changed.

Using a molecular self-organized monolayer as new surface the original surfaces´ symmetry can be changed. Figure 22 a) shows a six-fold symmetric HOPG surface with mirror symmetry. In figure 22 b) the same HOPG surface is now covered with an *n*-alkane adlayer, which effectively reduces the surface to a two-fold substrate and breaks the mirror symmetry (for results see chapter 9.5 and 9.7).

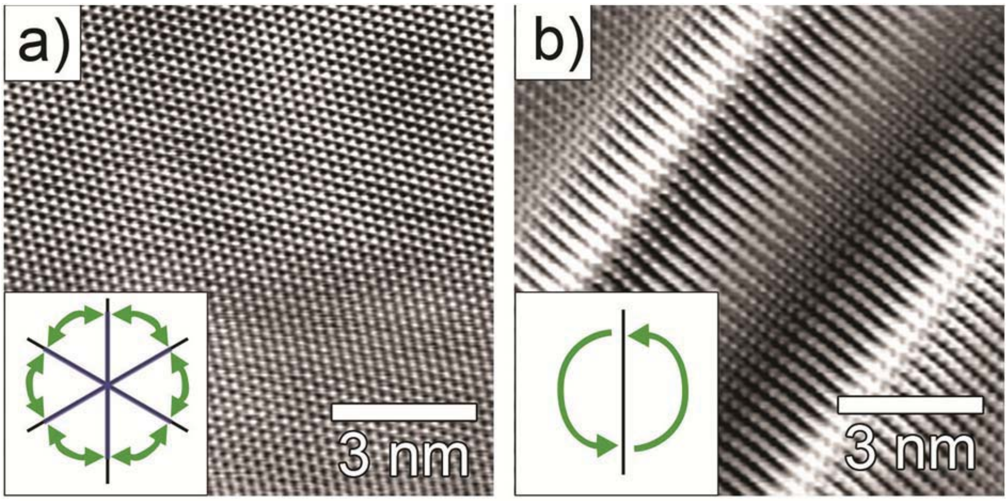

Figure 22. **Surface symmetry modification:** a) A scanning tunneling microscopy image of an HOPG surface exhibits six-fold rotational symmetry as well as mirror symmetry. b) An adlayer of pentacontane reduces the surface symmetry to a two-fold rotational symmetry and breaks the mirror symmetry. 10 nm x 10 nm, U_{Bias}= -50 mV - - 800 mV, $|I_T|$= 8 pA - -30pA.

7.2 Chirality

The term chirality derives from the Greek word for hand χειρ, and stands for the handedness of objects. Chirality means that the mirror operation applied to an object creates an object that is not superimposable by any number of rotations and translations with the original object. That explicitly means that the chiral object does not have any inverse symmetry elements. Therefore a chiral object always possesses a second mirror form. A detailed introduction on chirality can be found in the publication of S. M. Barlow[125].

Different forms of chirality can be found. Molecules can be truly chiral, i.e. non superimposable with its mirror image, in three dimensions. A second class of molecules is achiral in three dimensions, i.e. they have an inverse symmetry element. If these molecules are adsorbed onto a surface, rotation around one axis is blocked, which results in two possible adsorbed mirror forms, see figure 23a. These molecules that become chiral on surfaces are called prochiral. A third form is organizational chirality, in which molecules that are even achiral on the surface organize into patterns that are themselves chiral, see figure 23b.

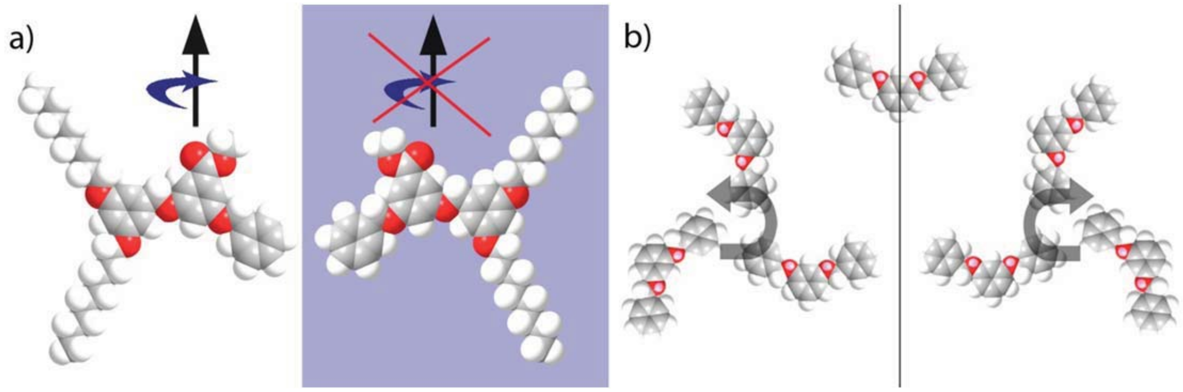

Figure 23. Forms of chirality: a) An achiral molecule in three dimensions becomes prochiral, when by adsorption onto a surface one off its rotational axis is blocked. b) Achiral molecules on surfaces can still organize into chiral motifs, which is called organizational chirality.

Separating the two mirror-images of a molecule after the chemical synthesis is of special importance for the pharmaceutical industry. Therefore inducing one kind of chirality in molecular self-organization is studied with great interest[32] [33] [31]. A variety of successful approaches for inducing or spatially separating chiral domains in self-organized monolayers have been reported They rely on chiral solvents[126], which induce organizational chirality with a chiral preference, the 'sergeants-and soldiers' principle[127], where a slight surplus of one chirality is added inducing large scale ordering of one chirality or the use of magnetic fields[128] to break the mirror symmetry on the surface. Regarding substrate effects to induce one chirality "…so far there are only a few systematic studies in which the substrate has a profound effect on monolayer chirality" [31]. This is reported in this thesis, see chapter 9.7

7.3 Hierarchical organization

Hierarchical ordering phenomena can arise as an emergent property during some self-assembly processes[34]. The term hierarchy has to be distinguished into to broad categories. One common usage of the term hierarchy denotes different objects, some of which have the property of a different hierarchy, e. g. worker and superior in a cooperation. This term is to distinguish from compositional containment hierarchy, where all elements are equal, but can form higher level elements by combination, e. g. individuals and a team[129]. This can also take the form of a nested hierarchy where atoms form molecules,

molecules form cells, cells form organs, and organs form individuals. The second understanding of hierarchy is relevant for molecular self-organization and is from now on only referred to as hierarchy.

The relationships between two levels of the hierarchy are: the higher level contains the lower level elements, while the lower level causes the higher level organization. The lower level properties dictate the higher level properties, while the higher level can produce additional emergent properties. Additionally elements at each level are found to be autonomous[130].

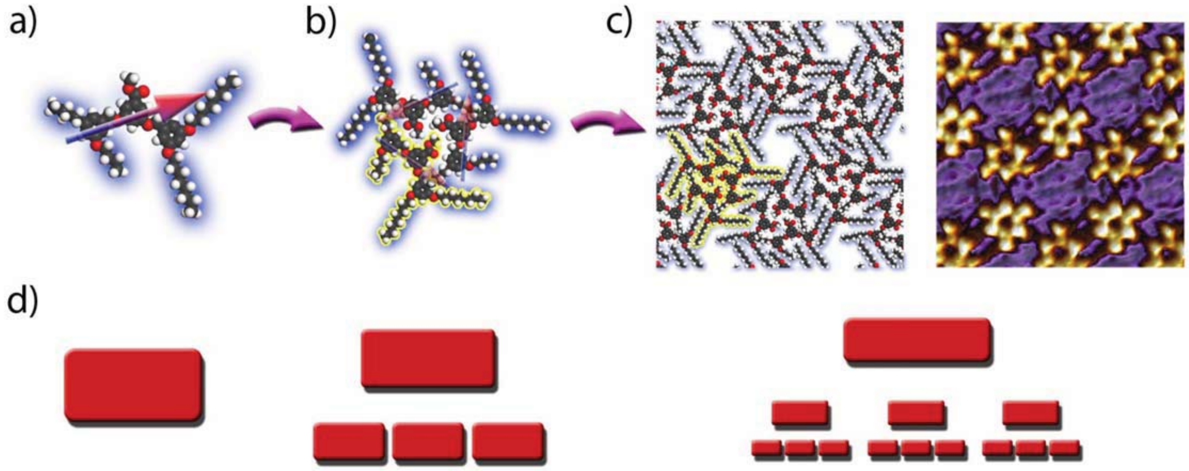

Figure 24. Hierarchical molecular organization: a) A molecule has two asymmetric types of interaction, a dipole moment and van der Waals interactions at the chains. b) Wile saturating the dipole forces a trimer forms. c) For the saturation of the van der Waals forces than a monolayer is formed, consisting hierarchically of trimmers.

In molecular self-organization hierarchical assembly is a rare, but not uncommon phenomenon[11, 131-135]. The causes for molecular hierarchical self-organization are found in the properties of the molecular building blocks. At least two interactions of different strength are needed, with at least one arranged asymmetrically at the molecule. Each subsequent level of assembly is held together by increasingly weaker interactions[34], see figure 24. Therefore hierarchical assemblies should be in principle step wise decomposable into lower levels of organization by breaking the bonds of the highest organizational levels which are weakest. This has so far only been achieved by de Feyter using surface potential increase to disrupt hydrogen bonding[136]. For another approach using surface modification see chapter 9.7

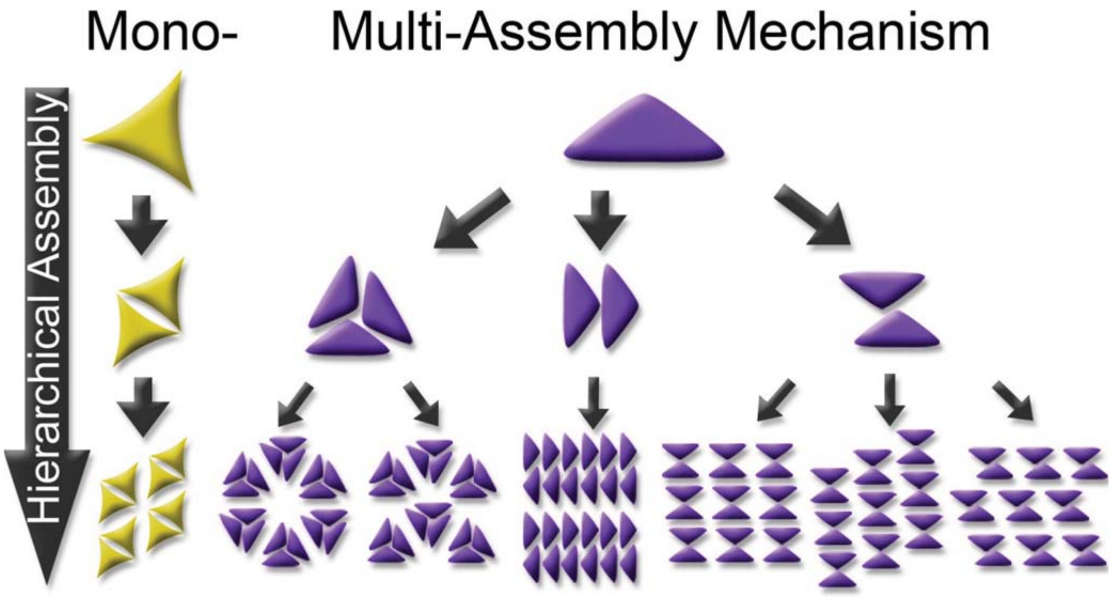

Figure 25. Multi-hierarchical Assembly: The two forms of hierarchical assembly. In mono hierarchical assembly the building block at each hierarchical level can only combine in *one* form to generate the next level. In multi hierarchical assembly the building block can combine in *multiple* forms to generate the next level, creating pattern variety.

Molecular self-organization on surface is of mono hierarchical assembly. That means that the building block at each hierarchical level can only combine in *one* form to generate the next level of assembly. Recently, the hierarchical construction of *multiple* structures from a common building block was demonstrated using self-organization of DNA origami[137]. In multi hierarchical assembly one building block can combine into *different* forms of higher level structures, see figure 25. This organization mechanism leads to a large phase variety of hierarchical self-organized monolayers, see chapter 9.6.

8 Summaries of Publications

Now following are the results of the thesis displayed. First all papers are briefly summarized to give an overview to the findings. The order reflects the three main portions of the thesis with some overlap between the parts.

Publication 1 answers to the question of the origin of the Fréchet Dendrons phase variety. It is attributed to the increasingly rugged energy landscape of the increasingly complex molecules.

Publication 2 - 5 develop an interaction-site model of the Fréchet dendron based on multi scale modeling. This model reproduces the pattern variety from random starting configurations. The local and global ordering of the phases is reproduced. Additionally the model is used to predict patterns on a modified substrate, which were afterwards experimentally confirmed.

Publication 6 - 7 concern general rules for self-organization. From basic properties of the molecular building blocks, like conformational flexibility, asymmetry and multiple interactions inferences about the resulting features of the organized patterns could be drawn. With the modification of the substrate it was possible to modify the patterns orientations, chirality and hierarchical assembly. Publication 8 deals with unification on two hitherto distinct classes of heterogeneous self-assembly due to the molecular properties of Fréchet Dendrons.

Publication 1: Size Matters in Ostwald´s Rule of Stages: Multiphase Transformations Caused by Structural Complexity

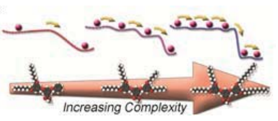

C. Rohr, K. Gruber, M. S. Malarek, L. J. Scherer, E. C. Constable, B. A. Hermann (submitted).

We report nanoscale observations of a system of high phase variety showing the most complex form of Ostwald´s law of stages in two dimensions. We found that the number of metastable states during this crystallization process is not predefined, but increases with the complexity of the building blocks. These additional transient states are an emergent property of the more rugged energy landscape for the more complex structures. This shows the relation between building block complexity and emergent properties in molecular self-organizaion.

Publication 2: Molecular Jigsaw: Pattern Diversity Encoded by Elementary Geometrical Features

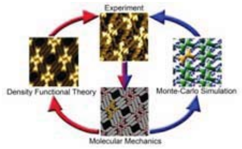

C. Rohr, M. Balbás Gambra, K. Gruber, E. C. Constable, E. Frey, T. Franosch, B. A. Hermann
Nano Letters, 2010, **10**, 833-837.

Scanning tunneling microscopy (STM) images of self-organized monolayers of Fréchet dendrons display a variety of two-dimensional ordering motifs. The emerging patterns are analyzed in a multi-modeling approach: the observed electronic structure is modeled with density functional theory (DFT), the molecular conformation with molecular mechanics (MM), and the question of the predictability of the ground state with interaction site model Monte Carlo Methods (MC). The Monte Carlo approach successfully predicts the various ordering motifs of the self-organization. This confirms that geometry as well as a few salient weak interaction sites encode this structural pattern variety.

Publication 3: Molecular self-organization: Predicting the pattern diversity and lowest energy state of competing ordering motifs

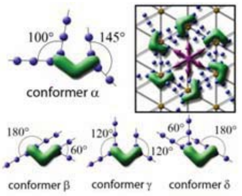

B. A. Hermann, **C. Rohr**, M. Balbás Gambra, A. Malecki, M. S. Malarek, E. Frey, T. Franosch
Physical Review B, 2010, **82**, 165451.

Scanning tunneling microscopy of a single Fréchet Dendron self-organizes with up to seven stable hierarchical ordering motifs. The essential molecular properties determined by molecular mechanics simulations are condensed to a coarse grained interaction-site model of various chain configurations. By varying the internal angles of the pairs of alkoxy chains in an interaction-site model, all facets of the experimentally found patterns can be predicted within our approach. A zero temperature analysis of the MC simulations leads to the thermodynamically most stable pattern that corresponds both to the local minimum derived from MM simulations and the experimental findings upon heating the monolayers.

Publication 4: Predicting the influence of a *p*2-symmetric substrate on molecular self-organization with an interaction-site model

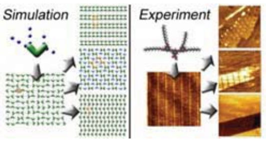

C. Rohr, M. Balbás Gambra, K. Gruber, C. Höhl, M. S. Malarek, L. J. Scherer, E. C. Constable, T. Franosch, B. A. Hermann
Chemical Communications, 2011, **47**, 1800-1802.

An interaction-site model predicts the molecular self-organization of a known molecule on a new substrate in Monte Carlo simulations prior to the measurements. The results are experimentally confirmed with scanning tunneling microscopy on self-organized Fréchet dendrons on a *n*-alkane modified surface. The new substrate has a different symmetry, unit cell and interaction strength compared to HOPG. The local and global ordering motifs, inclusion molecules and a rotated unit cell are correctly predicted.

Publication 5: Simulating patterns for molecular self-organization on surfaces using interaction-site Models

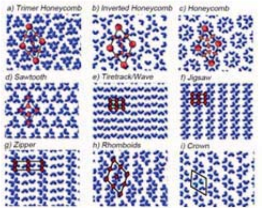

M. Balbás Gambra, **C. Rohr**, K. Gruber, B. A. Hermann, T. Franosch (submitted).

In this paper we provide a detailed discussion of the theoretical aspects of the use of interaction-site models for Fréchet dendrons. In particular, we discuss how salient features of the molecular structure can be identified and used to tailor a suitable coarse-grained model and then be studied by means of Monte-Carlo methods. Furthermore, we show that phase diversity naturally emerges in agreement with experimental studies and discuss the corresponding phase stability as the packing fraction on the substrate or the temperature is varied. Our method is suitable to investigate the stability of the emergent patterns as well as to identify the nature of the melting transition monitoring appropriate order parameters. Finally we provide a thorough discussion on the merits of the approach and its limitations as well as possible extensions.

Publication 6: Multi-hierarchical assembly via molecular flexibility

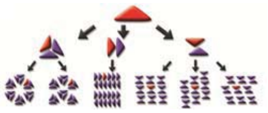

C. Rohr, K. Gruber, M. S. Malarek, E. C. Constable, B. A. Hermann (submitted).

Hierarchical ordering phenomena arise as an emergent property during some molecular self-assembly processes. Fréchet dendrons are an experimental system with *multi-hierarchical* organization and therefore distinctly different from normal hierarchical assemblies. The mult-hierarchy stems from the combination of three different types of second level building blocks. This diversity is caused by the conformational flexibility of the molecule and the resulting change in molecular dipole moment. Reasoning from the basic properties of the molecular building blocks leads to conclusions about specific features of higher level structures, for example symmetry, in the hierarchical assembly.

Publication 7: Surface control of chirality, orientation and hierarchical assembly of self-organized monolayers

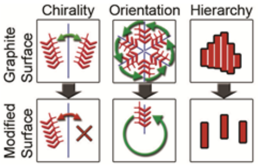

C. Rohr, K. Gruber, M. S. Malarek, E. C. Constable, B. A. Hermann (submitted).

We use an elegant way to modify the substrate for self-assembly with *n*-alkanes to direct the characteristics of the molecular adlayer. This allows the fabrication of monolayers of one chirality and orientation without external or chemical intervention and even influences the hierarchy of assembly. By this method one can fabricate monolayers of one chirality and orientation without external or chemical intervention, effectively standardizing the self-organization in a specific region. We explain these observations by an effective change in the substrates symmetry and interaction strength. Our study highlights the importance and utility of the substrate employed in self-assembly, a factor often neglected due to difficulties in influencing the surface.

Publication 8: A Versatile Fréchet-Dendron Compound Unifies Host-Guest and Templated Heterogeneous Self-Assembly

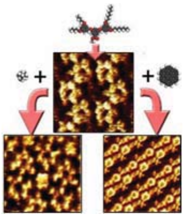

K. Gruber, **C. Rohr**, L. J. Scherer, M. S. Malarek, E. C. Constable, B. A. Hermann
Advanced Materials 2011, DOI: 10.1002/adma.201100013, in print.

We show for the first time that a molecular compound is able to build an independent host structure, a host-guest assembly incorporating guest molecules, and a templated polymorph assembly. The resulting patterns of the respective bimolecular system depend on the type of co-adsorbed guest molecule. This is the first molecular thin film that unifies guest selective confinement in pre-existing cavities as well as conformational switching into a templated new structure. We analyze the observed molecular ordering and differences in packing arrangement using complementary molecular mechanics (MM) and density functional theory (DFT) calculations. At the end, a possible mechanism behind this new and unexpected behavior by electronic properties is explained.

9 Publications

9.1 Size Matters in Ostwald´s Rule of Stages: Multiphase Transformations Caused by Structural Complexity

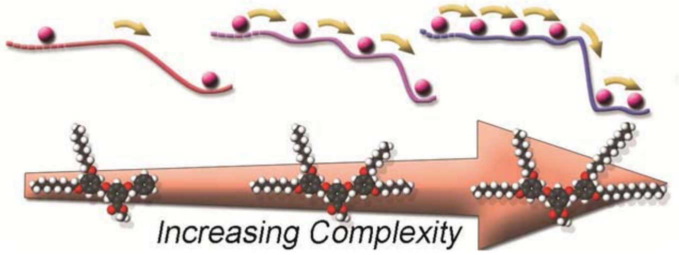
Increasing Complexity

C. Rohr, K. Gruber, M. S. Malarek, L. J. Scherer, E. C. Constable, B. A. Hermann
(submitted).

Multiphase Transformations

DOI: 10.1002/anie.200((will be filled in by the editorial staff))

Size Matters in Ostwald´s Rule of Stages: Multiphase Transformations Caused by Structural Complexity

Carsten Rohr*, Kathrin Gruber, Michael S. Malarek, Lukas J. Scherer, Edwin C. Constable and Bianca A. Hermann

The process of crystallization from melt or solution via metastable states has been formulated by Ostwald in his empirical law of stages[1] in 1897. He stated that: “When leaving a given state and in transforming to another state, the state which is sought out is not the thermodynamically stable one, but the state nearest in stability to the original state”, thus implying the involvement of metastable states in the crystallization process. The first atomistic measurements observing the actual process at the nanometer scale were published in 2009.[2] Simultaneously theoretical nanoscale calculations in two and three dimensions reached the timescales required to analyze the individual metastable states[3,4] and colloidal simulations identified metastable states.[5-9] In order to control the crystallization behavior, insight into transformation kinetics during crystallization and their causes is required, preferably emerging from an easy to handle, two-dimensional yet versatile system containing multiple metastable states.

In this work we present for the first time an illustrative two-dimensional example of Ostwald´s rule with multiple phase-transitions. We use this model system[10] to show that increased molecular complexity increases the number of metastable polymorphs observed during the crystallization. We explain this observation by the trapping of transient states caused by an increased barrier height for more complex molecules. Our study of Ostwald behavior and its dependence on chemical complexity is crucial for the development of increasingly complex supra-molecular chemistry. This appearance of emergent metastable states gives an exciting perspective to this 100 year old law that is important not only for chemistry, but for all aspects of self-organization.

Our system is composed of molecules, which are cast from 0,2 mM hexane solution onto a highly oriented pyrolitic graphite (HOPG) surface. During the rapid evaporation of the solvent, the molecules self-organize in regular patterns and crystallize into two-dimensional monolayers. The surface and its time evolution are imaged by a Nanoscope III scanning tunneling microscope (STM) with low-current converter under ambient conditions at room temperature, which allowed high resolution nanoscale observations of crystallization processes in real space. All images were flattened, drift-corrected and all small scale images were correlation averaged. The Fréchet dendrons[11] 1-3 chosen contain three benzene rings, two bearing flexible alkoxy chains[12] which interact with the surface and drive the molecular self-organization via chain interdigitation.

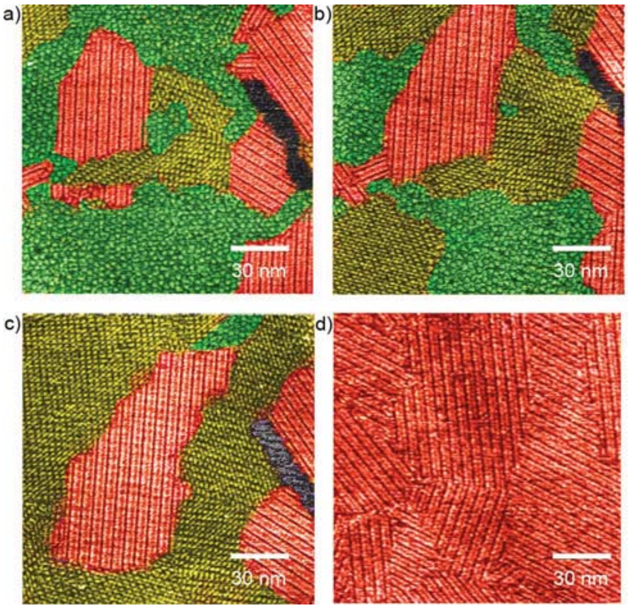

Figure 1. Scanning tunnelling microscopy (STM) measurements of the Ostwald law of stages in 2D with multiple metastable states transforming from green to yellow to red. a, Self-organized molecules crystallizing in a metastable honeycomb phase (green) after the evaporation of the solvent. b, c, Time series of subsequent phase transformation into a metastable chequered phase (yellow) within minutes. d, The concluded phase transformation results in the stable double row phase (red) in different orientations on HOPG, which was facilitated here by heating. 150 nm x 150 nm, U_{Bias}= - 800 mV, $|I_T|$= 8 pA.

(An image of the surface taken directly after solvent evaporation displays multiple, two dimensional crystals. These are different crystallization polymorphs of the molecule, which can be

---

[*] C. Rohr, K. Gruber, Dr. B. A. Hermann
Center for Nano Science (CeNS) and Walther-Meissner-Institute of Low Temperature Research of the Bavarian Academy of Sciences
Walther-Meissner-Str. 8, 85748 Garching (Germany)
Fax: (+49) 89 289 14206
E-mail: carstenrohr@gmx.de

Dr. L. J. Scherer, Dr. M. S. Malarek,
Prof. Dr. E. C. Constable
Department of Chemistry
University of Basel
Spitalstr. 51, 4056 Basel (Switzerland)

Dr. L. J. Scherer
EMPA
Laboratory for Protection and Physiology
Lerchenfeldstrasse 5, 9014, St.Gallen (Switzerland)

Dr. M. S. Malarek
Department of Chemistry and Biochemistry
La Sierra University
4500 Riverwalk Pkwy, Riverside, CA 92515 (USA)

[**] Financial support by the German Excellence Initiative via the program “Nanosystems Initiative Munich”, ERA-Chemistry, the Swiss National Science Foundation and the University of Basel is gratefully acknowledged. C.R. acknowledges the “Studienstiftung des deutschen Volkes“ and the “Elite Network Bavaria“ (IDK Nanobiotechnology).

distinguished by their morphology or pattern.[10] A time series of measurements off our octyloxy substituents shows the initially dominant honeycomb phase (green) transforming within minutes into a chequered phase (yellow) which then subsequently transforms into the thermodynamically stable double row phase (red), see figure 1. This transformation process can be facilitated by warming the sample to 50°C, after which the stable end phase is observed exclusively, see figure 1 d. This phase transformation of two-dimensional crystals starting from a metastable form and transforming via metastable, intermediate steps into the thermodynamically stable end form demonstrates the Ostwald´s law of stages in two dimensions at the nanometer scale.

A sequence of three related molecules was used to study the influence of increasing molecular complexity on their phase transformation behavior. The molecules differ in one pair of alkoxy chains.[12] The simplest molecule 1 exhibits a “naked” phenyl ring, whilst 2 and 3 have two hexyloxy or two dodecyloxy substituents respectively. See also the bottom of figure 2 for their space filling representations.

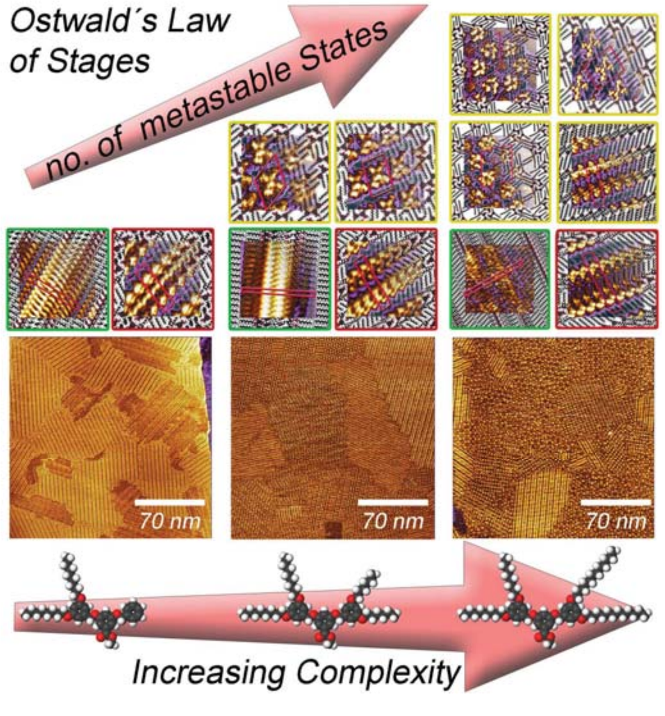

Figure 2. Phase behavior under the influence of increasing molecular complexity. Compound **1** (left) shows one metastable state (green), which transforms into the stable phase (red) within minutes. These two states coexist during the transformation. The more complex molecule **2** (middle) exhibits two additional metastable states (yellow) between the metastable start (green) and stable end phase (red). The overview image displays all four phases. The most complex molecule **3** (right) again with two additional metastable phases (yellow) shows five metastable polymorphs (green and yellow) and the stable double row phase (red). Thus, in two dimensions the number of metastable Ostwald polymorphs increases with molecular complexity. U_{Bias}= - 800 mV to - 1200 mV, $|I_T|$= 3 pA to 40 pA.

The simplest molecule 1 initially exhibits a dense row like ordering, where the molecules are assembled in an upright position in respect to the surface. This metastable start phase transforms subsequently into the thermodynamically stable double row phase, thus showing one metastable and one stable crystal configuration, see left part of figure 2.

Molecule 2, with increased structural complexity, also crystalizes initially as the upright phase (green). Surprisingly here the phase transformation into the thermodynamically stable double row phase (red) happens via two additional intermediate phases (yellow). The appearance of these two metastable orderings results in a four step process, see figure 2 middle. In the overview image of figure 2, middle, all four phases can be seen within one measurement.

The most complex molecule of this series, 3, shows the most intricate example of Ostwald´s law of stages. The initial upright phase (green) can only be measured rarely, since it is quickly replaced by two new intermediate crystallization forms, with honeycomb[13] and sawtooth appearances (yellow). These two phases are more complex in their structure than those previously observed and feature more molecules per unit cell and a higher symmetry (for the honeycomb phase). These metastable phases subsequently transform into one of the previously observed chequered phases (yellow). Before reaching the thermodynamic end product, the double row phase (red), another “pseudo double row” pattern (yellow) is also observed, see figure 2, right. This pattern is structurally similar to the double row phase, since half of one molecule´s conformation mirrors exactly the subsequent double row phase. This phase can, however, be clearly distinguished by its 15% smaller unit cell size. This observation of six phases for a single compound is an extremely complex form of Ostwald´s law of stages and unparalleled for 2D crystals.[14,15]

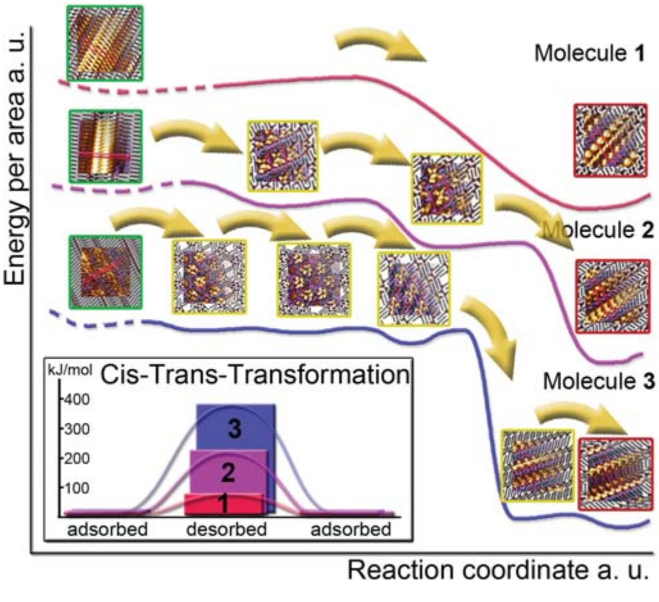

Figure 3. Phase transformations in an energy landscape of increasing complexity. Transformations start with the metastable upright phase (green) and end in the stable double row phase (red). For the more complex molecules the transformation can proceed via the intermediate phases (yellow). Successive phases have progressively higher adsorption energies per area leading to a step-like transformation cascade. Lifting one alkane chain out of the monolayer for an exemplary conformational change requires more energy for the more complex molecules, see inset. This higher energy barrier is expected to stabilize the additional intermediate phases in more complex molecules. U_{Bias}= - 800 mV to - 1200 mV, $|I_T|$= 3 pA to 40 pA.

The phase transformations proceed unidirectional. This means that a phase only transforms into another phase closer to the thermodynamically stable end phase, leading to a transformation cascade. In this process individual steps can be skipped or may be too short lived to be observed, but the steps are not reversible. This transformation cascade exhibits additional metastable stops for the molecular sequence from molecule 1 to 3. It follows that increasing molecular complexity increases the number of metastable phases as described by Ostwald´s law of stages.

Energy minimized molecular mechanics simulations of the relative energy per area of the different phases allows us to qualify these observations. The simulations were performed using the Forcite module of Materials Studio 4.4 employing a universal force field and periodic boundary conditions of the unit cell[16]. Figure 3 displays the respective relative energies calculated for the molecules 1, 2 and 3. The transformation cascade is here made apparent by the decreasing energy ΔG per area found for subsequent molecular phases. The calculated energy for the upright phase is, in general, not comparable to the other phases; upright standing molecules have an increased energy per area due to their increased height. The molecular mechanics calculations for all flat lying phases reproduce the experimentally observed transformation cascade even for the most complex process of molecule 3.

The appearance of additional transient states for molecules of higher complexity means that these states are stabilized by an additional energy barrier. The transformation between two phases also involves a change in molecular conformation. The larger, more complex molecules require more free energy ΔG to e.g. make a cis-trans conversion by partially desorbing from the surface, changing conformation and re-adsorbing, see the inset in figure 3. This is elegantly illustrated by the “pseudo double row” phase that partially mirrors the thermodynamically stable double row phase. Here, part of the molecule has transformed into the stable form, while the other part has not yet reached the final configuration. As expected, the addition of energy facilitates the transformation process. The molecular complexity therefore leads to a rugged energy landscape, which exhibits additional transient states as an emergent property.

In summary we here report nanoscale observations of Ostwald´s law of stages in a two dimensional model system of high phase complexity. We found that the number of transient states increases with the complexity of the molecule, leading to the most extreme form of Ostwald stage behavior observed to date. We show that these additional transient states are an emergent property of the more rugged energy landscape for more complex molecules. To control crystallization processes, new insights into transformation kinetics during crystallization and their dependence on the respective building blocks are crucial for the successful advancement of the field. This novel finding opens a new perspective onto the 100 year old Ostwald´s law of stages in the light of the increasingly complex building blocks utilized in supramolecular chemistry and other areas of technology.

Experimental Section

A Nanoscope III with low-current converter was utilized at ambient conditions for STM measurements. The molecules were cast from 0,2 mM hexane solution onto HOPG. All images were flattened, drift-corrected and all small scale images correlation averaged. The molecular mechanics energy minimizations were performed using the Forcite module of Materials Studio 4.4 employing a universal force field and periodic boundary conditions of the unit cell[16].

Received: ((will be filled in by the editorial staff))
Published online on ((will be filled in by the editorial staff))

Keywords: Scanning probe microscopy · Self-assembly · Supramolecular chemistry · Phase transitions · Ostwald law of stages

---

[1] W. Z. Ostwald, *Phys. Chem.***1897**, *22*, 289-330.

[2] S. Y. Chung, Y.-M. Kim, J.-G. Kim, Y.-J. Kim, *Nature Phys.* **2009**, *5*, 68-73.

[3] M. R. Walsh, C. A. Koh, E. D. Sloan, A. K. Sum, D. T. Wu, *Science* **2009**, *326*, 1095-1098.

[4] J. Baia, C. A. Angell, C. Z. Xiao, *Proc Natl Acad Sci.* **2010**, *107*, 5718-5722.

[5] P. Rein ten Wolde, D. Frenkel, *Science* **1997**, *277*, 1975-1978.

[6] S. Auer, D. Frenkel, *Nature* **2001**, *409*, 1020-1023.

[7] V. J. Anderson,H. N. W. Lekkerkerker, *Nature* **2002**, *416*, 811-815.

[8] J. F. Lutsko, G. Nicolis, *Phys. Rev. Lett.* **2006**, *96*, 046102.

[9] J. Bang, T. P. Lodge, *Phys. Rev. Lett.* **2004**, *93*, 245701.

[10] C. Rohr, M. Balbás Gambra, K. Gruber, E. C. Constable, E. Frey, T. Franosch, B. A. Hermann, *Nano Lett.* **2010**, *10*, 833-837.

[11] C. J. Hawker, J. M. J. Fréchet, *J. Am. Chem. Soc.* **1990**, *112*, 7638-7647.

[12] E. C. Constable, S. Graber, B. A. Hermann, C. E. Housecroft, M. S. Malarek, L. J. Scherer, *Eur. J. Org. Chem.* **2008**, *15*, 2644-2651.

[13] L. Merz, H.-J. Güntherodt, L. J. Scherer, E. C. Constable, C. E. Housecroft, M. Neuburger, B. A. Hermann, *Chem. Eur. J.* **2005**, *11*, 2307-2318.

[14] S. Ahn, A. J. Matzger, *J. Am. Chem. Soc.* **2010**, *132*, 11364-11371.

[15] K. E. Plass, A. L. Grzesiak, A.J. Matzger, *Acc. Chem. Res.* **2007**, *40*, 287-293.

[16] A. K. Rappé, C. J. Casewit, K. S. Colwell, W. A. Goddard III, W. M. Skiff, *J. Am. Chem. Soc.* **1992**, *114*, 10024-10035.

9.2 Molecular Jigsaw: Pattern Diversity Encoded by Elementary Geometrical Features

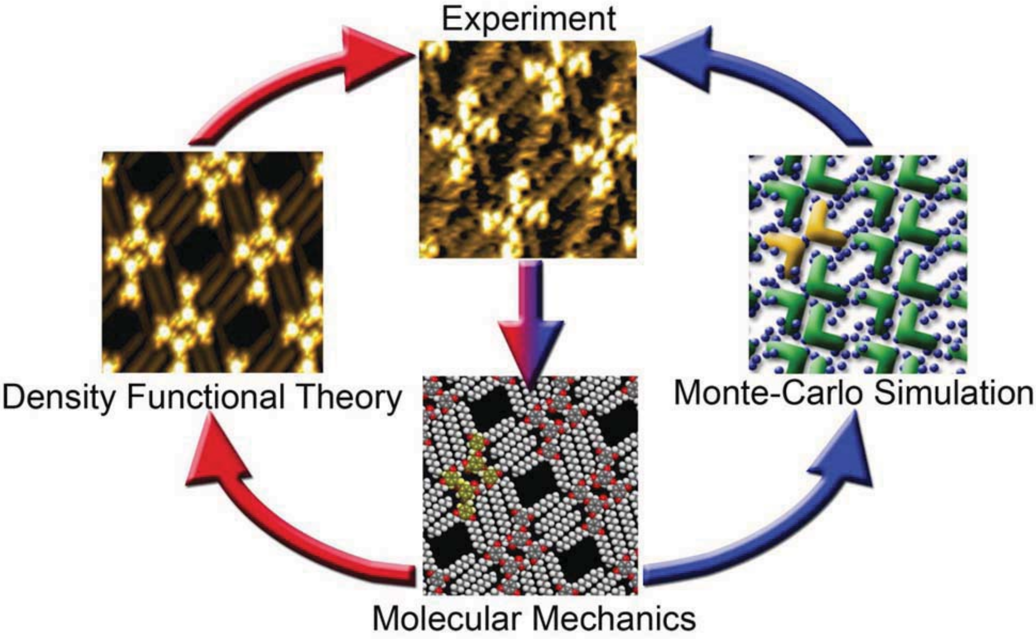
Experiment
Density Functional Theory
Monte-Carlo Simulation
Molecular Mechanics

C. Rohr, M. Balbás Gambra, K. Gruber, E. C. Constable, E. Frey, T. Franosch, B.A. Hermann

Nano Letters, 2010, **10**, 833-837

NANO LETTERS

pubs.acs.org/NanoLett

Molecular Jigsaw: Pattern Diversity Encoded by Elementary Geometrical Features

C. Rohr,[†] M. Balbás Gambra,[‡] K. Gruber,[†] E. C. Constable,[§] E. Frey,[‡] T. Franosch,[‡,∥] and B. A. Hermann*[,†]

[†]Center for NanoScience (CeNS) and Walther-Meissner-Institute of Low Temperature Research of the Bavarian Academy of Sciences and Humanities, Walther-Meissner-Strasse 8, 85748 Garching, Germany, [‡]Arnold Sommerfeld Center for Theoretical Physics (ASC) and Center for NanoScience (CeNS), Department of Physics, LMU München, Theresienstrasse 37, 80333 München, Germany, [§]Department of Chemistry, University of Basel, Spitalstrasse 51, 4056 Basel, Switzerland, and [∥]Institut für Theoretische Physik, Universität Erlangen-Nürnberg, Staudtstrasse 7, 91058 Erlangen, Germany

ABSTRACT Scanning tunneling microscopy (STM) images of self-organized monolayers of Fréchet dendrons display a variety of two-dimensional ordering motifs, which are influenced by engineering the molecular interactions. An interaction-site model condenses the essential molecular properties determined by molecular mechanics modeling, which in a Monte Carlo approach successfully predicts the various ordering motifs. This confirms that geometry as well as a few salient weak interaction sites encode these structural motifs.

KEYWORDS Supramolecules, molecular self-organization, scanning tunneling microscopy, pattern prediction, Monte Carlo simulation

Self-organization of supramolecular monolayers constitutes a major challenge for surface functionalization,[1] sensors,[2] catalysis,[3] and molecular electronic devices.[4] The main difficulty lies in making reliable predictions[5] and controlling[6] the complex molecular ordering on the nanometer scale. With its remarkable recognition and structural properties, DNA templates allow organization of nanomaterials in a programmable way; however, error control and scalability are hard to achieve.[7,8] Currently, scanning tunneling microscopy (STM) images of self-organized structures, in particular of alkane chains[9] and small rigid organic molecules,[10] are *analyzed* by atomistic modeling based on a combination of molecular mechanics (MM) and density functional theory (DFT). For *predicting* several coexisting metastable ordering motifs[11,12] a new multimodeling approach is required that does not presume an a priori knowledge of the resulting patterns.[13−15] Predictability and a deeper understanding of self-organization are expected.

In this Letter, we present high-resolution scanning tunneling microscopy (STM) measurements on self-organized Fréchet dendrons,[16,17] a class of highly flexible supramolecular building blocks. We find a surprisingly rich diversity of structural phases even for a single type of molecule. The emerging patterns are analyzed in a multimodeling approach: the observed electronic structure is modeled with density functional theory (DFT), the molecular conformation with molecular mechanics (MM), and the question of the predictability of the ground state with Monte Carlo Methods (MC). From energy-minimized MM calculations we derive (a) the atomic positions and (b) an effective interaction strength and pass these parameters to the DFT calculations and a coarse-grained interaction-site model for MC, respectively. As a result of this multimodeling approach, we explain how essential geometric features of the molecular architecture encode the observed patterns.

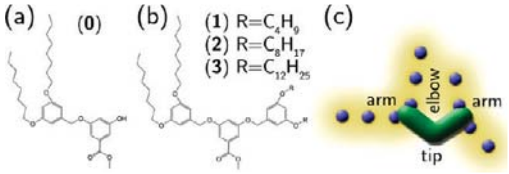

FIGURE 1. Structural model of Fréchet dendrons: (a) OH-terminated (molecule 0) and (b) with slightly varied alkyl chains R (molecules 1−3, butyl, octyl, dodecyl), which self-organize well on graphite surfaces and display up to 10 ordering motifs (seven for one molecule). In order to understand and predict this pattern diversity with Monte Carlo (MC) simulations, we conceived a coarse-grained model for (c) molecule 3 condensing the salient molecular architecture into 10 interaction sites (blue circles). Complementary *atomistic* modeling is achieved by molecular mechanics simulations (MM) combined with density functional theory (DFT).

We have synthesized a series of second generation Fréchet dendrons[18] (Figure 1). The Fréchet dendrons consist of three phenyl rings, two of which carry flexible alkoxychains which interact with the surface and drive the molecular self-organization via chain interdigitation. The alkoxy arms on one side of the Fréchet dendrons have been systematically varied in length in molecules **1**, **2**, and **3**. To study the effect of strong asymmetry, in molecule **0** a hydroxy group replaces one of the phenyl rings. Molecular monolayers are cast from 0.2 mM solutions in ethanol, hexane, or heptadecane onto highly oriented pyrolytic graphite (HOPG).

---

* To whom correspondence should be addressed: b.hermann@cens.de.

Received for review: 09/29/2009
Published on Web: 02/16/2010

© 2010 American Chemical Society

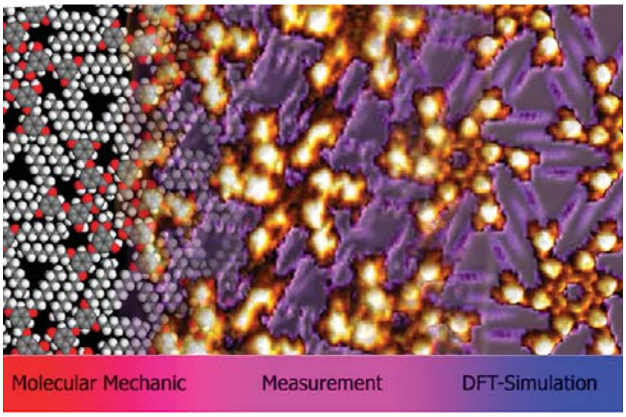

FIGURE 2. Atomistic modeling exemplified for molecule 0: positions and molecular conformation gained by energy-minimized molecular mechanics (MM) simulations on a graphite surface (left), based on starting values from the experimental STM image (middle), serve as input for density functional theory (DFT) calculations (right). The agreement of the measurement (middle) with a slice of the local density of states (LDOS) calculated by DFT (right) confirms the quality of the MM. For predicting ordering motifs, in particular the thermodynamically stable pattern, Monte Carlo methods (MC) are the complementary methods of choice. (12.5 nm × 7 nm, middle: $U_{\mathrm{Bias}} = -800$ mV, $|I_{\mathrm{T}}| = 18$ pA).

We have performed high-resolution STM imaging under ambient conditions employing a Nanoscope Multimode III equipped with a low-current converter. Ten general ordering motifs (21 different patterns) for the entire series **0**−**3** have been imaged at excellent submolecular resolution. To the best of our knowledge, such a large variety of ordering motifs in molecular self-organization cannot be found in the literature. The hexagonal "star" pattern (*p*6 symmetry) is one of four general ordering motifs[19] observed for molecule **0**; see Figure 2. (Images are flattened, correlation averaged, and drift-corrected.) With MM we have derived the molecular conformations and the relative positions of the individual molecules. On the basis of initial configurations extracted from the STM images, the molecular conformations are energy-minimized (local minima) on a fixed double layer of graphite relying on universal force fields.[20] The unit cell contains six molecules with periodic boundary conditions. The agreement of the energy-minimized molecular structures with the experiment (see left side of Figure 2) is significantly increased compared to the initial configurations as well as to energy-minimized single molecule conformations.

These energy-minimized MM simulations provide the atomic positions as input to derive the integrated local density of states (LDOS) of a free single molecule using DFT. For the DFT calculation we utilize the CASTEP module of Material Studio 4.3 employing Perdew−Wang '91 generalized gradient approximation exchange correlation functionals[21] and a plane wave basis set with an energy cutoff at 260 eV. For a direct comparison with the STM measurements convoluted (with a Gaussian function of 2x a Pt d_z orbital) density contours of a planar slice in the LDOS are calculated (24 free molecules at MM determined atomic positions). The phenyl rings of the molecular cores are discernible as pairs of bright protrusions and the atoms of the alkoxy arms emerge as a series of faint dots in the dark areas (right of Figure 2) agreeing with the experimental STM images (middle of Figure 2).

Thus far we have presented an atomically precise analysis of a pattern based on MM combined with DFT simulations. To predict the (meta-)stable patterns, the atomistic and electronic structure are not a suitable starting point, due to the many degrees of freedom. Hence, we shall complement the analysis by Monte Carlo methods employing a coarse grained model (see Figure 1c) to compute condensation energies. Experimentally, the thermodynamically stable pattern has been identified by slow heating. Here, we exemplify Fréchet dendron **3**, which exhibits 7 of the 10 ordering motifs coexisting in neighboring domains.

In two patterns, sawtooth and honeycomb, a molecular trimer in a tip-on-tip configuration is arranged in either *p*2 or a *p*6 symmetry, respectively, see Figure 3a,b. The remaining two patterns are built of dimeric molecular units: In the jigsaw case, the molecules arrange in a slightly distorted squarish repeat unit of *p*2 symmetry in a tip-on-tip geometry; see Figure 3c. The tiretrack pattern shows a rowlike arrangement in a tip-on elbow intermolecular configuration; see Figure 3d. (The fifth pattern found shall be discussed at the end of the paper, while the sixth and seventh patterns are omitted, because a large part of the molecule tilts out of the plane.) The two-dimensional molecular surface coverage in the various ordering motifs varies within a factor of 1.5. Comparing the detailed structural configurations for some patterns with X-ray structural data[22] of three-dimensional Fréchet dendron crystals yields excellent agreement not only in the core positions but also in the interdigitation of the alkyl chains. Most patterns of molecule **3** phase transform within hours into the tiretrack pattern, see Figure 3d, which can also be facilitated by raising the temperature to 60 °C.

Molecular mechanics modeling does not allow the determination of free energies, but the dominant part of the internal energy, the adsorption energies per area, can be extracted: Compared to the highest energy gain for adsorbing a free molecule into the tire-track pattern (Figure 3d), the honeycomb pattern (Figure 3b) and the sawtooth pattern (Figure 3a) show only 85% of the energy gain. The dominant intermolecular interaction term in the energy minimization stems from the alkyl chains. They statistically contribute an interaction strength of 14 kJ/mol per four CH_2 units for more than half but not fully interdigitated alkyl chains on graphite (previous studies yield 18 kJ/mol for fully and 8.5 kJ/mol for half-interdigitated alkyl chains on graphite surfaces[23]).

The interaction strength of 14 kJ/mol per four CH_2 units as determined in the MM and the main geometrical features of the molecular building blocks serve as input for our MC coarse-grained *interaction-site model*. This interaction-site model isolates the salient features: the substrate symmetry, the architecture of the molecule, and the interactions of the

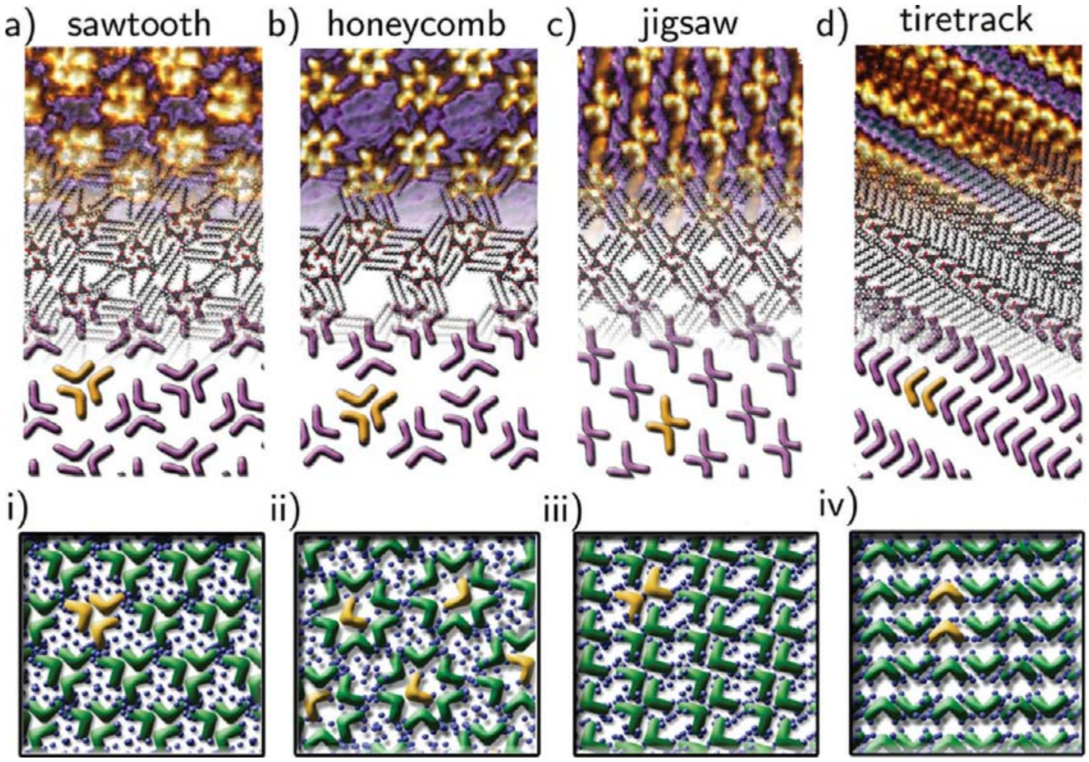

FIGURE 3. STM images of four experimentally found patterns (a−d) of molecule 3 and independent predictions by Monte Carlo (MC) simulations (i−iv). In each column from top to bottom, the high-resolution measurements are faded into the corresponding MM energy minimizations and are further reduced to a core representation indicating the long-range ordering motif of the respective assemblies as well as the local ordering motif displayed in yellow. These MM simulations provide the interaction strength and main geometrical considerations as input for the interaction site model (Figure 1c). The MC simulations of this coarse-grained model predict four (i−iv) patterns with striking resemblance to the measurements in long-range and local ordering. For determining the thermodynamically stable state, phase diagrams are generated (see Figure 4) (a−d: 12.5 nm × 22 nm, $U_{\mathrm{Bias}} = -700$ to -800 mV, $|I_{\mathrm{T}}| = 5-30$ pA).

chains. The building blocks complexity is drastically simplified, reducing the degrees of freedom, by considering the molecule as a rigid entity but preserving the crucial information of the geometry. In the coarse-grained model, a small number of beads, disposed in rigid, straight arms, model the chains; see Figure 1c.

The van der Waals attraction of the chains is described by a Lennard-Jones potential, $V(r) = 4\varepsilon[(\sigma/r)^{12} - (\sigma/r)^{6}]$. The role of the strong adsorbate−substrate π interaction is accounted for by fixing the molecules on the sites of a triangular lattice reflecting the symmetry of the graphite substrate and using typically found chain configurations.

We have performed Monte Carlo (MC) simulations following a Metropolis scheme to determine and better understand the equilibrium configurations and key points controlling the monolayer self-organization, respectively. The lattice constant a, accounting for the density, has been varied in steps of 0.2σ between 2.6σ and 4.2σ, corresponding to a change in coverage density by a factor of 2.8, while the dimensionless inverse temperature $\varepsilon/k_{\mathrm{B}}T$ ranged from 0.025 to 6. The MC moves consist of discrete $\pi/3$ rotations of the coarse-grained “molecules”. To minimize finite-size effects, periodic boundary conditions are employed for different system sizes ranging from several hundred to a few thousand molecules. The systems are slowly cooled to identify the different ground state configurations for varying densities. The ground states have proved reliable, as raising the temperature has shown that the different ordered phases are stable up to 300 °C.

Surprisingly, the MC simulations also show a striking variety of (meta-)stable patterns, exemplified here for molecule **3**. The first structure, Figure 3(i), reproduces the local tip-on-tip trimeric ordering, experimentally found for the sawtooth and the honeycomb motif, but differs in the global symmetry ($p3$ instead of $p2$ and $p6$, respectively). The second pattern, Figure 3(ii), in contrast, nicely captures the global ordering of the honeycomb pattern, Figure 3b, in particular, it displays an open-pore host structure with an included guest molecule of nonfixed orientation also found in the experiment[24] and theoretically predicted in colloidal molecular crystals.[15] The MC pattern in Figure 3(iii) exhibits the same long-range symmetry and local ordering as the experimentally found jigsaw structure, Figure 3c. The fourth MC pattern displays locally a tip-on-elbow arrangement of the tiretrack pattern, Figure 3d, with a tiretrack global ordering motif. The MC simulations also yield a phase consisting of tetramers as local motifs without long-range order (not shown) similar to experimental patterns of a different type of Fréchet dendrons.[25]

© 2010 American Chemical Society

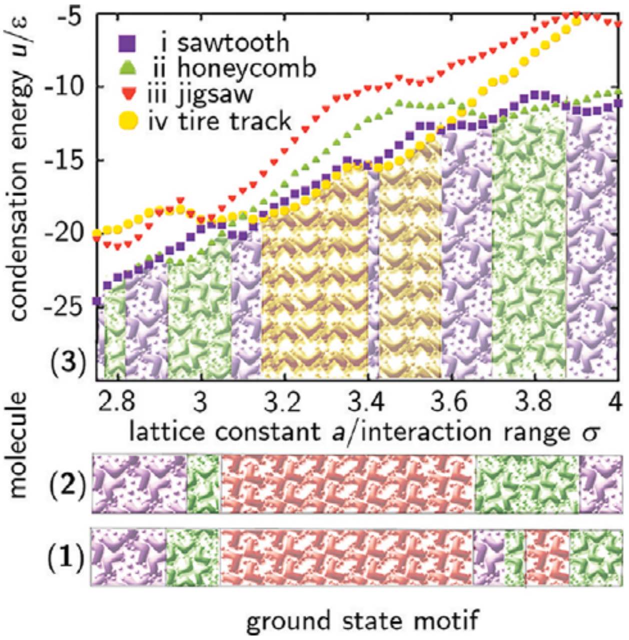

FIGURE 4. In order to predict ground states of the molecular ordering, the condensation energy per molecule of the four by Monte Carlo (MC) simulations predicted phases of molecule 3 (two times three and two times two interactions sites on the periphery) are displayed as a function of the dimensionless (lattice constant a)/(interaction range σ). With varying a/σ the ground state repeatedly alternates between various ordering motifs, predicting the tire-track pattern for molecule 3 in the experimental relevant range of $3.2a/\sigma$. The bars show the ground states at different lattice constants for molecule 2 (two times two and two times two interaction sites on the periphery) and 1 (two times one and two times two interaction sites on the periphery) using the same color coding. The multimodeling approach confirms that salient geometrical features and a few interaction sites encode the local as well as the long-range molecular ordering.

In a zero temperature analysis the condensation energies of the various MC determined patterns can be calculated to determine the ground-state pattern: The ground-state pattern varies abruptly with the packing fraction. A similar pattern diversity is found in our MC simulations for molecules **1** and **2**, modeled by a total of six and eight interaction sites, respectively, yet the stability of ordering motifs is altered; see Figure 4. Apparently all patterns found by MC possess very similar condensation energies in line with the experimental observation of many coexisting patterns, which transform into one another with time. In the experimentally relevant regime ($3.2a/\sigma$), the most favorable configuration is the tiretrack pattern in the case of molecule **3** (Figure 4). So from the coarse-grained MC simulations, the tiretrack pattern constitutes the ground state for molecule **3** in agreement with above-discussed experimental findings upon heating.

The agreement between the experimental patterns and the MC structures suggests that within our coarse-grained model all essential information is successfully contained. The lattice symmetry and typical chain configurations transferred into the interaction-site model allow an overall correct simulation of the local and global ordering motifs by MC. The question now is whether our multimodeling approach provides predictive power for supramolecular self-organization when multiple ordering motifs occur. A closer inspection of the MC pattern Figure 3(iv) reveals also an arm-on-arm local ordering motif; see top of Figure 5. This prediction has challenged us to conduct further STM experiments and to search for the new local ordering motif. Indeed in rare cases, we have found the predicted structure displayed in Figure 5e, i.e., a wave pattern consisting of dimers in an arm-on-arm arrangement in a rowlike assembly of $p2$ symmetry.

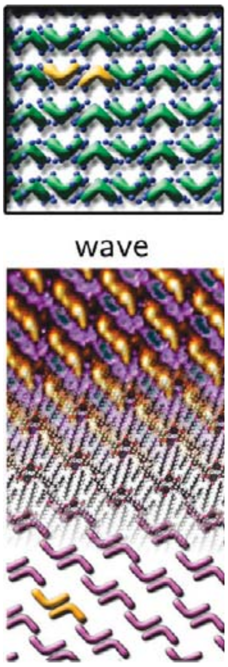

FIGURE 5. The Monte Carlo (MC) simulation (iv) (see Figure 3) predicts a second local ordering motive in a arm-on-arm configuration, which was discovered experimentally after the simulation as a fifth rare ordering phase: a wave pattern.) (12.5 nm × 22 nm, $U_{\mathrm{Bias}} = -800$ mV, $|I_{\mathrm{T}}| = 8$ pA).

In a control experiment Fréchet dendrimers have been cast on a substrate of a lower $p2$ symmetry obtained through a pentacontane monolayer on the HOPG. In this lower symmetry environment, some of the patterns discussed can no longer be observed in the STM measurements. The same conclusion arises from appropriately adapted MC simulations, which serves to strongly corroborate the predictive power of our multimodeling approach.

The concept presented herein is not limited to a particular supramolecular architecture. Extensions of the approach would be needed in the case of patterns derived from upright standing molecules or from species with a significant nonplanarity (such as octahedral metal complexes) to properly deal with the new degrees of freedom. When large flexible molecules adsorb on 10 or more substrate atoms, the assembly appears to be directed by steric hindrance; the role of the substrate is then to align the molecule and, e.g., the molecular chains. For small and rigid molecules or even single atoms one expects the molecule–substrate interaction to become more dominant as specific molecular recognition features become more important, e.g., preferred adsorption sites. In principle, the multimodeling approach can be extended to systems of atom adlayers and small molecules provided the information of the molecule–substrate interactions obtained from MM is reflected in the interaction-site model.

In conclusion, combinations of Monte Carlo and molecular mechanics simulations bear predictive power for molecular self-organization. When the relevant molecule–substrate and molecule–molecule interactions can be transferred into the geometry of an interaction-site model, surprisingly most of the chemical details appear to be of minor importance for the resulting self-organized patterns. Yet, salient geometrical features encode various, experimentally confirmed patterns; their stability depends sensitively on the molecular interactions. A fine-tuning of these interaction strengths may be utilized to organize *functional* cores. Since the symmetry of the underlying graphite restricts the preferred molecular orientations, only certain motifs are permitted, other symmetries can be realized with, e.g,. metal surfaces with 4-fold symmetry. In summary, our combined Monte Carlo and molecular mechanics modeling allows prediction of which of the elementary geometrical features such as molecular architecture, chain length, and relative angles is essential for the formation of a particular planar self-organized monolayer. Local and global ordering motifs as well as the ground states of molecular patterns can be determined by condensing the critical chemical information in a coarse-grained interaction site model. Hence, this approach of general validity will be able to guide future synthesis of complex molecules in order to program new surface patterns with designed ordering motifs.

Acknowledgment. Financial support by the German Excellence Initiative via the program "Nanosystems Initiative Munich (NIM)", DFG, ERA-Chemistry, Deutsche Studienstiftung, NRP47, the Swiss Nanoscience Institute, and Walther-Meissner-Institute is gratefully acknowledged.

REFERENCES AND NOTES

(1) Barth, J. V.; Costantini, G.; Kern, K. *Nature* **2005**, *437*, 671.
(2) Lehn, J.-M. *Science* **2002**, *295*, 2400.
(3) Lorenzo, M. O.; et al. *Nature* **2000**, *404*, 376.
(4) Joachim, C.; Gimzewski, J. K.; Aviram, A. *Nature* **2000**, *408*, 541.
(5) Barth, J. V. *Annu. Rev. Phys. Chem.* **2007**, *58*, 375.
(6) Swiegers, G.; Malefetse, T. *Chem. Rev.* **2000**, *100*, 3483.
(7) Seeman, N. C. *Nature* **2003**, *421*, 427.
(8) Aldaye, F. A.; Palmer, A. L.; Sleiman, H. F. *Science* **2008**, *321*, 1795.
(9) Ilan, B.; et al.*, Nano Lett.* **2008**, *8*, 3160.
(10) Shi, D. X.; et al. *Phys. Rev. Lett.* **2006**, *96*, 226101.
(11) Morgenstern, K. *Surf. Sci.* **2003**, *523*, 141.
(12) Meier, C. *J. Phys. Chem. B* **2005**, *109*, 21015.
(13) Weber, U. K. *Phys. Rev. Lett.* **2008**, *100*, 156101.
(14) Haran, M.; et al. *Langmuir* **2007**, *23*, 4897.
(15) Šarlah, A.; Franosch, T.; Frey, E. *Phys. Rev. Lett.* **2005**, *95*, 088302. Šarlah, A.; Franosch, T.; Frey, E. *Phys. Rev. E* **2007**, *75*, 021402.
(16) Hawker, C. J.; Fréchet, J. M. J. *J. Am. Chem. Soc.* **1990**, *112*, 7638. Hawker, C. J.; Fréchet, J. M. J. *J. Chem. Soc., Chem. Commun.* **1990**, *112*, 1010.
(17) Hermann, B. A.; et al. *Adv. Funct. Mat.* **2006**, *16*, 221.
(18) Constable, E.; et al. *Eur. J. Org. Chem.* **2008**, *15*, 2644.
(19) Miura, A.; et al. *Small* **2005**, *1*, 131.
(20) Rappé, A. K. *J. Am. Chem. Soc.* **1992**, *114*, 10024.
(21) Clark, S. J. *Z. Kristallogr.* **2005**, *220*, 567.
(22) Constable, E. C.; et al. *CrystEngComm* **2007**, *9*, 176.
(23) Yin, S.; et al. *Surf. Interface Anal.* **2001**, *32*, 248.
(24) Merz, L.; et al. *Chem. Eur. J.* **2005**, *11*, 2307.
(25) Mamdouh, W.; et al. *J. Am. Chem. Soc.* **2006**, *128*, 317.

© 2010 American Chemical Society

9.3 Molecular Self-Organization: Predicting the Pattern Diversity and Lowest Energy State of Competing Ordering Motifs

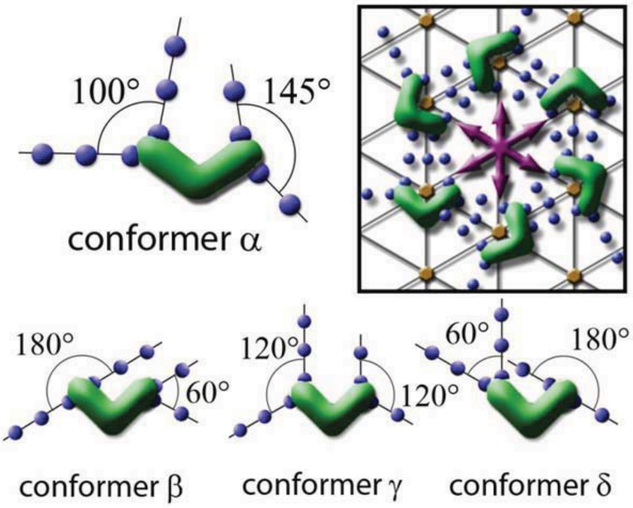
100°
145°
conformer α
180°
60°
conformer β
120°
120°
conformer γ
60°
180°
conformer δ

B. A. Hermann, **C. Rohr**, M. Balbás Gambra, A. Malecki, M. S. Malarek, E. Frey, T. Franosch

Physical Review B, 2010, **82**, 165451.

PHYSICAL REVIEW B **82**, 165451 (2010)

Molecular self-organization: Predicting the pattern diversity and lowest energy state of competing ordering motifs

B. A. Hermann,[1,*] C. Rohr,[1] M. Balbás Gambra,[2] A. Malecki,[1] M. S. Malarek,[3] E. Frey,[2] and T. Franosch[4,2]
[1]*Center for Nano Science (CeNS) and Walther-Meissner-Institute of Low Temperature Research of the Bavarian Academy of Sciences, Walther-Meissner-Str. 8, 85748 Garching, Germany*
[2]*Arnold Sommerfeld Center for Theoretical Physics (ASC) and Center for Nano Science (CeNS), Department of Physics, LMU München, Theresienstraße 37, 80333 München, Germany*
[3]*Department of Chemistry, University of Basel, Spitalstrasse 51, 4056 Basel, Switzerland*
[4]*Institut für Theoretische Physik, Universität Erlangen–Nürnberg, Staudtstraße 7, 91058 Erlangen, Germany*

(Received 22 March 2010; revised manuscript received 12 May 2010; published 29 October 2010)

Self-organized monolayers of highly flexible Fréchet dendrons were deposited on graphite surfaces by solution casting. Scanning tunneling microscopy (STM) reveals an unprecedented variety of patterns with up to seven stable hierarchical ordering motifs allowing us to use these molecules as a versatile model system. The essential molecular properties determined by molecular mechanics simulations are condensed to a coarse grained interaction-site model of various chain configurations. In a Monte Carlo approach with random starting configurations, the experimental pattern diversity can be reproduced in all facets of the local and global ordering. Based on an energy analysis of the Monte Carlo and molecular mechanics modeling, the thermodynamically most stable pattern is predicted and shown to coincide with the pattern which dominates the STM images after several hours or upon moderate heating.

DOI: 10.1103/PhysRevB.82.165451 PACS number(s): 68.43.−h, 68.37.Ef, 81.16.−c

I. INTRODUCTION

Organic molecules mainly self-organize via hydrogen bonds,[1,2] metal-coordination,[3] or van der Waals interactions.[4] The need has been established for[5,6] more innovative modeling approaches[7,8] that can analyze and predict molecular patterns, thus nurturing efficient application in surface functionalization,[9] sensors,[10] catalysis,[11] and molecular electronic devices.[12] Predictability of surface patterning could speed up molecular design and advance the understanding of the self-organization process itself. For *predicting* several coexisting ordering motifs (cf. Refs. 13 and 14) a new multimodeling approach is required, that does not rely on the prior knowledge of the resulting patterns.[15–19] In this paper we demonstrate that, based on a coarse grained interaction-site model (omitting chemical details), we are able to not only reproduce and predict all features of the local and global ordering motifs of self-organized molecular layers, but also, independently predict the thermodynamically most stable patterns and thus deliver an innovative method for understanding molecular self-organization.

In this paper, the self-organization of flexible supramolecular building blocks, Fréchet dendrons,[20,21] is investigated in highly resolved scanning tunneling micrographs and modeled with various techniques including density-functional theory (DFT), molecular mechanics (MM), and Monte Carlo (MC) simulation based on an interaction-site model. The second-generation asymmetric Fréchet dendrons consist of three phenyl rings, two of which are functionalized by two pairs of alkoxy chains, a longer dodecyloxy pair, and a shorter octyloxy pair (see Fig. 1 left), responsible for van der Waals and weak hydrogen bonds.[22] The fact, that Fréchet dendrons with longer and shorter chains are used, eases identification of angles within conformers. Otherwise, the irregular chain length is of no importance, as a large pattern variety is also obtained for chain-symmetric Fréchet dendrons (two pairs of octyloxy chains), see Ref. 15. The total van der Waals interactions are the sum of the individual intermolecular interactions [chain-neighboring-chain (c-n-c)] and the molecule-substrate interactions [molecule-substrate (m-s)]. By varying the internal angles of the pairs of alkoxy chains in an interaction-site model, all facets of the experimentally found patterns can be predicted within our approach. A zero-temperature analysis of the MC simulations leads to the thermodynamically most stable pattern that corresponds both to the local minimum derived from MM simulations and the experimental findings upon heating the monolayers.

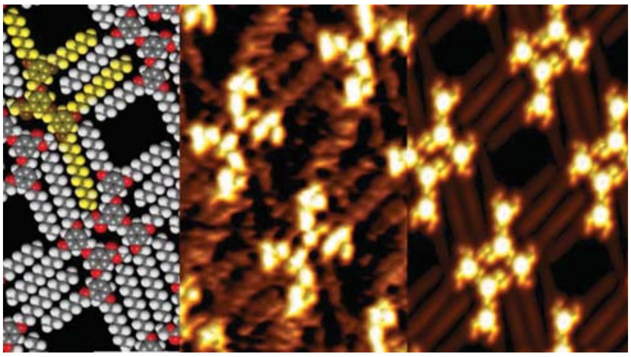

FIG. 1. (Color online) A single molecule of the dodecyl/octyl terminated Fréchet dendron is highlighted. One of seven different ordering patterns on HOPG is exemplified. *Middle*: STM image of a jigsaw pattern of the Fréchet dendron (7.5 nm × 12.5 nm, $U_{Bias}=-800$ mV, $|I_T|=8$ pA). *Left*: atomistic modeling by an energy minimized MM simulation (see text). *Right*: simulation of the LDOS by DFT calculations based on the input of the geometry determined by MM.

©2010 The American Physical Society

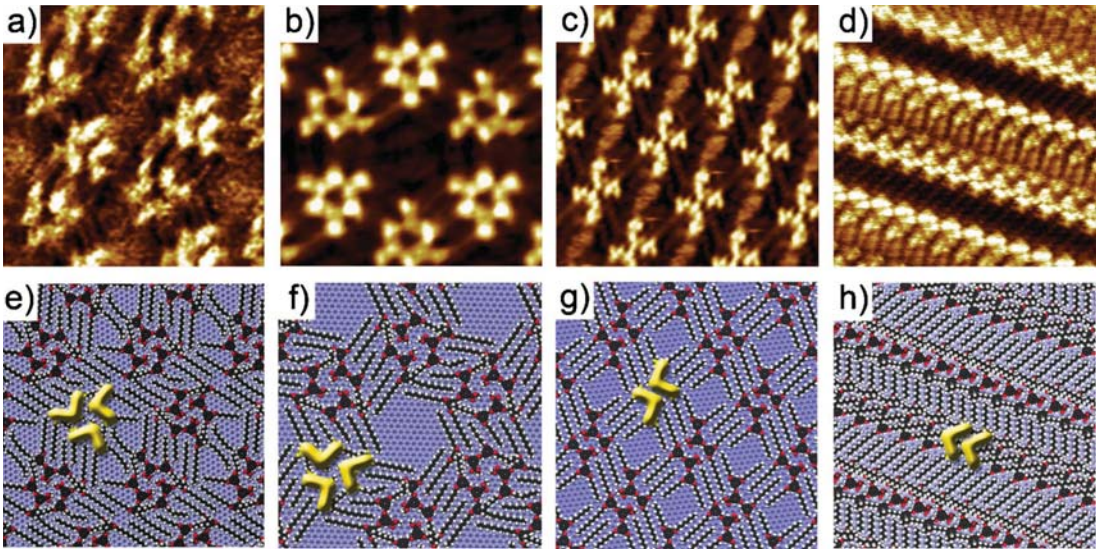

FIG. 2. (Color online) [(a)–(d)] STM results and corresponding [(e)–(f)] molecular mechanics modeling (see text) of four experimentally found patterns of Fréchet dendrons: (a) sawtooth, (b) honeycomb, (c) jigsaw, and (d) tiretrack. The molecular backbones (highlighted) indicate the local ordering motif. ($10\ \text{nm} \times 10\ \text{nm}$, $U_{Bias} = -700$ to -800 mV, and $|I_T| = 5-30$ pA)

II. METHODS

For the STM measurements a nanoscope multimode III instrument equipped with a low-current converter under ambient conditions was employed. Monolayers of Fréchet dendrons (3,5-bis[(3,5-bisoctyloxyphenyl)methyloxy]phenyl ester, synthesis, see Ref. 23), are cast from 0.2 mM solutions in ethanol, hexane, or heptadecane on highly oriented pyrolytic graphite (HOPG) surfaces. The emerging patterns are analyzed by combining several complementary approaches: (a) DFT, utilizing the CASTEP®module of Material Studio 4.3 employing Perdew-Wang'91 generalized gradient approximation exchange correlation functionals[24] and a plane-wave-basis set with an energy cutoff at 260 eV; (b) MM, performed on a fixed double layer of graphite (universal force fields[25] in periodic boundary conditions) based on starting values obtained from the STM experiments; and (c) MC annealing simulations in the METROPOLIS scheme based on 60° rotations of a coarse-grained interaction-site model, using periodic boundary conditions for minimizing finite-size effects in system sizes ranging from several hundreds to a few thousand objects.

III. RESULTS AND ANALYSIS

The mixed image in Fig. 1 (Ref. 26) exemplifies MM and DFT simulations together with experimental measurements of the jigsaw pattern. After applying a droplet of a solution in hexane, the jigsaw pattern ($p2$ symmetry)[27] appears as one of seven general ordering motifs in about 25% of the substrate area. A detailed analysis of many STM images yields starting configurations[28] for a MM energy minimization[29] to calculate molecular conformations (see left of Fig. 1) and relative positions. From the MM determined adsorption energy the dominant van der Waals part[30] can be extracted, as discussed later.

As the energy-minimized MM simulations can only provide atomic positions and not electronic states, we used these energy minimized geometries as input to derive the local density of states (LDOS) of a free single molecule using DFT. Convoluted[31] density contours of a planar slice in the LDOS are plotted[32] (right, Fig. 1) for a direct comparison with the STM measurement: the phenyl rings of the molecular cores are discernible as three bright protrusions and atoms of the alkoxy arms emerge (visible in the dark areas) as series of faint lines (right, Fig. 1) in agreement with the experimental STM images (middle, Fig. 1).

In a large STM study, we have imaged seven ordering motifs of this Fréchet dendron in excellent resolution. Here we focus on four main ordering motifs: sawtooth: honeycomb: jigsaw: tiretrack (see Fig. 2). $20\ \text{nm} \times 20\ \text{nm}$ sized domains of these patterns in ratios 1%:15%:25%:20% typically cover an HOPG surface roughly half an hour after applying a hexane droplet. About 39% of the HOPG surface is occupied by domain boundaries, mobile molecules or two other patterns: upright and small tiretrack. Minutes after casting a droplet of the Fréchet dendrons in hexane, the honeycomb pattern dominates. The sawtooth pattern seldom appears as an independent pattern and often as a stacking fault of the honeycomb pattern. After several hours, typically 60% of the HOPG surface is covered with the tiretrack pattern.

As DFT calculations can only poorly describe van der Waals interactions, the dominant part of the internal energy, the adsorption energy per unit cell or area, is evaluated from the MM minimization energy.[33] This covers the dominant intermolecular interactions stemming from the alkoxy chains, statistically contributing an interaction strength of 14 kJ/mol per four CH_2 units in case of alkoxy chains that are not fully (>50%) interdigitated on graphite (previous studies yield 18 kJ/mol for fully and 8.5 kJ/mol for half-interdigitated alkoxy chains on graphite surfaces[34]). We have calculated the van der Waals part of the total energy (I) of a

TABLE I. Van der Waals part of the adsorption energies determined by MM energy minimization. (a) *per molecule*. (b) *per area*. The labels refer to: m-s, molecule-substrate interactions and c-n-c, chain-neighboring-chain interactions.

Pattern	Molecules per unit cell	$I_{\text{m-s}}$/molecule (kJ/mol)	$I_{\text{c-n-c}}$/molecule (kJ/mol)
Sawtooth	6	−674	−147
Honeycomb	6	−691	−163
Jigsaw	2	−653	−117
Tiretrack	2	−528	−222

Pattern	Unit cell size (nm^2)	$I_{\text{m-s}}/\text{nm}^2$ (kJ/mol)	$I_{\text{c-n-c}}/\text{nm}^2$ (kJ/mol)
Sawtooth	24.5	−167	−38
Honeycomb	26.5	−155	−38
Jigsaw	8.4	−151	−25
Tiretrack	6.1	−172	−75

substrate supported monolayer in MM energy minimized geometry, i_{sup}, (II) of a gas phase net,[2] i_{gn}, and (III) of one isolated molecule, i_{iso}. With that we can carefully separate the intermolecular interaction (chain-neighboring-chain) part $I_{\text{c-n-c}}/\text{molecule}=(i_{gn}/n)-i_{iso}$ from the substrate interaction (molecule-substrate) part $I_{\text{m-s}}/\text{molecule}=(i_{gn}-i_{sup})/n$ of the van der Waals energy per molecule, with n, the number of molecules per unit cell (see Table I). If we then divide by the area per unit cell, the respective energies per nm^2 are derived (see Table I).

Molecular domains grow at the boundaries by the addition or loss of molecules that do not have a full complement of neighboring molecules as appropriate for the domain symmetry. When initially forming domains after applying a droplet, the gain in van der Waals adsorption energy $I_{\text{m-s}}+\delta(I_{\text{c-n-c}})$ *per molecule* with $\delta<1$ rules the process: the honeycomb pattern in Table I. Over time the HOPG surface is covered with some 100-nm^2-sized domains, which transform according to the Kitaigorodskii principle of avoiding free space.[35] Hence the highest gain in van der Waals adsorption energy $I_{\text{m-s}}+I_{\text{c-n-c}}$ *per area* dominates the outcome: the tiretrack pattern in Table I. This agrees with the thermodynamically stable pattern experimentally identified by moderate heating, which is the tiretrack pattern in hexane. Thus, the initial domains form open pore patterns dominated by the highest energy gain *per molecule* while with time the pattern with the largest energy gain *per area* wins. However, all calculated energies are very close, reflecting that the phases can coexist.

IV. MODELING

In order to identify the ground-state energy we performed independent MC simulations, based on coarse graining the dominant molecule and substrate properties in an interaction-site model. Rather than including as much chemical detail as possible, we investigated the crucial properties needed to reproduce key experimental findings. When large molecules adsorb on ten or more substrate atoms, the organization is dominated by steric hindrance; the role of the substrate is to align the molecular backbone and to some extent the molecular chains. In this work, we systematically varied the internal angles of the pairs of longer and shorter arms of interaction centers (see Fig. 3), thereby probing different molecular conformations, in order to determine how critical the angles are on the predictive power of the interaction-site model.

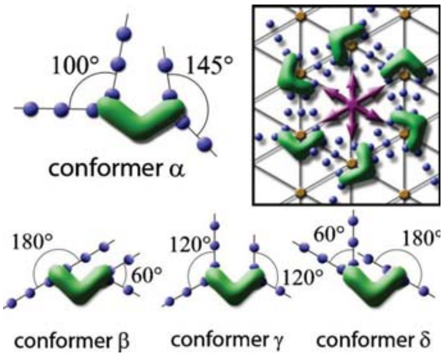

FIG. 3. (Color online) Top: angle configuration for conformer α. The box displays the six possible orientations on a fixed lattice of hexagonal symmetry. Bottom: conformers β, γ, and δ with the respective internal angles indicated.

As described in our previous work[15] the substrate symmetry is accounted for by allowing discrete $\pi/3$ rotations of the coarse grained molecules, see Fig. 3, on fixed sites in a lattice of hexagonal symmetry. The geometry and spacing of the molecular backbone is transferred from the MM modeling. The chains are modeled by a small number of beads, disposed in rigid, straight arms at distances determined by MM and with approximate angles of 100° and 145° between long and short pairs of alkoxy chains, respectively.[15] We refer to a Fréchet dendron with the latter chain conformation as conformer $\boldsymbol{\alpha}$. Here, the internal angle within each pair of arms has been systematically varied from 180° and 60°, referred to as conformer β, over 120° and 120°, conformer γ, to 60° and 180°, conformer δ, for long and short pairs of alkoxy chains, respectively. One bead represents four CH_2 units, exhibiting short-range van der Waals attractions, which are described by a Lennard-Jones potential, $U(r)=4\epsilon[(\sigma/r)^{12}-(\sigma/r)^{6}]$.

The MC simulations were performed by preparing random starting configurations [see (0) in Fig. 4] and relaxing the system by slowly "cooling." The lattice constant a, accounting for the density, has been varied between 2.95σ and 4.0σ, corresponding to a change in coverage density by a factor of 1.35, while the dimensionless inverse temperature ϵ/k_BT ranged from 0.025 to 6. The ordered patterns obtained, (i), (ii), (iii), and (iv) in Fig. 4, correspond well in long-range symmetry and local ordering with the structures found experimentally: (a), (b), (c), and (d) in Fig. 2, respectively. While the chain configuration of conformer α (100° and 145° for long and short pairs of alkoxy chains, respectively) leads to a striking variety of patterns (see Ref. 15), the systematic choice of internal angles in conformers β, δ, and γ narrows the pattern variety.

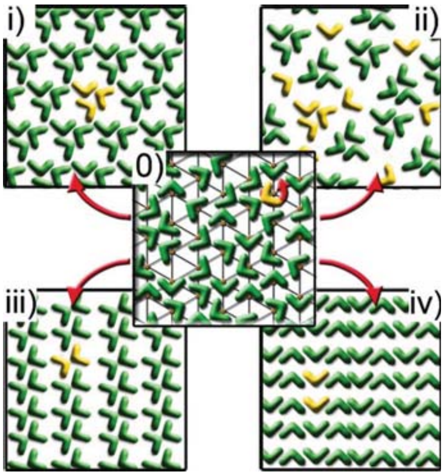

FIG. 4. (Color online) MC simulations (i)–(iv). (0) Random starting configurations allowing discrete $\pi/3$ rotations of the coarse grained molecules. Upon slow cooling the following patterns formed from random state (0) indicated with red arrows: (i) sawtooth pattern for conformer β and for conformer α, (ii) trimer honeycomb pattern for conformer δ, (iii) jigsaw pattern for conformer α, and (iv) tiretrack pattern for conformers α, β, and γ. All phases were stable upon heating to 300 °C.

The patterns that can be generated from the respective conformers are: sawtooth and tiretrack for β [see (i) and (iv) in Fig. 4], tiretrack, honeycomb, and inverted honeycomb for γ [see (iv) in Fig. 4 and (v) and (vi) in Fig. 5, respectively] and trimer honeycomb for δ [see (ii) in Fig. 4]. So with the conformer δ, even the intriguing open-pore host structure of the molecular trimers arranged in hexagonal symmetry [see (b) in Fig. 2] can now be generated from random starting configurations by slow cooling. The honeycomb pattern (b) in Fig. 2 displays an organizational chirality with an included guest molecule of nonfixed orientation (described in another publication[36]). Hence, all experimentally found patterns can be completely described. The MC patterns (i)–(iv), in very good correspondence with experimental findings, proved to be reliable, as raising the temperature showed that these phases stay ordered up to 300 °C and can thus be considered as stable states.

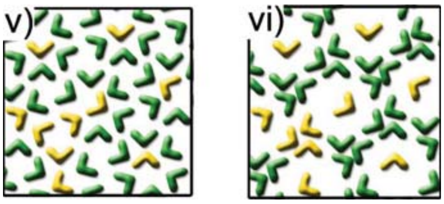

FIG. 5. (Color online) Alternative phases, that have been predicted, condensed from random starting configurations by the Monte Carlo approach: (v) honeycomb pattern of conformer α and γ, and (vi) inverted honeycomb pattern of conformer γ. Both the inverted honeycomb and honeycomb MC patterns proved unstable upon simulating a finite temperature and, thus, cannot be considered as likely patterns; these patterns find no close resemblance in the experimental data.

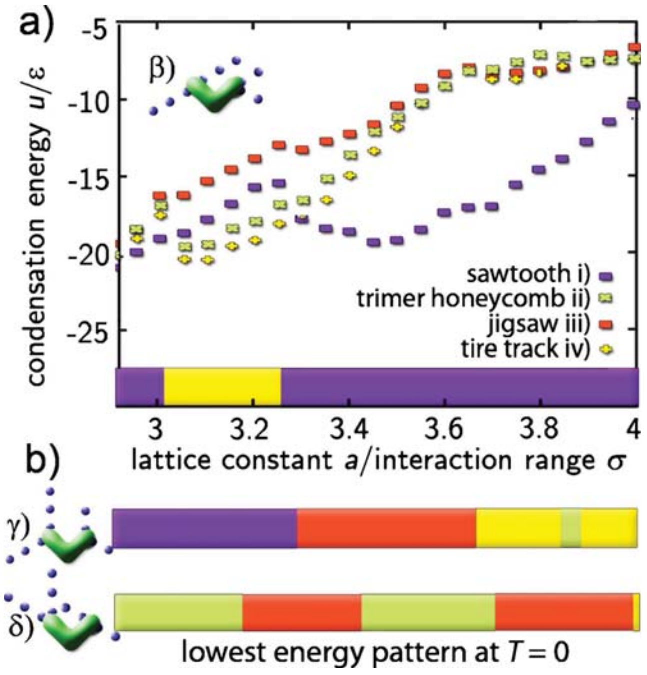

FIG. 6. (Color online) conformer β, coarse grained model with angles 180° and 60° between the long and short chains. (a) Zero-temperature energy analysis for determining the associated lowest energy state. The experimentally relevant regime corresponds to $3.2a/\sigma$. (b) The pattern of lowest energy in the zero-temperature analysis for conformations γ and δ. At the experimentally relevant regime of $3.2a/\sigma$, the sawtooth pattern for conformer γ and jigsaw pattern for conformer δ, did not prove stable upon heating and hence cannot represent the thermodynamically most stable pattern.

Furthermore, we now demonstrate two additional patterns (see Fig. 5) named (v) honeycomb pattern and (vi) inverted honeycomb pattern (both found for conformer γ), that were condensed from random starting configurations, but could not be verified in the STM experiments. The stability of these MC patterns was tested by simulating a finite temperature; both patterns proved unstable upon "heating" and, thus, cannot be considered likely ordering states. Although, all three honeycomb patterns have a similar appearance, upon closer examination, only the trimer honeycomb pattern (ii) displayed in Fig. 4 correctly describes the experimentally found pattern (b) of Fig. 2. Hence, the honeycomb and inverted honeycomb pattern are not experimentally observed and are unstable in a MC simulation of finite temperature.

In contrast to patterns generated from random starting configurations, patterns (i), (ii), (iii), and (iv) (see Fig. 4) can be pre-prepared for all conformers allowing to compute the associated energies in a zero-temperature energy analysis. So the state of lowest energy at $T=0$ can be identified in each case as a function of the packing density. In the case of artificially prepared patterns the energy analysis can only indicate how energetically attractive a structure is, not if the pattern is likely. The pattern that minimizes the energy varies, depending on the packing fraction [see bar graphs in Figs. 6(a) and 6(b)] and the internal angle, hence, the conformer. In the experimentally relevant regime ($3.2a/\sigma$), the most favorable configuration for conformer α (see Ref. 15) and conformer β) is the tiretrack pattern [see Fig. 6(a)]. As this pre-prepared pattern is stable upon heating to 300 °C

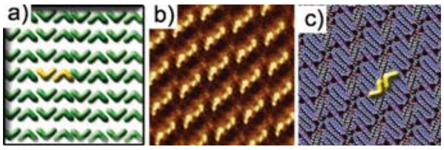

FIG. 7. (Color online) (a) Another local ordering motif of the MC simulation [Fig. 4(iv)] that was subsequently identified experimentally; (b) STM measurement of the rarely found fifth pattern with corresponding; and (c) MM modeling. (12.5 nm × 12.5 nm, $U_{Bias}=-800$ mV, $|I_T|=8$ pA)

and can also be generated from random starting configurations, the tiretrack pattern is identified as the thermodynamically most stable pattern in good agreement with the experimental findings and the MM energy analysis discussed above.

For the chain configurations of conformers γ and δ, the sawtooth and jigsaw patterns [Fig. 6(b)] appear to have the lowest energy at $T=0$ in the experimentally relevant regime. Probing the stability of the latter two patterns by raising the temperature leads to destabilization and, thus, clearly indicates that neither the sawtooth nor jigsaw can represent the thermodynamically most stable pattern around room temperature.

In summary, the systematic variation in internal angles within the pairs of chains (representing the chain-chain interdigitation) reveals that the local and global ordering motif of all experimentally found patterns can be reproduced by cooling random starting configurations. The zero-temperature analysis of pre-prepared patterns in all combinations of conformers/patterns underlines that only the tiretrack pattern found for conformer α (see Ref. 15) and β represents an ordered state with lowest energy at $T=0$ and is at the same time stable upon heating. Thus, the tiretrack pattern is confirmed both experimentally and theoretically as the thermodynamically most stable motif at finite temperatures, even for different molecular conformations in the interaction-site model.

In addition, it is not only possible to reproduce patterns by the MC approach but also to predict. In Fig. 4(iv) a second local ordering motif with a side by side arrangement of the molecular backbones is apparent [Fig. 7(a)]. This local ordering motif named "wave" has been experimentally identified subsequent to the theoretical prediction; it occurs rarely for dodecyl/octyl terminated Fréchet dendrons in ethanol [Fig. 7(b)].

V. CONCLUSIONS

Our study underlines the assertion that gross geometrical features are the dominant driving force of molecular self-organization. The various patterns found experimentally for the Fréchet dendron presented in this study serve as a versatile model system to systematically test our multimodeling approach. Five structural phases have been closely modeled by MM energy minimization; their quality is underlined in an exemplary manner by DFT LDOS simulations plotted adjacent to the STM image. Evaluating the van der Waals part of the MM determined adsorption energy favors an open pore trimer honeycomb structure in the initial phase of adsorption (energy per molecule maximized) and a densely packed pattern reminiscent of tire tracks after various phase transformations to reach the final state (energy per area maximized). The calculated energies are very similar reflecting the coexistence of phases for competing ordering motifs. Furthermore, we have refined our independent MC approach with a coarse grained interaction-site model of various internal angles and can successfully reproduce the experimental pattern diversity in all facets of the local and global ordering. The lowest energy pattern at $T=0$ can be identified in a zero-temperature analysis for the different chain conformations. All theoretical and experimental findings point to the tiretrack pattern as the thermodynamically most stable pattern for the dodecyl/octyl terminated Fréchet dendron. Furthermore, a newly predicted local ordering motif has been experimentally verified subsequently. We thoroughly and successfully tested an interaction-site approach to molecular self-organization, which will serve as an innovative analysis tool in the future fostering the application of self-organized molecular monolayers in various areas of science.

ACKNOWLEDGMENTS

Financial support by the German Excellence Initiative via the program "Nanosystems Initiative Munich (NIM)," ERA-Chemistry, Studienstiftung des dt. Volkes, IDK NanoBioTechnology, CeNS, NRP47, and the Swiss Nanoscience Institute is gratefully acknowledged. We thank K. Gruber for participating in the development of the interaction-site model and E. Constable for important chemical input to the latter model, C. Höhl for measuring the wave pattern with STM, L. Merz, M. Malarek, and L. Scherer for prior STM measurements on Fréchet-dendrons, L. Scherer and F. Trixler for discussing symmetries of patterns, D. Amann, L. Merz, and I. Widmer for finding measurement protocols, E. Constable, S. Graber, C. Housecroft, M. Malarek, P. B. Rheiner, D. Seebach, and L. Scherer for synthesis of compounds, M. Schönherr for input on MM energy optimization, P. Altpeter, H. Lorenz, and S. Schöffberger for support in the clean room, R. Gross, H. J. Güntherodt, J. Kotthaus, J. Rädler, and F. Simmel for usage of facilities and ongoing support. F. Jamitzky, R. Netz, P. Nielaba, S. Rohr, and A. Rubio are acknowledged for discussions.

[*] Author to whom correspondence should be addressed; b.hermann@cens.de

[1] G. Pawin, K. L. Wong, K. Y. Kwon, and L. Bartels, Science **313**, 961 (2006).

[2] J. Schnadt, E. Rauls, W. Xu, R. T. Vang, J. Knudsen, E. Lægsgaard, Z. Li, B. Hammer, and F. Besenbacher, Phys. Rev. Lett. **100**, 046103 (2008).

[3] A. Langner, S. L. Tait, N. Lin, C. Rajadurai, M. Ruben, and K. Kern, Proc. Natl. Acad. Sci. U.S.A. **104**, 17927 (2007).

[4] K. Tahara, S. Furukawa, H. Uji-i, T. Uchino, T. Ichikawa, J. Zhang, W. Mamdouh, M. Sonoda, F. C. De Schryver, S. De Feyter, and Y. Tobe, J. Am. Chem. Soc. **128**, 16613 (2006).

[5] J. V. Barth, Annu. Rev. Phys. Chem. **58**, 375 (2007).

[6] G. Tomba, L. C. Ciacchi, and A. De Vita, Adv. Mater. **21**, 1055 (2009).

[7] B. Ilan, G. M. Florio, M. S. Hybertsen, B. J. Berne, and G. W. Flynn, Nano Lett. **8**, 3160 (2008).

[8] D. X. Shi, W. Ji, X. Lin, X. B. He, J. C. Lian, L. Gao, J. M. Cai, H. Lin, S. X. Du, F. Lin, C. Seidel, L. F. Chi, W. A. Hofer, H. Fuchs, and H. J. Gao, Phys. Rev. Lett. **96**, 226101 (2006).

[9] J. V. Barth, G. Costantini, and K. Kern, Nature (London) **437**, 671 (2005).

[10] J.-M. Lehn, Science **295**, 2400 (2002).

[11] M. Ortega Lorenzo, C. J. Baddeley, C. Muryn, and R. Raval, Nature (London) **404**, 376 (2000).

[12] C. Joachim, J. K. Gimzewski, and A. Aviram, Nature (London) **408**, 541 (2000).

[13] K. Morgenstern, S. W. Hla, and K. H. Rieder, Surf. Sci. **523**, 141 (2003).

[14] C. Meier, U. Ziener, K. Landfester, and P. Weihrich, J. Phys. Chem. B **109**, 21015 (2005).

[15] C. Rohr, M. Balbás Gambra, K. Gruber, E. C. Constable, E. Frey, T. Franosch, and B. A. Hermann, Nano Lett. **10**, 833 (2010).

[16] A. Breitruck, H. E. Hoster, and R. J. Behm, J. Phys. Chem. C **113**, 21265 (2009).

[17] U. K. Weber, V. M. Burlakov, L. M. A. Perdigao, R. H. J. Fawcett, P. H. Beton, N. R. Champness, J. H. Jefferson, G. A. D. Briggs, and D. G. Pettifor, Phys. Rev. Lett. **100**, 156101 (2008).

[18] M. Haran, J. E. Goose, N. P. Clote, and P. Clancy, Langmuir **23**, 4897 (2007).

[19] A. Šarlah, E. Frey, and T. Franosch, Phys. Rev. Lett. **95**, 088302 (2005); Phys. Rev. E **75**, 021402 (2007).

[20] C. J. Hawker and J. M. J. Fréchet, J. Am. Chem. Soc. **112**, 7638 (1990); J. Chem. Soc., Chem. Commun. **1990**, 1010.

[21] B. A. Hermann, L. J. Scherer, C. E. Housecroft, and E. C. Constable, Adv. Funct. Mater. **16**, 221 (2006).

[22] Omitted due to a much smaller contribution.

[23] E. Constable, S. Graber, B. A. Hermann, C. E. Housecroft, M. S. Malarek, and L. J. Scherer, Eur. J. Org. Chem. **2008**, 2644 (2008).

[24] S. J. Clark, M. D. Segall, C. J. Pickard, P. J. Hasnip, M. I. J. Probert, K. Refson, and M. C. Payne, Z. Kristallogr. **220**, 567 (2005).

[25] A. K. Rappé, C. J. Casewit, K. S. Colwell, W. A. Goddard III, and W. M. Skiff, J. Am. Chem. Soc. **114**, 10024 (1992).

[26] Images flattened, correlation averaged, and drift-corrected.

[27] E. C. Constable, M. Haeusler, B. A. Hermann, C. E. Housecroft, M. Neuburger, S. Schaffner, and L. J. Scherer, Cryst. Eng. Comm. **9**, 176 (2007).

[28] Starting with an energy-minimized free molecule has failed at 150% minimization energies.

[29] Unit cell of two molecules in periodic boundary conditions.

[30] Electrostatic interactions contribute only 30%.

[31] With a Gaussian function of 2× a Pt d_z orbital, 200 pm.

[32] Eight free molecules at precisely MM-determined positions.

[33] Omitting electrostatic interactions.

[34] S. Yin, C. Wang, X. Qiu, B. Xu, and C. Bai, Surf. Interface Anal. **32**, 248 (2001).

[35] A. I. Kitaigorodskii, C. Wang, X. Qiu, B. Xu, and C. Bai, *Molecular Crystals and Molecules* (Academic Press, New York, 1973).

[36] L. Merz, H.-J. Güntherodt, L. J. Scherer, E. C. Constable, C. E. Housecroft, M. Neuburger, and B. A. Hermann, Chem.-Eur. J. **11**, 2307 (2005).

9.4 Predicting the Influence of a *p2*-Symmetric Substrate on Molecular Self-Organization with an Interaction-Site Model

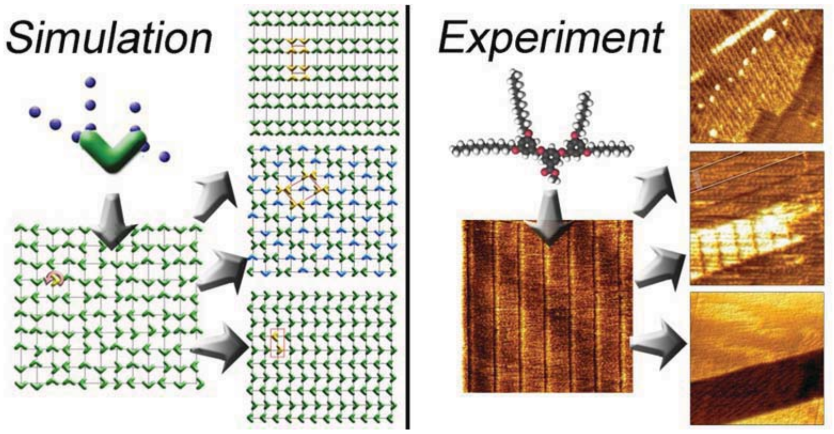

C. Rohr, M. Balbás Gambra, K. Gruber, C. Höhl, M. S. Malarek, L. J. Scherer, E. C. Constable, T. Franosch, B. A. Hermann

Chemical Communications, 2011, **47**, 1800-1802.

View Online

COMMUNICATION www.rsc.org/chemcomm | ChemComm

Predicting the influence of a *p*2-symmetric substrate on molecular self-organization with an interaction-site model†

Carsten Rohr,*[a] Marta Balbás Gambra,[b] Kathrin Gruber,[a] Cornelia Höhl,[a] Michael S. Malarek,‡[c] Lukas J. Scherer,§[c] Edwin C. Constable,[c] Thomas Franosch[bd] and Bianca A. Hermann*[a]

Received 1st September 2010, Accepted 1st November 2010
DOI: 10.1039/c0cc03603j

Downloaded by Technische Universitaet Muenchen on 01 February 2011
Published on 03 December 2010 on http://pubs.rsc.org | doi:10.1039/C0CC03603J

An interaction-site model can *a priori* predict molecular self-organisation on a new substrate in Monte Carlo simulations. This is experimentally confirmed with scanning tunnelling microscopy on Fréchet dendrons of a pentacontane template. Local and global ordering motifs, inclusion molecules and a rotated unit cell are correctly predicted.

Self-organization of supramolecular monolayers constitutes a major challenge for surface functionalization, sensors, catalysis, and molecular electronic devices.[1] The difficulty has been neatly summarized recently by Tomba *et al.*[2] who state "[...] the increasing complexity of the assembly units used makes it generally more difficult to control the supramolecular organization and *predict* the assembling mechanisms." Various approaches,[3] *via* synthetic routes, atomistic modelling or coarse-grained Monte-Carlo methods, have been adopted to predict patterns in a particular experiment. The ultimate goal is a generalized model, which can be fitted to individual experimental circumstances *e.g.* molecules, conformations, substrates, solvents while retaining its predictive power. Based on an interaction-site model, developed in a multi-modelling approach, we recently found with Monte-Carlo simulations that geometry as well as a few salient weak interaction-sites encode a large variety of structural motifs of a particular molecular conformation on a graphite substrate.[4]

In this communication, we demonstrate the versatility of interaction site models by predicting patterns on a new substrate with Monte Carlo simulations prior to measurements. Fréchet dendrons[5] exhibit a wide range of self-organized ordering motifs on highly oriented pyrolytic graphite (HOPG).[4] By employing pentacontane modified HOPG, we change the substrate's symmetry, lattice constant and adsorption energy. This serves as an intricate test for the applicability of the recently introduced interaction-site model[4] to a wider variety of experimental systems. New simulations have been performed on a rectangular lattice and successfully compared with scanning tunnelling microscopy (STM) images of Fréchet dendrons, growing on top of a pentacontane monolayer. Hence, we corroborate the predictive power of interaction site models for molecular self-organization. In particular, we highlight the importance of substrate symmetry on pattern formation.

The Fréchet dendron[6] methyl (3-[3,5-bis(dodecyloxyphenyl)-methoxy]-5-[3,5-bis(octyloxyphenyl)methoxy]benzoate) displays seven different ordering motifs on HOPG.[4] This second generation Fréchet dendron consists of three benzene rings, two of which carry flexible alkoxychains[6] which interact with the surface and drive the molecular self-organization *via* chain interdigitation,[7] see Fig. 1c. A variety of ordering motifs is expected,

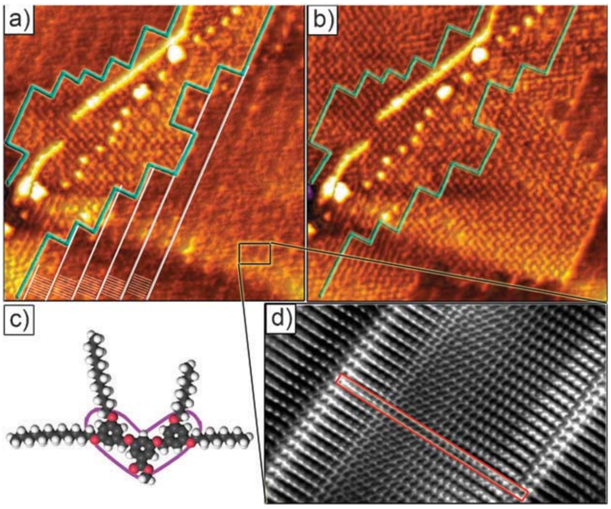

Fig. 1 Self-organized Fréchet dendron domains on top of a pentacontane monolayer: the upper STM images display the domain growth over time. (a) Rows of pentacontane are indicated in white, Fréchet dendron domain borders in green. The green outline of the Fréchet dendron domain follows the pentacontane rows. (b) Subsequent STM¶ image of the same spot. The distinct HOPG surface defects serve as recognition markers. The domain size from the left image is outlined in green. This indicates that the Fréchet dendron domains grow on top of pentacontane. (c) Space filling structure of the Fréchet dendrons with outlined molecular core. (d) High resolution image of a pentacontane monolayer on HOPG. The row like structure changes the HOPG surface from a sixfold to a twofold symmetry. Parameters: (a), (b) $U_{\mathrm{Bias}} = -400$ mV, $|I_{\mathrm{T}}| = 0.5$ pA, 80 nm × 80 nm; (d) $U_{\mathrm{Bias}} = -150$ mV, $|I_{\mathrm{T}}| = 30$ pA, 10 nm × 6 nm.

---

[a] *Center for Nano Science (CeNS) and Walther-Meissner-Institute of Low Temperature Research of the Bavarian Academy of Sciences, Walther-Meissner-Str. 8, 85748 Garching, Germany. E-mail: carstenrohr@gmx.de, b.hermann@cens.de*
[b] *Arnold Sommerfeld Center for Theoretical Physics (ASC) and Center for Nano Science (CeNS), Department of Physics, LMU München, Theresienstraße 37, 80333 München, Germany*
[c] *Department of Chemistry, University of Basel, Spitalstrasse 51, 4056 Basel, Switzerland*
[d] *Institut für Theoretische Physik, Universität Erlangen-Nürnberg, Staudtstrasse 7, 91058 Erlangen, Germany*

† Electronic supplementary information (ESI) available: STM measurement of the third pattern (wave), MC simulation of two additional interlaced patterns. See DOI: 10.1039/c0cc03603j

‡ Current address: Department of Chemistry and Biochemistry, La Sierra University, 4500 Riverwalk Pkway, Riverside, CA 92515, USA.

§ Current address: EMPA St. Gallen, Laboratory for Protection and Physiology, Lerchenfeldstrasse 5, 9014 St. Gallen, Switzerland.

This journal is © The Royal Society of Chemistry 2011

Downloaded by Technische Universitaet Muenchen on 01 February 2011
Published on 03 December 2010 on http://pubs.rsc.org | doi:10.1039/C0CC03603J

when these Fréchet dendrons organize on the new pentacontane modified HOPG substrate. The feasibility of modifying substrates with pentacontane was successfully introduced by Bai and Fichou *et al.*,[8] allowing us to change the surface symmetry to *p*2 and the lattice constants to (x = 0.4 nm, y = 0.3 nm).

Pentacontane was dissolved in tetradecane before applying a droplet onto the HOPG surface and raising the substrate temperature to 50 °C to evaporate the tetradecane. The Fréchet dendrons were applied from 0.2 mM solution in phenyloctane or ethanol. We have performed high-resolution STM imaging under ambient conditions employing a Nanoscope Multimode III equipped with a low-current converter.

In the STM images (see Fig. 1a and b) the uncovered row structure of pentacontane is visible, emphasized by white lines. A high-resolution close-up reveals the ladder-like pentacontane pattern with a unit cell of 6.5 nm × 0.4 nm in atomic resolution, see Fig. 1d. On pentacontane monolayers Fréchet dendrons self-organize in domains, encased in green in Fig. 1a. These domains precisely follow the row structure of the pentacontane substrate. We use the distinct bright HOPG defect features as position markers. A follow-up image of the same location has been taken, see Fig. 1b: the domain size indicated by the green borders shows that Fréchet dendrons domains grow on the pentacontane monolayer.

Two ordering motifs of self-organized Fréchet dendrons, "jigsaw" and "tiretrack", are identified on pentacontane. These domains grow and show Ostwald ripening over minutes to hours. An extended domain of a *p*2 symmetric "jigsaw" pattern is shown in Fig. 2a adjacent to rows of unoccupied pentacontane (indicated by white lines). In the "jigsaw" ordering two molecules arrange in a tip-on-tip geometry in a nearly rectangular unit cell, see inset Fig. 2a. This ordering motif is also found on HOPG.[4] The unit cell a = 3.2 nm, b = 2.6 nm, α = 86° is tilted with respect to the pentacontane rows and features an additional bright protrusion in the middle of four adjacent molecules. This might be an included molecule, which partially fits into the provided host cavity. On HOPG yet another pattern, referred to as "tiretrack", emerges.[4] There Fréchet dendrons interdigitate in a *p*2 symmetric double-row ordering. Such Fréchet "tiretrack" rows (blue lines) are found to run roughly perpendicularly to the pentacontane rows (white lines), as indicated in Fig. 2b. The unit cell parameters are a = 6.0 nm, b = 1.0 nm, α = 87°. The unit cells of all patterns show no measurable difference to HOPG within the error. The width of the Fréchet dendrons double-rows amounts to 6.0 nm which is close to the width of pentacontane rows (6.5 nm). Nevertheless, an easy identification is possible, since single Fréchet dendrons, measuring half the width of a double-row, accompany the regular double-row structure (marked with a red arrow in Fig. 2b). A third ordering motif, the "wave" patterns, resembles a similar pattern found on HOPG, the wave pattern.[4] This rarely occurring pattern is displayed in the ESI.† In summary, Fréchet dendrons grow on a pentacontane monolayer exhibiting twofold symmetry in two (three) ordering motifs, all with a *p*2 symmetric unit cell.

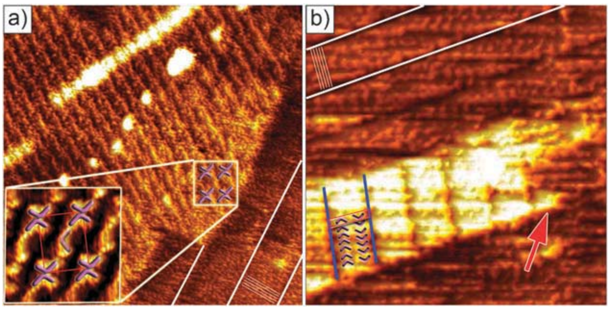

Fig. 2 Ordering motifs of Fréchet dendrons on pentacontane imaged by STM. (a) "Jigsaw" domain: the pentacontane rows are indicated in white. The black rectangle marks a 6 nm × 6 nm sized area. The inset in the lower left corner shows a high resolution image. Molecular backbones are overlaid and a unit cell is marked in red. (b) "Tiretrack" domain: again, pentacontane rows are marked in white. Fréchet dendron "tiretrack" rows are indicated in blue with a unit cell in red. The schematic representation of the molecular backbones illustrates the ordering.[4] The red arrow marks half a double-row of Fréchet dendrons (discussion see text). Parameters: (a) U_{Bias} = −400 mV, $|I_T|$ = 0.5/1 pA, 50 nm × 50 nm/6 nm × 6 nm; (b) U_{Bias} = −1000 mV, $|I_T|$ = 8 pA, 50 nm × 50 nm.

Prior to the STM measurements, we have predicted ordering motifs on a *p*2-symmetric lattice by independent Monte Carlo (MC) simulations. Based on a coarse-grained interaction-site model[4] the essential geometric features of the molecule and the substrate are condensed without including every chemical detail. The patterns discussed in this communication are obtained for two different pairs of internal angles (see Fig. 3e): conformer ε, 60° and 120°, conformer ζ, 60° and 180°, for long and short pairs of alkoxy chains. More chain angles on a hexagonal substrate are described elsewhere.[9] Here a new lattice is implemented in this interaction site model. The twofold symmetric substrate is realized *via* (a) model molecules arranged on a rectangular lattice and *via* allowing (b) four possible orientations of each model molecule.

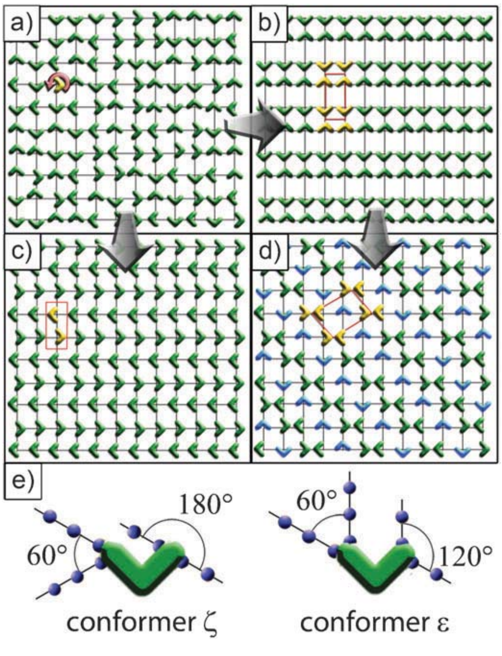

Fig. 3 Pattern prediction based on MC simulations of an interaction-site model. (a) Random starting configuration. The individual model molecules can rotate in fixed π/2 angles in a Monte-Carlo step. Slow cooling predicts the following patterns: (b) "jigsaw" and (d) "jigsaw with inclusion" for the chain configuration ε and: (c) "tiretrack" for the chain configuration ζ (two other patterns are displayed in the ESI†). (e) Detailed view of the chain configurations ζ and ε.

Downloaded by Technische Universitaet Muenchen on 01 February 2011
Published on 03 December 2010 on http://pubs.rsc.org | doi:10.1039/C0CC03603J

The MC simulations have been performed by preparing random starting configurations (see Fig. 3a) and slowly "cooling" them. The aspect ratio of the two lattice constants is held at a value of 7/8, which approximately reflects reaching equivalent positions perpendicular and along pentacontane rows. In a Monte Carlo step, $\pi/2$-rotations are possible on each lattice site. Allowing only π rotations would limit the freedom of orientations and would hence possibly restrict the so found patterns. The lattice constant a (and $b = 8/7a$) has been varied between $2.8a/\sigma$ and $4.2a/\sigma$, corresponding to a change in coverage density by a factor of 1.5, while the dimensionless inverse temperature ε/k_BT ranges from 0.025 to 6. All simulated patterns proved stable in the simulations up to 300 °C and are therefore considered to be stable at room temperature.

Fig. 3 displays three of the five found patterns for the conformers ε and ζ. Conformer ε: the first ordering exhibits dimeric units in a $p2$ symmetric tip-on-tip arrangement (for $3.8a/\sigma$), see Fig. 3b. Such a tip-on-tip arrangement matches the experimentally found "jigsaw" pattern (see Fig. 2a). When the lattice constant is increased ($4.0a/\sigma$) an "interlaced jigsaw" structure can be observed with inclusions of one model molecule per unit cell in non-fixed orientation, see Fig. 3d. The unit cell is then rotated with respect to the lattice axis, for another "interlaced jigsaw" pattern see ESI.† Conformer ζ: a $p2$ symmetric double-row pattern is found, comparable to the experimental "tiretrack" pattern ($3.8a/\sigma$), see Fig. 3c. (For this conformer an interlaced double-row structure can be obtained for a few other a/σ, see ESI.†) In the double-row pattern the third experimentally discovered pattern, "wave", is also encoded (again, see ESI†). Hence, the predicted patterns reflect the local and global symmetry of the experimentally identified ordering motifs as well as the interlacing with non-fixed molecules.

Fréchet dendrons on pentacontane molecules have a reduced adsorption energy (80.3 kJ mol^{-1} nm^{-2}) compared to Fréchet dendrons on HOPG (167.1 kJ mol^{-1} nm^{-2}), which we calculated using molecular mechanics (MM)‖ in Material Studio.[10] This reduced adsorption energy leads to a high orientational freedom ($\pi/2$ rotations instead of π-rotations) on the lattice sites. The experimentally observed inclusions in the "jigsaw" pattern can only be obtained in simulations when $\pi/2$ rotations are allowed.

The prediction of local molecular arrangements by the interaction-site model in its detail goes beyond considerations feasible by group theory. Nevertheless let us comment on the influence of a lower symmetric substrate for molecular self-organization. The symmetry groups of a twofold symmetric substrate are included in four-fold, *e.g.* Cu(100), or six-fold symmetric substrates, *e.g.* HOPG. Therefore, ordering motifs found on twofold surfaces can be expected to occur also on *e.g.* six-fold symmetric surfaces. The "tiretrack", "wave", and "jigsaw" ordering motifs observed on pentacontane are also found on the six-fold HOPG surface. Yet on HOPG two more hierarchical flat lying patterns are recognized exhibiting molecules with $\pi/3$ orientations relative to each other.[4] Strong molecule–surface interactions can constrain the molecular orientation along the symmetry axis of the substrate; hence, $\pi/3$ symmetric patterns are omitted on pentacontane. This underlines that the substrate, despite reduced adsorption energy, has a big influence and that substrates symmetry dictates molecular ordering.

In conclusion, we gain *a priori* predictability of ordering motifs of Fréchet dendrons on a new substrate. We have generalized the interaction-site approach to the most general surface symmetry ($p2$). The general applicability has been successfully demonstrated in a template experiment. Additionally, we find that a $p2$ symmetric substrate selects a subset of $p2$ symmetric patterns from a larger pattern variety observed on higher-symmetry substrates. Hence, substrate symmetry constrains the allowed ordering motifs. Prediction of ordering motifs on new substrates, prior to experimental observation, will not only greatly ease future surface functionalization, in particular of layered assemblies (3D), but also allow application directed chemical synthesis.

Financial support by the German Excellence Initiative *via* the "Nanosystems Initiative Munich (NIM)", ERA-Chemistry, Studienstiftung des dt. Volkes, IDK NanoBioTechnology, Elite Netzwerk Bayern (ENB), CeNS, NRP47, the University of Basel, Swiss Nanoscience Institute, Walther-Meissner-Institute and LMU-München is gratefully acknowledged. We thank S. Graber for help with molecule synthesis, E. Frey for help in the development of the interaction-site model, J. Büttner for fruitful discussions. J. Kotthaus for usage of his Nanoscope III and cleanroom facilities.

Notes and references

¶ All images are flattened, drift-corrected. Fig. 1d and the inset of Fig. 2a are correlation averaged. The color scale ranges from dark brown, over light brown, yellow to white.

‖ Molecular mechanics is performed with the Forcite module of Materials Studio 4.4 employing a universal force field. Energy calculations were performed on the "jigsaw" pattern.

1 (*a*) J. V. Barth, G. Costantini and K. Kern, *Nature*, 2005, **437**, 671; (*b*) J.-M. Lehn, *Science*, 2002, **295**, 2400; (*c*) O. Lorenzo, C. J. Baddeley, C. Muryn and R. Raval, *Nature*, 2000, **404**, 376; (*d*) C. Joachim, J. K. Gimzewski and A. Aviram, *Nature*, 2000, **408**, 541.
2 G. Tomba, L. C. Ciacchi and A. De Vita, *Adv. Mater.*, 2009, **21**, 1055.
3 J. V. Barth, *Annu. Rev. Phys. Chem.*, 2007, **58**, 375; B. Ilan, G. M. Florio, M. S. Hybertsen, B. J. Berne and G. W. Flynn, *Nano Lett.*, 2008, **8**, 3160; U. K. Weber, V. M. Burlakov, L. M. A. Perdigao, R. H. J. Fawcett, P. H. Beton, N. R. Champness, J. H. Jefferson, G. A. D. Briggs and D. G. Pettifor, *Phys. Rev. Lett.*, 2008, **100**, 156101; A. Breitruck, H. E. Hoster and R. J. Behm, *J. Phys. Chem. C*, 2009, **113**, 21265; A. Sarlah, T. Franosch and E. Frey, *Phys. Rev. Lett.*, 2005, **95**, 088302; A. Sarlah, E. Frey and T. Franosch, *Phys. Rev. E: Stat., Nonlinear, Soft Matter Phys.*, 2007, **75**, 021402.
4 C. Rohr, M. Balbás Gambra, K. Gruber, E. C. Constable, E. Frey, T. Franosch and B. A. Hermann, *Nano Lett.*, 2010, **10**, 833.
5 C. J. Hawker and J. M. J. Fréchet, *J. Am. Chem. Soc.*, 1990, **112**, 7638; C. J. Hawker and J. M. J. Fréchet, *J. Chem. Soc., Chem. Commun.*, 1990, 1010; B. A. Hermann, L. J. Scherer, C. E. Housecroft and E. C. Constable, *Adv. Funct. Mater.*, 2006, **16**, 221.
6 E. Constable, S. Graber, B. A. Hermann, C. E. Housecroft, M. S. Malarek and L. J. Scherer, *Eur. J. Org. Chem.*, 2008, 2644.
7 L. Merz, H.-J. Güntherodt, L. J. Scherer, E. C. Constable, C. E. Housecroft, M. Neuburger and B. A. Hermann, *Chem.–Eur. J.*, 2005, **11**, 2307.
8 B. Xu, S. Yin, C. Wang, X. Qiu, Q. Zeng and C. Bai, *J. Phys. Chem. B*, 2000, **104**, 10502; L. Piot, A. Marchenko, J. Wu, K. Müllen and D. Fichou, *J. Am. Chem. Soc.*, 2005, **127**, 16245.
9 B. A. Hermann, C. Rohr, M. Balbás Gambra, A. Malecki, E. Frey and T. Franosch, *Phys. Rev. B: Condens. Matter Mater. Phys.*, 2010, **82**, 165451.
10 A. K. Rappé, C. J. Casewit, K. S. Colwell, W. A. Goddard and W. M. Skiff, *J. Am. Chem. Soc.*, 1992, **114**, 10024.

Supplementary Material (ESI) for Chemical Communications
This journal is (c) The Royal Society of Chemistry 2011

Electronic Supplementary Information (ESI)

Interaction-site model prediction of molecular self-organization on *p2*-substrate symmetry

C. Rohr,*[a] M. Balbás Gambra,[b] K. Gruber,[a] C. Höhl,[a] M. Malerek,[c] L. Scherer,[c] E. C. Constable,[c] T. Franosch,[b,d] B.A. Hermann*[a]

[a] *Center for Nano Science (CeNS) and Walther-Meissner-Institute of Low Temperature Research of the Bavarian Academy of Sciences, Walther-Meissner-Str. 8, 85748 Garching, Germany*
[b] *Arnold Sommerfeld Center for Theoretical Physics (ASC) and Center for Nano Science (CeNS), Department of Physics, LMU München, Theresienstraße 37, 80333 München, Germany*
[c] *Department of Chemistry, University of Basel, Spitalstrasse 51, 4056 Basel, Switzerland*
[d] *Institut für Theoretische Physik, Universität Erlangen-Nürnberg, Staudtstrasse 7, 91058 Erlangen, Germany*
E-Mail: b.hermann@cens.de

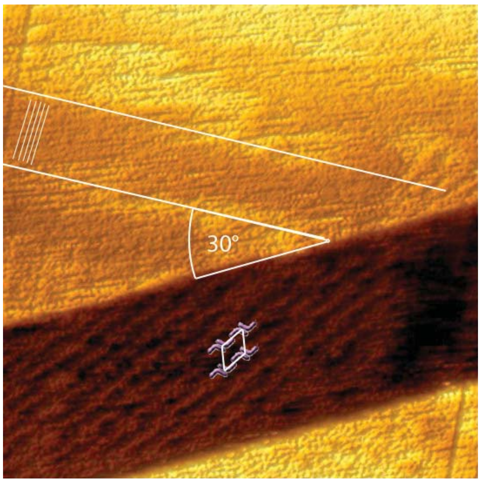

Fig.S1: “Wave” ordering of Fréchet-dendrons on pentacontane imaged by STM. Rarely observed “wave” domain is visible in the dark brown graphite depression. The schematic ordering is indicated with the unit cell and schematic molecular backbones. Slightly visible are adjacent pentacontane rows on the higher graphite terraces (yellow area) indicated by the white lines. The pentacontane rows have the characteristic 30° angle with respect to the graphite substrate. Parameters: a) U_{Bias} = - 800 mV, $|I_{\mathrm{T}}|$ = 0.3 pA, 40 nm x 40 nm.

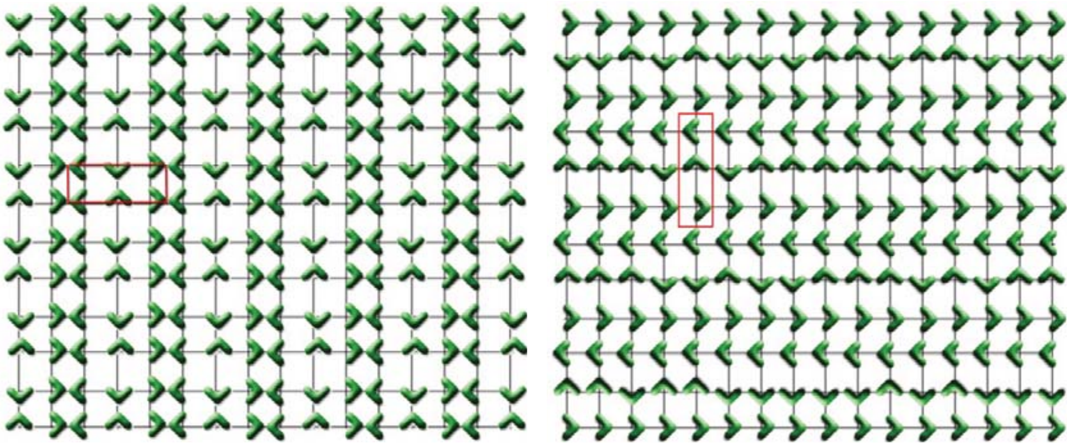

Fig.S2: Monte-Carlo simulated interlaced ordering motifs. (a) Second interlaced “jigsaw” structure found for conformer ζ. The interlacing molecules have a fixed orientation (b) Interlaced “tiretrack” structure found for conformer ε with interlacing rows of non-fixed orientation.

9.5 Simulating Patterns for Molecular Self-Organization on Surfaces Using Interaction-Site Models

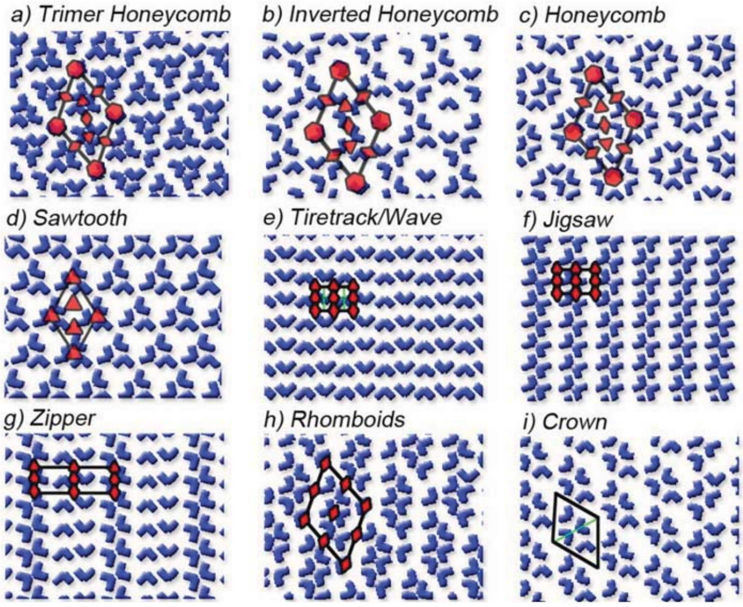
a) Trimer Honeycomb
b) Inverted Honeycomb
c) Honeycomb
d) Sawtooth
e) Tiretrack/Wave
f) Jigsaw
g) Zipper
h) Rhomboids
i) Crown

M. Balbás Gambra, **C. Rohr**, K. Gruber, B. A. Hermann, T. Franosch
(submitted).

Predicting patterns for molecular self-organization on surfaces using interaction-site models

Marta Balbás Gambra,[1] Carsten Rohr,[2] Kathrin Gruber,[2] Bianca Hermann,[2] and Thomas Franosch[3, 1]

[1] *Arnold Sommerfeld Center for Theoretical Physics (ASC) and Center for Nano Science (CeNS),*
Fakultät für Physik, Ludwig-Maximilians-Universität München, Theresienstraße 37, 80333 München, Germany
[2] *Walther–Meißner Institute for Low Temperature Research and Center for NanoScience,*
Department of Physics, Ludwig-Maximilians-Universität München,
Walther–Meißner Str. 8, 85748 Garching, Germany
[3] *Institut für Theoretische Physik, Friedrich-Alexander-Universität*
Erlangen-Nürnberg, Staudtstraße 7, 91058 Erlangen, Germany

(Dated: 13th January 2011)

Molecular building blocks interacting at the nanoscale organize spontaneously into stable monolayers that display intriguing long-range ordering motifs on the surface of atomic substrates. The patterning process, if appropriately controlled, represents a viable route to manufacture practical nanodevices. With this goal in mind, we seek to capture the salient features of the self-assembly process by means of an *interaction-site model*. The geometry of the building blocks, the symmetry of the underlying substrate, and the strength and range of interactions encode the self-assembly process. By means of Monte Carlo simulations, we have predicted an ample variety of ordering motifs which nicely reproduce the experimental results. Here, we explore in detail the phase behavior of the system in terms of the temperature and the lattice constant of the underlying substrate. Our method is suitable to investigate the stability of the emergent patterns as well as to identify the nature of the melting transition monitoring appropriate order parameters.

PACS numbers: 89.75Fb, 81.16.Dn, 81.16.Fg, 05.65.+b, 89.75.Kd

I. INTRODUCTION

Molecular building blocks interacting at the nanoscale organize spontaneously into stable ordered monolayers [1]. The patterns that emerge upon self-organization of simple supramolecular units display a variety of symmetries and local ordering motifs with different degrees of packing on the surface. Currently such surface coatings are under active research due to their potential applications in nanoscience, such as surface functionalization [2], sensor surfaces [3], or molecular electronics [4]. The theoretical challenge is to provide tools that allow to predict the patterns without performing the actual measurements for the supramolecular units [5]. Most approaches rely on atomistic modeling where the stable conformations are calculated using experimental measurements of the molecular conformations on the surface as input. There, the molecular subunit is resolved in all chemical details, resulting in a large number of degrees of freedom that have to be included in the modeling. In molecular mechanics calculations (MM) [6] and molecular dynamics simulations (MD) [7, 8] the molecular interactions are parametrized by semi-empirical force fields which requires a significant number of additional parameters. In MM the starting conformations are energy-minimized resulting in a stable configuration, yet the method intrinsically provides only the closest local minimum. In contrast, MD simulations sample different minima and incorporate, in principle, also dynamical reconfigurational processes. The quantum aspects such as the electronic density of states (DOS) measurable in scanning tunneling microscopy (STM) can be computed using density functional theory (DFT) [8, 9], yet these calculations are limited to small systems.

Recently, a complementary approach has been introduced employing coarse-grained models which aim at predicting certain features of the patterns with the benefit of a great reduction of complexity. For example, using an effective hamiltonian accounting for the energetics of the respective orientations of neighboring molecules, local ordering motifs for oligopyridine supramolecules on a surface have been successfully reproduced [10]. For mixtures of melamines, PTCDI, and PTCDA structural stability diagrams of two competing patterns have been reported [11, 12] using effective pair energies between neighboring molecules on a lattice. For the case of flexible organic molecules, we have recently shown that a multi-method approach combining MM, DFT, and Monte Carlo simulations is capable of providing reliable predictions for the emerging multiple coexisting patterns on surfaces [13–15].

In this paper we provide a detailed discussion of the theoretical aspects of the use of interaction-site models for Fréchet dendrons. In particular, we discuss how salient features of the molecular structure can be identified and used to tailor a suitable coarse-grained model and then be studied by means of Monte-Carlo methods. Furthermore, we show that a phase diversity naturally emerges in agreement with experimental studies and discuss the corresponding phase stability as the packing fraction on the substrate or the temperature is varied. Then we provide a thorough discussion on the merits of the approach and its limitations as well as possible extensions.

II. EXPERIMENTALLY OBSERVED PATTERNS

In this Section we first summarize the experimental findings on molecular self-organization for Fréchet dendrons [16, 17]. These second generation Fréchet dendrons are flexible supramolecules, which consist of three phenyl rings symmetrically disposed at the vertices of a triangle with two alkoxychains attached at each lateral phenyl ring. The arms of these chains consist at one side of the molecule of twelve carbon atoms, and on the other side of eight carbon atoms—see the structural formula in Fig. 1.

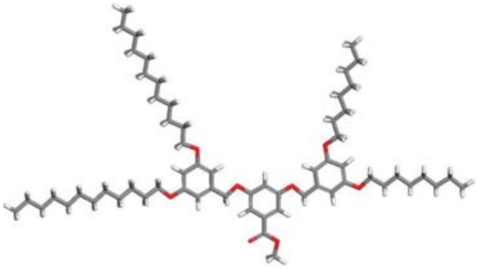

Figure 1: Stick model of the asymmetric Fréchet dendron used in the experiments.

Scanning tunneling microscopy (STM) images show that a large variety of self-organized ordering motifs on top of highly oriented pyrolytic graphite (HOPG) emerges [18, 19]. This substrate exhibits a honeycomb-like surface with a six-fold rotational symmetry. Seven general ordering motifs have been reported, five of which are flat-lying configurations [13]. The tiretrack, wave, honeycomb, sawtooth, and jigsaw motifs are displayed in Fig. 2. These patterns coexist on the HOPG surface and phase transform over time into the thermodynamically stable tiretrack pattern. The schematics of the ordering motifs, Fig. 2, have been obtained employing atomistic modeling by molecular mechanics energy minimizations using the Forcite module of Materials studio 4.3 and employing a universal force field.

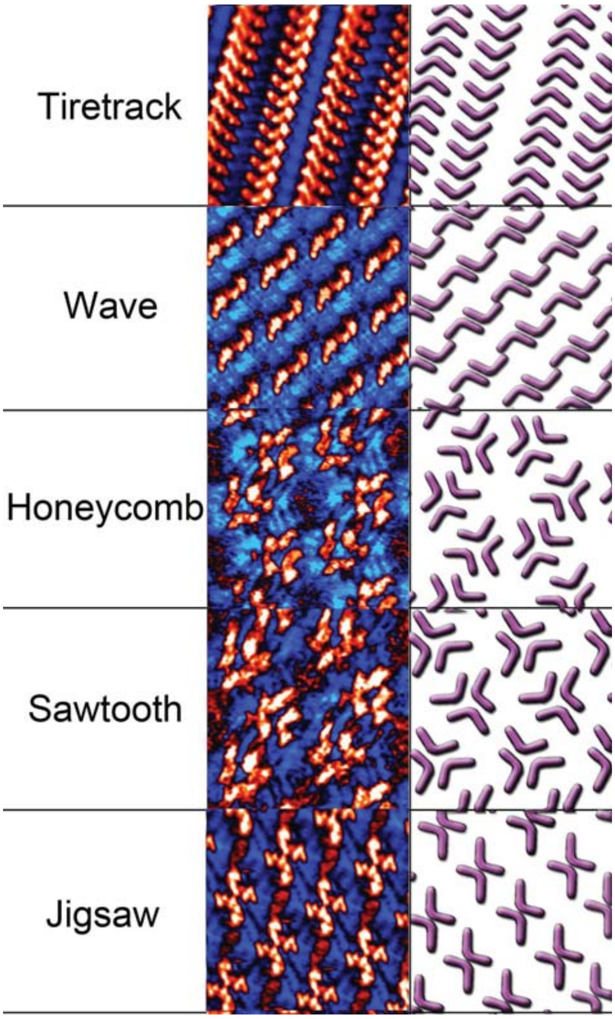

Figure 2: Five experimentally observed patterns for Fréchet dendrons. STM images on the left and the corresponding schematic ordering motifs on the right.

III. THE INTERACTION-SITE MODEL

To obtain reliable predictions of the emergent pattern in the assembly of monolayers without any *a priori* knowledge from the experiments, a drastic reduction of complexity is highly desirable. Here, we propose an *interaction-site model* which aims to provide a suitable description of the self-organization process. The basic idea is to reduce the numerous microscopic forces to a few representative interactions acting on groups of selected points. The major challenge consists of appropriately identifying the positions of the interaction centers and forces relevant for the self-organization. We will demonstrate in this paper that the geometry of the building blocks, the symmetry of the substrate, and the coupling of both are key elements in the self-organization of monolayers. We will show for an experimental model based on Fréchet dendrons, that the interaction-site model properly captures the essence of the system, predicts the observed patterns, as well as the temperature regime at which they are stable. Moreover, monitoring suitable order parameters, we are able to identify in principle the nature and location of the melting transition.

A. Construction of the interaction sites

The Fréchet dendron introduced above is a suitable and especially versatile model system to asses the validity of an interaction-site approach in the prediction of self-organized monolayers. According to the experimental observations the crucial features leading to the self-organization are the steric repulsion between the molecular rings, the weak interactions of the carbonated chains, as well as the coupling of the building blocks with the substrate. We model the symmetric molecular core as three *hard spheres* of radii r_r located at the vertices of a flattened isosceles triangle—large spheres in the sketch of Fig. 3. The long base of the triangle is twice of its height l, hence all three interaction sites have equal distance l from the center of the base. The carbonated chains of the molecules are modeled by a small number of sites with Lennard-Jones interactions. Four neighboring CH_2 units of the alkoxychain are coarse-grained to one Lennard-Jones site—small spheres in Fig. 3. The interaction sites are arranged in straight, rigid arms with their centers separated by a distance σ.

The radii of the hard spheres and the range of Lennard-Jones interaction, the distance of the former to the molecular center, as well as the length and orientation of the arms are the parameters of the model. These geometrical features are obtained from the conformations which minimize molecular mechanics simulations (MM) starting from an initial configuration derived from a detailed analysis of the experimental STM images, Fig. 2. The relevant length scales of the Fréchet dendrons range approximately from 15 Å of the skeleton to 50 Å for the extended molecule, with $l = 6.1$ Å, $r_r = 2.6$ Å and $\sigma = 6$ Å.

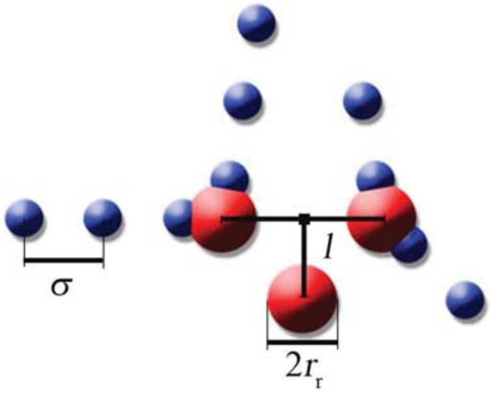

Figure 3: Interaction-site model for a Fréchet dendron in conformation α. Large spheres account for aromatic rings, whereas the small spheres represent subunits in the carbonated chains. Every sphere represents four CH_2 units in the arms of the dendrons.

We encode the strong intermolecular steric interaction between the aromatic rings by hard-sphere repulsions between the three central spheres of different molecules, preventing the cores of the molecules from overlapping. The weak, short-ranged van-der-Waals attraction of the lateral chains is described by a Lennard–Jones potential: $V(r) = 4\,\epsilon\left[(\sigma/r)^{12} - (\sigma/r)^{6}\right]$ among beads in chains of different molecules. Thus ϵ corresponds to the minimum energy which occurs at $r = 2^{1/6}\sigma$.

The atomically flat graphite surface which constitutes the template for the pattern formation, offers six energetically equivalent orientations for the molecule. The molecule-substrate attraction is mainly mediated by π-interactions between the phenyl-rings and the chains with the graphite surface, and the total adsorption energy is about ten times larger than the total intermolecular interaction. In addition, as the size of the entire molecule, around 45 Å, is up to ten times larger than the lattice constant (a few Å), only the symmetry of the underlying substrate plays a role in the monolayer assembly. In our modeling the molecules are fixed at the sites of a coarse-grained, fully occupied triangular lattice. The lattice constant a is comparable to the size of the building blocks and the lattice exhibits the same symmetry as the original graphite honeycomb structure. The Fréchet dendrons may rotate by discrete angles as rigid bodies around their centers and adopt one of the six preferred orientations of the underlying graphite.

The interaction-site model accomplishes a significant reduction of degrees of freedom, setting the flexibility of the molecule aside. While the actual physical system contains hundreds of atoms per molecule able to displace and rotate independently, the coarse-grained interaction-site model consists of a rigid object with no other degrees of freedom than the rotation around its center.

In addition to the conformation closest to the experimental findings, Fig. 3, we explore the Fréchet dendron in five alternative conformations by varying the orientations of the arms, as displayed in Fig. 4, where the angles follow the symmetry directions of the substrate.

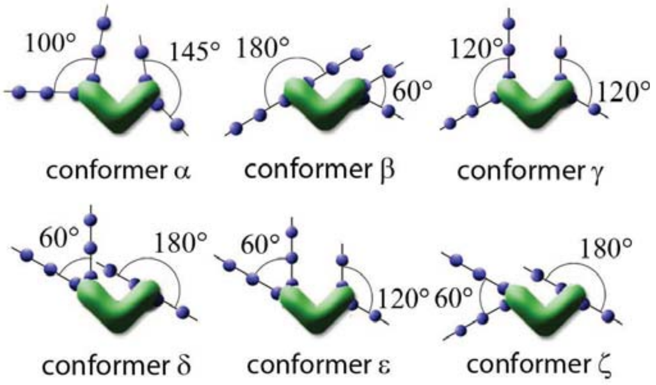

Figure 4: Molecular conformations showing different orientations of the lateral straight arms. The angles of the arms with respect to the positive x-axis are given clockwise from the left to the right for the five additional conformations: $\beta = (-5\pi/6, 5\pi/6, 5\pi/6, -\pi/6)$, $\gamma = (-5\pi/6, \pi/2, \pi/2, -\pi/6)$, $\delta = (-5\pi/6, \pi/6, \pi/2, \pi/6)$ $\epsilon = (-5\pi/6, \pi/2, \pi/2, \pi/6)$, $\zeta = (-5\pi/6, \pi/6, \pi/6, -\pi/6)$.

B. Predictions of the model

To find the regular patterns emerging in the self-organized monolayers we have run Monte Carlo (MC) simulations [20–22] considering some hundred to a few thousand molecules which corresponds also to the experimental situation: a single dendron covers a surface of approximately 4 nm^2 and the samples imaged with STM occupy some hundred nm^2. The lattice constant which essentially fixes the packing fraction of the monolayer has been varied from $a = 2.8\,\sigma$ to $a = 4.2\,\sigma$ covering the experimental regime. To ensure that the stable patterns are assumed in the simulations, simulated annealing [23–25] has been employed. Random configurations, where molecules assume a random direction among the six possible orientations, have been chosen as initial configurations. Starting at a given temperature the system evolves via Monte Carlo moves by performing $\pi/3$ rotations. We have run 500 MC sweeps [32] to equilibrate the sample and measure the energy and order parameters during another 1000 Monte Carlo sweeps before lowering or raising the temperature. Then the temperature is lowered and the process is repeated. The system is cooled down to temperatures around 170 K, low enough for our purpose, given that the experiments were performed at room temperature.

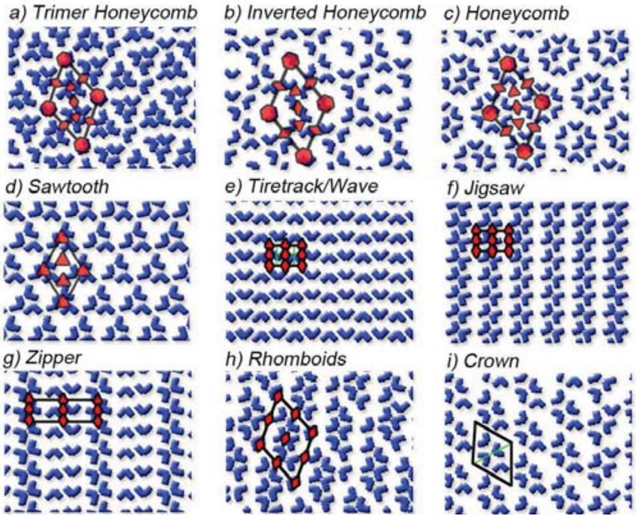

Figure 5: Ordered motifs found by simulated annealing for the Fréchet dendrons with different conformations within the interaction-site model. Molecules are represented as wedges matching their three aromatic rings. The carbonated arms are omitted for clarity.

An abundant variety of ordered patterns arises by cooling samples of the interaction-site model in all conformations, see Fig. 5. These patterns display different degrees of symmetries [26] which are subgroups of the $p6m$ symmetry (six-fold rotation, mirror symmetry) of the underlying lattice mimicking the graphite substrate. The honeycomb, trimer and inverted honeycomb structure, see Fig. 5, display a $p6$ symmetry, i.e. the sixfold rotational symmetry is still present, yet the mirror symmetry of the substrate is broken. The sawtooth pattern exhibits only a $p3$ with threefold rotations of the unit cell. In the tiretrack/wave pattern rows of aligned units emerge with opposite directions resulting in a $p2gg$ symmetry, i.e. a twofold rotational symmetry and glide-mirror axes. The class of $p2$ symmetric patterns consists of the jigsaw, zipper and rhomboid ordering. Here the jigsaw unit cell is comprised only of two units arranged in a head-to-head configuration, whereas the more exotic zipper contains four molecules in a unit cell, the rhomboid pattern even six building blocks. The lowest symmetry cm consisting of a mirror axis and a glide mirror axis, yet no rotational symmetry, is realized in the crown pattern, where four molecules order in a head-in fashion.

Table I lists the patterns found in the cooling process for the different conformations. Some patterns turn out to be only metastable and the ground state may change upon varying the packing fraction. The configuration α which resembles most closely the experimental configuration displays a significantly larger variety of patterns.

To asses the stability of the emergent patterns, we have prepared perfectly ordered configurations at low temperatures and heated them up slowly while monitoring the evolution of the energy and suitable order parameters. Thus, one can identify metastable phases which directly transform into a disordered state. In particular, one can estimate the melting temperature of the broken symmetry phase and determine whether the transition is continuous or discontinuous.

The order parameter is defined explicitly for every pattern, based on the fraction of molecules in a given sublattice following its preferred orientation. Indeed, one can distinguish various sublattices in which the molecules point in the same direction; for instance, alternating rows in the tiretrack/wave pattern represent two different sublattices. Thus, for a sublattice A with N_A molecules and preferred orientation σ^A, the partial order parameter reads

$$m_A = \frac{N_A^{\sigma_A}}{N_A} - \frac{1}{5} \sum_{\sigma_i \neq \sigma_A} \frac{N_A^{\sigma_i}}{N_A}. \qquad (1)$$

The factor 1/5 is introduced to ensure that $m_A = 0$ in a disordered phase where all six orientations are equiprobable. The global order parameter we monitor is just the average of the order parameters m_i over all sublattices n_s

$$m = \sum_{i=1}^{n_s} \frac{m_i}{n_s}. \qquad (2)$$

The thermal fluctuations of the order parameter encode the linear response of the system with respect to a fictitious external aligning field. Then a susceptibility can be defined as

$$\chi_m = \frac{N}{k_B T} \left(\langle m^2 \rangle - \langle m \rangle^2 \right). \qquad (3)$$

and its behavior as a function of temperature is indicative of the nature of the transition. Similarly, we measure in the Monte Carlo simulation the average energy per molecule $\langle u \rangle$ and the corresponding fluctuations

$$c_N = \frac{N}{k_B T^2} \left(\langle u^2 \rangle - \langle u \rangle^2 \right), \qquad (4)$$

which represents the specific heat per particle.

The simulation results are exemplified in Fig. 6 for the melting transition of the sawtooth phase as a function of the reduced temperature k_BT/ϵ. The average energy and the order parameter drop in a small temperature interval suggesting a first order melting transition. The corresponding susceptibilities exhibit corresponding peaks close to the transition temperature, and are interpreted as smeared delta functions. Yet, we cannot exclude a continuous transition, and finite size scaling would be needed to clarify the order of the transition. In this work we focus on the pattern diversity and have not pursued this issue any further.

Configuration	Patterns
α	**Tiretrack/wave** **Sawtooth** **Jigsaw** **Honeycomb** Rhomboid
β	**Sawtooth** **Tiretrack/wave**
γ	**Tiretrack/wave** Honeycomb inverted Honeycomb
δ	**Trimer Honeycomb**
ϵ	**Jigsaw** **Trimer Honeycomb** Crown
ζ	**Tiretrack/wave** Zipper

Table I: Emerging ordered phases by cooling down samples with $N = 576$ Fréchet dendrons for the chain conformations $\alpha, \ldots, \zeta$. The phases in bold font are stable under heating, while the other phases would be unstable in an experiment at room temperature.

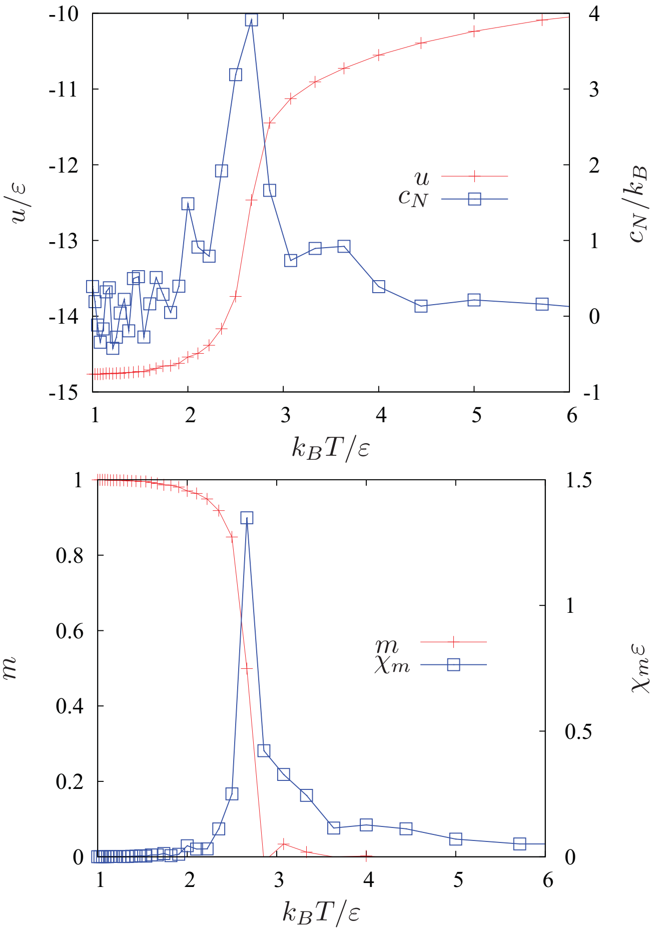

Figure 6: Melting transition for the sawtooth phase. Top: Energy and heat capacity per molecule as a function of the dimensionless temperature. Botom: Order parameter and susecptibility. The simulation was performed for $N = 576$ Fréchet dendrons in the β conformation on a lattice with $a/\sigma = 3.8$.

C. Comparison to experiments

The interaction-site model reproduces many of the features of the experimental model system consisting of Fréchet dendrons on graphite surfaces. First, in both systems an ample diversity of patterns emerges suggesting that the basic building blocks are correctly transferred from the Molecular Mechanics calculations to the interaction-site model. Furthermore, the patterns found in the theoretical model closely resemble the experimental ones both in its global and local ordering motifs, i.e. the structure displays the same wallpaper group [26] and a similar arrangement of the molecules in a unit cell.

In the highly symmetric trimer honeycomb structure three molecules align in a subunit facing each other. The resulting trimer exhibits a threefold rotational symmetry without additional mirror symmetry implying that the trimer is chiral. These trimers order in sixfold symmetric arrangement where a single molecule of unspecified orientation resides at its center, see Fig. 5a). In the experimental system precisely the same structure has been observed where the center of the hexagons appear as blurred regions in the STM measurements [15]. Thus it appears that these unpaired molecules are free to change their orientation rapidly, much faster than the time resolution of the STM [27].

The tiretrack/wave pattern is characterized by alternating columns of molecules pointing in the same direction. Then in the corresponding rows of this pattern every second molecule possesses the same orientation. Depending on the conformation of the arms of the molecule, the pattern is formed by strong intracolumn interactions with moderately coupled columns, or by strongly linked rows that then arrange in a parallel fashion. Similar to the theoretical model, the experimental system displays a tiretrack and a wave pattern where molecules arrange in rows or columns, respectively, see Fig. 2e. Experimentally the coupling in the rows and columns is significantly different resulting into two clearly distinguishable phases, although wave and tiretrack belong to the same wallpaper group. For the simulations on a coarse-grained lattice this distinction can no longer be made and both phases merge into a single tiretrack/wave pattern.

Our simulations also reproduce the sawtooth pattern, Fig. 5d, which has been observed in STM measurements on Fréchet dendrons. Here three molecules form a composite which constitutes the repeat unit on a triangular lattice. In contrast the experiments report a lower wallpaper group, *p*2 rather than *p*3, since here two trimers arrange in a opposite orientation to form a unit cell, compare Fig. 2.

For the case of the jigsaw pattern, Fig. 5f, we find almost perfect agreement with the STM images, both with respect to the local ordering as well as with respect to the wallpaper group.

The remaining patterns we have generated in the interaction-site model have not been found for Fréchet dendrons. The first group of patterns (Fig. 5a-c) are all highly symmetric and very similar in their respective local motifs and therefore these structures may be very sensitive to the conformation and the details of the molecule. Thus it appears promising to modify the chemical structure of the Fréchet dendron only slightly to realize also the inverted honeycomb and the honeycomb structure. The second group of simulated patterns without corresponding experimental result consists of large complex unit cell with low symmetry (Fig. 5g-i). Therefore even if some of these patterns constitute the ground state of the system it is likely that they are not realized experimentally due to kinetic barriers.

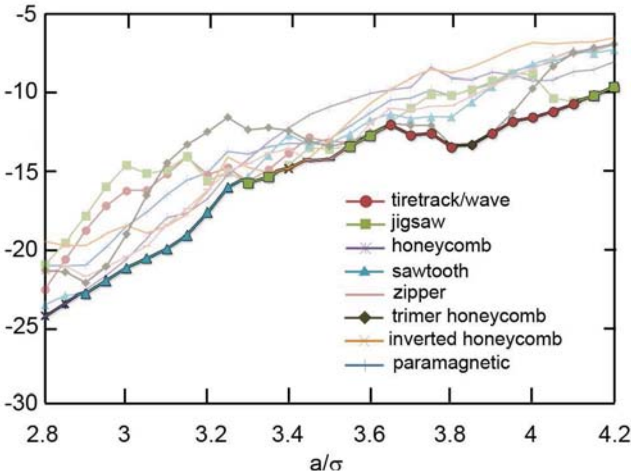

Figure 7: Zero temperature energies for conformation γ as a function of the lattice constant. The ground state corresponding to the lowest energy depends sensitively on the packing fraction demonstrating that the competing ordering motifs display similar energies.

The energies of the various patterns are rather similar in agreement with the experimental observation of coexisting metastable phases. After annealing in the experiments or sufficiently many Monte Carlo steps in the simulation the patterns are expected to transform to the stable pattern. For temperatures relevant in the experiment these patterns are almost always identified with the ground state of the system. Which of the suggested patterns actually represents the ground state depends critically on the density. We exemplify the subtle interplay of the effects of packing and ordering for conformation γ in Fig. 7 which displays one of the most complex behaviors. For high packing fractions (small lattice constant) first the honeycomb pattern and then the sawtooth pattern corresponds to the ground state. For moderate densities the tiretrack/wave exhibits the lowest energy and experimentally it also is found as the most stable pattern.

We have shown that interaction-site models are a powerful approach to model pattern formation of complex supramolecules on a substrate. In particular, the pattern diversity is correctly transferred from the molecular mechanics minimizations and also details of the patterns such as symmetries and local ordering motifs are surprisingly well reproduced. Let us discuss limitations and possible improvements of the current model. First, the interaction-site model so far accounts only for the dominant van der Waals interactions, yet on closer inspection electrostatic interactions could be also important for the selection of a particular motif. From the molecular mechanics calculations one infers that these forces are responsible for up to 30% of the intermolecular interaction. It would be desirable to model also these electrostatic interactions and test if more accurate results can be achieved. Similarly, in the case of highly directional forces, such as hydrogen bonds, one should explicitly incorporate these specific interactions in the interaction site model. Second, the model does not account for the effects of the solvent. Nevertheless some solvents interact via hydrogen bonds with the Fréchet dendrons and may favor conformations of the Fréchet dendrons where oxygen atoms are exposed to the solvent. Since the conformations are crucial for the corresponding patterns one should also account for the solvent effect in the interaction-site model. For example, one could attribute an additional conformational energy for each molecule and then compare the total energy, consisting of both conformational as well configurational energy, and thus determine the stable pattern and stable conformation in a specific solvent. Furthermore the lattices considered so far are fully occupied, which excludes complex motifs with host structures. In the interaction-site model one could account for this possibility by either a fixed partial coverage density (canonical ensemble) or a fixed chemical potential (grand canonical ensemble) and include hopping processes in addition to the rotational Monte Carlo moves. Last, we have reduced the molecule-substrate interaction to the lattice symmetry and spacing. The major justification for this simplification is that the supramolecules are significantly larger than a unit cell of the substrate and correspondingly experience only an averaged adsorption energy with preferential directions. Yet, for smaller molecules, larger substrate lattice constants, or specific interactions one should include explicit space-resolved molecule-substrate interactions.

IV. CONCLUSIONS AND OUTLOOK

In this work, we have developed an interaction-site model which correctly predicts the ordered motifs of assembled monolayers. By reducing the degrees of freedom and considering the building-blocks as rigid bodies with a reduced set of interacting points, we have demonstrated that the self-organization relies on very general features of the system considered: the coupling with the substrate, the geometry of the building blocks, and their weak interactions. These are universal principles in self-organizing systems which do not depend on the specific nature of the building blocks and the underlying substrate—our method also works for substrates exhibiting different geometries. Therefore, the predictive power provided by our model may guide the synthesis of suitable building blocks to engineer arbitrary patterns for specific goals. The versatility offered to construct the building blocks makes our model especially suitable to explore a wide range of geometries.

In addition, we have shown that by combining simulated annealing with a subsequent slow heating of the system, one can not only predict the emergent patterns, but also their stability upon heating and the nature of the transition into a disordered phase. We have found that a broad variety of long-range ordered phases are stable for various conformations of the building blocks and density regimes which may indeed coexist, as it has been observed in the experiments. The melting temperatures of the ordered motifs range from approximately 500 K to 1500 K, much higher than the room temperature where the experiments were performed.

However, the model still lacks an active determination of the intramolecular conformation. Here we have considered the building blocks as rigid bodies with the conformations observed in the molecular mechanics minimizations. A natural generalization would be to make the building blocks flexible and explore the interplay between intra and inter-molecular ordering. This extension implies including at least four new degrees of freedom per molecule, the orientations of the arms, which makes the Monte Carlo simulations computationally very expensive. An interesting alternative to speed up simulations would be to rely on genetic algorithms [28, 29]. They are suitable methods to compute the ground states of two-dimensional systems by minimizing the energy of single unit cells [30, 31]. The conformations and motifs resulting from this minimization can serve as input configurations for the Monte Carlo simulations to assess their stability. In this way, the interaction-site model is less dependent on the details of the external input. In addition, when employing genetic algorithms one can relax the constraint of the substrate. Instead considering the building blocks to be attached to the sites of a lattice, one can mimic the role of the substrate through arbitrary potentials. This opens a way to investigate systems whose substrates display more complex symmetries and interactions with the building-blocks.

V. ACKNOWLEDGEMENTS

We thank Erwin Frey stimulating discussions. MBG gratefully acknowledges the financial support of La Caixa and DAAD. C.R. has been supported by the "Studienstiftung des deutschen Volkes“ and the "Elite Network Bavaria“. This project is supported by the German Excellence Initiative via the program "Nanosystems Initiative Munich (NIM)."

[1] L. Bartels, Nature Chemistry **2**, 87 (2010).
[2] J. V. Barth, G. Costantini, and K. Kern, Nature **437**, 671 (2005).
[3] J. M. Lehn, Science **295**, 2400 (2002).
[4] C. Joachim, J. K. Gimzewski, and A. Aviram, Nature **408**, 541 (2000).
[5] G. Tomba, L. Ciacchi, and A. D. Vita, Adv. Mat. **21**, 1055 (2009).
[6] D.X. Shi, W. Ji, X. Lin, B. He, J.C. Lian, et al., Phys. Rev. Lett. **96**, 226101 (2006).
[7] W. Chen, H. Li, H. Huang, Y.X. Fu, H. L. Zhang, et al., J. Am. Chem. Soc. **130**, 12285 (2008).
[8] B. Ilan, G. M. Florio, M. S. Hybertsen, B. J. Berne, and G. W. Flynn, Nano Letters **8**, 3160 (2008).
[9] H. Glowatzki, B. Bröker, R. P. Blum, O. T. Hofmann, A. Vollmer, et al., Nano Letters **8**, 3825 (2008).
[10] A. Breitruck, H. Hoster, and R. Behm, J. Phys. Chem. C **113**, 21265 (2009).
[11] F. Silly, U.K. Weber, A.Q. Shaw, V.M. Burlakov, M.R. Castell, et al., Phys. Rev. B **77**, 201408 (2008).
[12] U.K. Weber, V. M. Burlakov, L.M.A. Perdigão, R.H.J. Fawcett, P.H. Beton, et al., Phys. Rev. Lett. **100**, 156101 (2008).
[13] C. Rohr, M. Balbás Gambra, K. Gruber, E. Constable, E. Frey, et al., Nano Letters **10**, 833 (2010).
[14] B. Hermann, C. Rohr, M. Balbás Gambra, A. Malecki, M.S. Malarek, et al., Phys. Rev. B **82**, 165451 (2010).
[15] C. Rohr, M. Balbás Gambra, K. Gruber, C. Höhl, M.S. Malarek, L.J. Scherer, et al., Chem. Comm. (2011), doi: 10.1039/c0cc03603j.
[16] C.J. Hawker, J.M.J. Fréchet, J. Am. Chem. Soc. **112**, 7638 (1990).
[17] C.J. Hawker and J.M.J. Fréchet, J. Chem. Soc., Chem. Commun, 1010 (1990).
[18] B. A. Hermann, L. J. Scherer, C. E. Housecroft, and E. C. Constable, Adv. Funct. Mater. **16**, 221 (2006).

[19] E. C. Constable, M. Häusler, B. A. Hermann, C. E. Housecroft, M. Neuburger, et al., Cryst. Eng. Comm. **9**, 176 (2007).

[20] D. Frenkel and B. Smit, *Understanding molecular simulation: from algorithms to applications* (Academic Press, 2002).

[21] D. P. Landau and K. Binder, *A guide to Monte Carlo simulations in statistical physics* (Cambridge University Press, 2005).

[22] K. Binder and D. Heermann, *Monte Carlo simulation in statistical physics: an introduction* (Springer Verlag, 2002).

[23] S. Kirkpatrick, Journal of Statistical Physics **34**, 975 (1984).

[24] S. Kirkpatrick, C. Gelatt, and M. Vecchi, Science **220**, 671 (1983).

[25] V. Černý, Journal of optimization theory and applications **45**, 41 (1985).

[26] D. Schattschneider, Amer. Math. Monthly **85**, 439 (1978).

[27] L. Merz, H.-J. Güntherodt, L. J. Scherer, E. C. Constable, C. E. Housecroft, et al., Chem.-Eur.J. **11**, 2307 (2005).

[28] S. Forrest, Science **261**, 872 (1993).

[29] J. H. Holland, Scientific American **267**, 66 (1992).

[30] J. Fornleitner, F. L. Verso, G. Kahl, and C. N. Likos, Soft Matter **4**, 480 (2008).

[31] D. Gottwald, G. Kahl, and C. N. Likos, J. Chem. Phys. **122**, 204503 (2005).

[32] The orientation of every molecule is updated on average once at every MC sweep.

9.6 Multi-Hierarchical Assembly via Molecular Flexibility

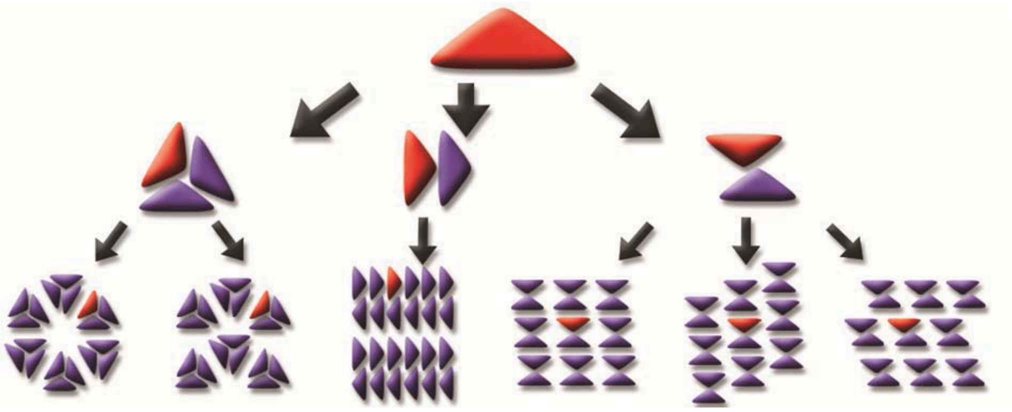

C. Rohr, K. Gruber, M. S. Malarek, E. C. Constable, B. A. Hermann
(submitted).

Hierarchical Self-Organization

DOI: 10.1002/anie.200((will be filled in by the editorial staff))

Multi-hierarchical assembly via molecular flexibility**

Carsten Rohr, Kathrin Gruber, Michael S. Malarek, Edwin C. Constable and Bianca A. Hermann*

Molecular monolayers on surfaces exemplify the emergent property of hierarchical ordering phenomena in self-organization processes.[1-6] Recently, the hierarchical construction of multiple structures from a common building block was demonstrated using self-organization of DNA origami.[7] For self-organization at surfaces, such hierarchical organization into multiple structures has not yet been demonstrated. Molecular multi-purpose building blocks, would give access to a wide variety of self-organized patterns, for the creation of functional surfaces. The ability to predict possible properties of the resulting patterns purely from the chemical structure could replace the prevalent trial and error approach and aids in the design of self-organized structures.

In this work we present a Fréchet Dendron building block that organizes into multiple second level structures, which in turn order into multiple third level patterns on an HOPG surface. While the pattern variety itself can be successfully reproduced by Monte-Carlo modeling[8], the mechanism behind this multi pattern formation is left open by the simulation. We explain this versatility to form multiple second level structures by the flexibility of the molecule. Finally, we connect the general properties of the lower level building blocks with resulting features such as the symmetry of the higher level structures.

In hierarchical self-organization individual molecular building blocks create regular second level aggregates. These in turn order into larger third level structures. Each subsequent level of assembly is held together by increasingly weaker interactions.[1,2] making it possible to disassemble the structure into its lower level constituents by breaking the weakest bonds.[9] In a more interesting type of hierarchical assembly, molecules do not form a single second level structure, but rather form several different second level structures, which can then themselves create multiple third level structures, see figure 1 a.

Our system is composed of molecules, which order into regular hierarchic patterns on the surface of highly oriented pyrolitic graphite (HOPG). The employed Fréchet dendrons,[10] see figure inset in figure 1 b, are flexible molecules containing three benzene rings, two bearing alkoxy chains[11,12] which can change their conformation and drive the molecular self-organization via chain interdigitation. The three Fréchet dendrons of slightly varying alkoxy chains lengths (**1**-**3**) all show multi-hierarchical assembly. The multiple orderings are imaged by a Nanoscope III scanning tunneling microscopy (STM) with low-current converter under ambient conditions at room temperature. A typical STM measurement of the hierarchical pattern highlighting the different levels of organization is displayed in figure 1 b. The first level encompasses the individual molecule. Two molecules in an antiparallel orientation form a second level building block, which then builds the next stage at the pattern level.

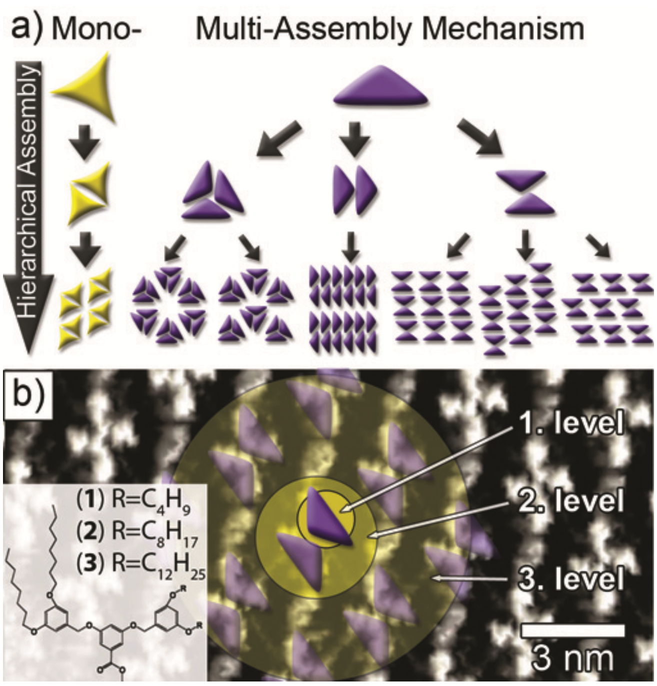

Figure 1. Types of hierarchical self-organization. a, Scheme of hierarchical assembly via three levels that results in one pattern for the common mono-hierarchical. In the more interesting multi-hierarchical case different second level building blocks are possible, which assemble into several multiple third-level structures. b, Scanning tunneling microscopy measurement of a hierarchical self-organized pattern of **3**. The three levels of assembly (1st level building block, 2nd level building block, pattern) are highlighted in yellow. 20 nm x 10 nm, U_{Bias}= - 800 mV, $|I_T|$= 8 pA.

When observing the Fréchet dendrons cast from different solvents (tetradecane, 2,2,2-trifluorethanol, dichlormethane, *N,N*-dimethylformamide, hexanoic acid, hexane and ethanol) onto highly oriented pyrolitic graphite (HOPG) multiple patterns exhibiting

---

[∗] C. Rohr, K. Gruber, Dr. B. A. Hermann
Center for Nano Science (CeNS) and Walther-Meissner-Institute of Low Temperature Research of the Bavarian Academy of Sciences
Walther-Meissner-Str. 8, 85748 Garching (Germany)
Fax: (+49) 89 289 14206
E-mail: carstenrohr@gmx.de

Dr. L. J. Scherer, Dr. M. S. Malarek,
Prof. Dr. E. C. Constable
Department of Chemistry
University of Basel
Spitalstr. 51, 4056 Basel (Switzerland)

Dr. M. S. Malarek
Department of Chemistry and Biochemistry
La Sierra University
4500 Riverwalk Pkwy, Riverside, CA 92515 (USA)

[∗∗] Financial support by the German Excellence Initiative via the program “Nanosystems Initiative Munich”, ERA-Chemistry, the Swiss National Science Foundation and the University of Basel is gratefully acknowledged. C.R. acknowledges the “Studienstiftung des deutschen Volkes“ and the “Elite Network Bavaria“ (IDK Nanobiotechnology).

different hierarchical orderings can be found.[8] A similar multiplicity of patterns can be found when observing the Fréchet dendrons after the evaporation of hexane solutions over time. In total eight different patterns were found, six of which are flat-lying configurations and will be discussed in detail, the measurements are depicted in figure 2. The different patterns can be observed experimentally under two different conditions, either as metastable states towards thermodynamic equilibrium in one solvent e. g. hexane or as the thermodynamic end phases for different solvents. Through molecular mechanics modelling (MM) we found that all six patterns are hierarchical three level assemblies. The molecular mechanics energy minimizations were performed using the Forcite module of Materials Studio 4.4 employing a universal force field and periodic boundary conditions of the unit cell.[13] The insets of figure 2 schematize the ordering of the different patterns. The molecular cores are represented by boomerang shapes. Three different second level building blocks build up the six different patterns.

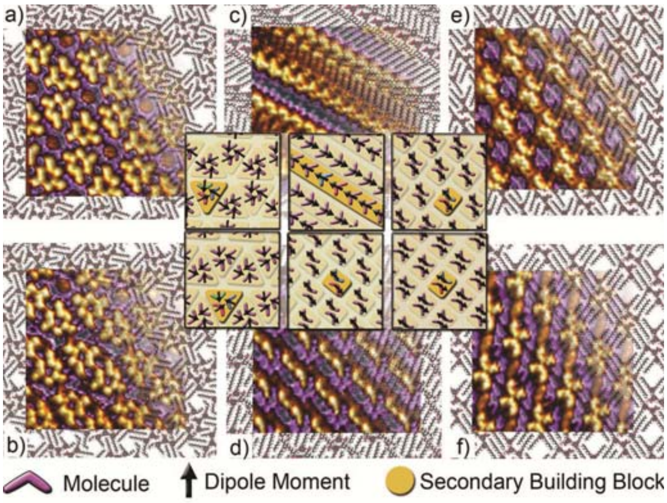

Figure 2. Multi-hierarchical assembly resulting in phase variety. STM measurements of the complete series of six flat-lying multi-hierarchical assemblies, most of which are found for each of the three flexible Fréchet dendrons in different solvents. The measurements are faded into the corresponding molecular mechanics simulations. The inset displays each molecular ordering schematically. The dipole moment of each molecule is indicated. The secondary building blocks highlighted in yellow, show either an anti-parallel, closed-flux or a parallel ordering of the dipole moments. The same secondary building blocks are the constituents of different patterns, leading to the branched multi-hierarchical assembly of figure 1. 12 nm x 12 nm U_{Bias}= - 800 mV, $|I_T|$= 8 pA to 80 pA. (see supporting information for large scale version.)

Focusing on the second level building blocks the molecules can order in triplets resulting in a triangular unit. These can be arranged in either a hexagonal honeycomb pattern or sawtooth appearance resulting from a row wise dislocation compared to the honeycomb pattern, see figure 2 a,b. In the next type of second level structure the molecules point in the same direction, thereby forming a row-like next level unit. These rows arrange in an antiparallel manner producing a double-row structure, see figure 2 c. The third kind of building block is comprised of two molecules in an antiparallel orientation. Three different third level patterns, a checkerboard assembly and patterns with row displacements in vertical and horizontal directions, are formed from this second level building block, see figure 2 d-f. Of these ordering motifs molecule **1** shows the four patterns in figure 2 a-c, f, molecule **2** the patterns a-e and molecule **3** the patterns a-d,f. In all, this self-organised system shows six hierarchical patterns with overlapping second level building blocks demonstrating the versatility of this multi-hierarchical assembly for self-organisation on surfaces.

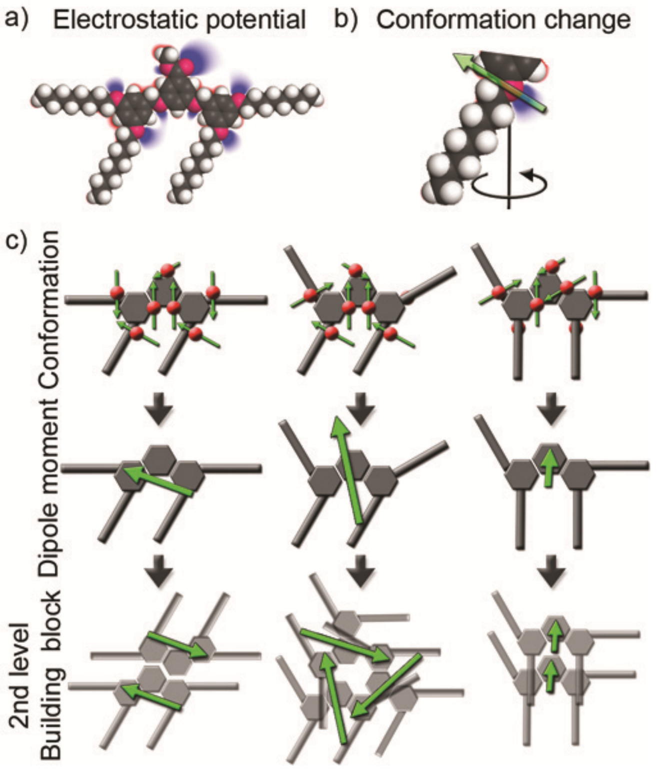

Figure 3. Formation of different second level building blocks from a flexible molecule. a, Electrostatic potential overlaid over the space filling model of the flexible Fréchet dendron. b, The dipole moment (green arrow) at each of the alkoxy arms can change its orientation via a change in conformation. c, The flexible Fréchet dendron in different arm conformations results in different orientations and magnitudes of the net molecule dipole moment. Depending on the orientation and strength of the dipole moment the second level building blocks prefer the anti-ferromagnetic, flux closure or ferromagnetic ordering.

Although several different solvents and three different Fréchet dendrons were studied, all three second level building blocks are found for each of the three molecules. Their formation can be understood in the light of the molecules flexibility and its dipole moment. Other interactions like higher electrostatic expansions and hydrogen bonds are omitted due to their small contribution. The van der Waals forces are mainly mediated by the chains of the molecule and are important for next higher level of organisation.[1]

The Fréchet dendrons have an electrostatic potential of intermediate strength, which is mainly located at the alkoxy chains, see figure 3 a. The electrostatic potential was calculated using the DMol³ module of Materials studio 4.4 using the Perdew Wang ′91 (GGA) potential. The oxygen atom located at the beginning of the alkoxy chains gives rise to a small dipole moment. When changing the conformation of the alkoxy side chain the direction of the dipole moment associated with the oxygen atom also changes its orientation, see figure 3 b. For a given fixed conformation of the Fréchet dendron the multiple smaller dipole moments of the different parts of the molecule can be added up and reduced to a global in plane dipole moment for the whole molecule. Depending on the molecule´s conformation this dipole moment has different orientations and magnitudes, see figure 3 c.

The three second level building blocks differ in the orientation of the dipole moment of their constituent molecules and thus in their resulting ordering. In the first case the dipole moment parallel to the molecular core leads to an anti-parallel arrangement of the molecules within the second level building block, see figure 3 c left. The largest dipole moment, see figure 3 c middle results in a larger second level building block, where three molecules order triangularly in a closed flux motif. The upward pointing dipole moment of the third configuration in figure 3 c right orders the molecules in a parallel row structure. This conformation with the smallest magnitude of molecular dipole moment is also the only second level building block with a net dipole moment, which is only balanced in the next level of the assembly. In summary, the configurational flexibility allows the molecule to arrange in three different second level structures induced by their varying molecular dipole moments.

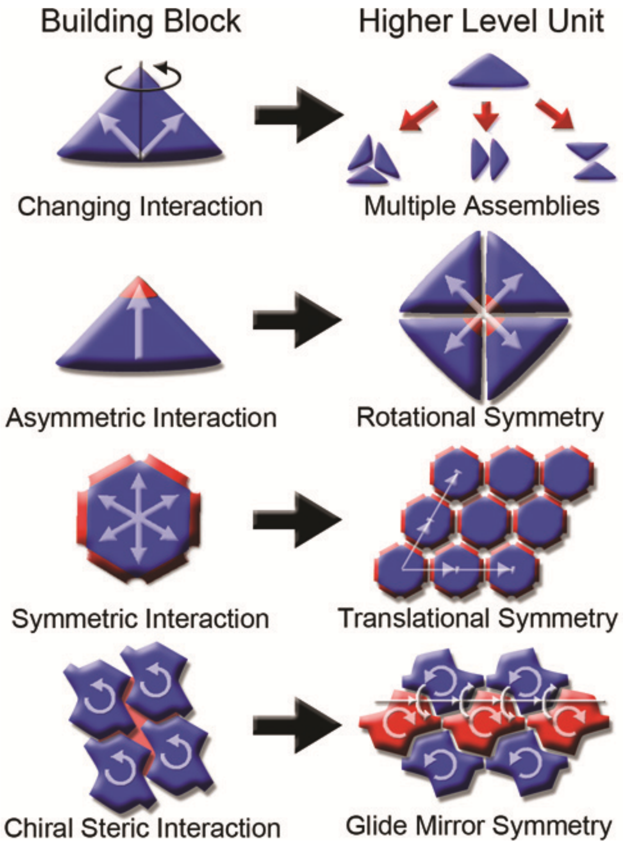

Figure 3. Scheme of the properties of the molecular building block and the resulting features of the pattern. Changing direction, strength or type of the dominant interaction produces multiple possible assemblies for the next level. Asymmetric interactions within a building block result in the next level of hierarchical assembly in a rotational symmetric building block. Building blocks of rotationally symmetric interactions lead to a repeat attachment in different directions and translational symmetry. Glide mirror symmetries result from the more dense racemic packing compared to sterically hindered enantiomerically pure assemblies.

The possibility of changing the interactions of the building block (direction, magnitude or type) enables the formation of different subsequent level assemblies, branching the hierarchical distribution; see figure 1 a and 4. In general, the properties of the building block enable different types of features for upper level structures in the hierarchical assembly,[1,8,14] see figure 4. Building blocks with an interaction of non-rotational symmetry will form a rotationally symmetric unit at the upper levels. If the building blocks have rotationally symmetric interactions the assembly of the subsequent level has translational symmetry. These two properties can also be seen in our hierarchical assembly. For completeness glide mirror symmetry results from steric chiral interactions, a two-dimensional variant of Wallach´s rule.[15] It states that racemic mixtures in general have a denser packing than their enantiomerically pure counterparts which is favourable in Kitajgorodskij´s principle of close packing.[16] So the properties of the building blocks used in the self-organisation process fundamentally predetermine the type of resulting assembly

In this paper we have shown an experimental system with multi-hierarchical assembly in two dimensions using self-organised molecules. The six hierarchical patterns shown by this one type of molecule are a combination of three different types of second level building blocks. Their diversity is caused by the conformational flexibility of the molecule and the resulting differences in dipole moments. Knowledge of the basic properties of the building blocks leads to conclusions about specific features of higher level structures, for example symmetry, in the hierarchical assembly. The control of building block properties of the self-organised pattern is crucial know-how for the conscious tailoring of functional surfaces. Correlating elementary features to the emergent properties of hierarchical assemblies is essential for the progressing change from a trial and error approach to full prediction of the self-organization in advance.

Experimental Section

A Nanoscope III with low-current converter was utilized at ambient conditions for STM measurements. The molecules were cast from 0.2 mM hexane or ethanol solutions onto HOPG. All images were flattened, drift-corrected and all small scale images correlation averaged. The molecular mechanics energy minimizations were performed using the Forcite module of Materials Studio 4.4 employing a universal force field and periodic boundary conditions of the unit cell.[13] The electrostatic potential was calculated using the $DMol^3$ module of Materials studio 4.4 using the Perdew Wang ´91 (GGA) potential.

Received: ((will be filled in by the editorial staff))
Published online on ((will be filled in by the editorial staff))

Keywords: Scanning probe microscopy · Self-assembly · Supramolecular chemistry · Hierarchy · Building block

---

[1] Y. Yang, C. Wang, *Chem. Soc. Rev.* **2009**, *38*, 2576-2589.
[2] F. Vonau, D. Suhr, D. Aubel, L. Bouteiller, G. Reiter, L. Simon, *Phys. Rev. Lett.* **2005**, *94*, 066103.
[3] H. Spillmann, A. Dmitriev, N. Lin, P. Messina, J. V. Barth, K. Kern, *J. Am. Chem. Soc.* **2003**, *125*, 10725-10728.
[4] D. Écija, K. Seufert, D. Heim, . Auwärter, C. Aurisicchio, C. Fabbro, D. Bonifazi, J. V. Barth, *ACS Nano* **2010**, *4*, 4936-4942.
[5] L. Piot, C. Marie, X. Feng, K. Müllen, D. Fichou, *Adv. Mater.* **2008**, *20*, 3854-3858.
[6] M.-C. Blüm, E. Ćavar, M. Pivetta, F. Patthey, W.-D. Schneider, *Angew. Chem.* **2005**, *44*, 5334-5337.

[7] Y. He, T. Ye, M. Su, C. Zhang, A. E. Ribbe, W. Jiang, C. Mao, *Nature* **2008**, *452*, 198-202.

[8] C. Rohr, M. Balbás Gambra, K. Gruber, E. C. Constable, E. Frey, T. Franosch, B. A. Hermann, *Nano Lett.* **2010**, *10*, 833-837.

[9] A. S. Klymchenko, S. Furukawa, K. Müllen, M. Van der Auweraer, S. De Feyter, *Nano Lett.* **2007**, *7*, 791-795.

[10] C. J. Hawker, J. M. J. Fréchet, *J. Am. Chem. Soc.* **1990**, *112*, 7638-7647.

[11] E. C. Constable, S. Graber, B. A. Hermann, C. E. Housecroft, M. S. Malarek, L. J. Scherer, *Eur. J. Org. Chem.* **2008**, *15*, 2644-2651.

[12] L. Merz, H.-J. Güntherodt, L. J. Scherer, E. C. Constable, C. E. Housecroft, M. Neuburger, B. A. Hermann, *Chem. Eur. J.* **2005**, *11*, 2307-2318.

[13] A. K. Rappé, C. J. Casewit, K. S. Colwell, W. A. Goddard III, W. M. Skiff, *J. Am. Chem. Soc.* **1992**, *114*, 10024-10035.

[14] B. A. Hermann, C. Rohr, M. Balbás Gambra, A. Malecki, M. S. Malarek, E: Frey, T. Franosch, *Phys. Rev. B* **2010**, *82*, 165451.

[15] O. Wallach, *Liebigs Ann. Chem.* **1895**, *286*, 90-143.

[16] A. I. Kitajgorodskij, *Acta Crystallogr.* **1965**, *18*, 585-590.

Supporting Information:

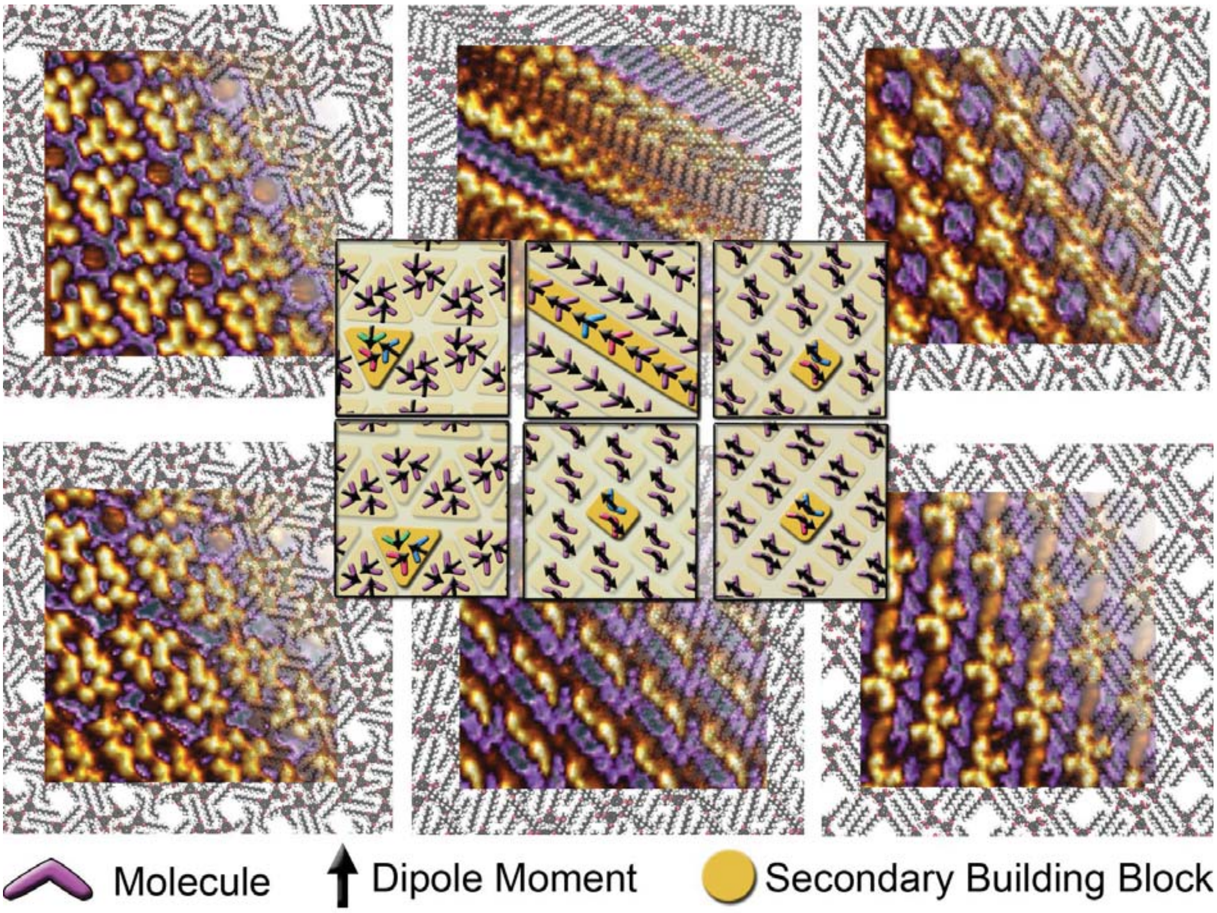

Figure S1. Multi-hierarchical assembly resulting in phase variety. STM measurements of the complete series of six flat-lying multi-hierarchical assemblies, most of which are found for each of the three flexible Fréchet dendrons in different solvents. The measurements are faded into the corresponding molecular mechanics simulations. The inset displays each molecular ordering schematically. The dipole moment of each molecule is indicated. The secondary building blocks highlighted in yellow, show either an anti-parallel, closed-flux or a parallel ordering of the dipole moments. The same secondary building blocks are the constituents of different patterns, leading to the branched multi-hierarchical assembly of figure 1. 12 nm x 12 nm U_{Bias}= -800 mV, $|I_{\mathrm{T}}|$= 8 pA to 80 pA

9.7 Surface Control of Chirality, Orientation and Hierarchical Assembly of Self-Organized Monolayers

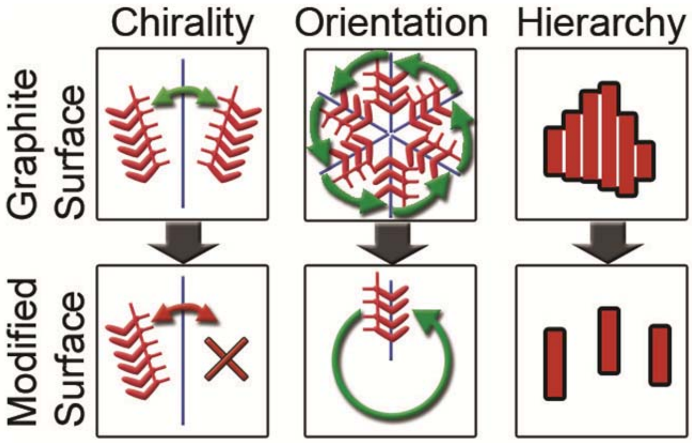
Chirality
Orientation
Hierarchy
Graphite Surface
Modified Surface

C. Rohr, K. Gruber, M. S. Malarek, E. C. Constable, B. A. Hermann
(submitted).

Self-Organization

DOI: 10.1002/anie.200((will be filled in by the editorial staff))

Surface control of chirality, orientation and hierarchical assembly of self-organized monolayers[**]

Carsten Rohr[*], Kathrin Gruber, Michael S. Malarek, Edwin C. Constable and Bianca A. Hermann

The simple and convenient control of functional monolayers[1,2] is a major prerequisite for their applicability in real world devices such as sensors[3], catalysis[4] and molecular electronic devices.[5] To this end, the following subset of monolayer properties have been engineered: chirality, domain orientation and hierarchy of assembly. Of these properties, the study of chirality is the most prevalent in recent reports.[6,7] A variety of successful approaches for inducing or spatially separating chiral domains in self-organized monolayers have been reported, relying on chiral solvents[8], the 'sergeants-and soldiers'[9] principle or the use of magnetic fields.[10] Regarding substrate effects "…so far there are only a few systematic studies in which the substrate has a profound effect on monolayer chirality"[6]. While the number of domain orientations is changed by the substrate´s symmetry, hierarchical assembly is usually not influenced by the substrate.[11] The routes taken to change hierarchical nature, i.e. the levels of an assembly, include chemical modification[12] of the building blocks or increasing/decreasing kinetic barriers between the building blocks via temperature[13] or electrostatic potential[14]. Up until now, methods have relied on special conditions such as ultra-high vacuum or magnetic fields, necessitating the use of advanced equipment thereby limiting the study of these self-assembly controls to only the most well-equipped laboratories. A new methodology allowing for the study of these controls under ambient conditions would undoubtedly contribute greatly to their applicability and the potential combination with other methods.

In this work we present an alternative approach to direct self-organized monolayers on surfaces combining the control of chirality, orientation and the hierarchy of assembly. We achieve this control by employing a buffer layer of self-organized *n*-alkanes, conveniently altering the surface properties and directing the molecular self-assembly on top. We explain the observed behavior employing symmetry arguments as well as complementary molecular mechanics calculations. Our study highlights the importance and utility of the substrate employed in self-assembly, a factor often neglected due to difficulties in influencing the surface. Our elegant method yields a novel perspective and provides new tools for scientists trying to direct molecular self-assembly.

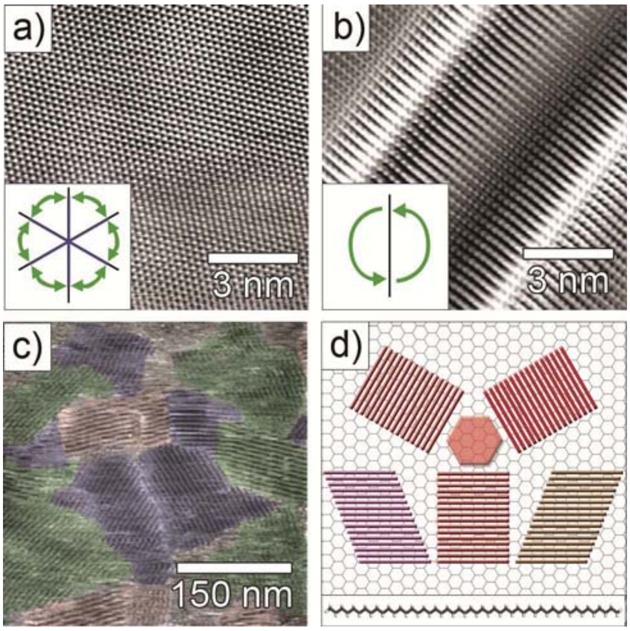

Figure 1. Properties of the pentacontane surface. a) A scanning tunneling microscopy image of an HOPG surface exhibits six-fold rotational symmetry as well as mirror symmetry. b) An adlayer of pentacontane reduces the surface symmetry to a two-fold rotational symmetry and breaks the mirror symmetry. c) In an overview image pentacontane can be seen to form multiple sets of *p2* symmetric domains on *p6* symmetric HOPG with relative angles within a set of multiples of 60°. d) The different domain orientations of the pentacontane (inset) result from a combination of the three orientations along the HOPG axes (red) and different possibilities of pentacontane stacking. 10 nm x 10 nm, 400 nm x 400 nm, U_{Bias}= -50 mV - - 800 mV, $|I_T|$= 8 pA - -30pA.

The feasibility of modifying substrates with adlayers of *n*-alkanes was first successfully introduced by Bai[15] and Fichou[16]. We dissolved pentacontane in tetradecane before applying a droplet onto the HOPG surface and raising the substrate temperature to 50 °C to evaporate the tetradecane solvent completely. The surface was imaged by a Nanoscope III scanning tunneling microscope (STM) with low-current converter under ambient conditions at room temperature, which allowed high resolution nanoscale observations of the ordering on the modified and unmodified surfaces in real space. All images were flattened, drift-corrected and all small scale images were correlation averaged.

An unmodified graphite surface exhibits a six-fold rotational symmetry as well as mirror symmetry, see figure 1a. If this substrate

---

[*] C. Rohr, K. Gruber, Dr. B. A. Hermann
Center for Nano Science (CeNS) and Walther-Meissner-Institute of Low Temperature Research of the Bavarian Academy of Sciences
Walther-Meissner-Str. 8, 85748 Garching (Germany)
Fax: (+49) 89 289 14206
E-mail: carstenrohr@gmx.de

Dr. L. J. Scherer, Dr. M. S. Malarek,
Prof. Dr. E. C. Constable
Department of Chemistry
University of Basel
Spitalstr. 51, 4056 Basel (Switzerland)

Dr. M. S. Malarek
Department of Chemistry and Biochemistry
La Sierra University
4500 Riverwalk Pkwy, Riverside, CA 92515 (USA)

[**] Financial support by the German Excellence Initiative via the program "Nanosystems Initiative Munich", ERA-Chemistry, the Swiss National Science Foundation and the University of Basel is gratefully acknowledged. C.R. acknowledges the "Studienstiftung des deutschen Volkes" and the "Elite Network Bavaria" (IDK Nanobiotechnology). We thank C. Höhl for measurements.

is modified by an ordered adlayer of pentacontane, the observed rotational symmetry is two-fold and the mirror symmetry is broken, see figure 1b, which results in a chiral surface stemming from the prochiral pentacontane molecule, see figure 1d inset. Additionally, the adlayer changes the lattice constant of the surface and the adsorption energy of molecules compared to an HOPG surface. On a larger scale, domains of ordered pentacontane of diverse orientations are visible. These domains form different sets, which have relative angles of multiples of 60° within a set of domains, see figure 1c. The differing orientations of the pentacontane rows result from a combination of two factors. First, the pentacontane molecules can align along one of the three distinguishable graphite axes. The second cause for the different row orientations originates from the stacking of the molecules within a row. They can either order directly perpendicular to the long molecule axis or their ordering is shifted by one CH_2-group to the left or right, resulting in a tilted row angle, see figure 1d.

The self-organizing molecule we employed on the unmodified graphite and the modified pentacontane surface is the Fréchet dendron[17-21] **1** methyl 3-[3,5-bis(octyloxy)benzyloxy]-5-benzyloxybenzoate), see figure 2a inset. The Fréchet dendron chosen contains three benzene rings, one of which bears flexible alkoxy chains[22] that interact with the surface and drive the molecular self-organization via chain interdigitation. The Fréchet dendrons are cast from 0.2 mM phenyloctane and toluene solutions onto the respective surface, where the molecules self-organize in regular row like patterns.

On graphite the Fréchet dendrons hierarchically organize into one dimensional rows of molecules, which in turn stick together to form two dimensional domains. These domains have six different orientations on the graphite surface, no individual rows can be observed, only molecular domains, see figure 2a.

When molecule **1** organizes on a pentacontane modified surface a distinctly different self-organization behavior is observed. In figure 2b, three domains of different pentacontane orientations have Fréchet dendron adlayers. The domain structure is frayed and the domain borders are oriented along the pentacontane rows, with individual rows of molecule **1** in between. Additionally, only one domain orientation with an angle of 17° can be found on each pentacontane domain. These observations are in strong contrast to the assembly on graphite, where multiple domain orientations with varying angles exist.

An apparent disparity on the two different surfaces is in the chirality of the respective adlayer. On HOPG, domains with a relative angle, not equal to a multiple of 60° can be found, representing the two kinds of chiral ordering of molecule **1**. More precisely, two sets of domains with 60° angles within each set are observed, each representing one chirality, see figure 3a and 2a. In contrast, on a pentacontane surface of a specific orientation always only one orientation of ordered adlayer rows is found. These rows span an angle of *either* +17° or -17° with the normal on the pentacontane rows. Figure 3b displays the domains 1 and 2 from figure 2b to specifically show this angle effect, illustrating that only one form of handed ordering is present on a pentacontane surface.

A second obvious change can be seen in the rotational symmetry of the pattern on the two surfaces. Even when focusing on only one set of domains with 60° angles on HOPG, three distinct orientations are observable, while only one orientation is found on a pentacontane surface, see figure 3c,d. This difference originates in the rotational symmetry of the two surfaces. The *p6* HOPG surface with its six-fold symmetry allows for a maximum three distinguishable orientations of the two-fold symmetric molecular adlayer. The two-fold symmetric pentacontane surface standardizes the alignment to one orientation of the two-fold symmetric molecular rows.

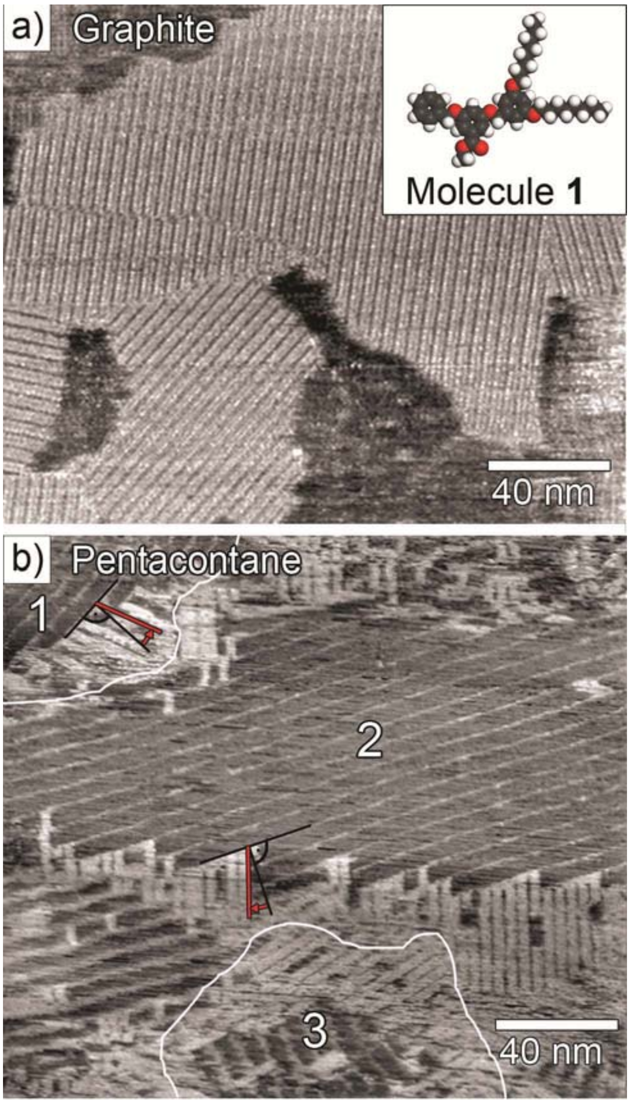

Figure 2. Differences in adlayer assembly on an HOPG and a pentacontane surface. a) A Fréchet dendron (inset) orders in large striped domains of different orientations on HOPG. b) Ordering of the same molecule on three different pentacontane surfaces (1, 2, 3). A distinctly different assembly is observed for the Fréchet dendrons containing only one orientation and one chirality, visible by the angle with respect to the pentacontane domain. For an comparison see figure 3. 180 nm x 160 nm, U_{Bias}= - 800 mV, $|I_T|$= 8 pA.

Thirdly, two different hierarchical assembly behaviors are observed. The row pattern of molecule **1** on HOPG is a hierarchically ordered pattern in the sense that it encompasses at least two interactions of different strength[11] that in turn are responsible for the formation of second level building blocks (rows) and third level structures (domains). Here the molecules within the rows are connected together by chain-chain interactions, while interactions between rows are mediated by weaker π-interactions of the outermost ring. On HOPG, fully formed domains develop, while on the modified pentacontane surface a much more frayed domain formation with individual rows of molecule **1** protruding or completely detached, see figure 3e,f. This kind of detachment of precursors of hierarchical assembly has only been realized by two other methods in self-organized monolayers. One method hinders

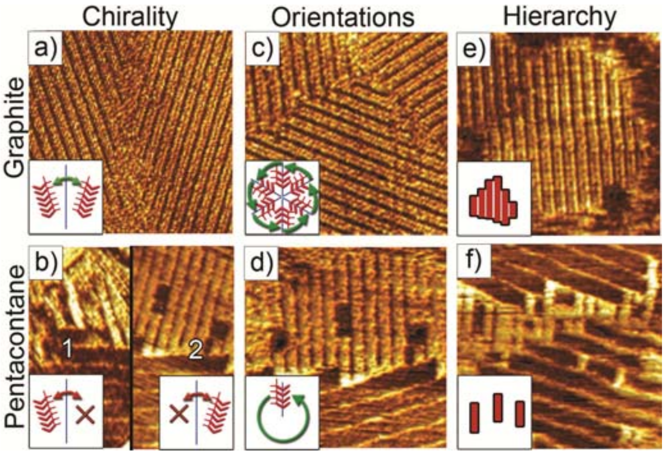

Figure 3. Assembly properties of a molecule adlayer on HOPG and pentacontane surfaces. a) While on HOPG both chiral orderings of the molecule can be observed, b) on one pentacontane surface only one chirality can be found, while the other is omitted. (Example domains 1 and 2 taken from figure 2b) c) The three different rotationally symmetric orientations of the molecule adlayer on HOPG are reduced to d) one orientation on a pentacontane surface. e) Molecules form rows which in turn assemble in domains on HOPG. f) On pentacontane molecules only combine into rows partly omitting the second hierarchical step of forming domains. 70 nm x 70 nm, U_{Bias}= - 800 mV, $|I_T|$= 8 pA.

the last hierarchical stage from forming by omitting the last heating step[13]. The other method separates a fully formed hierarchical assembly by increasing the work potential.[14] Both methods alter the interaction strength or the kinetic barriers, thereby stabilizing the precursor of the finished assembly. On a pentacontane surface the molecule-surface interaction as found by molecular mechanics[23] is reduced to half the strength that is observed on HOPG[21] and the intermolecular π-interaction strength is effectively altered since no t-stacking (edge to face π-interaction) with the aromatic HOPG surface can occur. An alteration of the relative interaction strength via the surface modifications thus allows an easier separation of the hierarchical assembly into precursor building blocks.

All three observations on chirality, orientation and hierarchy are caused by the alteration of the substrate properties. Pentacontane breaks the surface´s mirror symmetry and alters it to a chiral substrate. Additionally, the surfaces' rotational symmetry is reduced by a factor of three, which in turn results in the reduction of domain orientations. Finally, the modified surface alters the intermolecular interaction strength, allowing the observation of individual one dimensional rows of an otherwise two-dimensional layer. These three effects, the selection of one chirality, the standardization into one domain orientation and the stabilization of hierarchical precursors can be achieved by means of *n*-alkane surface modification.

We have shown that by an elegant modification of the substrate with *n*-alkanes one can control the chirality and number of domain orientations and even influence the hierarchy of assembly of a self-organized monolayer. By this method one can fabricate monolayers of one chirality and orientation without external or chemical intervention, effectively standardizing the self-organization in a specific region. The limiting factor here becomes the size of the pentacontane domains; increasing their size should be actively investigated. The stabilization of the hierarchical building blocks by our surface modification transforms a two-dimensional assembly into a partially one-dimensional ordering. This represents a new way of influencing hierarchical assemblies, which currently emerge due the increasing complexity of employed building blocks resulting in more complex ordering. Our method offers a new tool for the elegant control of self-organized monolayers by utilizing the too often neglected surface, thus enabling scientists working in this field to tailor molecular assemblies to their wishes.

Experimental Section

A Nanoscope III with low-current converter was utilized at ambient conditions for STM measurements. Pentacontane is solved in tetradecane and applied onto HOPG. The substrate temperature is raised to 50 °C to evaporate solvent completely. The molecules were cast from 0.2 mM hexane or phenyloctane solutions onto pentacontane. All images were flattened, drift-corrected and all small scale images correlation averaged.

Received: ((will be filled in by the editorial staff))
Published online on ((will be filled in by the editorial staff))

Keywords: Scanning probe microscopy · Self-assembly · Supramolecular chemistry · Hierarchy · Chirality

---

[1] J. V. Barth, *Annu. Rev. Phys. Chem.* **2007**, *58*, 375-407.
[2] J. V. Barth, G. Costantini, K. Kern, *Nature* **2005**, *437*, 671-679.
[3] J. M. Lehn, *Science,* **2002**, *295*, 2400-2403.
[4] M. O. Lorenzo, C. J. Baddeley, C. Muryn, R. Raval, *Nature* **2000**, *404*, 376-379.
[5] C. Joachim, J. K. Gimzewski, A. Aviram, *Nature* **2000**, *408*, 541-548.
[6] J. A. A. W Elemans, I. De Cat, H. Xu, S. De Feyter, *Chem. Soc. Rev.*, **2009**, *38*, 722-736
[7] Raval, R; *Chem. Soc. Rev.*, **2009**, *38*, 707-721.
[8] N. Katsonis, Katsonis, H. Xu, R. M. Haak, T. Kudernac, Z.Tomovic, S. George, M. Van der Auweraer, A. P. H. J. Schenning, E. W. Meijer, B. L. Feringa, S. De Feyter, *Angew. Chem.*, **2008**, *47*, 4997-5001.
[9] A. R. A. Palmans, E. W. Meijer, *Angew. Chem.,* **2007**, *47*, 8948-8968.
[10] A. M. Berg, D. L. Patrick, *Angew. Chem.*, **2005**, *44*, 1821-1823.
[11] Y. Yang, C. Wang, *Chem. Soc. Rev.* **2009**, *38*, 2576-2589.
[12] D. Bléger, D. Kreher, F. Mathevet, A.-J. Attias*, G. Schull, L. Douillard, A. Huard, C. Fiorini-Debuisschert, F. Charra.;*Angew. Chem.*, **2007**, *46*, 7404-7407.
[13] H. Spillmann, A. Dmitriev, N. Lin, P. Messina, J. V. Barth, K. Kern, *J. Am. Chem. Soc.* **2003**, *125*, 10725-10728.
[14] A. S. Klymchenko, S. Furukawa, K. Müllen, M. Van der Auweraer, S. De Feyter, *Nano Lett.* **2007**, *7*, 791-795.
[15] B. Xu, S. Yin, C. Wang, X. Qiu, Q. Zeng, C. Bai. *J. Phys. Chem. B,* **2000**, *104*, 10502-10505.
[16] L. Piot, C. Marie, X. Feng, K. Müllen, D. Fichou, *Adv. Mater.* **2008**, *20*, 3854-3858.
[17] C. J. Hawker, J. M. J. Fréchet, *J. Am. Chem. Soc.* **1990**, *112*, 7638-7647.
[18] L. Merz, H.-J. Güntherodt, L. J. Scherer, E. C. Constable, C. E. Housecroft, M. Neuburger, B. A. Hermann, *Chem. Eur. J.* **2005**, *11*, 2307-2318.
[19] C. Rohr, M. Balbás Gambra, K. Gruber, E. C. Constable, E. Frey, T. Franosch, B. A. Hermann, *Nano Lett.* **2010**, *10*, 833-837.
[20] B. A. Hermann, C. Rohr, M. Balbás Gambra, A. Malecki, M. S. Malarek, E: Frey, T. Franosch, *Phys. Rev. B* **2010**, *82*, 165451.
[21] C. Rohr, M. Balbás Gambra, K. Gruber, M. S. Malarek, L. S. Scherer, E. C. Constable, T. Franosch, B. A. Hermann *Chem. Comm.*, **2011**, *47*, 1800-1802.
[22] E. C. Constable, S. Graber, B. A. Hermann, C. E. Housecroft, M. S. Malarek, L. J. Scherer, *Eur. J. Org. Chem.* **2008**, *15*, 2644-2651.
[23] A. K. Rappé, C. J. Casewit, K. S. Colwell, W. A. Goddard III, W. M. Skiff, *J. Am. Chem. Soc.* **1992**, *114*, 10024-10035.

9.8 A Versatile Fréchet-Dendron Compound Unifies Host-Guest and Templated Heterogeneous Self-Assembly

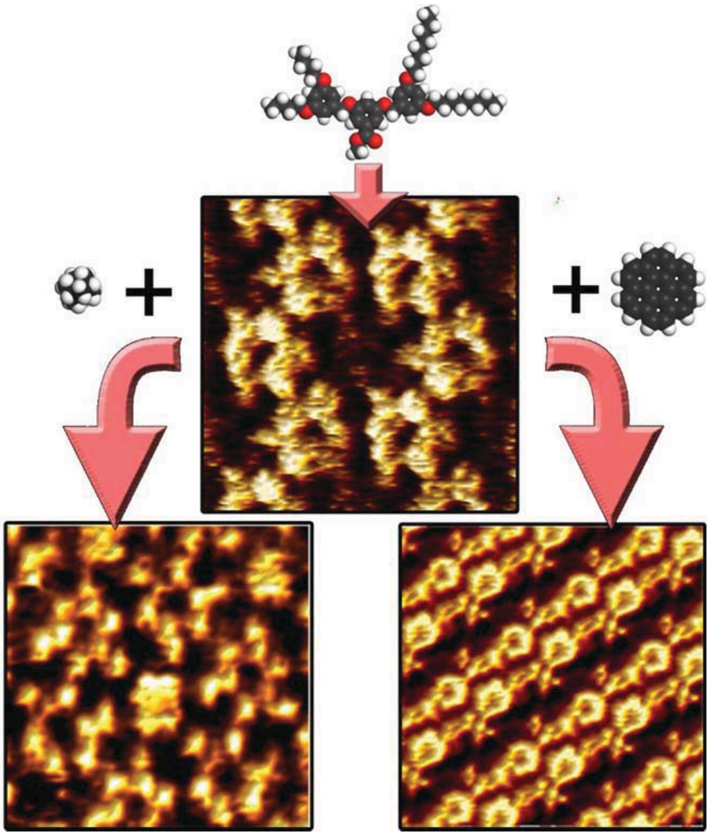

K. Gruber, **C. Rohr**, L. J. Scherer, M. S. Malarek, E. C. Constable, B. A. Hermann

Advanced Materials 2011, DOI: 10.1002/adma.201100013, in print.

A Versatile Fréchet-Dendron Compound Unifies Host-Guest and Templated Heterogeneous Self-Assembly

Kathrin Gruber, Carsten Rohr, Lukas J. Scherer, Michael S. Malarek, Edwin C. Constable, and Bianca A. Hermann**

2D molecular self-assembly is key to the design of functional surfaces[1] and the bottom-up approach of bicomponent systems.[2] Applications are aimed at catalysis[3] and molecular electronic devices.[4] One of the recent trends is towards control over networks with two or more molecular compounds and the inclusion of functional molecules.[5]

In heterogeneous molecular materials, two distinct categories stand out: host-guest networks[6] and templated polymorph structures.[7] The addition of a guest species leaves the host structure of the host-guest system unchanged, the guest is incorporated into pre-existing cavities. This guest selectivity and spatial confinement leads to control over the behavior and reactivity of the included functional molecules.[5] In contrast, for templated assemblies the co-adsorbed guest influences the ordering and thus templates a new ordering motif that is not observed for the pure assembly.[7a] This switching ability of the second class of heterogeneous assemblies completely reorganizes the molecular layer, yielding different symmetries and altered distances between the molecular components. Up to now these two different material functionalities of selective guest inclusion in host-guest systems and conformational switching into a templated new ordering were never found in one host species. The crucial link, a system combining both functionalities, i.e., a host system that shows host-guest behavior as well as templated structures, was missing. The availability of such a system will allow confinement inside nanocavities of the host-guest system, as well as the switching into templated molecular monolayers, depending on the guest molecule, thus merging these two material functions in one host species. Applying both processes subsequently would enable a variety of two-step protocols within one molecular material.

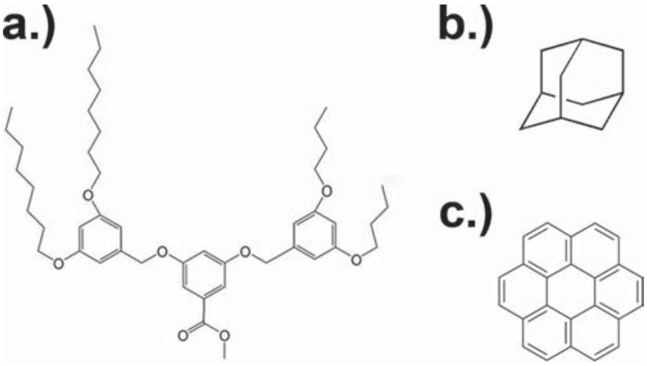

Scheme 1. Molecular structures. a) Second-generation ester-decorated Fréchet dendrons with octyl chains on one side and butyl termination on the other side of the phenyl rings. b) Structure of the adamantane guest. c) Structure of the coronene guest.

Here, we present high-resolution scanning tunneling microscopy (STM) measurements made at room temperature on heterogeneous assemblies of one Fréchet-dendron compound, methyl (3-[3,5-bis(butyloxyphenyl)methoxy]-5-[3,5-bis(octyloxyphenyl) methoxy] benzoate,[8] co-adsorbed with adamantane and coronene guest molecules (**Scheme 1**) on highly oriented graphite (HOPG). While adamantane, a small saturated hydrocarbon structure, only interacts via van der Waals forces, coronene is an example of a small aromatic hydrocarbon compound that additionally allows for electrostatic and π-interactions. De Feyter and co-workers showed an empty host structure[9] and a templated assembly upon the addition of guest molecules to an assembly from dehydrobenzo[12] annulene (DBA) derivatives.[7a] Here, we show for the first time that a molecular compound is able to build an independent host structure, a host-guest assembly incorporating guest molecules, and a templated polymorph assembly. The resulting patterns of the respective bimolecular system depend on the type of co-adsorbed guest molecule. This is the first molecular thin film that unifies guest selective confinement in pre-existing cavities as well as conformational switching into a templated new structure. We analyze the observed molecular ordering and differences in packing arrangement using complementary molecular mechanics (MM) and density functional theory (DFT) calculations. At the end, we explain a possible mechanism behind this new and unexpected behavior by electronic properties.

K. Gruber, C. Rohr, Dr. B. A. Hermann
Center for Nano Science (CeNS) and Walther-Meissner-Institute of Low Temperature Research of the Bavarian Academy of Sciences
Walther-Meissner-Str. 8, 85748 Garching, Germany
E-mail: kathrin.gruber@gmx.de; b.hermann@cens.de
Dr. L. J. Scherer, Prof. M. S. Malarek, Prof. E. C. Constable
Department of Chemistry
University of Basel
Spitalstr. 51, 4056 Basel, Switzerland
Dr. L. J. Scherer
EMPA, Laboratory for Protection and Physiology
Lerchenfeldstrasse 5, 9014, St. Gallen, Switzerland
Prof. M. S. Malarek
Department of Chemistry and Biochemistry
La Sierra University
4500 Riverwalk Pkwy, Riverside, CA 92515, USA

DOI: 10.1002/adma.201100013

© 2011 WILEY-VCH Verlag GmbH & Co. KGaA, Weinheim

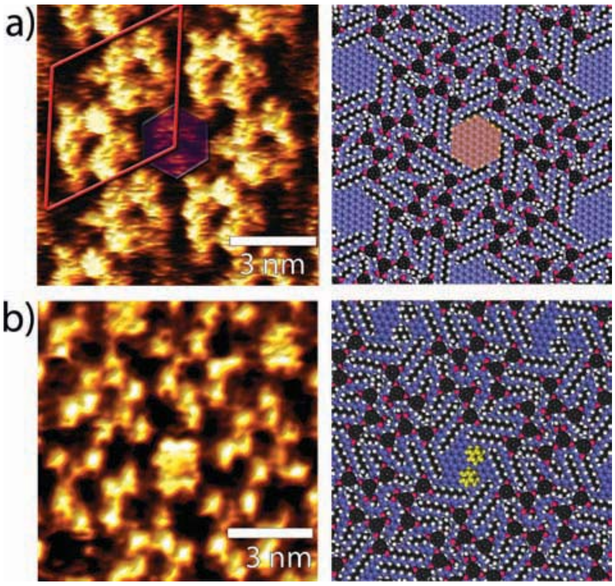

Figure 1. Host-guest assembly. The host network of the self-assembled Fréchet-dendron compound remains unchanged by adamantane guest inclusion. a) High-resolution STM image and MM calculation of the guest-free honeycomb host pattern. b) Close-up and corresponding MM energy minimizations with additional adamantane in the pores of the unchanged honeycomb pattern. Tunneling bias $U_{\mathrm{Bias}} = -700$ to -800 mV and current setpoint $|I_{\mathrm{T}}| = 8$ to 10 pA.

For the pure Fréchet-dendron assembly we focused on the honeycomb pattern that is observed in hexane and toluene after solvent evaporation. This assembly is stable for hours with domains extending up to several hundred nanometers. **Figure 1**a shows an STM image of a honeycomb structure with pores of 1.3 nm diameter, the *p*6 unit cell of the pattern ($a1 = a2 =$ 4.7 nm and angle, $\measuredangle$, = 60.8°), as well as the corresponding MM energy minimization (enthalpy per area = 187.1 kJ mol^{-1} nm^{-2}). The bright moieties in the measurement correspond to the phenyl rings of the Fréchet backbone, and three molecules assemble in a triangular shape while six of these triangles form one ring in the honeycomb pattern. For the sawtooth pattern, which is the other observed pattern in hexane, the triangles are lined up in zigzag rows resulting in a *p*2 symmetric arrangement.[10] This pattern will not be discussed here. The dark contrast observed in the STM measurement inside the honeycomb pores in Figure 1a indicates that no additional Fréchet molecules are included, making this compound an ideal host network for heterogeneous assemblies.[9b]

After adding adamantane molecules to the assembly and letting the hexane solvent evaporate, we observed the same hexagonal honeycomb pattern with unchanged unit cell parameters ($a1 = a2 = 4.7$ nm, $\measuredangle = 60.4°$). However the pores then showed a much higher brightness and were clearly filled. Figure 1b shows a close-up image and the MM simulation (enthalpy per area = 196.8 kJ mol^{-1} nm^{-2}) of a filled pore. The pores are filled with one or two adamantane molecules, as MD simulations suggest (see Supporting Information) for this host-guest assembly.

A distinctly different pattern is always observed when coronene molecules are added to the original Fréchet-host assembly, which represents the second class of templated materials with switching behavior. This new row-like structure differs strongly from the honeycomb structure of the pure assembly or the adamantane guest molecule inclusion. **Figure 2**a shows a typical STM image obtained after the addition of coronene and evaporation of the solvent. A correlation averaged close-up with the *p*2 symmetric unit cell ($a1 = 2.6$ nm, $a2 = 3.4$ nm, $\measuredangle = 81.2°$, enthalpy per area = 203.2 kJ mol^{-1} nm^{-2}) is shown in the inset. While the bright circular contrast is attributed to the coronene molecules, the triangular granular shapes represent the Fréchet backbone. A simulated STM image, depicted in the left inset of Figure 2 a, fits well to the measurements and confirms the interpretation of the switching to a new templated arrangement.

To analyze the cause of this first time observation of host-guest inclusion as well as templated assembly, depending on the guest, several possible reasons were examined. The pore size in both patterns was comparable (1.30 nm and 1.35 nm, respectively), therefore the size factor was excluded as a cause for pattern-selecting. Since the solution casting method involves the evaporation of the solvent, the influence of the solvent used for deposition on the pattern formation was negligible. Comparing the enthalpies calculated for the two assemblies (host-guest/adamantane and templated/coronene) with their

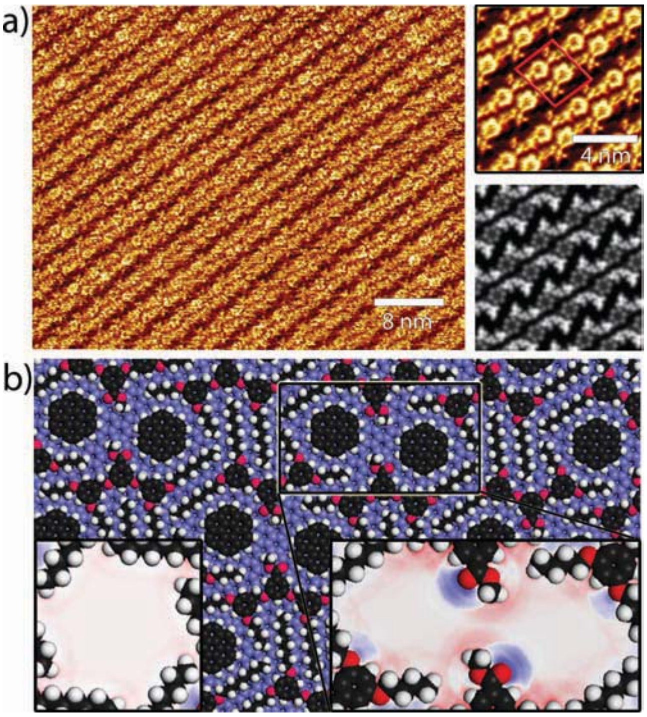

Figure 2. Templated assembly. A templated new pattern forms from heterogeneous self-assembly of Fréchet dendrons and coronene. a) Large-scale STM image of the pattern with a high-resolution close-up and DFT-simulated STM image of the integrated local density of states (ILDOS) with an applied Gauss filter to simulate the effect of the extended tip. b) Corresponding MM calculation of the new guest-induced pattern. Inset: Comparison of the electrostatic potential calculations within the pores formed by both patterns (host-guest and templated). $U_{\mathrm{Bias}} = -800$ mV and $|I_{\mathrm{T}}| = 8$ pA.

© 2011 WILEY-VCH Verlag GmbH & Co. KGaA, Weinheim

respective, not experimentally observed, counterparts (templated/adamantane and host-guest/coronene) sheds light on a possible cause. Adamantane in the host-guest pattern generates 196.8 kJ mol^{-1} nm^{-2}, while the templated structure with adamantane guests would gain only 183.5 kJ mol^{-1} nm^{-2}. In contrast, coronene in the host-guest structure is, with an enthalpy of 199.8 kJ mol^{-1} nm^{-2}, less favorable than in the experimentally observed templated form that has an enthalpy of 203.2 kJ mol^{-1} nm^{-2}. These simulated enthalpies support the experimental observations, while the question about the origin of the difference in pattern formation and enthalpy remains.

The most striking difference between the two patterns lies in the electrostatic potential within the pores of the Fréchet-dendron network. For the Fréchet honeycomb pattern a homogeneous electrostatic potential of nearly zero intensity is calculated. In contrast, the templated pattern pores show a heterogeneous electrostatic potential of higher intensity (Figure 2b, insets).

The main difference between the two guest molecules with respect to their electronic properties is that adamantane only interacts via van der Waals forces, while the polarizable coronene guest also interacts with its electrostatic environment (dipole-induced dipole interaction) and perhaps even forms weak C–H…O hydrogen bonds. The Fréchet dendron has two spatially separated interaction regions. On the one hand, it interacts through van der Waals forces via its alkane chains; on the other hand the polar molecular core allows electrostatic (dipole-induced dipole) interaction. The two types of interaction are also spatially separated in the two self-organized networks of the molecule (see the color coding in **Figure 3**). Adding the adamantane guest, this separated structure is retained, since the adamantane interacts via van der Waals forces with the alkane chains surrounding the pores. The pattern rearranges itself when coronene is added to allow interaction with the electrostatic Fréchet-dendron cores, resulting again in a spatially separated arrangement of the interaction types (Figure 3). The effect may be explained with a crude separation of the molecule into only two distinct regions, omitting chemical details, and thus it might be applicable to new molecular thin films. This new kind of behavior is only possible because of the two spatially separated interaction parts of the Fréchet-dendron.

This study reports a novel combination of two previously separated functionalities in one molecular material. A Fréchet-type dendron assembled in an independent host pattern, a host-guest network, and as a templated 2D network. The decision for one of the two heterogeneous assemblies thus depended on the interactions with the guest molecule. We showed that the type of interaction between either the saturated adamantane or the aromatic coronene molecules is responsible for the selection of the material function and the observed assembly pattern. Either the host-guest or the templated network is selected to spatially separate the two available interaction types. The Fréchet dendron connects these two, previously separated, molecular functionalities of heterogeneous molecular self-assembly. This linking opens new possibilities of manufacturing host-guest and templated molecular thin films within one system for the development of two-step protocols.

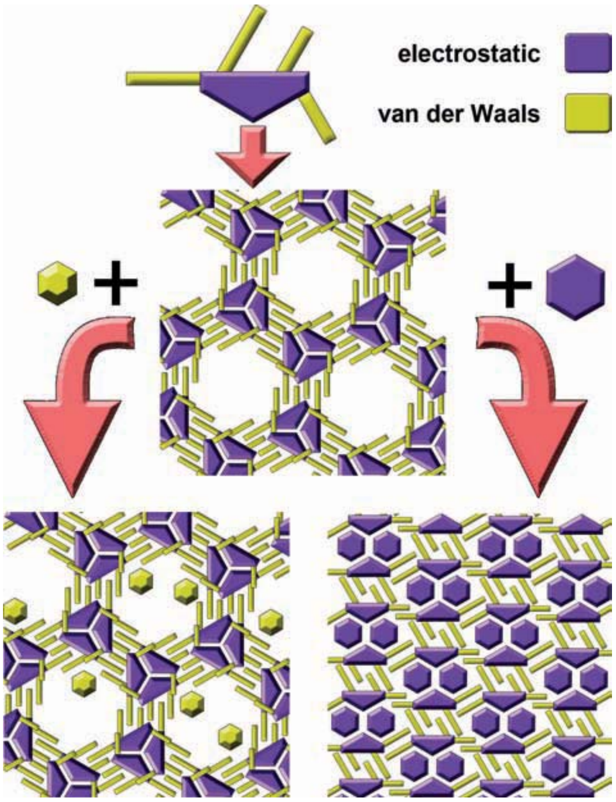

Figure 3. Separation of the molecular interaction types within the heterogeneous patterns. The two interaction types (van der Waals and electrostatic), which are found in the Fréchet-dendron ordering, are spatially separated within the pattern. The guest molecules either interact through van der Waals forces (adamantane, yellow) or react to electrostatic forces (coronene, blue). When added to the pattern, they either integrate easily into the spatial separation (adamantane) or change the pattern and create a new separation of interaction types.

Experimental Section

Molecular monolayers were prepared by solution casting. Fréchet dendrons were applied from solutions in hexane or toluene (0.2 to 0.4 mM). Adamantane was added in hexane (8 mM) and coronene was dissolved in toluene (2 mM) due to solubility. Both were either in the same solution as the Fréchet dendrons or in successive evaporating droplets. STM images were recorded under ambient conditions employing a Nanoscope Multimode III equipped with a low-current converter. All images were flattened.

All simulations were done with Materials Studio 4.4. MM used the Forcite Plus module with a universal force field.[11] The molecules were placed on a fixed double layer of graphite in vacuum and energy minimized, optimizing the molecule–molecule as well as the molecule–substrate interactions. One unit cell was repeated with periodic boundary conditions. For enthalpy calculations of the structures not observed, one coronene was added in the pore of a honeycomb pattern and four adamantanes (two per pore) were added in the templated structure.

The energy-minimized MM simulations provided the atomic positions and were used as input to derive the integrated local density of states (LDOS). Calculated STM images utilized the CASTEP module employing Perdew–Wang '91 (PW91)[12] generalized gradient approximation exchange correlation functionals (GGA) and a plane-wave basis set with an energy cutoff at 260 eV. For a direct comparison with the STM measurements, density contours of a planar slice, convoluted with a Gaussian function of 2× a Pt dz orbital, in the LDOS were calculated.

Electrostatic potential calculations used the Dmol^3 DFT module, employing a PW91 GGA functional.

Supporting Information

Supporting Information is available from the Wiley Online Library or from the author.

Acknowledgements

This work was supported by the German Excellence Initiative via the Nanosystems Initiative Munich (NIM), CeNS, ERA-Chemistry, the Elite Network of Bavaria (ENB and IDK), and the Studienstiftung des Deutschen Volkes. The authors thank Prof. J. Kotthaus for the use of facilities.

Received: January 3, 2011
Revised: February 15, 2011
Published online:

[1] a) J. V. Barth, *Annu. Rev. Phys. Chem.* **2007**, *58*, 375; b) J. V. Barth, G. Costantini, K. Kern, *Nature* **2005**, *437*, 671.
[2] H. Liang, Y. He, Y. Ye, X. Xu, F. Cheng, W. Sun, X. Shao, Y. Wang, J. Li, K. Wu, *Coord. Chem. Rev.* **2009**, *253*, 2959.
[3] M. Ortega Lorenzo, C. J. Baddeley, C. Muryn, R. Raval, *Nature* **2000**, *404*, 376.
[4] C. Joachim, J. K. Gimzewski, A. Aviram, *Nature* **2000**, *408*, 541.
[5] D. Bonifazi, S. Mohnani, A. Llanes-Pallas, *Chem. Eur. J.* **2009**, *15*, 7004.
[6] a) J. A. Theobald, N. S. Oxtoby, M. A. Phillips, N. R. Champness, P. H. Beton, *Nature* **2003**, *424*, 1029; b) S. Lei, K. Tahara, X. Feng, S. Furukawa, F. C. De Schryver, K. Müllen, Y. Tobe, S. De Feyter, *J. Am. Chem. Soc.* **2008**, *130*, 7119; c) G. Schull, L. Douillard, C. Fiorini-Debuisschert, F. Charra, *Nano Lett.* **2006**, *6*, 1360; d) S. J. H. Griessl, M. Lackinger, F. Jamitzky, T. Markert, M. Hietschold, W. M. Heckl, *Langmuir* **2004**, *20*, 9403.
[7] a) S. Furukawa, K. Tahara, F. C. De Schryver, M. Van Der Auweraer, Y. Tobe, S. De Feyter, *Angew. Chem. Int. Ed.* **2007**, *46*, 2831; b) D. Bléger, D. Kreher, F. Mathevet, A.-J. Attias, G. Schull, A. Huard, L. Douillard, C. Fiorini-Debuischert, F. Charra, *Angew. Chem. Int. Ed.* **2007**, *46*, 7404; c) S. Yoshimoto, Y. Honda, O. Ito, K. Itaya, *J. Am. Chem. Soc.* **2008**, *130*, 1085; d) J.-R. Gong, H.-J. Yan, Q.-H. Yuan, L.-P. Xu, Z.-S. Bo, L.-J. Wan, *J. Am. Chem. Soc.* **2006**, *128*, 12384.
[8] a) E. C. Constable, S. Graber, B. A. Hermann, C. E. Housecroft, M. S. Malarek, L. J. Scherer, *Eur. J. Org. Chem.* **2008**, 2644; b) L. Merz, H.-J. Güntherodt, L. J. Scherer, E. C. Constable, C. E. Housecroft, M. Neuburger, B. A. Hermann, *Chem. Eur. J.* **2005**, *11*, 2307.
[9] S. Lei, K. Tahara, F. C. De Schryver, M. Van Der Auweraer, Y. Tobe, S. De Feyter, *Angew. Chem. Int. Ed.* **2008**, *47*, 2964.
[10] C. Rohr, M. Balbás Gambra, K. Gruber, E. C. Constable, E. Frey, T. Franosch, B. A. Hermann, *Nano Lett.* **2010**, *10*, 833.
[11] A. K. Rappé, C. J. Casewit, K. S. Colwell, W. A. Goddard III, W. M. Skiff, *J. Am. Chem. Soc.* **1992**, *114*, 10024.
[12] S. J. Clark, M. D. Segall, C. J. Pickard, P. J. Hasnip, M. I. J. Probert, K. Refson, M. C. Payne, *Z. Kristallogr.* **2005**, *220*, 567.

© 2011 WILEY-VCH Verlag GmbH & Co. KGaA, Weinheim

Copyright WILEY-VCH Verlag GmbH & Co. KGaA, 69469 Weinheim, Germany, 2010.

ADVANCED MATERIALS

Supporting Information

for Adv. Mater., *DOI: 10.1002/adma.201100013*

A Versatile Fréchet-Dendron Compound Unifies Host-Guest and Templated Heterogeneous Self-Assembly

Kathrin Gruber,* Carsten Rohr, Lukas J. Scherer, Michael S. Malarek, Edwin C. Constable, and Bianca A. Hermann*

DOI: 10.1002/adma.201100013

Versatile Fréchet-dendron compound unifies Host-Guest and Templated Heterogeneous Self-Assembly

By *Kathrin Gruber*, Carsten Rohr, Lukas J. Scherer, Michael S. Malarek, Edwin C. Constable, and Bianca A. Hermann**

[*] K. Gruber, C. Rohr, Dr. B. A. Hermann
Center for Nano Science (CeNS) and Walther-Meissner-Institute of Low Temperature Research of the Bavarian Academy of Sciences
Walther-Meissner-Str. 8, 85748 Garching (Germany)
Fax: (+49) 89 289 14206
E-mail: kathrin.gruber@gmx.de, b.hermann@cens.de

Dr. L. J. Scherer, Prof. Dr. M. S. Malarek, Prof. Dr. E. C. Constable
Department of Chemistry
University of Basel
Spitalstr. 51, 4056 Basel (Switzerland)

Dr. L. J. Scherer
EMPA
Laboratory for Protection and Physiology
Lerchenfeldstrasse 5, 9014, St.Gallen (Switzerland)

Prof. Dr. M. S. Malarek
Department of Chemistry and Biochemistry
La Sierra University
4500 Riverwalk Pkwy, Riverside, CA 92515 (USA)

Supporting Information

S1. Number of Incorporated Adamantane Guest Molecules

The number of adamantane molecules enclosed within a single pore of the honeycomb host pattern can be determined with the aid of molecular mechanics and molecular dynamics simulations and a subsequent comparison to the experimental measurements. Molecular mechanics simulations show that at most three adamantane molecules per pore are possible (see **Figure S1** left). A molecular dynamics simulation of these three confined molecules results in a three lobed structure since the adamantane molecules are sterically confined and therefore unable to move within the pore. This result is at odds with the experimental observation of a six lobed STM contrast structure within the pore of the host pattern (see Figure S1 middle). This observation can be reproduced in the simulation, if one or two adamantane molecules are used in the simulation instead of three. In these cases the guest molecules are able to move within the pore, resulting in a six lobed structure (see Figure S1 right). Therefore the pores of the honeycomb host pattern are filled with either one or two moving adamantane molecules.

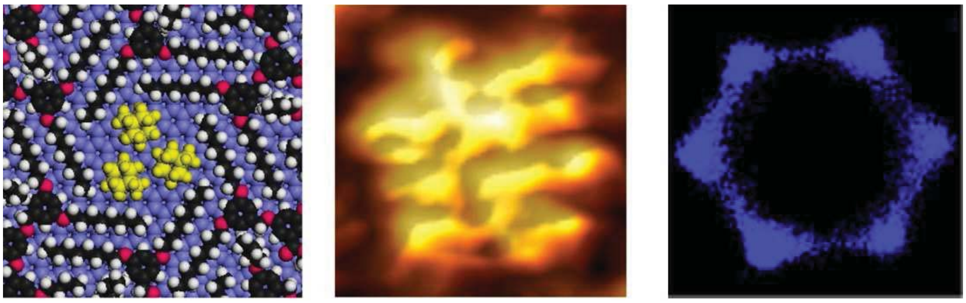

Figure S1: Dynamics of adamantane molecules in the pores of the honeycomb host pattern. Left: Molecular mechanics energy minimization of the honeycomb pattern with three included adamantane molecules. Middle: Correlation averaged STM image of the adamantane filled pore region of the honeycomb pattern showing a six lobed structure. Right: Molecular dynamic simulation of a single adamantane molecule within a host pore exhibiting a six lobed pattern. Depicted is the trajectory of the center of mass.

10 Perspectives

10.1 From Prediction and Complexity in Self-Organization

Going back to the beginning chapters of this thesis, one of the defining challenges posed for molecular self-organization was given by de Vita[30]:

> "*… the increasing complexity of the assembly units used makes it generally more difficult to control the supramolecular organization and* ***predict*** *the assembling mechanisms. This creates a case for developing novel analysis methods and ever more advanced modeling techniques*"

Building on the unprecedentedly large variety of self-organized patterns found for the different variations of Fréchet dendrons during my diploma thesis[138], the question arose for the underlying causes and effects, and the utility of this find. How does such a complexity contribute besides being a curious effect and can it add to principles and control?

Within the multiple self-organized patterns displayed by the different molecules, a trend is visible as the molecules become larger and more complex. More patterns are found during phase transformation the more complex the molecule becomes. These additional patterns are an emergent property of the more rugged energy landscape for more complex molecules. Self-organization in supra-molecular chemistry employs increasingly more complex molecules, but very little attention is generally given to the fact, that in self-organization larger can not only mean larger, but also different.

The large phase variety is a challenge to every attempt to predict the self-organized ordering of this system in advance, since the model would need to incorporate this fact as well. The created interaction-site model and its unexpectedly exact fitting not only of the phase variety, but also the local and global ordering of the individual motifs, distinguish this approach. It has not only been tested against the most complex self-organized monolayer, but also predicted experimental results in advance. The idea behind the model is radically reductionistic. Only the molecules' overall geometry, the coarse grained main-interaction and the surfaces' symmetry are included, while all further chemical detail was omitted. The fact that geometry as well as a few salient weak interaction sites encode these varied structural motifs makes this approach adoptable to a wide range of other molecules and paves the way from trial and error to predictability.

One approach to fore knowledge is the utilization of simulation programs, another one would consist of rules demanding or excluding certain outcomes of the self-organization process, depending on the general properties of the building block. Both approaches differ from the tecton idea[16], which restricts variety by key-lock interactions and therefore manages relatively good predictability. The synthon ansatz interchanges predictability with pattern flexibility and therefore has uses in process control or pattern direction after the organization. The phase variety of the Fréchet Dendron system follows from multi-hierarchical assembly. This form of hierarchical assembly is the first of its kind that was observed for self-organized monolayers. Key for this system property was the conformational flexibility of the molecular building block. The other rules concerned rotational and translational symmetry which follow from asymmetric and symmetric building blocks, respectively. Together with the insight that multiple interactions of different strength are necessary for hierarchical assembly in general[34] these generic building block properties predetermine a lot of parameters of the resulting pattern.

By restriction of the observed variety, the influence of a lower symmetric surface came to light. Only $p2$ symmetric patterns were found on a $p2$ symmetric surface. The number of domain orientations was reduced, as well as the chirality, since the surface lacked mirror symmetry. On the one hand many assembly possibilities are offered by a highly symmetric surface; on the other hand surface control can restrict variety and effectively standardize the resulting patterns.

This pattern variety can be utilized by host-guest assembly. Here the system's flexibility allowed two forms of heterogeneous ordering that have till now been exclusive to either one or the other form. This change in pattern assembly depending on the guest molecule allows execution of two step assembly protocols on the surface. This property again could be derived from the molecular structure of the building block.

The main conclusion of this thesis is: Fundamental building block properties necessarily cause specific pattern properties. These causes can be found. This knowledge in turn can be used to predict patterns in advance, either by simulation or cognition, and skillfully applied lead the direction to a more conscious, more complex self-organization.

10.2 Towards Design and Functionality

The trial and error approach in molecular self-organization should be successively replaced by the conscious design of building block properties with the resulting pattern already in mind. The here outlined rules give a solid starting point for many pattern properties. Other questions still remain, like the cause for the appearance of mirror and glide mirror symmetries within the patterns. Can they be traced back to fundamental properties too? What are the rules governing heterogeneous self-organization and their mixing or separation into different domains? Changes in designing a new molecular building block can take place, resulting in more time spent in front of the whiteboard.

The computer simulations have already the potential to include multiple types of interactions to give rise to more accurate predictions. Two great challenges for the next generation of programs would be the simulation of phase diagrams and phase transitions with the interaction site model. This would not only provide the knowledge about the existence of the different phases, but also the possible experimental conditions for them to be observed.

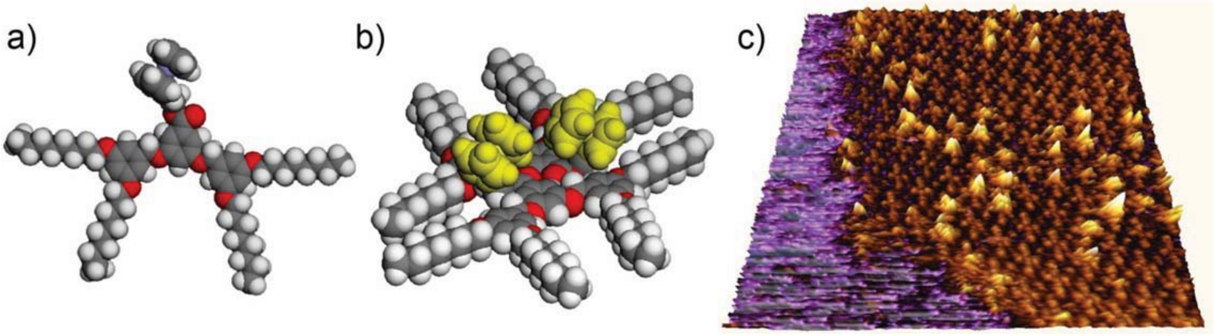

Figure 26. Fréchet adapter molecule: a) Fréchet Dendron coupled with Ferrocene functionality. b) The Fréchet adapter provides the ordering for the functional part. c) Mixture of functionalized and un-functionalized self-organized molecules[3].

Controlling self-organization with the best designs and modeling techniques still need to be employed in real-life applications. Here functional monolayers are already key. The Fréchet Dendrons are apart from their phase variety interesting due to another property. They can be employed as adapter molecules. The idea here is that the Fréchet Dendron part of the molecule is responsible for the molecular self-organization, while the functionality is contained in a part attached to the molecule, see figure 26. This way a molecular separation of organization capability and functionality is achieved.

---

[3] Measurement by Johannes Büttner.

One of my personal quests is the idea of creating hierarchical assemblies with three or more levels of hierarchical organization by employing the here mentioned rules in a creative way, which already works in my personal theory.

References

[1] Camazine, S., *Self-Organization in Biological Systems*. Princeton University Press: Princeton, N.J. ; Oxford, 2001; p viii, 538 p., 8 p. of plates.

[2] Whitesides, G. M. and Grzybowski, B. Self-Assembly at All Scales. *Science* **2002,** 295, 2418-2421.

[3] Barth, J. V.; Costantini, G. and Kern, K. Engineering Atomic and Molecular Nanostructures at Surfaces. *Nature* **2005,** 437, 671-679.

[4] Lehn, J. M. Toward Self-Organization and Complex Matter. *Science* **2002,** 295, 2400-2403.

[5] Lorenzo, M. O.; Baddeley, C. J.; Muryn, C. and Raval, R. Extended Surface Chirality from Supramolecular Assemblies of Adsorbed Chiral Molecules. *Nature* **2000,** 404, 376-379.

[6] Joachim, C.; Gimzewski, J. K. and Aviram, A. Electronics Using Hybrid-Molecular and Mono-Molecular Devices. *Nature* **2000,** 408, 541-548.

[7] Plass, K. E.; Grzesiak, A. L. and Matzger, A. J. Molecular Packing and Symmetry of Two-Dimensional Crystals. *Accounts of Chemical Research* **2007,** 40, 287-293.

[8] Morgenstern, K.; Hla, S. W. and Rieder, K. H. Coexisting Superstructures of Iodobenzene on Cu(111) near Saturation Coverage. *Surface Science* **2003,** 523, 141-150.

[9] Meier, C.; Ziener, U.; Landfester, K. and Weihrich, P. Weak Hydrogen Bonds as a Structural Motif for Two-Dimensional Assemblies of Oligopyridines on Highly Oriented Pyrolytic Graphite: An Stm Investigation. *Journal of Physical Chemistry B* **2005,** 109, 21015-21027.

[10] Ahn, S. and Matzger, A. J. Six Different Assemblies from One Building Block: Two-Dimensional Crystallization of an Amide Amphiphile. *Journal of the American Chemical Society* **2010,** 132, 11364-11371.

[11] Cañas-Ventura, M. E.; Aït-Mansour, K.; Ruffieux, P.; Rieger, R.; Müllen, K.; Brune, H. and Fasel, R. Complex Interplay and Hierarchy of Interactions in Two-Dimensional Supramolecular Assemblies. *Acs Nano* **2010,** 5, 457-469.

[12] Roos, M.; Hoster, H. E.; Breitruck, A. and Behm, R. J. Coverage Dependent Structures of Oligopyridine Adlayers on (111) Oriented Ag Films. *Physical Chemistry Chemical Physics* **2007,** 9, 5672-5679.

[13] Busse, C.; Weigelt, S.; Petersen, L.; Laegsgaard, E.; Besenbacher, F.; Linderoth, T. R.; Thomsen, A. H.; Nielsen, M. and Gothelf, K. V. Chiral Ordering and Conformational Dynamics for a Class of Oligo-Phenylene-Ethynylenes on Au(111). *Journal of Physical Chemistry B* **2007,** 111, 5850-5860.

[14] Ha, S. D.; Kaafarani, B. R.; Barlow, S.; Marder, S. R. and Kahn, A. Multiphase Growth and Electronic Structure of Ultrathin Hexaazatrinaphthylene on Au(111). *Journal of Physical Chemistry C* **2007,** 111, 10493-10497.

[15] Gutzler, R.; Sirtl, T.; Dienstmaier, J. r. F.; Mahata, K.; Heckl, W. M.; Schmittel, M. and Lackinger, M. Reversible Phase Transitions in Self-Assembled Monolayers at the Liquid−Solid Interface: Temperature-Controlled Opening and Closing of Nanopores. *Journal of the American Chemical Society* **2010,** 132, 5084-5090.

[16] Barth, J. V. Molecular Architectonic on Metal Surfaces. *Annual Review of Physical Chemistry* **2007,** 58, 375-407.

[17] Swiegers, G. F. and Malefetse, T. J. New Self-Assembled Structural Motifs in Coordination Chemistry. *Chemical Reviews* **2000,** 100, 3483-3537.

[18] Lei, S. B. and De Feyter, S. Stm, Sts and Bias-Dependent Imaging on Organic Monolayers at the Solid-Liquid Interface. *Stm and Afm Studies on (Bio)Molecular Systems: Unravelling the Nanoworld* **2008,** 285, 269-312.

[19] Llanes-Pallas, A.; Palma, C. A.; Piot, L.; Belbakra, A.; Listorti, A.; Prato, M.; Samori, P.; Armaroli, N. and Bonifazi, D. Engineering of Supramolecular H-Bonded Nanopolygons Via Self-Assembly of Programmed Molecular Modules. *Journal of the American Chemical Society* **2009,** 131, 509-520.

[20] Palma, C.-A.; Bjork, J.; Bonini, M.; Dyer, M. S.; Llanes-Pallas, A.; Bonifazi, D.; Persson, M. and Samorì, P. Tailoring Bicomponent Supramolecular Nanoporous Networks: Phase Segregation, Polymorphism, and Glasses at the Solid−Liquid Interface. *Journal of the American Chemical Society* **2009,** 131, 13062-13071.

[21] Llanes-Pallas, A.; Palma, C.-A.; Piot, L.; Belbakra, A.; Listorti, A.; Prato, M.; Samorì, P.; Armaroli, N. and Bonifazi, D. Engineering of Supramolecular H-Bonded Nanopolygons Via Self-Assembly of Programmed Molecular Modules. *Journal of the American Chemical Society* **2008,** 131, 509-520.

[22] Tahara, K.; Furukawa, S.; Uji-I, H.; Uchino, T.; Ichikawa, T.; Zhang, J.; Mamdouh, W.; Sonoda, M.; De Schryver, F. C.; De Feyter, S. and Tobe, Y. Two-Dimensional Porous Molecular Networks of Dehydrobenzo 12 Annulene Derivatives Via Alkyl

Chain Interdigitation. *Journal of the American Chemical Society* **2006,** 128, 16613-16625.

[23] Ilan, B.; Florio, G. M.; Hybertsen, M. S.; Berne, B. J. and Flynn, G. W. Scanning Tunneling Microscopy Images of Alkane Derivatives on Graphite: Role of Electronic Effects. *Nano Letters* **2008,** 8, 3160-3165.

[24] Glowatzki, H.; Broker, B.; Blum, R. P.; Hofmann, O. T.; Vollmer, A.; Rieger, R.; Mullen, K.; Zojer, E.; Rabe, J. P. and Koch, N. "Soft" Metallic Contact to Isolated C-60 Molecules. *Nano Letters* **2008,** 8, 3825-3829.

[25] Silly, F.; Weber, U. K.; Shaw, A. Q.; Burlakov, V. M.; Castell, M. R.; Briggs, G. A. D. and Pettifor, D. G. Deriving Molecular Bonding from a Macromolecular Self-Assembly Using Kinetic Monte Carlo Simulations. *Physical Review B* **2008,** 77.

[26] Weber, U. K.; Burlakov, V. M.; Perdigao, L. M. A.; Fawcett, R. H. J.; Beton, P. H.; Champness, N. R.; Jefferson, J. H.; Briggs, G. A. D. and Pettifor, D. G. Role of Interaction Anisotropy in the Formation and Stability of Molecular Templates. *Phys Rev Lett* **2008,** 100, 156101.

[27] Breitruck, A.; Hoster, H. E. and Behm, R. J. r. Short-Range Order in a Metal−Organic Network. *The Journal of Physical Chemistry C* **2009,** 113, 21265-21268.

[28] Sarlah, A.; Franosch, T. and Frey, E. Melting of Colloidal Molecular Crystals on Triangular Lattices. *Physical Review Letters* **2005,** 95.

[29] Sarlah, A.; Frey, E. and Franosch, T. Spin Models for Orientational Ordering of Colloidal Molecular Crystals. *Physical Review E* **2007,** 75.

[30] Tomba, G.; Ciacchi, L. C. and De Vita, A. Atomic-Level Studies of Molecular Self-Assembly on Metallic Surfaces. *Advanced Materials* **2009,** 21, 1055-1066.

[31] Elemans, J. A. A. W.; De Cat, I.; Xu, H. and De Feyter, S. Two-Dimensional Chirality at Liquid-Solid Interfaces. *Chemical Society Reviews* **2009,** 38, 722-736.

[32] Linares, M.; Minoia, A.; Brocorens, P.; Beljonne, D. and Lazzaroni, R. Expression of Chirality in Molecular Layers at Surfaces: Insights from Modelling. *Chemical Society Reviews* **2009,** 38, 806-816.

[33] Raval, R. Chiral Expression from Molecular Assemblies at Metal Surfaces: Insights from Surface Science Techniques. *Chemical Society Reviews* **2009,** 38, 707-721.

[34] Yang, Y. L. and Wang, C. Hierarchical Construction of Self-Assembled Low-Dimensional Molecular Architectures Observed by Using Scanning Tunneling Microscopy. *Chemical Society Reviews* **2009,** 38, 2576-2589.

[35] Bonifazi, D.; Mohnani, S. and Llanes-Pallas, A. Supramolecular Chemistry at Interfaces: Molecular Recognition on Nanopatterned Porous Surfaces. *Chemistry-a European Journal* **2009,** 15, 7004-7025.

[36] Theobald, J. A.; Oxtoby, N. S.; Phillips, M. A.; Champness, N. R. and Beton, P. H. Controlling Molecular Deposition and Layer Structure with Supramolecular Surface Assemblies. *Nature* **2003,** 424, 1029-1031.

[37] Lei, S. B.; Tahara, K.; Feng, X. L.; Furukawa, S. H.; De Schryver, F. C.; Mullen, K.; Tobe, Y. and De Feyter, S. Molecular Clusters in Two-Dimensional Surface-Confined Nanoporous Molecular Networks: Structure, Rigidity, and Dynamics. *Journal of the American Chemical Society* **2008,** 130, 7119-7129.

[38] Griessl, S. J. H.; Lackinger, M.; Jamitzky, F.; Markert, T.; Hietschold, M. and Heckl, W. A. Incorporation and Manipulation of Coronene in an Organic Template Structure. *Langmuir* **2004,** 20, 9403-9407.

[39] Schull, G.; Douillard, L.; Fiorini-Debuisschert, C.; Charra, F.; Mathevet, F.; Kreher, D. and Attias, A. J. Single-Molecule Dynamics in a Self-Assembled 2d Molecular Sieve. *Nano Letters* **2006,** 6, 1360-1363.

[40] Lei, S.; Surin, M.; Tahara, K.; Adisoejoso, J.; Lazzaroni, R.; Tobe, Y. and De Feyter, S. Programmable Hierarchical Three-Component 2d Assembly at a Liquid-Solid Interface: Recognition, Selection, and Transformation. *Nano Letters* **2008,** 8, 2541-2546.

[41] Aldaye, F. A.; Palmer, A. L. and Sleiman, H. F. Assembling Materials with DNA as the Guide. *Science* **2008,** 321, 1795-1799.

[42] Seeman, N. C. DNA in a Material World. *Nature* **2003,** 421, 427-431.

[43] Rothemund, P. W. K. Folding DNA to Create Nanoscale Shapes and Patterns. *Nature* **2006,** 440, 297-302.

[44] Binning, G.; Rohrer, H.; Gerber, C. and Weibel, E. Surface Studies by Scanning Tunneling Microscopy. *Physical Review Letters* **1982,** 49, 57-61.

[45] Crommie, M. F.; Lutz, C. P. and Eigler, D. M. Confinement of Electrons to Quantum Corrals on a Metal-Surface. *Science* **1993,** 262, 218-220.

[46] Crommie, M. F.; Lutz, C. P. and Eigler, D. M. Imaging Standing Waves in a 2-Dimensional Electron-Gas. *Nature* **1993,** 363, 524-527.

[47] Rosei, F.; Schunack, M.; Naitoh, Y.; Jiang, P.; Gourdon, A.; Laegsgaard, E.; Stensgaard, I.; Joachim, C. and Besenbacher, F. Properties of Large Organic Molecules on Metal Surfaces. *Progress in Surface Science* **2003,** 71, 95-146.

[48] Hla, S. W. and Rieder, K. H. Stm Control of Chemical Reactions: Single-Molecule Synthesis. *Annual Review of Physical Chemistry* **2003,** 54, 307-330.

[49] Hermann, B. A.; Scherer, L. J.; Housecroft, C. E. and Constable, E. C. Self-Organized Monolayers: A Route to Conformational Switching and Read-out of Functional

Supramolecular Assemblies by Scanning Probe Methods. *Advanced Functional Materials* **2006,** 16, 221-235.

[50] Moresco, F.; Meyer, G.; Rieder, K. H.; Tang, H.; Gourdon, A. and Joachim, C. Conformational Changes of Single Molecules Induced by Scanning Tunneling Microscopy Manipulation: A Route to Molecular Switching. *Physical Review Letters* **2001,** 86, 672-675.

[51] Morgenstern, K. Isomerization Reactions on Single Adsorbed Molecules. *Accounts of Chemical Research* **2009,** 42, 213-223.

[52] Bode, M. Spin-Polarized Scanning Tunnelling Microscopy. *Reports on Progress in Physics* **2003,** 66, 523-582.

[53] Eigler, D. M. and Schweizer, E. K. Positioning Single Atoms with a Scanning Tunneling Microscope. *Nature* **1990,** 344, 524-526.

[54] Binnig, G. and Smith, D. P. E. Single-Tube 3-Dimensional Scanner for Scanning Tunneling Microscopy. *Rev. Sci. Instrum.* **1986,** 57, 1688-1689.

[55] Hofer, W. A. Challenges and Errors: Interpreting High Resolution Images in Scanning Tunneling Microscopy. *Progress in Surface Science* **2003,** 71, 147-183.

[56] Hermann, B. A., *Scanning Probe Microscopy*. Wiley-VCH Verlag GmbH & Co. KGaA: 2007; p 337-390.

[57] Bardeen, J. Tunnelling from a Many-Particle Point of View. *Physical Review Letters* **1961,** 6, 57-&.

[58] Drakova, D. Theoretical Modelling of Scanning Tunnelling Microscopy, Scanning Tunnelling Spectroscopy and Atomic Force Microscopy. *Reports on Progress in Physics* **2001,** 64, 205-290.

[59] Hofer, W. A.; Foster, A. S. and Shluger, A. L. Theories of Scanning Probe Microscopes at the Atomic Scale. *Reviews of Modern Physics* **2003,** 75, 1287-1331.

[60] Nieminen, J. A.; Niemi, E. and Rieder, K. H. Interference between Competing Tunneling Channels and Chemical Resolution of Stm. *Surface Science* **2004,** 552, L47-L52.

[61] Tersoff, J. and Hamann, D. R. Theory and Application for the Scanning Tunneling Microscope. *Physical Review Letters* **1983,** 50, 1998-2001.

[62] Chen, C. J., *Introduction to Scanning Tunneling Microscopy*. Oxford University Press: New York ; Oxford, 1993; p xxii, 412 p., 31 p. of plates.

[63] Repp, J.; Meyer, G.; Stojkovic, S. M.; Gourdon, A. and Joachim, C. Molecules on Insulating Films: Scanning-Tunneling Microscopy Imaging of Individual Molecular Orbitals. *Phys Rev Lett* **2005,** 94, 026803.

[64] Lukas, S.; Witte, G. and Woll, C. Novel Mechanism for Molecular Self-Assembly on Metal Substrates: Unidirectional Rows of Pentacene on Cu(110) Produced by a Substrate-Mediated Repulsion. *Physical Review Letters* **2002,** 88.

[65] Kohn, W. Nobel Lecture: Electronic Structure of Matter-Wave Functions and Density Functionals. *Reviews of Modern Physics* **1999,** 71, 1253-1266.

[66] Batra, I. P.; Garcia, N.; Rohrer, H.; Salemink, H.; Stoll, E. and Ciraci, S. A Study of Graphite Surface with Stm and Electronic-Structure Calculations. *Surface Science* **1987,** 181, 126-138.

[67] Pong, W. T. and Durkan, C. A Review and Outlook for an Anomaly of Scanning Tunnelling Microscopy (Stm): Superlattices on Graphite. *Journal of Physics D-Applied Physics* **2005,** 38, R329-R355.

[68] Cai, C.; Bösch, M.; Bosshard, C.; Müller, B.; Tao, Y.; Kündig, A.; Weckesser, J.; Barth Johannes, V.; Bürgi, L.; Jeandupeux, O.; Kiy, M.; Biaggio, I.; Liakatas, I.; Kern, K. and Günter, P., Self-Assembly Growth of Organic Thin Films and Nanostructures by Molecular Beam Deposition. In *Anisotropic Organic Materials*, American Chemical Society: 2001; Vol. 798, pp 34-49.

[69] Meyer, E.; Overney, R.; Brodbeck, D.; Howald, L.; uuml; thi, R.; Frommer, J. and ntherodt, H. J. Friction and Wear of Langmuir-Blodgett Films Observed by Friction Force Microscopy. *Physical Review Letters* **1992,** 69, 1777.

[70] Rauschenbach, S.; Stadler, F. L.; Lunedei, E.; Malinowski, N.; Koltsov, S.; Costantini, G. and Kern, K. Electrospray Ion Beam Deposition of Clusters and Biomolecules. *Small* **2006,** 2, 540-547.

[71] Tanaka, H.; Hamai, C.; Kanno, T. and Kawai, T. High-Resolution Scanning Tunneling Microscopy Imaging of DNA Molecules on Cu(111) Surfaces. *Surface Science* **1999,** 432, L611-L616.

[72] De Feyter, S. and De Schryver, F. C. Self-Assembly at the Liquid/Solid Interface: Stm Reveals. *The Journal of Physical Chemistry B* **2005,** 109, 4290-4302.

[73] Heckl, W. M.; Smith, D. P.; Binnig, G.; Klagges, H.; Hänsch, T. W. and Maddocks, J. Two-Dimensional Ordering of the DNA Base Guanine Observed by Scanning Tunneling Microscopy. *Proceedings of the National Academy of Sciences* **1991,** 88, 8003-8005.

[74] Deegan, R. D.; Bakajin, O.; Dupont, T. F.; Huber, G.; Nagel, S. R. and Witten, T. A. Capillary Flow as the Cause of Ring Stains from Dried Liquid Drops. *Nature* **1997,** 389, 827-829.

[75] Henriksen, K. and Stipp, S. L. S. Image Distortion in Scanning Probe Microscopy. *American Mineralogist* **2002,** 87, 5-16.

[76] Yurov, V. Y. and Klimov, A. N. Correction of Drift and Slope Distortions in Stm Image and Scanner Calibration. *Surface and Interface Analysis* **1994,** 22, 84-88.

[77] Soethout, L. L.; Gerritsen, J. W.; Groeneveld, P.; Nelissen, B. J. and Vankempen, H. Stm Measurements on Graphite Using Correlation Averaging of the Data. *Journal of Microscopy-Oxford* **1988,** 152, 251-258.

[78] Lehn, J. M., *Supramolecular Chemistry : Concepts and Perspectives*. VCH: 1995.

[79] Lehn, J. M. Cryptates - Inclusion Complexes of Macropolycyclic Receptor Molecules. *Pure and Applied Chemistry* **1978,** 50, 871-892.

[80] Lehn, J. M. Supramolecular Chemistry - Scope and Perspectives Molecules, Supermolecules, and Molecular Devices. *Angewandte Chemie-International Edition in English* **1988,** 27, 89-112.

[81] Dance, I. What Is Supramolecular? *New Journal of Chemistry* **2003,** 27, 1-2.

[82] Gilli, G. and Gilli, P. Towards an Unified Hydrogen-Bond Theory. *Journal of Molecular Structure* **2000,** 552, 1-15.

[83] Hunter, C. A. and Sanders, J. K. M. The Nature of Pi-Pi Interactions. *Journal of the American Chemical Society* **1990,** 112, 5525-5534.

[84] Lehn, J. M. Toward Complex Matter: Supramolecular Chemistry and Self-Organization. *Proceedings of the National Academy of Sciences of the United States of America* **2002,** 99, 4763-4768.

[85] Lehn, J. M. Supramolecular Chemistry: From Molecular Information Towards Self-Organization and Complex Matter. *Reports on Progress in Physics* **2004,** 67, 249-265.

[86] Scherer, L. J. Octyl-Decorated Fréchet-Type Dendrons: A General Motif for Visualisation of Static and Dynamic Behaviour Using Scanning Tunnelling Microscopy. University of Basel, Basel, 2006.

[87] Hawker, C. J. and Frechet, J. M. J. Preparation of Polymers with Controlled Molecular Architecture - a New Convergent Approach to Dendritic Macromolecules. *Journal of the American Chemical Society* **1990,** 112, 7638-7647.

[88] Hawker, C. J. and Frechet, J. M. J. A New Convergent Approach to Monodisperse Dendritic Macromolecules. *Journal of the Chemical Society-Chemical Communications* **1990**, 1010-1013.

[89] Uemura, S.; Sengupta, S. and Wurthner, F. Cyclic Self-Assembled Structures of Chlorophyll Dyes on Hopg by the Dendron Wedge Effect. *Angewandte Chemie-International Edition* **2009,** 48, 7825-7828.

[90] Zhang, X.; Chen, T.; Chen, Q.; Deng, G. J.; Fan, Q. H. and Wan, L. J. One Solvent Induces a Series of Structural Transitions in Monodendron Molecular Self-Assembly from Lamellar to Quadrangular to Hexagonal. *Chemistry-a European Journal* **2009,** 15, 9669-9673.

[91] Constable, E. C.; Hermann, B. A.; Housecroft, C. E.; Merz, L. and Scherer, L. J. Monitoring Conformational Diversity in Self-Organised Monolayers with Scanning Tunnelling Microscopy at near Atomic Resolution. *Chemical Communications* **2004**, 928-929.

[92] Merz, L.; Guntherodt, H.; Scherer, L. J.; Constable, E. C.; Housecroft, C. E.; Neuburger, M. and Hermann, B. A. Octyl-Decorated Frechet-Type Dendrons: A General Motif for Visualisation of Static and Dynamic Behaviour Using Scanning Tunnelling Microscopy? *Chemistry-a European Journal* **2005,** 11, 2307-2318.

[93] Scherer, L. J.; Merz, L.; Constable, E. C.; Housecroft, C. E.; Neuburger, M. and Hermann, B. A. Conformational Analysis of Self-Organized Monolayers with Scanning Tunneling Microscopy at near-Atomic Resolution. *Journal of the American Chemical Society* **2005,** 127, 4033-4041.

[94] Constable, E. C.; Graber, S.; Hermann, B. A.; Housecroft, C. E.; Malarek, M. S. and Scherer, L. J. The Introduction of Asymmetry into Alkyl-Decorated Frechet-Type Dendrons. *European Journal of Organic Chemistry* **2008**, 2644-2651.

[95] Constable, E. C.; Haeusler, M.; Hermann, B. A.; Housecroft, C. E.; Neuburger, M.; Schaffner, S. and Scherer, L. J. Self-Assembled Monolayers as Two-Dimensional Crystals: Relationship to Three-Dimensional Crystals. *Crystengcomm* **2007,** 9, 176-180.

[96] Desiraju, G. R. Supramolecular Synthons in Crystal Engineering - a New Organic-Synthesis. *Angewandte Chemie-International Edition in English* **1995,** 34, 2311-2327.

[97] Yokoyama, T.; Yokoyama, S.; Kamikado, T.; Okuno, Y. and Mashiko, S. Selective Assembly on a Surface of Supramolecular Aggregates with Controlled Size and Shape. *Nature* **2001,** 413, 619-621.

[98] Yoshimoto, S.; Suto, K.; Tada, A.; Kobayashi, N. and Itaya, K. Effect of Adlayer Structure on the Host-Guest Recognition between Calcium and Crown-Ether-Slubstituted Phthalocyanine Arrays on Au Single-Crystal Surfaces. *Journal of the American Chemical Society* **2004,** 126, 8020-8027.

[99] Spillmann, H.; Kiebele, A.; Stohr, M.; Jung, T. A.; Bonifazi, D.; Cheng, F. Y. and Diederich, F. A Two-Dimensional Porphyrin-Based Porous Network Featuring Communicating Cavities for the Templated Complexation of Fullerenes. *Advanced Materials* **2006,** 18, 275-+.

[100] Hoeben, F. J. M.; Wolffs, M.; Zhang, J.; De Feyter, S.; Leclere, P.; Schenning, A. and Meijer, E. W. Influence of Supramolecular Organization on Energy Transfer Properties in Chiral Oligo(P-Phenylene Vinylene) Porphyrin Assemblies. *Journal of the American Chemical Society* **2007,** 129, 9819-9828.

[101] Dobson, C. M.; Šali, A. and Karplus, M. Protein Folding: A Perspective from Theory and Experiment. *Angewandte Chemie International Edition* **1998,** 37, 868-893.

[102] Shea, J. E. and Brooks, C. L. From Folding Theories to Folding Proteins: A Review and Assessment of Simulation Studies of Protein Folding and Unfolding. *Annual Review of Physical Chemistry* **2001,** 52, 499-535.

[103] Wales, D. J.; Miller, M. A. and Walsh, T. R. Archetypal Energy Landscapes. *Nature* **1998,** 394, 758-760.

[104] Wales, D. J., *Energy Landscapes*. Cambridge University Press: Cambridge, 2003; p 681.

[105] Fejer, S. N.; Chakrabarti, D. and Wales, D. J. Emergent Complexity from Simple Anisotropic Building Blocks: Shells, Tubes, and Spirals. *Acs Nano* **2010,** 4, 219-228.

[106] Cheng, S. Z. D. and Keller, A. The Role of Metastable States in Polymer Phase Transitions: Concepts, Principles, and Experimental Observations. *Annual Review of Materials Science* **1998,** 28, 533-562.

[107] Goldstein, J. Emergence as a Construct: History and Issues. *Emergence : a Journal of Complexity Issues in Organizations and Manadgement. The New England Complex Systems Institute* **1999,** 1, 49-72.

[108] Born, M. and Oppenheimer, R. Quantum Theory of Molecules. *Annalen Der Physik* **1927,** 84, 0457-0484.

[109] Ehrenreich, H. and Cohen, M. H. Self-Consistent Field Approach to the Many-Electron Problem. *Physical Review* **1959,** 115, 786-790.

[110] Casewit, C. J.; Colwell, K. S. and Rappe, A. K. Application of a Universal Force-Field to Organic-Molecules. *Journal of the American Chemical Society* **1992,** 114, 10035-10046.

[111] Casewit, C. J.; Colwell, K. S. and Rappe, A. K. Application of a Universal Force-Field to Main Group Compounds. *Journal of the American Chemical Society* **1992,** 114, 10046-10053.

[112] Rappe, A. K.; Casewit, C. J.; Colwell, K. S.; Goddard, W. A. and Skiff, W. M. Uff, a Full Periodic-Table Force-Field for Molecular Mechanics and Molecular-Dynamics Simulations. *Journal of the American Chemical Society* **1992,** 114, 10024-10035.

[113] Payne, M. C.; Teter, M. P.; Allan, D. C.; Arias, T. A. and Joannopoulos, J. D. Iterative Minimization Techniques for Abinitio Total-Energy Calculations - Molecular-Dynamics and Conjugate Gradients. *Reviews of Modern Physics* **1992,** 64, 1045-1097.

[114] Fletcher, R. and Reeves, C. M. Function Minimization by Conjugate Gradients. *Computer Journal* **1964,** 7, 149-&.

[115] Szabo, A. and Ostlund, N., *Modern Quantum Chemistry: Introduction to Advanced Electronic Structure Theory*. {Dover Publications}: 1996.

[116] Hohenberg, P. and Kohn, W. Inhomogeneous Electron Gas. *Physical Review B* **1964,** 136, B864-&.

[117] Kohn, W. and Sham, L. J. Self-Consistent Equations Including Exchange and Correlation Effects. *Physical Review* **1965,** 140, 1133-&.

[118] Perdew, J. P. and Wang, Y. Accurate and Simple Analytic Representation of the Electron-Gas Correlation-Energy. *Physical Review B* **1992,** 45, 13244-13249.

[119] Gambra, M. B. The Role of Structures in Collective Processes: Social Dynamics and Molecular Self-Assembly. LMU München, München, 2010.

[120] Binder, K. and Heermann, D. W., *Monte Carlo Simulation in Statistical Physics --- an Introduction*. Springer: 1988.

[121] Metropolis, N.; Rosenbluth, A. W.; Rosenbluth, M. N.; Teller, A. H. and Teller, E. Equation of State Calculations by Fast Computing Machines. *The Journal of Chemical Physics* **1953,** 21, 1087-1092.

[122] Hastings, W. K. Monte-Carlo Sampling Methods Using Markov Chains and Their Applications. *Biometrika* **1970,** 57, 97-&.

[123] Kurzweil, H. and Stellmacher, B., *The Theory of Finite Groups: An Introduction*. Springer: 2003.

[124] Vidal, F.; Delvigne, E.; Stepanow, S.; Lin, N.; Barth, J. V. and Kern, K. Chiral Phase Transition in Two-Dimensional Supramolecular Assemblies of Prochiral Molecules. *Journal of the American Chemical Society* **2005,** 127, 10101-10106.

[125] Barlow, S. M. and Raval, R. Complex Organic Molecules at Metal Surfaces: Bonding, Organisation and Chirality. *Surface Science Reports* **2003,** 50, 201-341.

[126] Katsonis, N.; Xu, H.; Haak, R. M.; Kudernac, T.; Tomovic, Z.; George, S.; Van der Auweraer, M.; Schenning, A.; Meijer, E. W.; Feringa, B. L. and De Feyter, S. Emerging Solvent-Induced Homochirality by the Confinement of Achiral Molecules against a Solid Surface. *Angewandte Chemie-International Edition* **2008,** 47, 4997-5001.

[127] Palmans, A. R. A. and Meijer, E. W. Amplification of Chirality in Dynamic Supramolecular Aggregates. *Angewandte Chemie-International Edition* **2007,** 46, 8948-8968.

[128] Berg, A. M. and Patrick, D. L. Preparation of Chiral Surfaces from Achiral Molecules by Controlled Symmetry Breaking. *Angewandte Chemie-International Edition* **2005,** 44, 1821-1823.

[129] Dawkins, R. In *Hierarchical Organization: A Candidate Principle for Ethology*, Growing points in ethology: based on a conference sponsored by St. John's College and King's College, Cambridge, Bateson, P. P. G.; Hinde, R., Eds. Cambridge University Press: 1996; pp 7-54.

[130] Lane, D., Hierarchy, Complexity, Society. In *Hierarchy in Natural and Social Sciences*, Pumain, D., Ed. Springer Netherlands: 2006; Vol. 3, pp 81-119.

[131] Vonau, F.; Suhr, D.; Aubel, D.; Bouteiller, L.; Reiter, G. and Simon, L. Evolution of Multilevel Order in Supramolecular Assemblies. *Physical Review Letters* **2005,** 94.

[132] Spillmann, H.; Dmitriev, A.; Lin, N.; Messina, P.; Barth, J. V. and Kern, K. Hierarchical Assembly of Two-Dimensional Homochiral Nanocavity Arrays. *Journal of the American Chemical Society* **2003,** 125, 10725-10728.

[133] Ecija, D.; Seufert, K.; Heim, D.; Auwarter, W.; Aurisicchio, C.; Fabbro, C.; Bonifazi, D. and Barth, J. V. Hierarchic Self-Assembly of Nanoporous Chiral Networks with Conformationally Flexible Porphyrins. *Acs Nano* **2010,** 4, 4936-4942.

[134] Piot, L.; Marie, C.; Feng, X. L.; Mullen, K. and Fichou, D. Hierarchical Self-Assembly of Edge-on Nanocolumnar Superstructures of Large Disc-Like Molecules. *Advanced Materials* **2008,** 20, 3854-+.

[135] Blum, M. C.; Cavar, E.; Pivetta, M.; Patthey, F. and Schneider, W. D. Conservation of Chirality in a Hierarchical Supramolecular Self-Assembled Structure with Pentagonal Symmetry. *Angewandte Chemie-International Edition* **2005,** 44, 5334-5337.

[136] Klymchenko, A. S.; Furukawa, S.; Mullen, K.; Van der Auweraer, M. and De Feyter, S. Supramolecular Hydrophobic-Hydrophilic Nanopatterns at Electrified Interfaces. *Nano Letters* **2007,** 7, 791-795.

[137] He, Y.; Ye, T.; Su, M.; Zhang, C.; Ribbe, A. E.; Jiang, W. and Mao, C. D. Hierarchical Self-Assembly of DNA into Symmetric Supramolecular Polyhedra. *Nature* **2008,** 452, 198-U41.

[138] Rohr, C. Supra- Und Biomoleculare Selbstorganisation Und Phasentransformation Auf Hopg - Visualisiert Mit Rastersondenmikroskopie. LMU Munich, Munich, 2007.

Appendix

A Book Chapter: Die Suche nach dem tiefsten Tal: Selbstorganisation von Molekülen in geschlossenen Systemen

C. Rohr

Emergenz, Editor: Christoph Schalley, to be published.

Die Suche nach dem tiefsten Tal: Selbstorganisation von Molekülen in geschlossenen Systemen

Hauptidee/Ziel des Kapitels:

> *Dieses Kapitel beschäftigt sich mit den Strukturen, die auf Grund von Energieminimierung entstehen und dabei emergente Eigenschaften ausbilden. Dabei betrachten wir das wichtige Konzept der Selbstorganisation. Zwei Sorten von Selbstorganisation, die sich in ihren Bausteinen unterschieden, spielen dabei eine Rolle. Einerseits organisieren sich gleiche Bausteine und bilden emergente Strukturen auf Grund ihrer Wechselwirkungen. Andererseits zeigen programmierte Bausteine ein ähnliches Verhalten basierend auf der Information die verteilt in den einzelnen Teilen gespeichert ist. Die Selbstorganisation wird auf der Nanometerskala betrachtet und anhand von molekularer Selbstorganisation wie beispielsweise DNA verdeutlicht.*

1. Wechselwirkungen unter gleichen Bausteinen

Emergente Eigenschaften sind Überstrukturen zu eigen, nicht aber den darin enthaltenen Bestandteilen. Die Überstrukturen entstehen dabei durch Selbstorganisation - ein natürlicher Prozess mit dessen Ergebnissen wir alle vertraut sind. Selbstorganisation findet auf allen Größenskalen unserer beobachtbaren Welt statt: Atome bilden Moleküle, Lipide bilden Membranen, Zellen bilden Kolonien, Sandkörner bilden Dünen, Vögel bilden Schwärme, Sterne bilden Galaxien. In allen diesen Beispiele entsteht die Überstruktur durch Selbstorganisation und bringt emergente Eigenschaften hervor.

Selbstorganisation wird oft darüber definiert, was sie nicht ist: Es organisieren sich die einzelnen Komponenten hier nicht über einen globalen, vorgegebenen Plan. Um beispielsweise ein Haus zu bauen, braucht man einen globalen Plan des Endproduktes um eine solche Überstruktur (Haus) aus seinen Bestandteilen zu schaffen. Genauso wenig wie einen globalen Plan gibt es bei der Selbstorganisation ein Anführerprinzip, bei dem die globale Struktur durch eine oder mehrere herausgehobene Bestandteile vorherbestimmt und geformt wird, wie es zum Beispiel bei hierarchisch organisierten Firmen der Fall ist. Die Ordnung wird auch nicht nach einem Vorlagenprinzip mit Hilfe eines vorgefertigten Templats geschaffen. Das heißt, dass eine Ordnung nicht durch das Anpassen an eine Form ausgebildet wird, die ihrerseits wiederum eine planvolle Erzeugung bedingt. Bei Selbstorganisation entsteht aus lokalen Interaktionen der einzelnen Bestandteile eine globale Ordnung. Daraus ergibt sich die Frage, was lokale Interaktionen sind und wo wir ein anschauliches Beispiel für sie finden.

1.1. Der Einzelne und das Ganze und die Interaktion dazwischen

Schwärme sind ein faszinierender Anblick. Wir alle haben schon einmal Fischschwärme, beispielsweise Heringe oder Sardinen gesehen. Diese Schwärme sind ein exzellentes Beispiel für Selbstorganisation. Der gesamte Schwarm agiert von außen betrachtet wie eine Einheit. Er ändert gemeinsam die Richtung, weicht Hindernissen aus und öffnet und schließt sich, um Fressfeinden auszuweichen. Das alles passiert ohne die Führung eines Alphatieres oder einer genauen Planung, die jeder Sardine einen speziellen Platz innerhalb des Schwarmes zuweist. Wie in Abbildung 1a-c gezeigt, unterliegt unser selbstorganisierter Schwarm lediglich drei simplen Regeln, die jeder einzelne Fisch einhält.

1. Schwimme in die Nähe von anderen Fischen. Wenn du zu weit von deinen nächsten Nachbarn entfernt bist, probiere zu ihnen aufzuschließen.
2. Halte einen Abstand zu deinen nächsten Nachbarn. Diese Regel ermöglicht Manövrierfähigkeit der einzelnen Fische.
3. Schwimme in die gleiche Richtung wie deine nächsten Nachbarn

Bei diesen Regeln fällt auf, dass sie alle lediglich lokal wirksam sind. Das heißt, die Regeln beziehen sich nicht auf den Schwarm als Ganzes, sondern treffen nur Aussagen über die Beziehungen eines Fisches zu seinen nächsten Nachbarn, also die lokale Umgebung jedes einzelnen Fisches. Das heißt der einzelne Fisch muss nur auf seine direkten Nachbarn achten und nicht auf den Schwarm als Ganzes. Wenn durch lokale Wechselwirkungen - hier die ziemlich einfachen Regeln, die das Verhalten der Fische steuern - globale Strukturen - hier der Schwarm - emergieren, wird dieser Vorgang als Selbstorganisation bezeichnet. Wie man theoretisch mit einem simplen Regelnwerk ein komplexes Verhalten erzeugt, haben wir ja schon im Kapitel zu Conways Game of Life sehr eindrucksvoll gesehen.

Dieselben Prinzipien der Selbstorganisation finden sich auch in der unbelebten Welt auf allen Größenskalen wieder. Auch subnanometergroße Moleküle organisieren sich nach den gleichen Grundprinzipien, die wir gerade am Beispiel der Fischschwärme diskutiert haben. Wie in Abbildung 1 gezeigt, treten die Moleküle dabei ebenfalls nur mit ihren nächsten Nachbarn in Wechselwirkung. Dabei ziehen sie sich auf Grund einer ganzen Reihe von verschiedenen attraktiven Kräften an, beispielsweise durch Coulomb-Kräfte zwischen gegennamigen Ladungen, durch Wasserstoffbrücken oder durch die eher schwachen Van-der-Waals-Kräfte, und bewegen sich aufeinander zu. Kommen sich die Moleküle zu nahe, sorgt die Pauliabstoßung der gleichartig geladenen Elektronenhüllen für die Einhaltung eines Mindestabstands. Desweiteren richten sich die Moleküle zueinander aus, ein Prozess der vor allem über gerichtete Wechselwirkungen wie Dipol-Dipol-Wechselwirkungen vermittelt wird. Analog zu den Polen eines Magneten hat ein Dipol ein elektrisch positiv und ein elektrisch negativ geladenes Ende. Die günstigste Anordnung der Moleküle ergibt sich dann, wenn das positive Ende eines Moleküls möglichst nahe beim negativen Ende des Nachbarn ist und zugleich möglichst weit entfernt von seinem positiven Ende. Auch hier wirken alle Wechselwirkungen lediglich lokal zwischen nächsten Nachbarn und resultieren in einem globalen Muster.

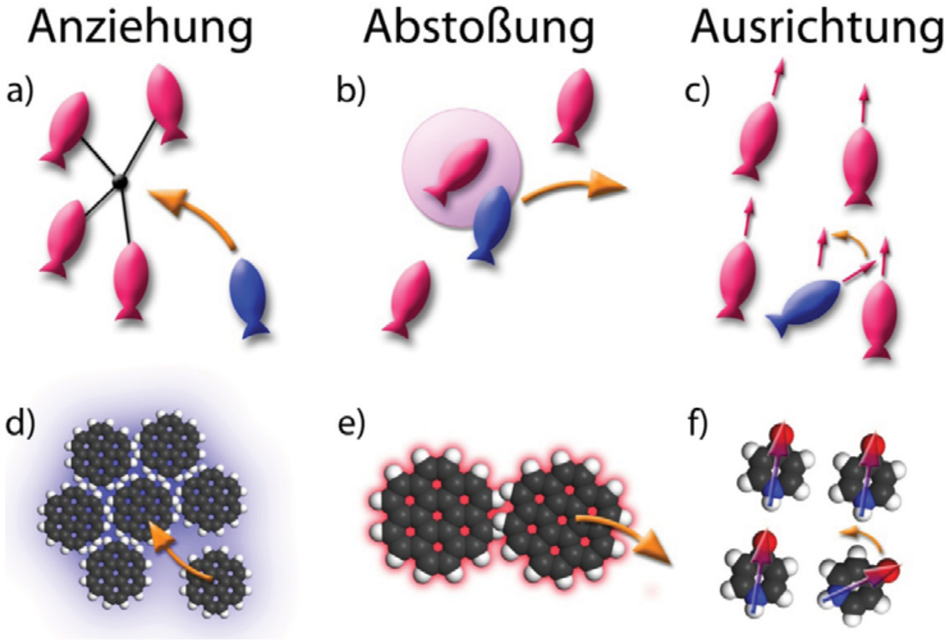

Abb.1: Lokale Wechselwirkungen und Selbstorganisation. Oben: Die drei Regeln der Schwarmbildung bei Fischen: a) Schwimme in die Nähe deiner Nachbarn. b) Halte zum Manövrieren genügend Abstand zu deinen Nachbarn. c) Richte dich an deinen Nachbarn aus. Unten: Äquivalente Prinzipien bei molekularer Selbstorganisation: d) langreichweitige, schwache Anziehungskräfte zwischen Molekülen begünstigen ihre Annäherung. e) Bei zu kleinen Abständen sorgt die Pauli-Abstoßung der Elektronenhüllen zweier Nachbarmoleküle für eine Abstandsvergrößerung. f) Die Ausrichtung an Nachbarmolekülen wird durch gerichtete Wechselwirkungen wie z.B. Dipol-Dipol-Wechselwirkungen bewirkt, die für eine möglichst günstige Ladungsverteilung im Molekülverband sorgen.

1.2 In Flagranti erwischt: Moleküle bei der Selbstorganisation

Moleküle sind so klein, dass sie auch mit dem stärksten Lichtmikroskop nicht direkt sichtbar gemacht werden können. Die Frage ist also, wie man ihre Selbstorganisation untersuchen kann. Grundsätzlich existieren die anziehenden und abstoßenden Kräfte zwischen Molekülen immer und Selbstorganisationsprozesse finden ständig statt. Die experimentellen Methoden, mit denen Naturwissenschaftler solche Prozesse untersuchen, sind genauso vielfältig, wie die Bedingungen, unter denen sie ablaufen. Wir wollen uns im ersten Teil dieses Kapitels auf einen speziellen Fall beschränken, der eine sehr direkte Beobachtung der Selbstorganisation erlaubt. Die Moleküle, die wir uns anschauen wollen, werden auf einer extrem glatten Oberfläche abgelegt. Das Oberflächenmaterial muss leitfähig sein. Dafür kommt Graphit mit seinen ausgedehnten Kohlenstoffschichten ebenso in Frage wie extrem glatte Metalloberflächen. Durch Selbstorganisation finden die Moleküle darauf ihre genauen Plätze, ohne, dass von außen eingegriffen wird. Da sie jetzt auf der Oberfläche liegen, kann man sie mit Hilfe von Rastertunnelmikroskopen sichtbar machen.

Während ein normales Lichtmikroskop wie unser Auge funktioniert und dieses verstärkt, indem es das zu betrachtende Objekt vergrößert, arbeitet ein Rastertunnelmikroskop viel eher wie unser Tastsinn und ist am besten mit einem Finger zu vergleichen. Mit einer atomar scharfen Metallspitze werden die Moleküle auf der Oberfläche abgetastet. Dabei wird kein Druck zur Sondierung verwendet, sondern ein sehr geringer Strom, der durch den quantenmechanischen Tunneleffekt zustande kommt und dessen Betrag abhängig vom Abstand zwischen Spitze und Oberfläche ist. Liegt ein Molekül zwischen Oberfläche und Spitze, ändert das den Tunnelstrom. Eine hochempfindliche Messung dieser Änderungen erlaubt es oft, selbst verschiedene Teile von Molekülen zu unterscheiden. Die Metallspitze fährt dabei die Oberfläche linienweise ab, ähnlich wie das Bild in einem Fernseher aufgebaut wird, siehe Abbildung 2. Durch die Verwendung des Tunnelstromes zur Bildgewinnung werden nicht alleine die Erhebungen der Oberfläche, sondern eine Mischung aus der mechanischen und der elektronischen Struktur der Oberfläche abgebildet. Die Bilder, die aus den Schwankungen des Tunnelstroms in Abhängigkeit vom Ort der Spitze auf der Oberfläche errechnet werden, geben daher auf verblüffende Weise den Aufbau der Moleküle wieder. Auf diese Weise ist es möglich, mit dem vordersten Atom der Spitze Moleküle abzutasten und ihre selbstorganisierten Muster zu beobachten.

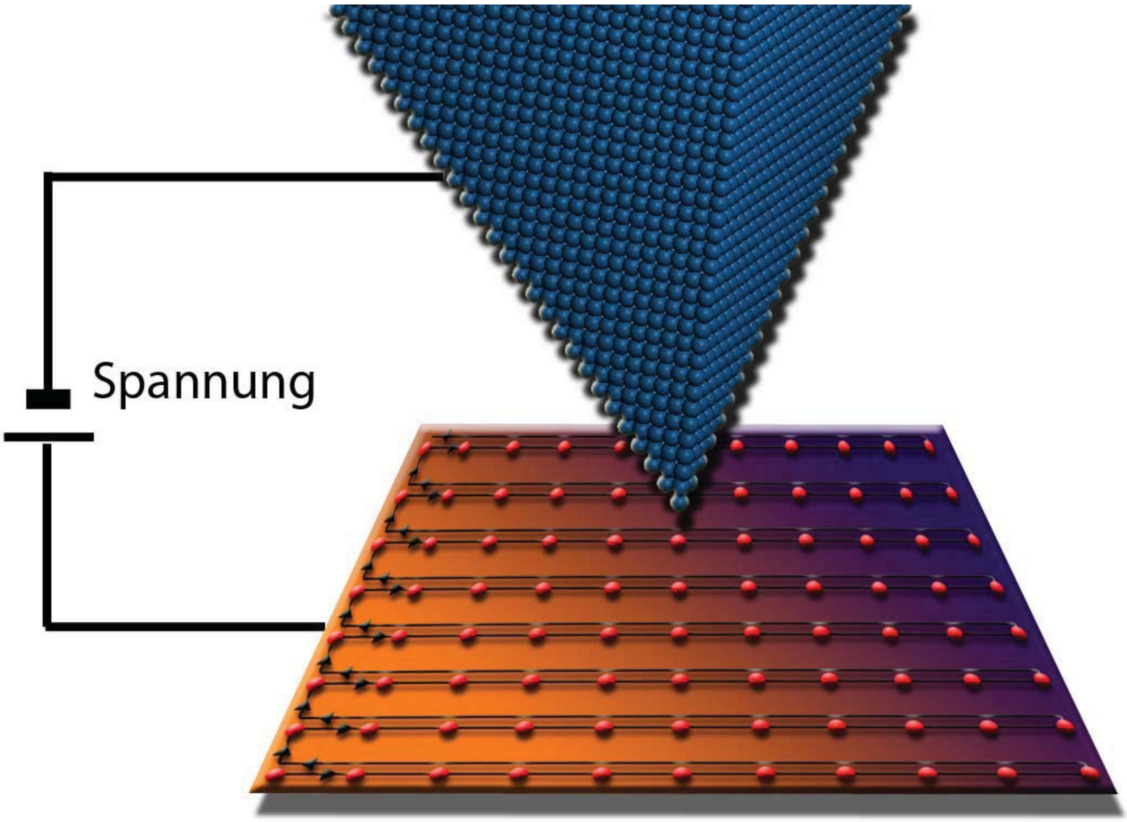

Abb. 2: Das Rastertunnelmikroskop: Der Abstand zwischen der atomar scharfen Metallspitze und dem zu untersuchenden Substrat wird über die Stärke des fließenden Tunnelstromes bestimmt. Durch die Rasterbewegung der Tunnelspitze kann dabei ein zweidimensionales Bild der Oberfläche aufgenommen werden. Auf diese Weise lassen sich selbst einzelne Moleküle abbilden.

1.3 Emergente Eigenschaften in selbstorganisierten Mustern

Die Anordnung mehrerer Moleküle zu einem globalen Muster bringt Symmetriebrechung und damit das Auftreten von emergenten Eigenschaften mit sich. Ein schönes Beispiel für Symmetriebrechung als emergente Eigenschaft bietet die Anordnungs-Chiralität. Chiralität beschreibt generell die Eigenschaft eines Objektes durch Drehung nicht mit seinem Spiegelbild zur Deckung gebracht werden zu können. Betrachten wir das Beispiel von rechtem und linkem Fuß. Der rechte Fuß ist ein Spiegelbild des linken Fußes. Man kann aber den rechten Fuß drehen so viel man will, er wird niemals wie der linke Fuß sein. Solche Objekte von denen es rechtsläufige und linksläufige gibt, werden als chiral bezeichnet. Sie haben einen Drehsinn und sind nicht spiegelsymmetrisch.

Abbildung 3 zeigt den Fall einer chiralen Anordnung von Molekülen auf Oberflächen, die selbst nicht chiral sind. Im Bild 3a liegt zunächst ein einzelnes spiegelsymmetrisches Molekül auf der Oberfläche. Das Molekül ist leicht herzustellen und besteht aus drei ebenen, sechseckingen Benzolringen, die so miteinander über Etherbrücken verbunden sind, dass insgesamt eine bananenförmige Krümmung erreicht wird. Bild und Spiegelbild sind eindeutig als identisch zu erkennen. Kombiniert man aber drei Moleküle miteinander zu einem zyklischen Verband, definiert man einen Drehsinn. Ein solcher flacher Molekülverband ist immer noch achiral, weil die Ebene, in der die drei Moleküle liegen, selbst eine Spiegelebene ist. Legt man ihn aber auf einer Oberfläche ab, bricht man diese letzte Spiegelsymmetrie. Das ganze Gebilde ist nun chiral, weil Ober- und Unterseite durch die Oberfläche verschieden werden.

Die Symmetriebrechung geschieht ganz spontan zu dem Zeitpunkt, an dem sich das zweite Molekül an das erste anlagert. Wegen der Symmetrie des ersten auf der Oberfläche abgelegten Moleküls wird das zweite gleich wahrscheinlich rechts oder links davon positioniert (symmetrische Situation). Nachdem es auf einer Seite angelagert wurde, ist die Situation für alle nachfolgenden Moleküle anders. Es gibt eine bevorzugte Stelle, an der das dritte Molekül stärker mit den ersten beiden wechselwirkt, und eine benachteiligte Stelle für die weitere Anlagerung, in der das dritte Molekül weniger starke Anziehung verspürt (asymmetrische Situation). Die Symmetrie wurde gebrochen und das Muster hat einen Drehsinn erhalten (Abbildung 2b).

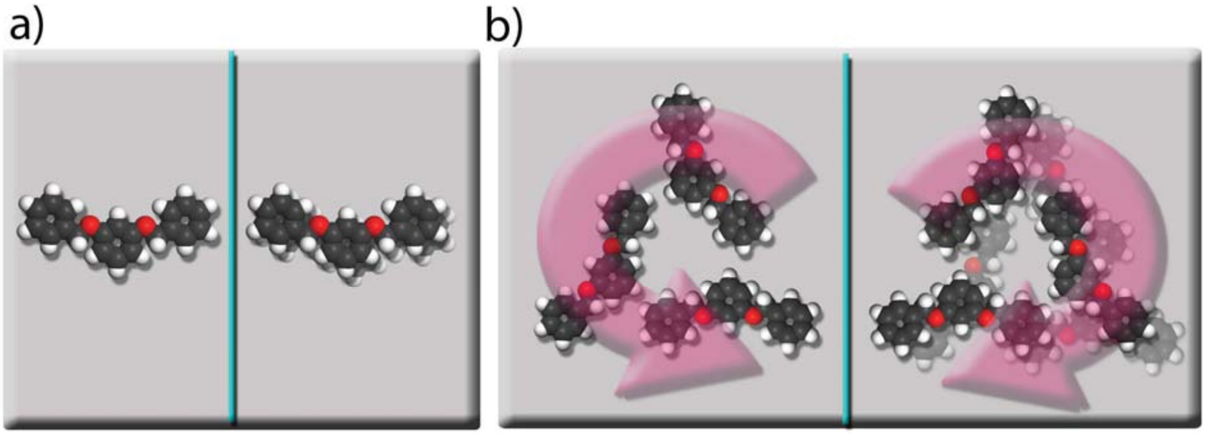

Abb. 3: Entstehung von chiralen Mustern durch Anordnung von Molekülen auf Oberflächen: a) Ein spiegelsymmetrisches Molekül auf einer Oberfläche ist achiral. Es ist mit seinem an der blauen Linie gespiegelten Gegenüber identisch. b) Lagern sich mehrere solcher achiralen Moleküle auf einer Oberfläche in einem Verbund mit Drehsinn zusammen, entsteht durch Symmetriebrechung ein chirales globales Muster. Bild und Spiegelbild lassen sich nicht durch Drehung zur Deckung bringen, ohne die Moleküle wieder von der Oberfläche abzulösen.

Hieran kann man erkennen, dass lokale Wechselwirkungen - ein neues Molekül hat lokal zwei Möglichkeiten sich anzulagern - durch Fortsetzungen zu einer globalen Eigenschaft - Chiralität des Musters - führen können.

Ordnen sich Moleküle zu komplexeren Mustern auf Oberflächen, dann sind diese Muster in den meisten Fällen drehsymmetrisch, auch wenn die Moleküle selbst keine Drehsymmetrie haben. Sind die Wechselwirkungen an einem Molekül asymmetrisch, gleichen sich diese zusammen mit den asymmetrischen Nachbarmolekülen aus und bilden auf diese Weise eine drehsymmetrische Anordnung. Auch diese emergente Eigenschaft entsteht lokal. Ein Beispiel dafür zeigt die Anordnung der Moleküle in Abbildung 4a und 4b

1.4 Hierarchiebildung

In den meisten Fällen zeigen selbstorganisierte Moleküle verschiedene Sorten von Wechselwirkungen, mit denen sie mit ihren Nachbarn interagieren können. Durch multiple Arten von Kräften, die zur Musterbildung beitragen, kommt es zu einer weiteren Form von emergenten Eigenschaften: der Hierarchiebildung. Ein Muster von selbstorganisierten Molekülen besitzt also bestimmte globale Symmetrien. Zusätzlich dazu können diese Muster lokal in kleinere Untereinheiten unterteilt sein, welche größere Einheiten bilden, die sich dann wieder zu noch größeren Einheiten zusammensetzen. Diese hierarchische Anordnung wird dabei durch die unterschiedlichen Kräfte, durch die die Grundbausteine des Musters wechselwirken können, hervorgerufen. In Abbildung 4 ist ein Beispiel zu sehen: Das gleiche Molekül wie eben wurde wieder auf einer Oberfläche abgelegt, jetzt aber ausgestattet mit vier längeren Kohlenwasserstoffketten in seiner Peripherie. Wieder lagern sich drei Moleküle zu einer größeren dreieckigen Einheit zusammen (Abbildung 4b). Diese Einheit wird durch die stärkste Wechselwirkung zwischen den Molekülen, der elektrostatischen Wechselwirkung, zusammengehalten. Diese Wechselwirkung wird in Abbildung 4b durch Dipolpfeile verdeutlicht, wobei man sieht, dass immer ein blaues gekennzeichnetes, negatives Ende an ein rot markiertes positives Ende grenzt. Durch den Zusammenschluss zu dieser größeren Einheit ist diese Wechselwirkung nun abgesättigt. Das heißt, diese Einheit als Ganzes wird kaum noch elektrostatisch mit ihrer Umgebung in Interaktion treten. Dafür treten nun die nächst schwächeren Wechselwirkungen in Aktion und sorgen auf der nächsthöheren Hierarchieebene für eine weitere Strukturierung der auf der Oberfläche liegenden Moleküle.

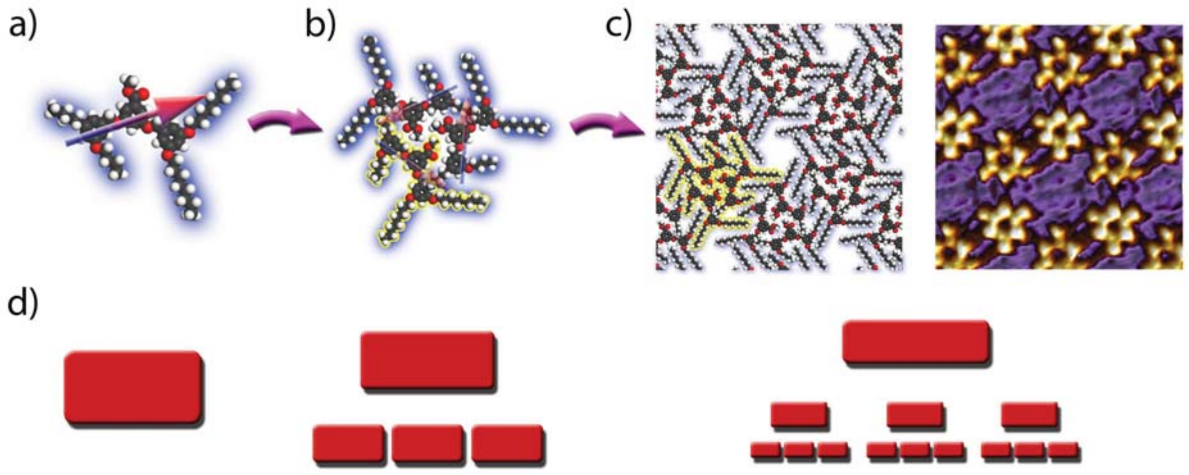

Abb. 4: Hierarchieebenen und Wechselwirkungen: a) Ein einzelnes Molekül mit einem Dipol und Kohlenwasserstoffketten, die über schwache van-der-Waals-Wechselwirkungen miteinander interagieren können. b) Drei Moleküle lagern sich auf Grund von Dipol-Dipol-Wechselwirkungen zu trimeren Einheiten zusammen. c) Diese Einheiten bilden ein Netzwerk über van-der-Waals-Wechselwirkungen, das mit einem Rastertunnelmikroskop sichtbar gemacht werden kann. d) Schematische Darstellung der Hierarchie der Strukturbildung

Diese nächste Stufe der Ordnung hat auf Grund der neuen dominanten Wechselwirkung meist einen anderen Charakter als die vorhergehende Stufe (Übergang von Abbildung 4b zu 4c. Die trimeren Einheiten (Abb. 4b) setzen sich zu einem großen Netzwerk aneinander, dass in diesem Fall durch die Wechselwirkung der blau hinterlegten Kohlenwasserstoffketten zusammengehalten wird. Eine der trimeren Einheiten ist in Abbildung 4c gelb angedeutet. Auch auf dieser Stufe der Organisation gibt es die Möglichkeit, dass sich die (nun schon aus Untereinheiten zusammengesetzten) größeren Grundbausteine wieder so finden, dass ein weiteres Mal abgeschlossene Einheiten entstehen, wenn die Wechselwirkungen lokal abgesättigt werden können. Wie schematisch in Abbildung 4d dargestellt, entstehen so Hierarchien von ineinander geschachtelten, lokal abgeschlossenen Einheiten, die sich zu komplex aufgebauten Netzwerken aus Molekülen ausdifferenzieren.

Diese Ordnungen können unter den richtigen Bedingungen auch wieder aufgebrochen werden, zerfallen dann von der größten Einheit angefangen und gehen auf lokalere Einheiten zurück. Auch hierbei wird sichtbar, wie der lokale Charakter der Selbstorganisation mit abnehmender Stärke zu einer langreichweitigen Ordnung führt.

Die bisher betrachteten multiplen Wechselwirkungen hatten aufeinander keinen großen Einfluss. Was entsteht aber nun, wenn die Wechselwirkungen miteinander in Konkurrenz stehen und jede Wechselwirkung für sich genommen ein anderes resultierendes Muster bevorzugen würde? Dazu ein anschauliches Beispiel: Betrachten wir eine regelmäßig gewellte Unterlage. In der Tat weisen die Unterlagen, auf denen unsere Moleküle liegen, genau so eine Wellung auf, da sie aus aneinander gereihten Atomen aufgebaut sind und damit automatisch gewellt sind. Legen wir nun eine Reihe von Kugeln auf der Unterlage ab, die sich untereinander und mit der Unterlage anziehen. Diese Kugeln sollen in ihrem Durchmesser ein wenig kleiner sein als der Abstand der Wellen der Unterlage (Abbildung 5). Damit haben wir zwei miteinander konkurrierende Wechselwirkungen, die Anziehung der Kugeln untereinander und die Wechselwirkung der Kugeln mit der Unterlage.

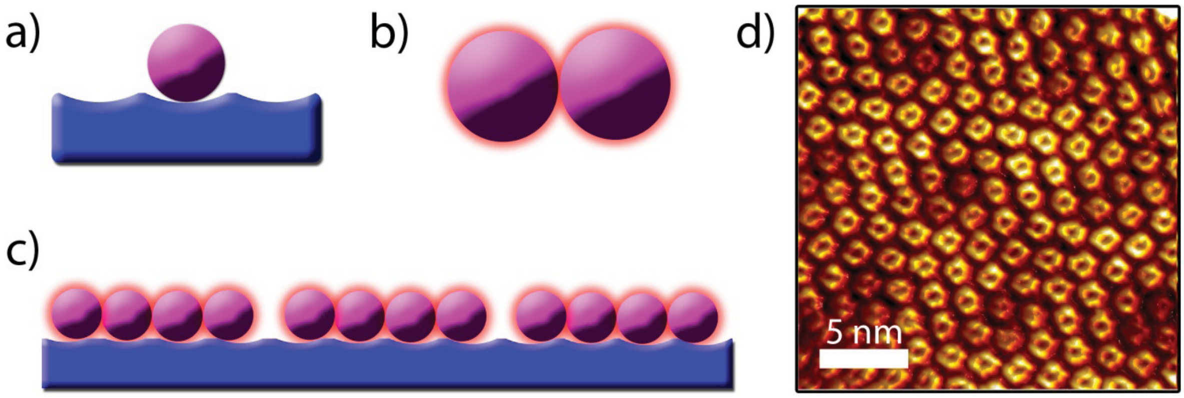

Abb. 5: Konkurrierende Wechselwirkungen: Konkurrenz zwischen dem a) energetisch günstigsten Zustand in der Unterlage und b) der günstigsten Wechselwirkung mit den direkten Nachbarn. c) Aus dem Wechselspiel der beiden Kräfte resultierende Ordnung mit periodischen, emergenten Freistellen nach jeweils vier Einheiten. d) Rastertunnelmikroskopische Aufnahme eines hexagonalen Moiré-Musters in einer Schicht von selbstorganisierten Molekülen, das - auf den zweidimensionalen Fall der Oberfläche übertragen - nach diesem Prinzip zustande kommt. Das Moiré-Muster ist an den unterschiedlichen hellen Farbtönen der verschiedenen kleinen Sechsecke im Bild zu erkennen.

Einerseits wirkt die Wechselwirkung der einzelnen Kugel mit der Unterlage, die am höchsten ist, wenn die Kugel am tiefsten Punkt der Mulde liegt. Andererseits wirkt die Interaktion zwischen zwei Kugeln, die am größten ist, wenn die Kugeln sich berühren. Trägt eine der beiden Wechselwirkungen viel stärker als die andere zum Energiegewinn bei, dominiert diese Wechselwirkung die Ordnung. Beispiel: Die Kugel-Unterlage Wechselwirkung ist stärker. Resultat: Jede Kugel liegt in ihrer eigenen Mulde. Wenn jedoch die konkurrierenden Kräfte ungefähr gleich stark sind, entsteht eine emergente Ordnung.

Abbildung 5c zeigt, wie eine solche Ordnung aussehen könnte. Einige Kugeln bilden eine Gruppe und sind aus ihrer Ruhelage aus der Mitte der Mulde ausgelenkt. An einem bestimmten Punkt schlägt diese Auslenkung um und es entstehen gleichmäßige Abstände, sehr ähnlich einem Moiré-Muster. Diesen Effekt kann man auch bei selbstorganisierten Molekülen beobachten. Wenn die Moleküle auf der Oberfläche dicht packen und die Abstände dieser dichten Packung nicht mit Periodizität der Unterlage übereinstimmen, kommen unterschiedliche Moleküle an unterschiedlichen Stellen der Unterlage (auf einer Erhöhung oder in einer Mulde) zu liegen. Diese unterschiedlichen Höhen, sowie die leicht unterschiedliche elektronische Struktur, werden im Rastertunnelmikroskop durch unterschiedliche Helligkeite der Moleküle sichtbar (Abbildung 5d). So entstehen durch konkurrierende lokale Wechselwirkungen langreichweitige Ordnungen. Wir haben gesehen, dass es die Wechselwirkungen sind, die die entscheidende Rolle bei der Entstehung von emergenten Eigenschaften spielen. Allerdings sind es nicht die Wechselwirkungen an sich, sondern vielmehr das Vorhandensein multipler Wechselwirkungen, die eine Grundvoraussetzung darstellen. Neuartiges Verhalten entsteht also vor allem durch ein subtiles Ausbalancieren widerstreitender Wechselwirkungen.

Betrachten wir unter diesem Aspekt die hierarchische Organisation von selbstorganisierten Molekülen. Durch die Beziehung der verschiedenen Interaktionen - in diesem Fall ihre unterschiedlichen Stärken relativ zueinander - emergiert die neue Eigenschaft des Musters, die Hierarchiebildung, indem nacheinander die unterschiedliche starken Kräfte abgesättigt werden.

Auch bei unserem Beispiel mit den Kugeln entsteht die emergente Eigenschaft, das Moiré-Muster, siehe Abbildung 5 durch die, in diesem Fall antagonistische, Wechselwirkung der beiden Arten von Kräften. Die Wechselwirkungen der Kugel untereinander und der Kugel mit der Unterlage stehen hier in Konkurrenz zueinander. Eine einzelne Kraft hätte ein solches Muster nicht hervorbringen können.

Ein weiterer wichtiger Aspekt ist, dass die verschiedenen Wechselwirkungen in starker wechselseitiger Beziehung zueinander stehen müssen. Bei dem Kugelbeispiel bedeutet dies, dass beide Kräfte ungefähr gleich stark sind. Würde eine Kraft die andere dominieren, hätten wir keine starke oder nur einseitige Beziehung zwischen den Kräften. Emergenz entsteht in der Selbstorganisation deshalb hauptsächlich „in der Mitte“, wo unterschiedliche Wechselwirkungen ähnlicher Stärke miteinander agieren.

1.5 Das tiefste Tal und der mühsame Weg dorthin

Stellen wir uns eine Hügellandschaft vor, in der wir nach dem tiefsten Punkt suchen. In dieser Landschaft gibt es aber auch andere Senken, die in ihrer näheren Umgebung den tiefsten Punkt darstellen. Solche Täler sind lokale Minima, während der tiefste Punkt ein globales Minimum darstellt. Ähnlich wie diese Hügellandschaft kann man sich auch die Energielandschaft der selbstorganisierten Moleküle vorstellen. Hierbei entspricht ein bestimmtes Tal in unserer Landschaft einem bestimmten Muster der Moleküle. Geht man in ein anders Tal, so ändert sich auch die Struktur des Musters. Wie hoch oder tief eine Talsohle liegt, entspricht der Energie dieses bestimmten Musters. Das tiefste Tal in dieser Landschaft entspricht dem energetisch günstigsten Zustand. Ein Muster in einem lokalen Minimum ist dann metastabil, wenn es von seinen umgebenden, energetisch günstigeren Minima durch vergleichsweise hohe Passstraßen getrennt ist (Abbildung 6). Es besteht die Möglichkeit, dass sich das Muster des lokalen Minimums in ein energetisch günstigeres Muster umwandelt. Dazu müssen die Passstraßen niedrig genug sein. Wenn dem so ist, ist die Umwandlung auch reversibel. Ansonsten kann selbst ein energetisch ungünstiges Muster in seinem Zustand „eingefroren“ bleiben.

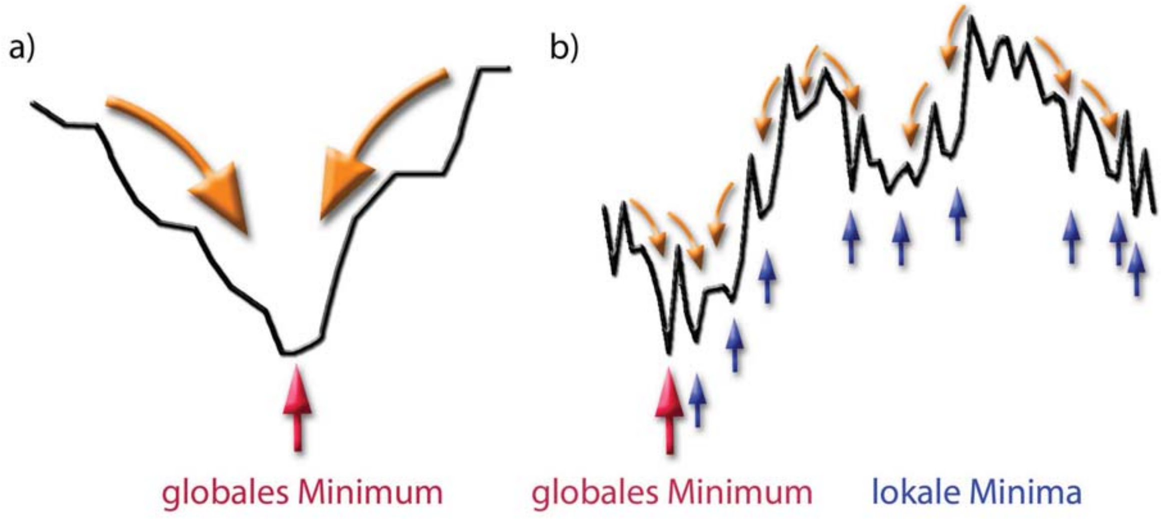

Abb. 6: Energielandschaft: a) Der energetisch günstigste Zustand ist bei einem einzelnen Minimum unabhängig vom Ausgangspunkt des Systems immer zu erreichen. b) Bei einer zerfurchten Energielandschaft kann das System je nach Startpunkt in einem lokalen Minimum hängen bleiben. Komplexe Systeme haben in den meisten Fällen zerfurchte Energielandschaften mit mehreren lokalen Minima.

Manchmal ist der energetisch günstigste Zustand durch eben jene widerstreitenden Wechselwirkungen definiert, die wir uns im letzten Abschnitt angesehen hatten. Meist führt ein energetisch erreichbarer Pfad vom Ausgangszustand in unserer Energielandschaft zum energetisch günstigsten Zustand. Dieser Pfad in der Energielandschaft ist es, der uns in diesem Abschnitt beschäftigen wird. Dabei wird auf einmal nicht nur der beste Endzustand, der unser Ziel ist, interessant, sondern auch der Weg vom Startpunkt aus dorthin. Welches Muster kann sich am schnellsten bilden? Wie hoch sind die Passstraßen, also die Barrieren, die den schnell entstehenden Zustand von den anderen, energetisch günstigeren trennt? In unserem Gebirgsmodell macht es einen erheblichen Unterschied, ob wir am Rande der tiefsten Senke starten und einfach nur nach unten laufen müssen oder ob wir in entlegenen Tälern beginnen und mühsam über mehrere Pässe klettern müssen. Außerdem stellt sich die Frage nach der Art unserer (Energie-)Landschaft. Haben wir es mit einer einzigen tiefen Senke in einer Ebene zu tun oder sieht unsere Landschaft eher wie die Alpen aus?

Bei selbstorganisierten Molekülen kann der Fakt, dass sich bestimmte Muster sehr schnell bilden und auch sehr stabil sind, dazu führen, dass metastabile Ordnungen sich nie in stabile umwandeln. Die hohen Energiebarrieren die diesen Zustand von den anderen günstigeren Zuständen trennen, können dann nur durch externe Maßnahmen wie zum Beispiel längeres Erwärmen überwunden werden. Wärme ermöglicht es den Molekülen sich zu bewegen und damit ihr Muster zu verändern. Das entspricht einer Bewegung der Muster innerhalb der Energielandschaft und erlaubt so das Überklettern höherer, trennender Energiebarrieren, so dass die metastabile Struktur den Weg ins globale Minimum finden kann.

Auch bei den Energielandschaften können wir emergente Eigenschaften beobachten. Durch die zunehmende Komplexität der Moleküle werden die Energiebarrieren zwischen den einzelnen Mustern größer. Dies geschieht, weil die Moleküle unterschiedliche Stellungen (Konformationen) einnehmen müssen, was bei größeren Molekülen mehr Energie beansprucht, unter anderem da größere Teile bewegt werden müssen. Durch die ansteigende Zerfurchung der Energielandschaften mit ansteigender Molekülkomplexität werden metstabile Muster stabilisiert. Dabei entstehen neue lokale Energietäler, d.h. es emergieren mit zunehmender Molekülkomplexität auch neue metastabile Ordnungen, die bei simpleren Mustern nicht vorhanden waren.

Bei dieser Emergenz von neuen Mustern gilt ein weiteres Mal, dass sich Komplexität „in der Mitte“ abspielt. Wenn die Moleküle zu einfach sind, entsteht ein globales Minimum und wir erhalten ein einziges Muster. Sind die Moleküle zu groß, entstehen zu hohe Energiebarrieren zwischen den einzelnen Ordnungen und das gesamte System bleibt in seinem ersten metstabilen Zustand gefangen. Nur wenn die Energiebarrieren im richtigen Bereich im Vergleich zur Raumtemperatur und der damit im System vorhanden Energie zur Überwindung von Barrieren sind, ist Mustervielfalt möglich.

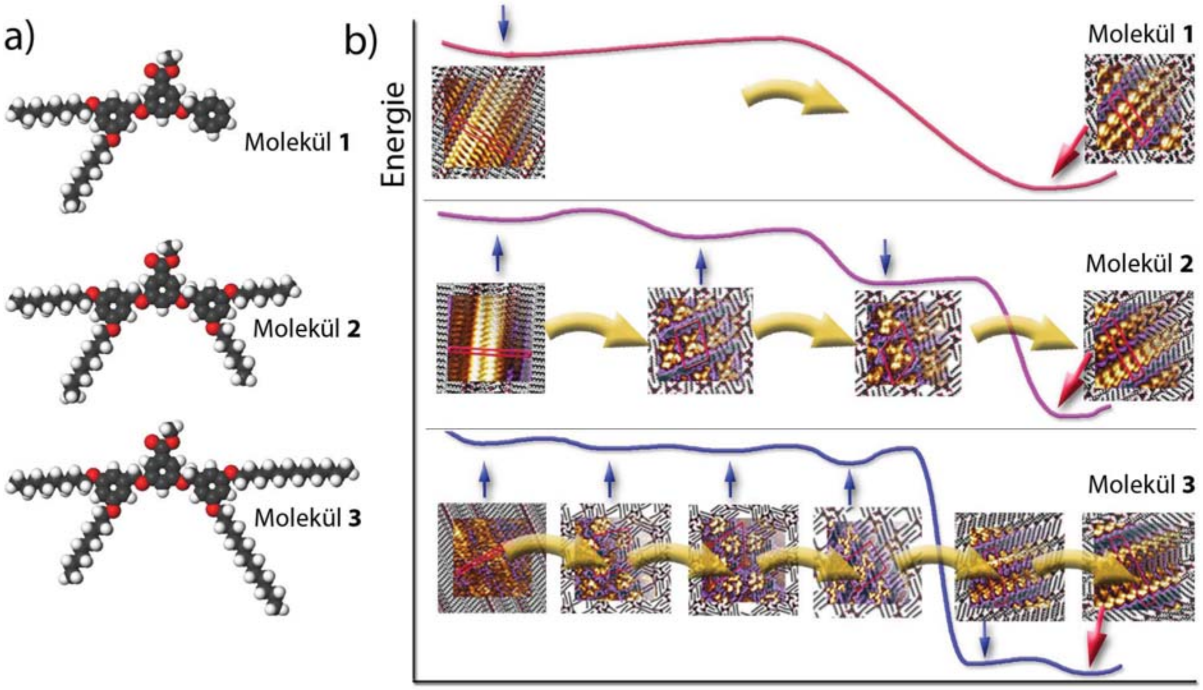

Abb.7: Emergierende metastabile Ordnungen bei steigender Molekülkomplexität: a) Drei verschiedene Moleküle mit steigender Komplexität. b) Experimentell gefundene metastabile Muster der drei Moleküle. Mit zunehmender Seitenkettenlänge emergieren mehr Zwischenzustände. Das heißt, die hier theoretisch berechnete Energielandschaft wird zerfurchter.

Abbildung 7 zeigt ein solches Beispiel der Emergenz metastabiler Muster für verzweigte organische Moleküle. Wir verwenden wieder unser Arbeitspferd von eben und modifizieren nun die Kohlenwasserstoffketten: Die Moleküle unterscheiden sich nun nur in der Länge ihrer Seitenketten auf einer der beiden Seiten, die von null zu sechs zu zwölf Kohlenstoffatomen erhöht wird, während die linken Ketten in ihrer Länge konstant bleiben (Abbildung 7a). Experimentell sind beim einfachsten Molekül zwei Muster zu finden. Die Anzahl der beobachteten Muster nimmt dann mit der Kettenlänge der Moleküle von zwei zu vier und sechs Mustern zu. Die theoretisch berechnete Energielandschaft ist bei den einzelnen Molekülen abgebildet (Abbildung 7b). Alle drei Systeme starten mit dem gleichen Ausgangsmuster und fallen nach verschiedenen Umwandlungen in das globale Minimum was bei allen drei Molekülen wiederum das gleiche Muster ist. Durch die zunehmende Seitenkettenlänge werden die schwachen Wechselwirkungen zwischen den Ketten verschiedener Moleküle moduliert. Dadurch wird die Energielandschaft zerfurchter und resultiert in mehr metastabilen Ordnungen.

Fassen wir kurz zusammen: Die emergenten Eigenschaften von gleichen Bausteinen sind vielfältig. Symmetriebrüche führen zu links- oder rechtsdrehenden Anordnungen. Vor multiple Wechselwirkungen, die auf ähnlichen Stärkeskalen arbeiten, erzeugen vielfältige emergente

Eigenschaften und komplexe Muster auf höheren Hierarchieebenen. Auch fein ausbalancierte antagonistische Kräfte zwischen Molekülen sorgen für die Entstehung von Vielfalt. Verschiedene Muster werden möglich, die abhängig von den genauen experimentellen Parametern zugänglich werden. Mehr und mehr Zwischenzustände treten dabei auf dem Weg ins tiefste Tal auf, wenn die Energielandschaft zunehmend zerfurchter wird.

2. Wechselwirkungen unter unterschiedlichen programmierten Bausteinen

Im ersten Abschnitt war der in ihren Bindungsstellen enthaltene Informationsgehalt der Bausteine eher gering. Komplexität und Emergenz entstanden durch Selbstorganisation. Im zweiten Teil wollen wir uns mit Bausteinen beschäftigen, die selbst komplexer und gezielt programmierbar sind. Die Frage ist also: Könnte man nicht Bausteine herstellen, deren Eigenschaften so spezifisch zueinander passen, dass diese nur noch zusammengebracht werden müssen, um dann eigenständig eine genau definierte Struktur auf molekulare Ebene herzustellen? Was für Eigenschaften müssten ein solcher Prozess und die beteiligten Bausteine haben? In diesem Teil werden wir uns mit programmierten Bausteinen beschäftigen, die genau dieses Verhalten zeigen. Das heißt, dass sie nach dem Zusammenbringen von selbst eine komplexe Struktur bilden, die ihnen einprogrammiert wurde.

Es gibt verschiedene Experimente, in denen mit solchen Bausteinen gearbeitet wird. Im Nachfolgenden werden wir uns beispielhaft auf den Bereich der DNA-Organisation fokussieren. Diese Selbstorganisation findet im Gegensatz zum vorherigen Kapitel in Lösung, d.h. dreidimensional statt. Wir vollziehen also gleich zwei gedankliche Sprünge: Hin zu gezielt programmierbaren Bausteinen und von der Zweidimensionalität der Oberfläche in das Volumen der Lösung.

Die Natur hält relativ leicht zu programmierende Moleküle für uns bereit: Die Desoxyribonukleinsäure (DNA) ist in der Zelle der Informationsträger der Erbsubstanz. Diese Eigenschaft eines Informationsträgers kann man gezielt nutzen, um DNA-Bausteine synthetisch zu programmieren, damit sie sich selbst organisieren.

2.1 Basenpaarung und die Struktur der DNA

Information wird in der DNA in einer Sequenz von Nukleobasen gespeichert, von denen es vier verschiedene gibt: Adenin, Thymin, Guanin und Cytosin (Abbildung 8a). Ein DNA-Strang besteht aus einem Rückgrat aus Desoxyribose, einem Zucker, und Phosphatresten, die die Desoxyriboseeinheiten miteinander verknüpfen. Von diesem Rückgrat zweigt in regelmäßigen Abständen an jeder Zuckereinheit eine der vier möglichen Nukleinbasen seitlich ab. Die

Erbinformation, die in der DNA enthalten ist, wird durch die Abfolge der variablen Nukleinbasen (Adenine, Thymin, Guanin, Cytosin) gespeichert. Wie bei einem Schlüssel und dem zugehörigen Schloss bilden jeweils zwei der vier Nukleinbasen bilden ein komplementäres Paar. Adenin paart immer nur mit Thymin und Guanin immer nur mit Cytosin. Diese Basenpaarungen sind energetisch günstig und haben zur Folge, dass eine bestimmte Abfolge von Nukleinbasen in der DNA eine sehr selektive Information enthält. Auf diese Weise kann ein zweiter Einzelstrang mit der korrekten zum ersten Strang komplementären Abfolge von Nucleinbasen sehr spezifisch an den ersten binden. Abbildung 8b zeigt im oberen Teil die korrekte Paarung bis zu der Stelle, an der zwei nicht komplementäre Basen miteinander paaren müssten. Hier können die Stränge nicht in der richtigen Weise zusammenkommen und laufen deswegen auseinander. Natürliche DNA existiert daher in einer Doppelstrangstruktur. Zur Replikation bei der Zellteilung werden die beiden Stränge voneinander getrennt und jeweils ein neuer Komplementärstrang synthetisiert. Danach existieren zwei identische Doppelstränge, von denen jeweils einer in jeder der beiden Tochterzellen bleibt. Die Doppelstränge falten sich dabei in eine Doppelhelix (Abbildung 8c), die einen Durchmesser von ca. 2 nm und eine Länge von bis zu 1 m haben kann.

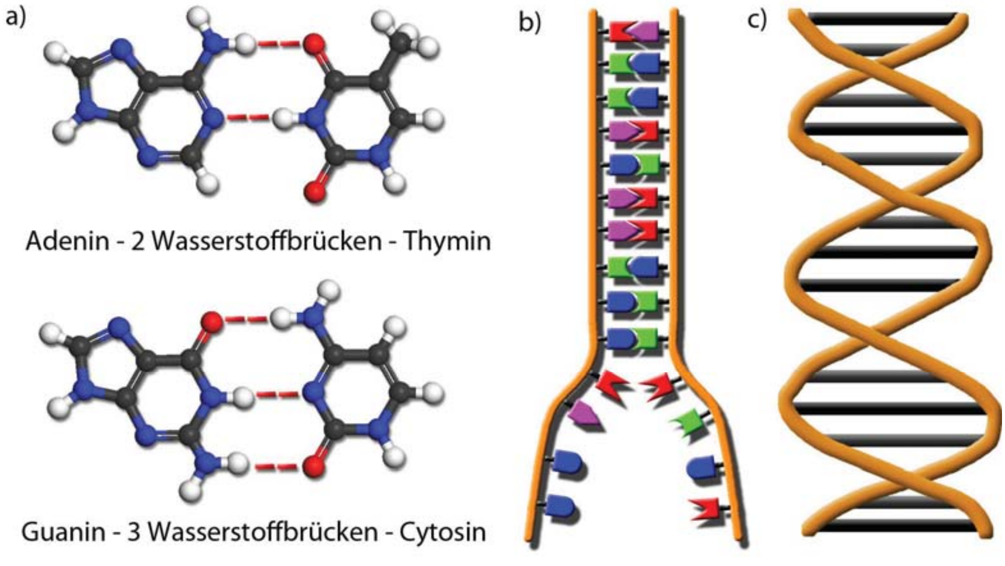
a)
Adenin - 2 Wasserstoffbrücken - Thymin
Guanin - 3 Wasserstoffbrücken - Cytosin
b)
c)

Abb.8: Eigenschaften der DNA: a) Komplementarität der DNA Basen; das Adenine-Thymin Paar wird durch zwei Wasserstoffbrücken, das Guanin-Cytosin Paar durch drei Wasserstoffbrücken miteinander verknüpft (rot gestrichelt). b) Ein DNA Strang kann mittels der DNA Basen programmiert werden und passt so nur zu seinem komplementären Gegenstück. c) Zwei komplementäre DNA-Stränge bilden eine Doppelhelixstruktur aus. Die schwarzen waagerechten Linien stehen jeweils für ein Basenpaar.

2.2 Programmierte DNA von 1D nach 2D

Trotz ihres Durchmessers, ist die DNA Helix im Wesentlichen eine eindimensionale Struktur und kann wie eine Linie betrachtet werden. Um nun auf synthetische Weise programmierte Bausteine zum Herstellen von räumlichen Strukturen zu verwenden, braucht man eine DNA-Anordnung in zwei oder drei Dimensionen. Wir werden uns hier zuerst auf den einfacheren Fall der zweidimensionalen Strukturen konzentrieren.

Die Idee einer zweidimensionalen Anordnung der DNA kommt aus der Natur und wird auch in Zellen verwendet. Dies geschieht in Zellen allerdings nicht zur DNA-Strukturbildung, sondern ist ein Zwischenschritt bei der DNA Rekombination. Bei dieser Struktur, genannt Holliday-Junction, werden nicht zwei DNA-Stränge miteinander kombiniert, sondern vier. Die Information auf den vier Bausteinen ist so gestaltet, dass jeweils eine Hälfte komplementär zu einem Strang und die andere Hälfte zu einem anderen Strang ist. Wenn dies reihum geschieht, entsteht eine Kreuzstruktur (Abbildung 9a). Diese Holliday Junction kann mit überstehenden, so genannten klebrigen Enden ausgestattet werden, die spezifisch an einen anderen komplementären Baustein binden. Setzt man in allen vier Richtungen immer wieder eine Holliday Junction an die nächste, entstehen zweidimensionale Netze (Abbildung 9b).

Diese überstehenden Enden halten anfangs durch Wasserstoffbrückenbindungen zusammen, können dann in einem zweiten Schritt durch starke chemische Bindungen zwischen den einzelnen Holiday Junctions fixiert werden. Das sorgt dafür, dass das gesamte Netzwerk aus zusammenhängenden DNA Strängen besteht.

Die DNA hat eine Doppelhelixstruktur und das trifft auch für die Doppelstränge zwischen zwei Holliday-Junctions zu. Auch diese Eigenschaft der DNA trägt zu den resultierenden Netzwerken bei. Haben zwei Holliday-Junctions einen Abstand von genau zwei Helixwindungen, entsteht ein Netzwerk von in sich verflochtenen Ringen ähnlich einem Kettenhemd (Abbildung 9c). Werden die einzelnen DNA Stücke nur ein wenig gekürzt, so dass nur eineinhalb Windungen resultieren, bevor die nächste Holliday-Junction erreicht ist, besteht das Netzwerk aus ineinander geflochtenen Fäden ähnlich einem gewebten Stoff.

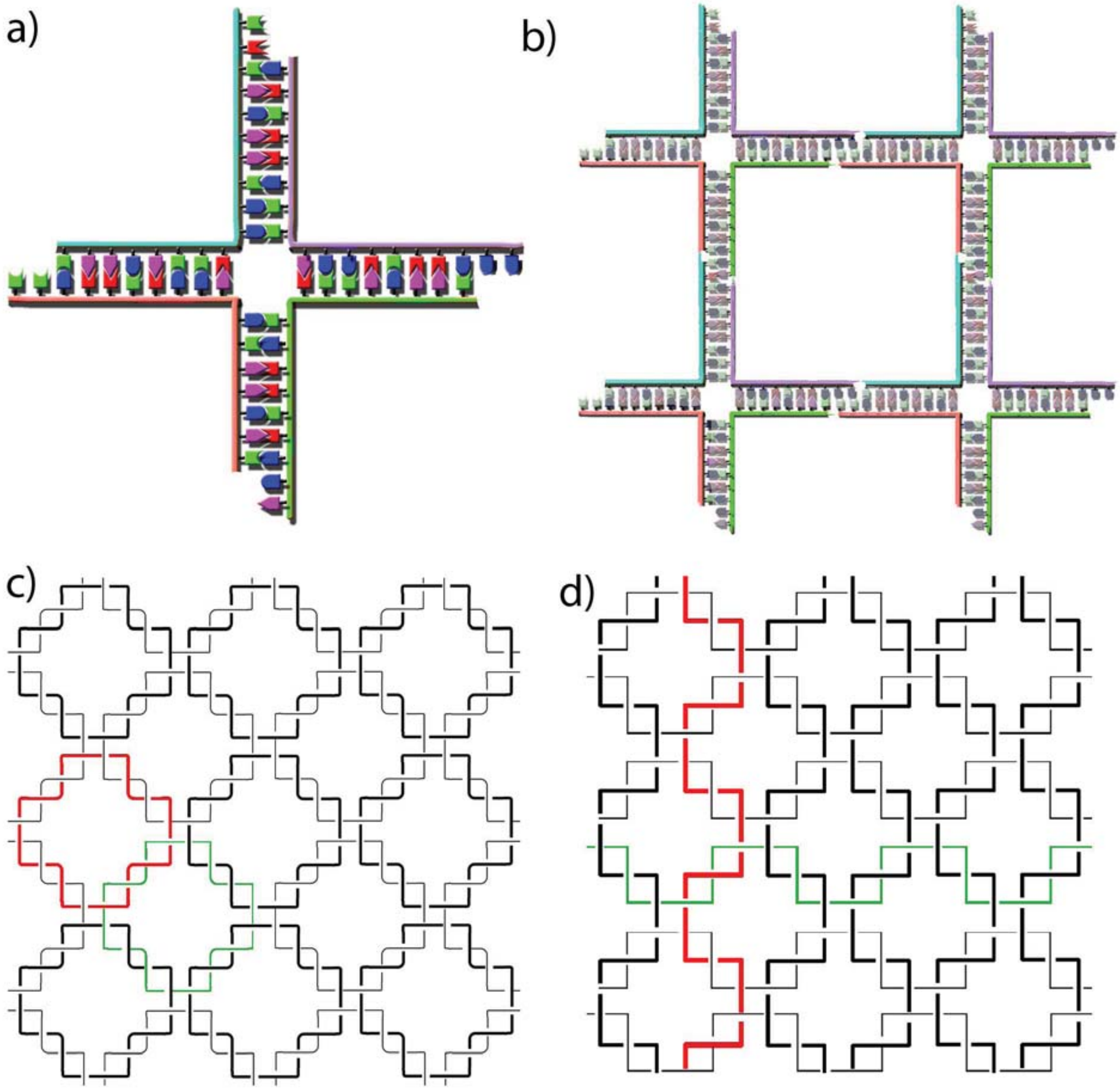

Abb. 9: 2D-DNA Strukturen: a) Die Holiday-Junction ist eine einfache Möglichkeit, zweidimensionale Strukturen zu konstruieren. Vier DNA-Stränge, die reihum jeweils zur Hälfte zu ihren beiden angrenzenden Strängen komplementär sind. Diese bilden eine Kreuzstruktur. b) Stehen an den Enden der Holiday-Junction selektive DNA-Enden über, können zweidimensionale Netzwerke konstruiert werden. Die Anzahl der DNA Helixwindungen bestimmt die Art des Netzwerkes. c) Bei zwei Windungen entstehen in sich geschlossene und wie bei einem Kettenhemd miteinander verschlungene Ringe, während d) bei eineinhalb Windungen einem Flechtwerk miteinander verwobener Fäden resultiert (jeweils rot und grün hervorgehoben).

Dieses Grundprinzip der selektiven Verknüpfung unterschiedlicher Teile verschiedener DNA-Stränge wurde von Nadrian Seeman nicht nur für die Herstellung der gezeigten Netzwerke, sondern auch für kompliziertere dreidimensionale Objekte angewandt. Darunter finden sich

Knoten aus DNA, Borromäische Ringe, die zu dritt untrennbar miteinander verbunden sind, solange keiner von ihnen aufgeschnitten wird und viele andere mehr. Durch dieses Grundprinzip entstehen sehr komplexe Strukturen aus kleinen, korrekt programmierten Bausteinen, die sich selbst zusammensetzen. Hierbei sehen wir das Prinzip, dass sich lokale Wechselwirkungen, nämlich die Basenpaarungen, zu einem globalen Muster organisieren, nämlich der Doppelhelix in der natürlichen DNA oder den Netzwerken und dreidimensionalen Gebilden aus synthetischer DNA.

2.3 DNA-Origami

Ein noch stärkerer Schritt in Richtung der programmierten Bausteine ist das DNA-Origami. Hierbei wird zunächst ein sehr langer DNA-Einzelstrang synthetisiert. Dieser Strang wird dann durch Zugabe verschiedener kleiner, programmierter DNA-Stücke gefaltet, die nur zu bestimmten Stellen des langen Strangs komplementär sind und nur dort andocken können. Aus der so induzierten Faltung stammt in Analogie zur japanischen Papierfaltkunst der Name "DNA-Origami".

Ein sehr anschauliches Beispiel ist in einer Arbeit von Paul Rothemund beschrieben. In dieser Arbeit wird ein DNA Strang von 7000 Basen Länge mit 200 kurzen DNA Stücken gefaltet. Dazu überlegt man sich die gewünschte Form der resultierenden Struktur und faltet zeilenweise den langen DNA Strang in diese Figur. In Abbildung 10a ist dieser lange DNA Strang (anthrazit) schematisch dargestellt. Um die einzelnen Zeilen des langen Stranges zusammenzuhalten und umzufalten sind kurze stabilisierende Querverbindungen nötig, in Abbildung 10a durch die farbigen Stränge dargestellt. Damit diese spezifisch nur an den ihnen zugedachten Stellen auf die richtige Weise binden, wird die Selektivität der unterschiedlichen DNA-Sequenzen ausgenutzt. Jede Querverbindung findet ihre passende Stelle durch eine spezifische Nukleotidsequenz. In Abbildung 10b ist diese Struktur nun schematisch als gefaltete Doppelhelix dargestellt, wobei auffällt, dass zusätzlich auch die Windung der DNA innerhalb der Struktur zu beachten ist. Nach der Synthese der einzelnen DNA Bausteine werden sie in wässriger Lösung zusammengegeben und die Struktur entsteht durch Selbstorganisation ohne äußeren Einfluss. Diese Information, wie die resultierende Struktur aussehen soll, ist in der Programmierung der einzelnen Bausteine enthalten; die Endstruktur ist der energetisch günstigste Zustand der Mischung. Die möglichen resultierenden Formen sind in Abbildung 10c dargestellt. Alle diese Quadrate, Dreiecke, Sterne und Smileys sind aus immer dem gleichen 7000 Basen langen Einzelstrang hergestellt, der auf verschieden Arten durch Selbstorganisation gefaltet wurde. Dabei zeigen die beiden oberen Reihen in Abbildung 10c den schematischen Aufbau der Struktur, während die beiden unteren Reihen Rasterkraftmikroskopiemessungen der ca. 100 nm x 100 nm großen Formen sind. In der untersten Zeile kann man einige Fehlfaltungen sehen, aber auch die präzise Wiederholbarkeit der Selbstorganisation beispielsweise über zwanzig identische Smileys im drittletzten Bildausschnitt von links.

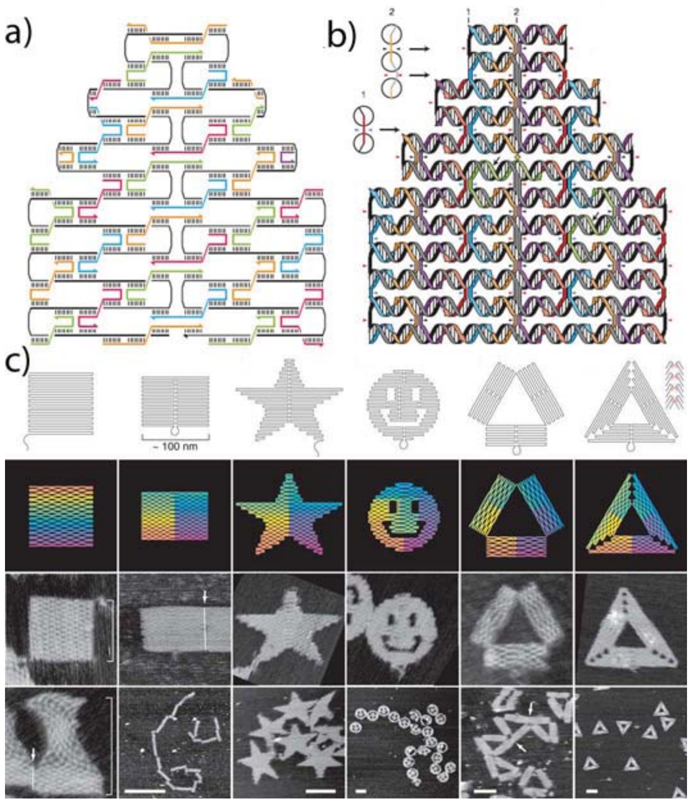

Abb.10: DNA Origami: a) Ein langer DNA-Strang (anthrazit) wird mit Hilfe vieler kleiner, programmierter Einzelstränge (farbig) gefaltet (Origami) und bildet als energetisch günstigsten Zustand eine zweidimensionalen Struktur. b) Schema der DNA-Struktur, in dem die Windungen der DNA sichtbar werden. c) Verschiedene Formen hergestellt aus unterschiedlich gefalteter, selbstorganisierter DNA. Die beiden oberen Reihen zeigen die schematischen Strukturen, die alle aus dem gleichen 7000 Basen langen Einzelstrang erhalten wurden. Die programmierten Bausteine werden lediglich zusammen in die Lösung gegeben und setzen sich selbst ohne weiteres Zutun des Chemikers aneinander. Die beiden unteren Reihen sind Rasterkraftmikroskopieaufnahmen der 100 nm x 100 nm großen Strukturen.

Beim Aufbau von größeren Strukturen aus geeignet programmierter DNA hilft die Selbstorganisation bei der Formgebung. Alle nötigen Informationen sind in den lokalen Wechselwirkung der einzelnen Teile enthalten. Es ist faszinierend, wie viel Kontrolle die richtige Programmierung der Bausteine über das Endergebnis ausübt und wie viele Gestaltungsmöglichkeiten sich ergeben, wenn man diese Programmierung beherrscht. Der Mensch kann sich die

Ausbildung höherer Strukturen durch Selbstorganisation zu Nutze machen, wenn er die Programmiersprache der Natur versteht. In diesem Kapitel wird auch klar, dass die Grenzen zwischen emergenten und gesteuerten Strukturen nicht fest sind, sondern auch fließend ineinander übergehen können.

3. Zusammenfassung und Diskussion

In diesem Kapitel wurde gezeigt, dass Selbstorganisation ein wichtiger Mechanismus ist, mit dessen Hilfe emergente Eigenschaften entstehen. Dabei müssen vier Grundvoraussetzungen gegeben sein:

a) Schwache Wechselwirkungen, die reversibel sind, damit Strukturen nicht in ihrem lokalen Startminimum hängenbleiben

b) Fehlerkorrektur, die nur durch Reversibilität möglich wird

c) Mobilität der Bausteine (bei Molekülen ist diese normalerweise durch die Brownsche Molekularbewegung gegeben) zur Suche nach der optimalen Struktur

d) die richtige Programmierung der Wechselwirkungen zwischen den Molekülen, damit ein eindeutiger Endzustand erreicht werden kann

Bei der Selbstorganisation bilden sich geordnete, globale Muster auf Grund von simplen lokalen Regeln aus. Diese Wechselwirkung zwischen nächsten Nachbarn führt durch Energieminimierung zu einer größeren Ordnung.

Größere Komplexität kann erreicht werden, wenn die Bausteine mehrere Wechselwirkungen miteinander haben, da dann Hierarchien in den Kräften entstehen, die sich in den Anordnungen niederschlagen. Antagonistische Wechselwirkungen zwischen den Bausteinen führen zu einem komplizierten Zwischenzustand, in dem beide Wechselwirkungen zum Teil befriedigt werden.

Der Weg von einem Ausgangszustand zum energetisch günstigsten Zustand verläuft in einer zerfurchten Energielandschaft. Zu beobachten sind dabei metastabile Zwischenzustände, in die sich das Ausgangsmuster sukzessive umwandelt. Die Erhöhung der Komplexität des Moleküls erschafft dabei neue mögliche Zwischenzustände die zusätzlich angenommen werden können.

Die emergente Endstruktur kann allerdings auch über Information in den einzelnen Bausteinen der Endstruktur gespeichert sein. Auch so entsteht auf Grund lokaler Wechselwirkungen und Energieminimierung eine emergente Endstruktur.

Literatur:
[1] N. C. Seeman, Nature 421, 427 (2003).
[2] F. A. Aldaye, A. L. Palmer, and H. F. Sleiman, Science 321, 1795 (2008).
[3] P. W. K. Rothemund Nature 440, 297 (2006).
[4] N. C. Seeman, Angew. Chem. Int. Ed. 37, 3220 (1998)

B Organic superconductors revisited

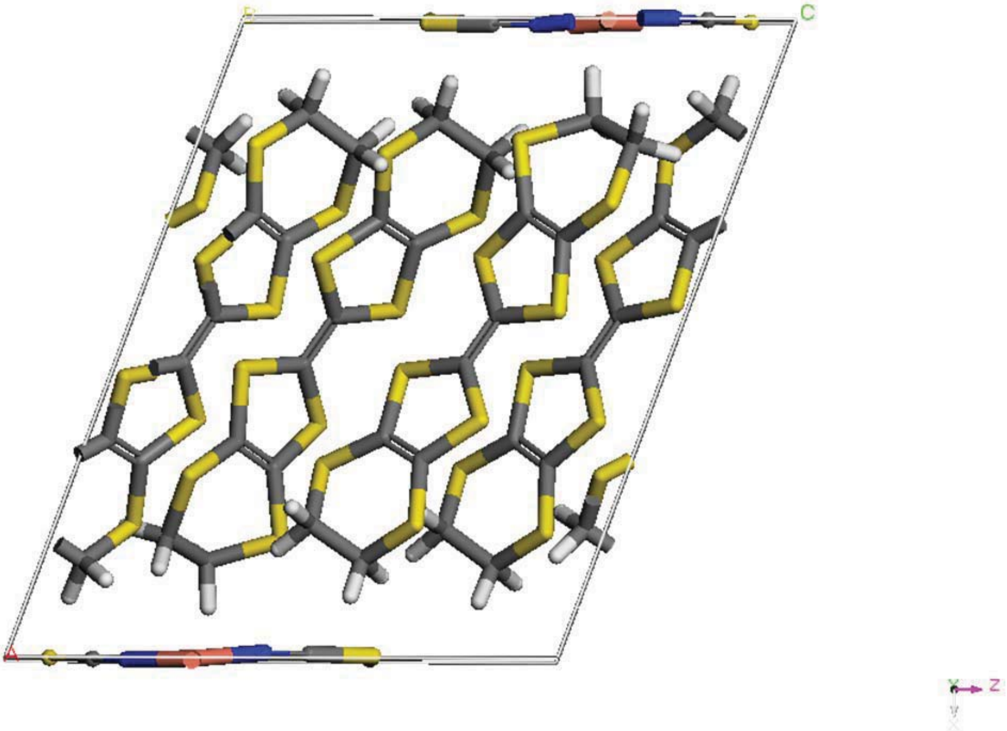

C. Rohr, J.M. Büttner, F.A. Palitschka, N.D. Kushch, M.V. Kartsovnik, W. Biberacher,R. Gross, B.A. Hermann

Eur. Phys. J. B **69**, 167–171 (2009)

Eur. Phys. J. B **69**, 167–171 (2009)
DOI: 10.1140/epjb/e2009-00135-2

THE EUROPEAN
PHYSICAL JOURNAL B

Regular Article

Organic superconductors revisited

STM imaging and DFT based simulations of the bc plane of κ-(BEDT-TTF)$_2$Cu(NCS)$_2$

C. Rohr[1], J.M. Büttner[1], F.A. Palitschka[1], N.D. Kushch[2], M.V. Kartsovnik[3], W. Biberacher[3], R. Gross[4], and B.A. Hermann[1,a]

[1] Walther-Meissner-Institute (WMI) of Low Temperature Research of the Bavarian Academy of Science and Faculty of Physics/Center for Nano Science (CeNS), LMU Munich, Walther-Meissner-Strasse 8, 85748 Garching b. München, Germany
[2] Institute of Problems of Chemical Physics, Russian Academy of Science, Chernogolovka, 142432 Moscow-region, Russia
[3] Walther-Meissner-Institut, Bayerische Akademie der Wissenschaften, 85748 Garching, Germany
[4] Walther-Meissner-Institut, Bayerische Akademie der Wissenschaften, 85748 Garching, Germany/Physik-Department, Technische Universität München, 85748 Garching, Germany

Received 5 August 2008 / Received in final form 4 March 2009
Published online 15 April 2009 – © EDP Sciences, Società Italiana di Fisica, Springer-Verlag 2009

Abstract. The surfaces of a ten years aged crystal and a freshly prepared κ-(BEDT-TTF)$_2$Cu(NCS)$_2$ crystal were compared by scanning tunneling microscopy (STM). The molecularly-resolved STM images of the *bc* plane of the crystals agree with each other and with the electronic contrast obtained by new density functional theory (DFT) based simulations. Even after ten years STM images of the molecular stacking of BEDT-TTF display a variation in brightness at the positions of different molecules. We attribute this symmetry breaking concerning the brightness in the STM images of the otherwise equivalent BEDT-TTF dimers to the electronic states of a relaxed surface.

PACS. 68.37.Ef Scanning tunneling microscopy – 74.70.Kn Organic superconductors – 71.15.Mb Density functional theory, local density approximation, gradient and other corrections

1 Introduction

κ-(BEDT-TTF)$_2$Cu(NCS)$_2$ (κ-di[bis(ethylenedithio)tetrathiafulvalene]di(thiocyane)cuprate) has one of the highest transition temperatures ($T_c = 10.4$ K) among organic superconductors. The synthesis of the κ- [1] and α- [2] phases were first reported in 1988. In the κ-phase two BEDT-TTF molecules form a pair with their central tetrathiafulvalene planes almost parallel. These dimers stack nearly perpendicular to each other to form the donor sheet along the *bc* plane [3] of the molecular composite crystal alternated in the *a*-direction by Cu(NCS)$_2^-$ anion sheets. The donor sheets are responsible for the electrical conductivity of the material [4] and hence its superconductivity. Scanning tunneling microscopy (STM) is an excellent tool to study the electronic surface morphology as well as spectroscopic details revealing the local gap structure of this superconductor [5,6]. Tunneling spectroscopy performed on the *bc* plane reveals an energy gap, supporting a *d*-wave pairing symmetry in κ-(BEDT-TTF)$_2$Cu(NCS)$_2$ [5]. When tunneling is performed on the lateral crystal side, perpendicular to the *bc* plane, the energy gap shows an angle dependence [5]. Spectroscopy above the critical temperature reveals a pseudogap similar to that found for cuprate superconductors [6]. When surface topography is studied with STM using constant current mapping, the obtained profile corresponds to the integrated density of available electronic states (DOS) between the Fermi-energy and applied potential (V_{Bias}) [7]. Hence, a comparison of the experimental data to a simulation of the integrated DOS in the relevant energy range gained by density functional theory (DFT) calculations or at least a comparison to the highest occupied molecular orbital (HOMO) calculation is desirable. Elaborate DFT calculations (Dmol^3) on the charge density expected on surfaces of the BEDT-TTF family were so far only reported for BEDT-TTF[FeBr$_4$] [8]; the latter material is interesting for its magnetic ordering. Also, exchange potentials for various organic superconductors [9–11], as well as the Fermi surface, Coulomb interaction and HOMO [12,13] are available.

In the past, the cation (donor) layers as well as the anion layers [19] of κ-(BEDT-TTF)$_2$Cu(NCS)$_2$ have been imaged with scanning tunneling microscopy. Various attempts were made to compare the images with ab initio calculations of the HOMO for the α-phase and the κ-phase [20] of (BEDT-TTF)$_2$Cu(NCS)$_2$. While usually the *bc* plane is addressed [14–20], Yoshimura et al. [21] investigated the *ab* plane of κ-(BEDT-TTF)$_2$Cu(NCS)$_2$

---

[a] e-mail: `b.hermann@cens.de`

and compared the STM results to calculations of the HOMO of the molecule. Protrusions of varying brightness were observed in the STM images and were attributed to the four molecules of the unit-cell. We present here DFT based simulations of a relaxed *bc* plane of κ-(BEDT-TTF)$_2$Cu(NCS)$_2$ and use them to discuss the brightness modulations observed in our STM-images.

The fragile [22–24] organic superconductor crystals are extremely hard to cleave and thus are usually investigated as grown. When left to aging, the surfaces of these organic composite materials are exposed to environmental influences. Hence, it is instructive to conduct a study of the aging effect on the crystal surfaces with a surface sensitive technique like scanning tunneling microscopy. In order to do so, we investigate the *bc* plane of κ-(BEDT-TTF)$_2$Cu(NCS)$_2$ single crystals of different ages (few months and 10 years aged under ambient conditions) with STM and compare the images with state-of-the-art CASTEP theoretical DFT based simulations of a relaxed and not relaxed surface. In this paper we show, that taking into account a surface relaxation explains all major features of the STM images.

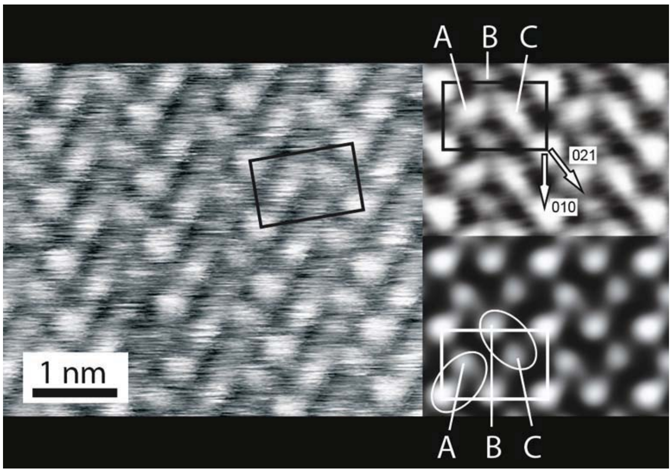

Fig. 1. Drift corrected STM image of the *bc* plane of a few month old κ-(BEDT-TTF)$_2$Cu(NCS)$_2$ crystal ($V_{Bias} = +30$ mV, $I_T = 3$ pA, 5.0 nm × 4.3 nm, ambient conditions); the black rectangle marks a unit cell. The insets show four complete (2 × 2) unit cells; the top graphics was gained from a correlation averaged cut of the STM-measurement; the bottom graphics displays the convoluted DFT based simulation presented in Figure 3b for comparison with the STM-measurements.

2 Results and discussion

The crystals were investigated at room temperature to study the microscopic structure of the surface layer. Figure 1 shows a drift corrected room temperature image of the *bc* plane of a freshly prepared crystal. The upper inset displays an averaged sub-image with a size chosen to show four complete crystal unit cells. The image reveals several regular protrusions partially arranged in rows exhibiting a high electronic contrast. Assuming that the brightest protrusions correspond to the corner BEDT-TTF molecules of the unit cell, the size of the unit cell is determined to be 0.84 nm × 1.33 nm, agreeing within the measurement error (4%) with the size of the *bc* plane unit cell of 0.844 nm × 1.31 nm of κ-(BEDT-TTF)$_2$Cu(NCS)$_2$ determined from x-ray analysis [3] at room temperature. In line with common belief, the bright protrusions inside the unit cell labeled counterclockwise A,B,C would correspond to the BEDT-TTF molecules of the multimolecular crystal basis of the *bc* plane of κ-(BEDT-TTF)$_2$Cu(NCS)$_2$. Along the [021]-direction a variation of brightness of the protrusions is observed. The corner molecules of the unit cell have a pronounced brightness, so that bright molecular rows appear along the [010]-direction of the crystal. To interpret the measured brightness variations, a DFT based simulation of the STM image proved helpful. The second inset, also of a size of roughly 2 × 2 crystal unit cells, displays a convoluted DFT based simulation (see later in the text) for comparison with the STM data. Now we compare the observed protrusion in the STM image with the DFT based simulation: protrusion B is placed in the lateral direction almost centric between two corner molecules of the unit cell. Protrusion A and protrusion C in the two insets of Figure 1 appear at the same positions and show a somewhat lower brightness than the corner molecules. The brightness of protrusion B seems to be lower than in the convoluted DFT-simulation. However, overall, the positions and brightness of the BEDT-TTF relaxed surface simulation match remarkably well the protrusions in the averaged STM sub-image. In the simulated BEDT-TTF image the dimers are marked with ovals according to the structural data of [25]. We can therefore interpret the molecules B and C as well as the molecule A and the adjacent corner molecule (not labeled) as BEDT-TTF molecular dimers (marked with ovals).

Figure 2 shows a drift corrected STM image of a ten years aged κ-(BEDT-TTF)$_2$Cu(NCS)$_2$ crystal. The inset of Figure 2 displays an averaged sub-image of an approximate size of 2 × 2 unit cells. The size of the unit cell could be determined as 0.82 nm × 1.34 nm corresponding, within the measurement error, to a unit cell of the *bc* plane of κ-(BEDT-TTF)$_2$Cu(NCS)$_2$ described above. Like in Figure 1, the cation layer consisting of ET-molecules is visible. Even after ten years the STM images show the surface of a κ-(BEDT-TTF)$_2$Cu(NCS)$_2$ crystal in very good resolution. The corner molecules of the unit cell also show slightly enhanced brightness, so that again bright molecular rows appear along the [010]-direction of the crystal. The variation in brightness along the [021]-direction of the BEDT-TTF crystal has been previously observed and attributed to a surface relaxation [13,26,27]. However, the elevated brightness along the [010]-direction (the corner molecules of the unit cell) was also found by others and was assigned either to a tip-molecule interaction or insulating layers [26]. As our measurements were performed at about a factor of 50 smaller tunneling current, we have significantly reduced tip-sample interactions. Despite that, we find a strongly elevated brightness of the corner molecules in the unit cell. Moreover, at a bias voltage of +30 mV, we can almost

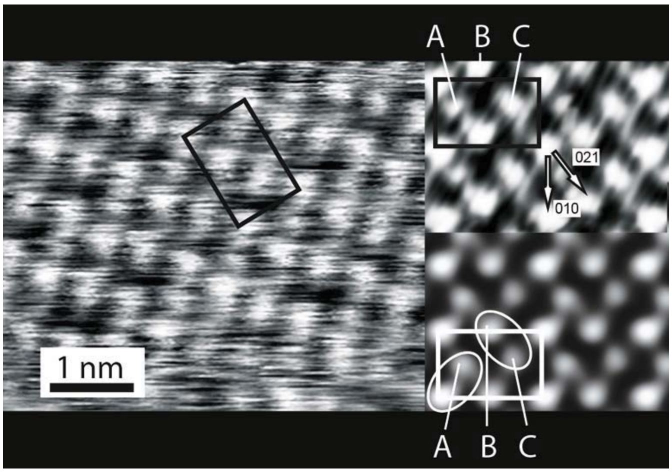

Fig. 2. Drift corrected STM image of the *bc* plane of a ten years aged κ-(BEDT-TTF)$_2$Cu(NCS)$_2$ crystal (V_{Bias} = +10 mV, I_T = 1 pA, 5.0 nm × 4.3 nm, ambient conditions); the black rectangle marks a unit cell. The insets represent a correlation averaged, rotated sub-image of the large STM-image with a size of about 2 × 2 unit cells (top) and a convoluted DFT based simulation to scale for comparison (bottom). Further discussion see text.

certainly exclude tunneling through an insulating barrier. Therefore the STM-contrast of the corner molecules is most likely dominated by surface electronic states of a relaxed surface, as the DFT based simulations suggest.

Cuts through the isosurfaces of the integrated local density of states (ILDOS) gained by a DFT based simulation of a relaxed and not relaxed surface are displayed in Figure 3 for comparison with the STM images (for further details see Experimental). The size is chosen to reveal a slightly larger set than 1 × 2 unit cells for the *bc* plane of BEDT-TTF. The two top images (Figs. 3a and 3b) simulate a STM image of a relaxed crystal surface, while the two bottom STM images (Figs. 3d and 3e) are a simulation of a not relaxed crystal surface. In the left row (Figs. 3a and 3d) a pure cut through the isosurface of the DFT calculation of the ILDOS is presented, in the right row (Figs. 3b and 3e) such a simulation convoluted by treatment with a Gauss function (see Experimental) is displayed, imitating the effect of a finite STM tip, as the CASTEP approach neglects the extended geometry of the STM tip. For better comparison with the measurements, Figure 3b doubled along [001] was added to Figures 1 and 2 as insets.

In the following we discuss the DFT results in greater detail. As already mentioned, the position and brightness of the molecules A, B, C as well as the corner molecules obtained by STM match well the DFT based simulation. The BEDT-TTF crystal unit cell has $P2_1$ symmetry. So along the [001]-direction a pair of BEDT-TTF molecules is transferred into another pair by a screw operation (see Fig. 3a bent arrow). Inside a crystal, these pairs of molecules are connected to one another by S...S contacts [26]. It was reported that the topmost ethylene group (-CH$_2$–CH$_2$-) is considerably relaxed in an optimized molecular structure [13]. In our surface relaxation, performed via the quasi-Newton scheme implemented in the CASTEP platform, we find a somewhat weaker intramolecular relaxation than [13] at this topmost ethylene group. However, the relaxation of the topmost ethylene group results in intermolecular changes: the topmost ethylene groups of the two molecules of a dimer move together and each topmost hydrogen of one of the molecules in a dimer stretches up (Figs. 3c and 3f). At this relaxed surface we performed a DFT calculation (Figs. 3a and 3b) of the ILDOS. A molecule of one dimer (marked with the left oval) falls on the corner molecule position of the unit cell, while the corresponding molecule in the second dimer (marked with the right oval) falls on position B. Alike the STM images, the simulation shows that the corner molecule of the unit cell appears brighter (encircled) than the corresponding molecule B of the second dimer (also encircled), thus revealing a symmetry breaking concerning the brightness of the otherwise equivalent dimers. In contrast to that, only a slight difference in brightness between the two dimers is visible in the electronic states gained by a cut of the isosurface of the ILDOS calculated for the not relaxed crystal surface (Figs. 3d and 3e). Dimers of a not relaxed surface would thus appear nearly symmetric. Calculation of BEDT-TTF bulk displays no difference in brightness between the different dimers (not shown). This

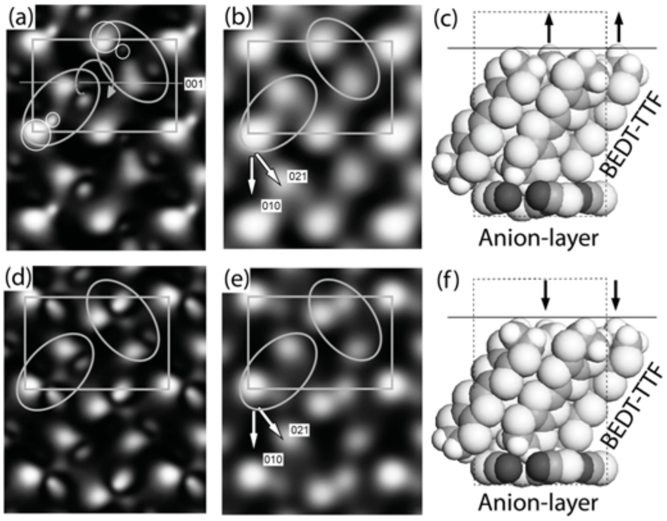

Fig. 3. A cut through the isosurface of a DFT based simulation of the *bc* plane of a relaxed and not relaxed κ-(BEDT-TTF)$_2$ crystal surface, with each sub-image showing roughly 1 × 2 unit cells: (a) Revealing a relaxed surface and (b) a convoluted (Gauss function treated) simulation imitating a finite STM-tip on the relaxed crystal surface. (c) Side view of a space-filling depiction of the relaxed unit cell gained by a quasi-Newton-scheme optimization – in the relaxed unit cell the topmost hydrogen atoms stretch up (marked with arrows). (d) Illustrating a bare and (e) a convoluted simulation imitating a finite STM-tip on the not relaxed crystal surface. (f) Side view of the non relaxed unit cell for comparison. The calculations include the Cu(NCS)$_2$ anionlayer, further details see text.

indicates that the experimentally observed modulation of brightness is due to electronic states influenced by missing molecular interaction at the surface resulting in the relaxation of the surface.

3 Conclusion

κ-(BEDT-TTF)$_2$Cu(NCS)$_2$ crystals were topographically characterized with STM and compared to a cut through the isosurface of the ILDOS of generalized gradient approximation exchange correlation functionals DFT-calculations. Even after ten years it is possible to get STM images on κ-(BEDT-TTF)$_2$Cu(NCS)$_2$ crystals in very good resolution without any further surface treatment, indicating that there is no deterioration of the surface with time. We confirmed the recently reported symmetry breaking [13,26,27] as well as the enhanced brightness along the [010] direction and find a close match of these properties to the here newly presented DFT-surface simulations of a relaxed *bc* plane of the cation layer of κ-(BEDT-TTF)$_2$Cu(NCS)$_2$ crystals. This suggests that the symmetry breaking is indeed caused by a surface relaxation [13,26,27]. Furthermore, the enhanced brightness of protrusions along the [010] direction is also caused by surface relaxation, rather than by tip-molecule interactions or insulation layers as suggested before [26]. An even closer correspondence between simulation and STM data has been obtained by convoluting the simulation data with a Gauss function, imitating a finite size tip.

4 Experimental

The crystals of the charge-transfer-salt κ-(BEDT-TTF)$_2$-Cu(NCS)$_2$ were obtained by electrochemical oxidation of BEDT-TTF (10^{-3} mol/l) in 1.1.2-TCE-alcohol absolute (10 v/v%) medium at constant current conditions (I = 1.0 μA and 1.5 μA, respectively, for the samples grown in 1997 and in 2007) at 20 °C. A mixture of the complex 18-crown-6, KSCN and CuSCN in a 1:1:1 molar ratio (4.5×10^{-3} mol/l) was used as an electrolyte. $1 \times 0.5 \times 0.2$ mm^3 crystals were grown on a Pt anode (diameter 1 mm) as hexagon-like black plates for 2 or 3 weeks, depending on the current applied. The older crystal was stored in a dark environment in air at room temperature. All measurements were performed on the *bc* plane. The crystals were mounted on a copper holder with silver paint. No special surface treatment (cleaving, etching or cleaning) was applied to the flat shiny crystal surfaces prior to the STM measurement.

The topographic images were obtained with a commercial DI Nanoscope III with a low current converter in air in a class 1000 clean room at room temperature. The tips were mechanically cut from a PtIr (Pt90%, Ir10%) wire.

From the images a background plane was subtracted and a horizontal line correction applied. The averaged images presented in the insets to Figures 1 and 2 were obtained by an averaging algorithm written for the SXM-shell of the Basel images analysis software and manually carefully checked for validity. A chosen subimage is compared to similar locations of the image via cross-correlation and averaged into a noise-reduced image [28,29].

DFT calculations with generalized gradient approximation exchange correlation functionals (Perdew-Wang 91 [30]) were performed on the CASTEP platform of Accelrys Material Studio [31] in self-consistent field (SCF) convergence (10^{-5} eV) with an energy cutoff of the plane wave basis set at 260 eV (k-points were fixed at $2 \times 3 \times 1$). The crystal structure (one unit cell) from reference [25] was used for the DFT calculations with periodic boundary conditions (one layer of BEDT-TTF molecules and one layer of CuNCS). For the simulation of the crystal surface 0.7 nm of vacuum were added. The surface relaxation was performed via the Broyden–Fletcher–Goldfarb–Shanno (BFGS) quasi-Newton scheme [32] implemented in the CASTEP platform of Accelrys Material Studio until the forces on individual ions were less then 0.1 eV Å^{-1}. Typical errors at atomic positions of the surface relaxation amounted to 0.01–0.02 nm, at single positions errors of 0.09 nm were encountered. The cut was placed above the cation layer in van-der-Waals distance to the topmost hydrogen atom. As CASTEP allows no correction for the finite size of a realistic tip, this was artificially introduced by folding the DFT images with a blurring size of a 0.13 nm × 0.13 nm Gauss function, mimicking the roughly 0.26 nm diameter of the tunneling d_z orbital.

We acknowledge M. Fuchs, A. Rubio, K. Gruber, C. Hoehl, M. Schönherr for discussions, H.J. Güntherodt, J. Kotthaus for usage of technical equipment and T. Brenninger, H. Thiess and his co-workers, U. Guggenberger, H. Schwaiger, J. Naundorf, P. Binkert, J. Geismann, S. Wanninger for technical support. Financial assistance from Nanosystems Initiative Munich (NIM), Center for Nano Science (CeNS), the Walther – Meissner – Institute, Ludwig – Maximilians – University of Munich and RFBR-DFG project No. 07-02-91562 is greatly appreciated.

References

1. H. Urayama, H. Yamochi, G. Saito, K. Nozawa, T. Sugano, M. Kinoshita, S. Sato, K. Oshima, A. Kawamoto, J. Tanaka, Chem. Lett. **1988**, 55 (1988)
2. N. Kinoshita, K. Takahashi, K. Murata, M. Tokumoto, H. Anzai, Solid State Commun. **67**, 465 (1988)
3. H. Urayama, H. Yamochi, G. Saito, S. Sato, A. Kawamoto, J. Tanaka, T. Mori, Y. Maruyama, H. Inokuchi, Chem. Lett. **1988**, 463 (1988)
4. T. Ishiguro, K. Yamaji, G. Saito, *Organic Superconductors*, 2nd edn. (Springer, Berlin, 2007)
5. T. Arai, K. Ichimura, K. Nomura, S. Takasaki, J. Yamada, S. Nakatsuji, H. Anzai, Phys. Rev. B **63**, 104518 (2001)
6. T. Arai, K. Ichimura, K. Nomura, S. Takasaki, J. Yamada, S. Nakatsuji, H. Anzai, Solid State Commun. **116**, 679 (2000)
7. Ø. Fischer, M. Kugler, I. Maggio-Aprile, Christophe Berthod, Rev. Mod. Phys. **79**, 353 (2007)

8. S.A. French, C.R.A. Catlow, J. Phys. Chem. Solids **65**, 39 (2004)
9. T. Kawakami, T. Taniguchi, S. Nakano, Y. Kitagawa, K. Yamaguchi, Polyhedron **22**, 2051 (2003)
10. B. Barszcz, A. Lapiński, A. Graja, A.M. Flakina, A.N. Chekhlov, R.N. Lyubovskaya, Chem. Phys. **330**, 486 (2006)
11. A. Fortunelli, A. Painelli, Synth. Metals **85**, 1631 (1997)
12. Y. Imamura, S. Ten-no, K. Yonemitsu, Y. Tanimura, J. Chem. Phys. **111**, 5986 (1999)
13. M. Ishida, O. Takeuchi, T. Mori, H. Shigekawa, Phys. Rev. B **64**, 153405 (2001)
14. H. Bando, S. Kashiwaya, H. Tokumoto, H. Anzai, N. Kinoshita, K. Kajimura, J. Vac. Sci. Technol. A **8**, 479 (1990)
15. M. Yoshimura, K. Fujita, N. Ara, M. Kageshima, R. Shioda, A. Kawazu, H. Shigekawa, S. Hyodo, J. Vac. Sci. Technol. A **8**, 488 (1990)
16. Y. Mori, Y. Maruyama, H. Mori, G. Saito, Jpn J. Appl. Phys. **30**, L358 (1991)
17. Y.F. Miura, A. Kasai, T. Nakamura, H. Komizu, M. Matsumoto, Y. Kawabata, Mol. Cryst. Liq. Cryst. **196**, 161 (1991)
18. S.N. Magonov, G. Bar, E. Keller, E.B. Yagubskii, E.E. Laukhina, H.-J. Cantow, Ultramicroscopy **42–44**, 1009 (1992)
19. R. Fainchtein, S.T. D'Arcangelis, S.S. Yang, D.O. Cowan, Science **256**, 1012 (1992)
20. H. Shigekawa, K. Miyake, H. Oigawa, Y. Nannichi, T. Mori, Y. Saito, Phys. Rev. B **50**, 15427 (1994)
21. M. Yoshimura, H. Shigekawa, H. Nejoh, G. Saito, Y. Saito, A. Kawazu, Phys. Rev. B **43**, 13590 (1991)
22. J. Moser, J.R. Cooper, D. Jérome, B. Alavi, S.E. Brown, K. Bechgaard, Phys. Rev. Lett. **84**, 2674 (2000)
23. C.E. Campos, J.S. Brooks, P.J.M. van Bentum, J.A.A.J. Perenboom, S.J. Klepper, P. Sandhu, M. Tokumoto, T. Kinoshita, N. Kinoshita, Y. Tanaka, H. Anzai, Physica B **211**, 293 (1995)
24. R. Li, V. Petricek, G. Yang, P. Coppens, M. Naughton, Chem. Mater. **10**, 1521 (1998)
25. M. Rahal, D. Chasseau, J. Gaultier, L. Ducasse, M. Kurmoo, P. Day, Acta Cryst. B **53**, 159 (1997)
26. S. Yoon, W.F. Smith, M. Yoo, A. L. deLozanne, R. Fainchtein, T.J. Kistenmacher, S.T. D'Arcangelis, D.O. Cowan, Phys. Rev. B **47**, 4802 (1993)
27. M. Ishida, O. Takeuchi, T. Mori, H. Shigekawa, Jpn. J. Appl. Phys. **39**, 3823 (2000)
28. S. Behler, S.H. Pan, M. Bernasconi, P. Jess, H.J. Hug, O. Fritz, H.-J. Güntherodt, J. Vac. Sci. Technol. B **12**, 2209 (1994)
29. L.J. Scherer, L. Merz, E.C. Constable, C.E. Housecroft, M. Neuburger, B.A. Hermann, J. Am. Chem. Soc. **127**, 4033 (2005)
30. J.P. Perdew, J.A. Chevary, S.H. Vosko, K.A. Jackson, M.R. Pederson, D.J. Singh, C. Fiolhais, Phys. Rev. B **46**, 6671 (1992)
31. Accelrys Software Inc., Materials Studio, Release 4.2 (San Diego: Accelrys Software Inc., 2008)
32. B.G. Pfrommer, M. Cote, S.G. Louie, M.L. Cohen, J. Comput. Phys. **131**, 233 (1997)

Acknowledgments

First of all I would like to thank my supervisor Bianca Hermann for the opportunity to work on this here presented topic, which not only taught me scientific skills, but also changed my way of seeing the world in terms of self-organization. Thank you for being always open and accessible to discussions. And I want to thank you for learning much about paper writing and the scientific freedom I enjoyed.

My next thanks go to Joachim Rädler, who responded to my need for a new first thesis advisor without hesitation. Thank you for this quick, unbureaucratic response. I am glad that Markus Lackinger took on the job of second referee for my thesis. I hope you will find it insightful and enjoyable to read. I would like to thank my Ph. D. committee Ulrich Schollwöck, Tim Liedl and Hermann Gaub for their invested time and energy.

Thank you Kathrin for the many different shared activities; for discussions, paper writing, corrections, poster preparation, listening to my ideas, being together on conferences, for ordering equipment, making tea, help in so many circumstances and being there in the lab, as well as in the office.

I would like to thank Johannes for lifting a large technical burden of my shoulders and letting me pursue scientific passion. Thank you for all the instances, when small technical things failed to make my life miserable due to your help. And thanks for putting up with my teasing nature. I´m thankful for the help of my diploma student Conny, who set this thesis on a solid footing with her large measurement contribution. At the end I would like to thank all the people at Walther-Meissner Institute for their support during the years foremost Rudolf Gross.

This work would not have been possible without the synthesized molecules and pre work done at the University of Basel. My thanks go to Edwin Constable, Michael Malarek and Lukas Scherer not only for the great system to work on, but also the language support in paper writing.

Thank you Thomas, for showing me, that I can write decent papers. This paper writing time meant a lot to me. Thank you both Thomas and Marta for the fruitful modeling discussions and last but not least the great interaction site model.

I would like to thank Prof. Kotthaus for the usage of his Nanoscope III which produced the all the beautiful measurements seen in this thesis.

I would like to thank Lorenz Kampschulte, who had a large impact onto my research, without knowing it, by showing me a little program I could do simulations with, that kindled my whole interest for simulating my results.

I thank my sister for her fresh outside view on my research which always helped me to clarify the explanations of my results. I enjoy our scientific discussions at the breakfast table and thank you for your graphics ideas, the theory discussions and your corrections to this thesis. I thank my friends, my girlfriend Hannah and my family for keeping my life outside of science vital and for helping me achieve the right balance.

I´m very much indebted for my scientific freedom by the Studienstiftung des deutschen Volkes and the Internationales Doktoranden Kolleg NanoBioTechnology des Elitenetzwerk Bayern. Without funding security, creativity is stifled by concerns. Thank you.

Genießt auch die Zeit,
in der ihr noch nicht erleuchtet seid.

S.R.Maharshi